

On-line Detection and Location of Partial Discharges in Medium-Voltage Power Cables

P.C.J.M. van der Wielen

Front cover: A 8/10 kV, $3 \times 150 \text{ mm}^2$ Al, belted paper-insulated lead-covered (PILC) cable (courtesy of Pirelli Cables and Systems N.V.) with a measurement (bottom) and injection (top) coil around it

Back cover: In front, a belted PILC cable (8/10 kV, $3 \times 150 \text{ mm}^2$ Al); left back, a three-core XLPE cable (6/10 kV, $3 \times 240 \text{ mm}^2$ Al); and right back, a single-core XLPE cable (6/10 kV, 400 mm^2 Al)

(Cover design by JWL Producties, Eindhoven)

**On-line Detection and Location of Partial Discharges
in Medium-Voltage Power Cables**

PROEFSCHRIFT

ter verkrijging van de graad van doctor aan de
Technische Universiteit Eindhoven, op gezag van de
Rector Magnificus, voor een commissie aangewezen
door het College voor Promoties in het openbaar te
verdedigen op donderdag 7 april 2005 om 14.00 uur

door

Petrus Carolina Johannes Maria van der Wielen

geboren te Hulst

Dit proefschrift is goedgekeurd door de promotoren:

prof.dr.ir. E.F. Steennis
en
prof.dr.ir. J.W.M. Bergmans

Copromotor:
dr. P.A.A.F. Wouters

Copyright © 2005 P.C.J.M. van der Wielen

All rights reserved. No part of this publication may be reproduced or transmitted in any form or by any means, electronic, mechanical, including photocopy, recording, or any information storage and retrieval system, without the prior written permission of the copyright owner.

Printed by Eindhoven University Press.

Kindly supported by Technology Foundation STW, KEMA Nederland B.V.,
N.V. Continuon Netbeheer, ENECO Netbeheer B.V.

CIP-DATA LIBRARY TECHNISCHE UNIVERSITEIT EINDHOVEN

Wielen, Petrus C.J.M. van der

On-line detection and location of partial discharges in medium-voltage power cables /
by Petrus Carolina Johannes Maria van der Wielen. -
Eindhoven : Technische Universiteit Eindhoven, 2005.
Proefschrift. - ISBN 90-386-1683-X
NUR 959

Trefw.: elektrische deelontladingen / elektrische kabels ; isolatie / foutendiagnose /
signaaldetectie

Subject headings: partial discharge measurement / power cable testing /
fault location / power cable insulation / condition monitoring

Aan Angelique

Summary

Partial-discharge measurements are a proven way to diagnose power-cables. Partial discharges are discharges that bridge only part of the insulation material in a cable or accessory and are indicative for the local insulation condition. A partial discharge induces a short current pulse in the surrounding conductors, which will propagate over the cable.

Several systems based on partial-discharge diagnostics on power cables are available. However, these systems require disconnection of the cable from the power grid and energize the cable with a separate generator. This ‘off-line’ measurement principle has obvious disadvantages (switching, short possible measurement time, separate high-voltage generator, etc.).

If partial discharges can be measured while the cable remains in-service, switching may not be necessary and important cable connections can be monitored (continuously). Consequently, the chances for detection of weak spots over time will be increased significantly. However, performing these ‘on-line’ measurements involves complications, which are investigated in this thesis. Furthermore, a measurement system that enables the on-line partial-discharge detection and location is discussed and designed.

A model is presented for the induced currents in the conductors of a three-phase structure inside a power cable or joint. In on-line situations the induced current magnitudes are dependent on the phase angle of the applied voltage. Furthermore, the phase-angle patterns can differ from off-line measurements.

A model of the propagation path(s) is required for optimal detection of the partial-discharge signals. A propagation model is presented and validated, tuned to the specific properties of power cables.

Research is performed on sensors and their optimal positioning for detection of partial discharges at the cable termination(s). The substation is the last part of the system model. A model is presented for the high-frequency behavior of the substation. Furthermore, a method is proposed to determine the properties of a substation and the cable sections while remaining in-service. This enables on-line system identification.

Several methods are presented to determine the location of the partial discharges. When measurements are conducted at both cable ends, the set-ups should be synchronized accurately. A patented method for this synchronization involves pulse injection at the cable termination of the power cable itself. This provides for an economically interesting and practically feasible method.

Principles for the design of an on-line partial-discharge detection system are given. This incorporates: system topology, data acquisition, communication, and software modelling. Experimental results have validated the research results and the practical applicability for diagnostics.

Samenvatting

Een bewezen methode voor het diagnostiseren van een energiekabelverbinding is het detecteren van partiële ontladingen. Dit zijn ontladingen die een gedeelte van het isolatiemateriaal van een kabel of kabel-accessoire overbruggen en indicatief zijn voor de plaatselijke conditie van de isolatie. Een partiële ontlading induceert een kortdurende stroompuls op de omringende geleiders, welke over de kabelverbinding zal propageren.

Er zijn verschillende systemen beschikbaar die van dit principe gebruik maken. Deze systemen vereisen echter, dat de kabelverbinding wordt losgekoppeld van het distributienet en met een aparte generator op spanning wordt gebracht. Dit ‘off-line’ meten heeft voor de hand liggende nadelen (schakelen, kort mogelijke meettijd, aparte hoogspanningsbron, etc.).

Indien partiële ontladingen gemeten kunnen worden terwijl de kabelverbinding in normaal bedrijf is, hoeft eventueel niet meer geschakeld te worden en kunnen belangrijke kabelverbindingen min of meer continu bewaakt worden. Hierdoor wordt de kans dat een zwakke plek tijdig wordt opgemerkt vergroot. Dit ‘on-line’ meten brengt echter complicaties met zich mee. In dit proefschrift worden de implicaties van het on-line detecteren en lokaliseren van partiële ontladingen onderzocht. Bovendien wordt een meetsysteem beschreven en gerealiseerd dat on-line detecteren van partiële ontladingen mogelijk maakt.

Een model wordt gegeven voor de geïnduceerde stromen ter plaatse van de partiële ontlading in de geleiders van een driefasestructuur van een energiekabel of mof. In een on-line situatie is de grootte van de geïnduceerde stromen afhankelijk van de fasehoek van de spanning. Bovendien kan het fasepatroon gewijzigd zijn ten opzichte van off-line metingen.

Teneinde de signalen van de partiële ontladingen goed te kunnen detecteren is een goed model van het propagatiepad noodzakelijk. Een model wordt gegeven voor signaalpropagatie door de kabel, toegespitst op de specifieke eigenschappen van energiekabels. Metingen verifiëren het model.

Voor het detecteren van partiële ontladingen aan de uiteinden van de kabels is onderzoek gedaan naar de verschillende mogelijkheden voor types en positionering van sensoren. Het laatste deel van het systeemmodel is het onderstation. Een model wordt gepresenteerd voor het hoogfrequent-gedrag van een onderstation. Bovendien wordt een methode gegeven om de eigenschappen van het onderstation en de kabelsecties te bepalen terwijl deze in bedrijf zijn. Dit is belangrijk om on-line systeem-identificatie mogelijk te maken.

Ter bepaling van de locatie van partiële ontladingen zijn verschillende methodes gepresenteerd. Indien aan twee zijden wordt gemeten, dienen de meetopstellingen nauwkeurig te worden gesynchroniseerd in tijd. Bij een inmiddels gepatenteerde

methode voor deze synchronisatie worden pulsen ten behoeve van tijdsreferentie in de kabel geïnjecteerd. Dit blijkt een economisch interessante en praktisch toepasbare methode.

Principes in het ontwerp van een systeem om partiële ontladingen te meten worden gegeven. Deze omvatten: systeem topologie, data acquisitie, communicatie en het software model. Experimentele resultaten hebben de resultaten van het onderzoek evenals de toepasbaarheid voor praktische diagnostiek geverifieerd.

Contents

| | |
|---|------------|
| Summary | vii |
| Samenvatting | ix |
| 1 Introduction | 1 |
| 1.1 Power cables | 1 |
| 1.1.1 Cables in power networks | 1 |
| 1.1.2 Distribution-class power-cable types | 2 |
| 1.2 Power-cable diagnostics | 6 |
| 1.2.1 Diagnostic methods | 6 |
| 1.2.2 Partial-discharge detection | 8 |
| 1.3 On-line partial-discharge detection and location | 10 |
| 1.3.1 Motivation | 10 |
| 1.3.2 Implications | 12 |
| 1.3.3 Project description | 13 |
| 1.4 Thesis outline | 13 |
| 2 Partial-discharge signal excitation | 15 |
| 2.1 Introduction | 15 |
| 2.2 Model of electric field and partial discharges in three-phase belted cables | 16 |
| 2.2.1 Rotating-field parameters | 16 |
| 2.2.2 Discharge model | 18 |
| 2.3 Induced charge in three-phase belted cables | 19 |
| 2.3.1 Induced-charge model | 19 |
| 2.3.2 Induced-charge simulations | 20 |
| 2.4 Partial-discharge phase-patterns in three-phase belted cables | 24 |
| 2.4.1 Phase patterns in a rotating field | 24 |
| 2.4.2 Simulation of partial discharges in a rotating field | 25 |
| 2.5 Conclusions | 27 |
| 3 Partial-discharge signal propagation | 29 |
| 3.1 Introduction | 29 |
| 3.2 Signal propagation in single-phase cables | 30 |
| 3.2.1 Propagation model | 30 |
| 3.2.2 Cable parameters | 31 |
| 3.3 Propagation model of three-phase belted cables | 34 |
| 3.3.1 Multi-conductor model | 34 |
| 3.3.2 Propagation channels in power cables | 35 |

| | | |
|----------|---|------------|
| 3.4 | Multi-conductor cable parameters | 38 |
| 3.4.1 | Model-based approximations | 38 |
| 3.4.2 | Propagation-measurement methods | 44 |
| 3.5 | Cascade-coupled cables and accessories: cable systems | 48 |
| 3.5.1 | Model of cable systems | 48 |
| 3.5.2 | Measurements on cable systems | 49 |
| 3.6 | Charge transport | 50 |
| 3.6.1 | Charge-transport estimation | 51 |
| 3.6.2 | Charge-transport measurements | 52 |
| 3.7 | Conclusions | 52 |
| 4 | Partial-discharge signal detection | 55 |
| 4.1 | Introduction | 55 |
| 4.2 | Sensors | 56 |
| 4.2.1 | Sensor types | 56 |
| 4.2.2 | Sensor shielding | 61 |
| 4.3 | Sensor locations | 64 |
| 4.3.1 | Measurement locations | 64 |
| 4.3.2 | Directional sensing | 67 |
| 4.4 | Substation impedance | 70 |
| 4.4.1 | Components in substations | 71 |
| 4.4.2 | Total substation impedance | 76 |
| 4.4.3 | On-line substation-impedance measurement | 78 |
| 4.5 | On-line system identification | 81 |
| 4.6 | Partial-discharge signal analysis | 83 |
| 4.6.1 | Signal extraction | 83 |
| 4.6.2 | Disturbance rejection | 87 |
| 4.6.3 | Simulations and measurements | 88 |
| 4.7 | Conclusions | 90 |
| 5 | Partial-discharge source location | 91 |
| 5.1 | Introduction | 91 |
| 5.2 | Methods for partial-discharge source location | 92 |
| 5.2.1 | Pulse-shape based location | 92 |
| 5.2.2 | Time-domain reflectometry | 93 |
| 5.2.3 | Double-sided measurement | 97 |
| 5.3 | Time-base alignment | 98 |
| 5.3.1 | Measurement set-up synchronization | 98 |
| 5.3.2 | Pulse-injection principle | 102 |
| 5.3.3 | Pulse-injection measurements | 104 |
| 5.3.4 | Time-wander correction | 106 |
| 5.4 | Time-of-arrival estimation | 108 |
| 5.5 | Conclusions | 110 |
| 6 | System design | 111 |
| 6.1 | Introduction | 111 |
| 6.2 | System topology | 112 |
| 6.3 | Hardware-design considerations | 114 |
| 6.3.1 | General component description | 114 |

| | | |
|----------|---|------------|
| 6.3.2 | Measurement and data acquisition | 115 |
| 6.3.3 | Pulse injection | 116 |
| 6.3.4 | Data communication | 117 |
| 6.4 | Software architecture | 120 |
| 6.4.1 | Software components | 120 |
| 6.4.2 | System-identification mode | 122 |
| 6.4.3 | Measurement mode: data acquisition | 122 |
| 6.4.4 | Data analysis: partial-discharge extraction | 125 |
| 6.4.5 | Result combination: partial-discharge location | 126 |
| 6.4.6 | Expert rules | 127 |
| 6.5 | Conclusions | 128 |
| 7 | On-line partial-discharge measurements | 129 |
| 7.1 | Introduction | 129 |
| 7.2 | Measurement set-up | 130 |
| 7.3 | System validation | 131 |
| 7.3.1 | Off-line reference measurement | 131 |
| 7.3.2 | On-line location with different time-base alignment methods | 133 |
| 7.3.3 | On-line charge magnitudes | 136 |
| 7.3.4 | Expert-rule validation | 138 |
| 7.4 | Partial-discharge measurements on defective cable and joint | 140 |
| 7.4.1 | Partial-discharge mapping | 140 |
| 7.4.2 | Partial-discharge density mappings | 141 |
| 7.4.3 | Partial-discharge magnitude histogram | 144 |
| 7.4.4 | Partial-discharge time-variations | 146 |
| 7.5 | Conclusions | 147 |
| 8 | Conclusions | 149 |
| 8.1 | Conclusions | 149 |
| 8.2 | Recommendations for future research | 151 |
| | Appendices | 153 |
| | A Measurement of Phase-to-Phase propagation properties | 153 |
| | B Rogowski-coil principle | 155 |
| | B.1 Mutual induction | 155 |
| | B.2 Self inductance | 156 |
| | B.3 Core material | 156 |
| | B.4 Relevant magnetic fluxes | 156 |
| | B.5 Transfer impedance | 157 |
| | C Software structures | 161 |
| | C.1 Software components | 161 |
| | C.2 Database structure | 163 |
| | Bibliography | 165 |
| | Glossary | 175 |

| | |
|------------------------------|------------|
| List of Abbreviations | 177 |
| Notation and Symbols | 179 |
| Acknowledgement | 187 |
| Curriculum vitae | 189 |

CHAPTER 1

Introduction

1.1 Power cables

1.1.1 Cables in power networks

Transmission and distribution of large quantities of power, as in power networks, can be established in two ways: with overhead lines (or overhead cables) and with underground power cables. In the early days of electrification, cable technology was just in its beginnings so mainly overhead lines were used. Nowadays, power cables are available for a wide range of voltage and power levels. Still, from an investment-costs point of view, overhead lines usually are preferred. However, regarding aesthetical and environmental considerations, safety issues, regulations but also technical matters, power cables can have the advantage (e.g. [Bar00]). Furthermore, if the operation costs, including maintenance, are taken into account, power cables can also be competitive, which especially applies for medium-voltage (MV) networks. The installed power-cable length is also increasing, because of the ever increasing demand for power. This is especially the case for distribution-class cables, operating in the range of 1 kV – 36 kV [Cig96]. In many countries, a large part of the medium and low voltage grid is constructed with power cables. In the Netherlands e.g., this is virtually 100 %. The total length of the MV cables in the Netherlands alone is already approximately 100,000 km, which corresponds to an investment of about $5 \cdot 10^9$ euros.

Medium-voltage power cables are usually applied for distribution of power from a substation to what are often called ‘ring main units’ (RMUs), where the voltage is usually further decreased to a low voltage (LV: < 1 kV) for the customers. The term ‘ring main unit’ is used, as the distribution grid is often, depending on the country, designed as a ring structure (or some variant), where the RMUs, together with the MV cables, form the ring. In Fig. 1.1 an example of a part of a ring-structured MV grid is drawn. As is indicated with dashed lines, several connections to other ring structures and substations are also possible and one substation usually feeds several rings. Medium-voltage networks, especially in highly populated areas, are often designed with some version of this ring structure, so power delivery can be routed via several paths, to increase reliability and provide maintenance possibilities. Due to limited maximum lengths of MV cables, or partial replacements, joints are used to interconnect cable sections.

Considering the total costs of the complete power grid, the distribution grid takes the major part, in the Netherlands approximately 75 %. Optimal design and mainte-

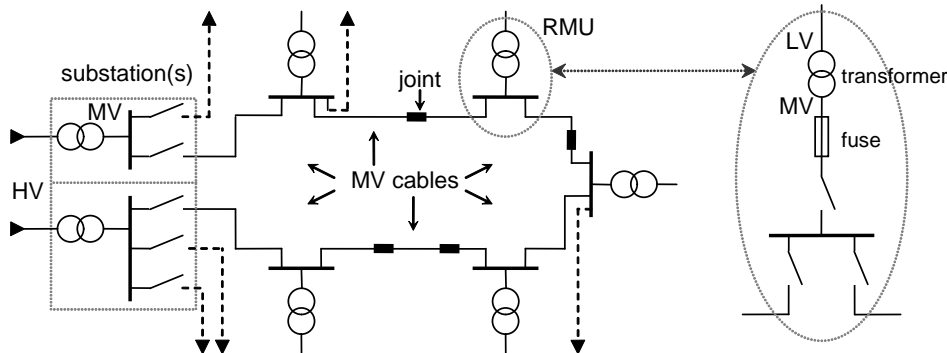


Figure 1.1 Example of relevant components in part of a medium-voltage grid which is designed as a ring structure. One ring main unit is enlarged to show its relevant components.

nance of the distribution grid is therefore crucial from an economical point of view. A large part of the investment costs of the distribution network is taken by the medium-voltage cables. Furthermore, the distribution grid is responsible for the majority of the time duration of power-delivery failure to the customer. In the Netherlands this figure is about 80 %. A vast majority of the distribution grid outage times is due to failures of MV cables and especially their joints. As many medium-voltage cable connections were already installed more than 30 years ago, a preventive maintenance strategy, as was often applied in the past, would require replacement. However, deregulation of the energy market and therefore the intensifying competition, bring utilities to pursue reduction of costs, postponing of investments, while maintaining or upgrading the reliability of power delivery. This, together with the ever increasing demand for energy, leads utilities to employ other maintenance and replacement strategies. Condition based maintenance (CBM) aims to postpone replacement and maintenance cost, based upon the current condition of the equipment. Provided that good knowledge of the condition of the system parts can be obtained, high cost reduction and reliability improvement can be established [Sch99]. As a consequence, good condition diagnostics for especially medium-voltage cables and their accessories (joints, splices, and terminations) have become very important.

Before considering the diagnostics presently available, the different relevant medium-voltage cable types themselves are discussed.

1.1.2 Distribution-class power-cable types

For medium-voltage cables, two main categories can be defined: paper-insulated and extruded cables. Several variations of the specific materials and dimensions exist, but the general lay-out principles are briefly described by the two categories below. A more detailed overview of power cables and more in-depth information can be found in e.g. [Bar00, Ste03a, Pes99, Kab].

Paper-insulated lead-covered cables

The paper-insulated lead-covered (PILC) cable is one of the oldest power-cable types and exists for almost a hundred years. For a long time, there have been no alternatives that could compete with the proven reliability of this type of cable and in many countries the majority of installed MV cables is still PILC. Fig. 1.2 shows an example of a commonly used PILC-type cable: a belted cable, which relates to the common belt (3) around the three phase cores (1+2). The phase conductors (1) can be stranded copper or aluminium or solid aluminium. The insulation consists of windings of paper tape, which is impregnated in a compound of oil, wax, and resin (2+3). The core- and belt-insulation thicknesses obviously depend on the operating voltage, which is for belted cables usually below 15 kV, [Bar00]. The lead shield (4), around the belt, serves as the earth conductor and ensures watertightness. Further coverings are bitumenized paper (5), jute (6), steel armor tape or wires (7), bitumenized jute (8), and chalk (9). The bitumen is applied for preservation. The chalk is used to avoid sticking of the cable to the reel. A polymer sheath from PVC (polyvinyl chloride) or PE (polyethylene) sometimes replaces the jute and gives better protection against e.g. pitting or corrosion (due to e.g. stray currents). For standardized names of the various layer, see [IECa].

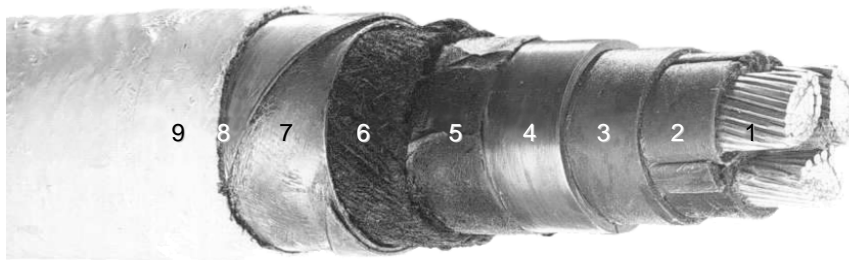


Figure 1.2 Typical PILC-cable lay-out: the belted construction type. The numbers correspond with the various layers, explained in the text. (Courtesy of TKF)

Some characteristics of PILC cables are: rugged, compact, continuous earth screen, high chemical resistance due to the lead sheath and proven long service life. Especially due to this last characteristic, some utilities still favor this type of cable. This belted PILC cable is used extensively for distribution-class cables. In the Netherlands, the vast majority of the medium-voltage cables are belted PILC cables, mainly 10 kV. Therefore, the main focus of this thesis will be pointed at this cable type, although most principles are cable-type independent.

For higher voltage classes (> 15 kV) field strengths between the conductors become too high due to their non-uniform distribution, as depicted in Fig. 1.3a, and cables with a separate shield around each round phase conductor are applied. This results in a radial field around each core, as shown in Fig. 1.3b. This power cable type is called a radial field or ‘Hochstädter’ cable. Other variations include e.g. the use of a separate lead sheath around each phase core and/or application of semi-conductor layers at the insulation-metal interfaces or as Hochstädter layers, to optimize field control. The maximum voltage class for this type of cable is 69 kV, although 10–35 kV PILC cables are most commonly used.

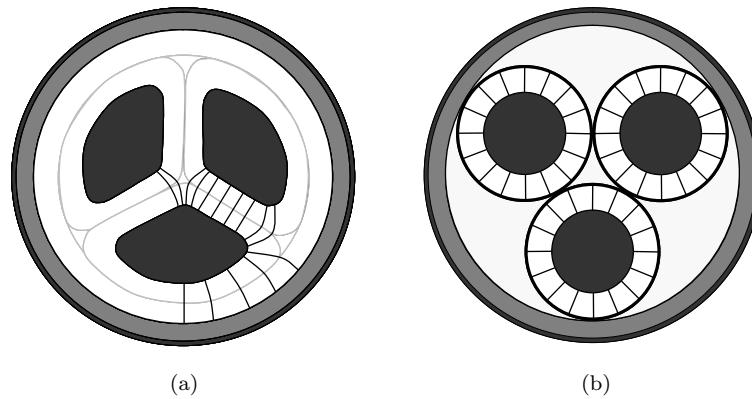


Figure 1.3 Electric field lines in typical PILC-cable lay-outs: (a) belted construction type, (b) Hochstädter layers around the cores

Extruded solid-dielectric power cables

Although polymeric cables are already available since the early 1950s, it was only until several tens of years later that the reliability increased enough to compete with PILC cables. Even nowadays, PILC cables sometimes get the advantage, depending on the utility and application.

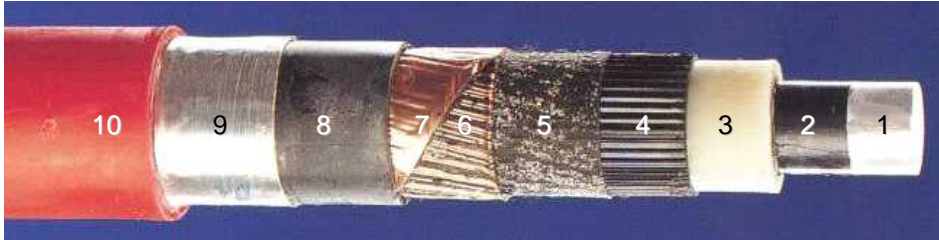


Figure 1.4 Typical single-phase MV XLPE cable lay-out. The numbers corresponds with the various layers, explained in the text. (Courtesy of TKF)

Although there are many different polymeric cable designs, an example of a single-phase XLPE (cross-linked polyethylene) cable is depicted in Fig. 1.4 to present the general structure. Details may differ for various designs. For standardized names of the various layer, see [IEC]. The conductor (1) can be stranded copper or aluminium or solid aluminium. A semi-conducting layer (often called conductor screen) (2) around the conductor serves for field control of the metal-insulation interface. The insulation material (3) can be PE, which is no longer used for new installations, EPR (ethylene-propylene-rubber) or XLPE. XLPE is by far the most popular choice, due to lower dielectric losses and price. Around the insulation, a semi-conducting shield (4) ensures smooth interfacing. This shield is also often denoted as insulation screen. Semi-conducting swelling tape (5) is applied for longitudinal watertightness. Copper or aluminium wires (6) and counter wound tape (7) serve as the earth conductor and should accommodate capacitive and short-circuit currents. Around this

screen, semi-conducting filling rubber (8) can ensure longitudinal watertightness at this location. An aluminium complex strip (9) and a PE or PVC sheath (10) serve as protection against water ingress and mechanical forces.

Properties of extruded cables are: low losses and relative permittivity, long expected lifetime, simple handling, long lengths and, especially if XLPE is used, high maximum operating temperature. Extruded cables are not restricted to distribution-class voltages. Maximum voltage rates are up to 500 kV, e.g. [Kam96].

Just as the three-core PILC cables with one common (lead) shield, MV polymeric cables can also embed three cores in one cable. Fig. 1.5 shows an example. The several layers and materials in this structure are similar to those of the single-core design. Now each of the phase conductors and their insulation layers have their own semi-conducting screen around them, resulting in radial electric field distributions in the core insulation, as in the Hochstädter PILC cable.

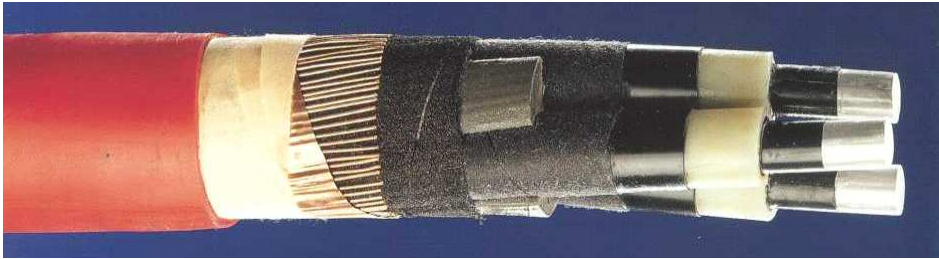


Figure 1.5 Example of an XLPE MV three-core cable design (Courtesy of TKF)

Terminology for high-frequency properties

For high-frequency properties of power cables, this thesis uses additional terminology for classification of power-cable types, based on the implementation of the shield, rather than the insulation material. Considering high frequencies (several MHz), two cable classes are defined here:

1. ‘Single-phase’ cables: cables with a metal screen around each individual core, irrespective of the surrounding construction, i.e. whether the compound is bundled together as one cable or left as three separate cables. This cable class incorporates e.g. radial field PILC cables with metal Hochstädter layers or single-core type extruded cables.
2. ‘Three-phase’, ‘common-screened’ or ‘belted’ cables: cables with three cable cores and one common metal earth-screen. This cable class incorporates e.g. belted PILC-type cables and extruded three-core cable designs, as depicted in Fig. 1.5.

‘Shielding’ of three individual cores in one cable by means of their semi-conducting layers (to establish radial electric fields) is not regarded as metal screening and will not influence the classification given above. Magnetic fields can easily penetrate the semi-conducting layers, since the skin-depth for these materials is much larger than the layer thickness. For high-frequency waves, this means that the main influence of the semiconducting layers is restricted to increased attenuation (Chapter 3).

1.2 Power-cable diagnostics

1.2.1 Diagnostic methods

This section will present a small overview of relevant diagnostic tests for medium-voltage cables. This summary is far from complete and too compressed to explain all the features and implications of the various test methods. The purpose of this section is to situate partial-discharge techniques in the context of diagnostics. More detailed information about power-cable diagnostics can be found in e.g. [Bar00, Ste03a, Tan83]. In this thesis the words “tests” and “diagnostic measurements” can refer to either destructive or non-destructive tests/diagnostics. If not trivial, destructive or non-destructive is added.

Mechanisms leading to breakdown

In general we can state that no breakdown will occur as long as the insulation is maintained. The causes of defects can be categorized in five main classes:

1. External influences: e.g. mechanical damage, chemical reactions, attack of vermin, etc., resulting in damage to the protective layers of a cable, and consequently to the other layers.
2. Production faults: e.g. inclusion of cavities, impurities or metal parts in the insulation, bad finishing of metal screen, etc.
3. Incorrect application: e.g. underestimation of maximum (short-circuit) current, voltage, load variation, environment temperature, temperature resistance of the environment, etc.
4. Incorrect installation: e.g. bad workmanship at installation of the cable and especially its accessories, violation of e.g. maximum forces during cable pulling, etc.
5. Aging of the insulation material.

Besides the causes that lead to immediate breakdown, categories 1–4 all lead to an acceleration of the natural aging process in category 5. The main aging processes, relevant for medium-voltage levels are:

- Thermochemical degradation. This degradation is accelerated by e.g. increasing temperature. Weakened insulation becomes increasingly prone to puncturing by energetic electrons or ions from partial discharges, see further e.g. [Kre91, Tan83].
- Partial discharges (PDs). These discharges cross a part of the insulating material (e.g. in a void, cavity, or electrical tree). If the electrical field in an insulation defect exceeds its inception voltage, a partial discharge over this region occurs. Due to the erosion, temperature increase, chemical reactions, and space-charge injection, PDs can be both a symptom and a cause of deterioration. See further e.g. [Kre89, Tan83, IECb].
- Electrical treeing. If partial discharges corrode the insulating material in such a way that carbonized channels appear and grow, then the process of electrical treeing has started. This aging mechanism can occur in all solid insulating materials or on the boundary areas of two (different) insulating materials. Elec-

trical treeing can be considered as a last step in the degradation before a final breakdown happens, see further e.g. [Kre91, Jon89].

- **Water treeing.** A water tree is a degradation of polyethylene by means of a combined action of water and an electric stress, resulting in a diffuse structure in a polymer with an appearance resembling a bush or a fan. Water trees reduce the electric breakdown stress level of a polyethylene insulating material. It will take many years for water trees to become large enough to be dangerous. In their final stage of life, water trees can result in the formation of PDs and electrical trees, causing rapid further deterioration and breakdown. See further e.g. [Ste89, Ild82].

As is indicated above, the different aging mechanisms are correlated, i.e. several mechanisms can be each other's cause and/or consequence.

Tests on MV cables

In Section 1.1.1, the reason for performing diagnostics on medium-voltage cables was motivated. Accurate determination of the cable condition and ultimately the expected lifetime is the goal. Many test methods are in principle available for every stadium of a power cable's life cycle: tests during development, (pre-)qualification, production, installation, service and finally failure [Ste03a]. In this thesis we are interested in non-destructive diagnostics during the service period.

Withstand tests

To test the insulation performance of power cables, a voltage that is related to the nominal voltage can be applied to test whether the cable's insulation holds. Considerations about the voltage level are important [IECa, IECc]. Since the test voltage is above the nominal voltage, an external test generator is necessary. For paper-insulated cables, a DC test can be applied. For XLPE cables this can lead to unnecessary breakdown of the cable insulation (due to accumulated space-charges and wrong field distribution in accessories) and usually does not provide useful information about the insulation under AC conditions, [Auc90, Sri95, Ste03a]. When AC tests are applied, the capacitance of the cable causes high power requirements for the test generator if normal power frequency is used. By means of a very low frequency (VLF) generator or a resonance test-set, this problem can be overcome. Obviously, this test is only non-destructive if the cable withstands the test.

Outer-sheath integrity tests

If the outer sheath of a cable is made from insulation material, the shield integrity can be tested by applying a high voltage between the metal screen of the cable and earth. If the sheath is damaged, the cable has lost the sheath's protecting function and will be more vulnerable to external influences. Obviously, this test does not provide indication of the present cable's insulation condition.

Loss-factor tests

The ratio of dielectric loss and permittivity is measured at e.g. VLF or power frequency and can serve as an indication of the overall insulation condition. For paper-insulated cables, this method can provide useful information. For XLPE the loss-factor only gives an indication of very severe degradation by water trees.

Dielectric spectroscopy

The dielectric permittivity and loss are measured as a function of frequency (0.1 mHz – 1 Hz, depending on the cable length) and as a function of voltage level (normally up to the nominal voltage). The variation of the measured parameters is a measure of the average presence of water trees in a polymer cable system, [Wer01, Hvi98], or e.g. water ingress in paper-insulated cables. As water trees are usually not concentrated on one location, but distributed along larger regions of the cable, this method provides in most cases a good assessment of the overall cable condition. Methods to detect and/or locate locally concentrated densities of water trees do not exist (yet). However, in [Pap03b] such a method is pursued.

Return-voltage, return-current tests (only extruded cables)

At present, publications are discussing the possibility to diagnose a water-tree aged medium-voltage cable with a return-voltage or return-current method. This method applies a relatively low DC voltage over the cable's insulation. After removal of the supply, the return voltage over the cable's insulation is measured. This voltage is caused by impurities, defects, but also normal polarization of the insulation under DC charging conditions. Instead of measuring the voltage, the return current through a small impedance can also be measured. Results of these methods might indicate the rate of water-tree presence, but confident, proven results are not present yet. Although, in principle, these methods measure the same properties in time domain as dielectric spectroscopy does in frequency domain [Gäf04, Hel98]. The effectiveness of the return-voltage and return-current measurements for power cables is still subject of research, e.g. [Hvi00].

Partial-discharge detection

Partial discharges induce high-frequency pulses over the cable insulation that will propagate to both cable ends. These high-frequency pulses can be measured at the termination(s) and can provide useful information about the condition of the cable insulation and its accessories. This method is especially applicable for paper-insulated cables and accessories and also provides for indication of possible problems in extruded-cable accessories. The extruded cables themselves can also be tested for PDs, but such cables do not often show PD related defects. A particularly powerful feature of PD detection is the possibility to locate the defect along the cable.

Partial-discharge detection is a reliable method for MV power-cable diagnostics. Especially PILC cables, which constitute the majority of installed MV cables in e.g. the Netherlands, can be diagnosed effectively by means of PDs. Furthermore, PD detection is the only non-destructive test that incorporates location of defective sites or regions along a complete cable length. Partial-discharge detection will be discussed in more detail in the next section.

1.2.2 Partial-discharge detection

Common practice for partial-discharge detection in medium-voltage cables is to disconnect the cable from the grid and apply the test off-line. A separate power generator is used to energize the cable under test in a conditioned matter, i.e. with low disturbance levels and on a voltage level of choice. Since energizing long cable systems

involves supplying its capacitive current, a VLF power generator (e.g. 0.1 Hz [Ste91]), a resonance system (e.g. [Gul98]) or other variants ([Lem96]) are applied to energize the cable up to the desired voltage level. All methods reduce the amount of needed power and can provide a low-noise energizing method. High-pass filters, e.g. high-voltage capacitors in series with a measurement impedance, are used to extract the high-frequency PD signal from the high-voltage conductors. Signals are stored in digital oscilloscopes or other digitizing equipment and further analysis can be performed.

Upon excitation of a partial discharge at the PD site, somewhere along the cable, a high-frequency pulse is induced on the surrounding conductors, see Chapter 2. This pulse will propagate in both directions and reflect at the cable ends. The difference in the time of arrival of the first pulse and the pulse that was reflected at the far end is a measure for the location of the PD site. This time-domain reflectometry (TDR) provides for a method to determine the insulation degradation as a function of the location. Fig. 1.6 shows an example of a mapping diagram of partial discharges on a 3 km long PILC-cable system, incorporating six joints. Various locations with high PD concentration and charge magnitude are shown, indicating possible high-risk locations, depending on the cable/accessory type.

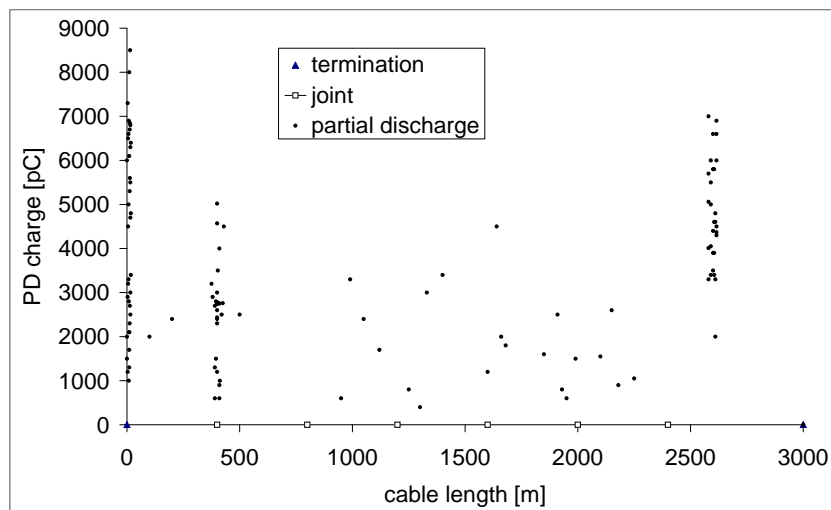


Figure 1.6 Example of a mapping diagram of a 3 km long MV PILC-cable connection. Charge levels and concentration indicate risk level, depending on cable and accessory type.

During the past years, a lot of research has been performed on PD diagnostic methods, resulting in several commercial apparatus, e.g. [Het95, Mas00, Ste91, Gul98, Lem96]. The maximum cable length for such systems is usually around 3–4 km, due to attenuation of high-frequency signals. In [Ste01], a system is described that is capable of measuring cable lengths up to about 8 km as well as branched cables by detecting PDs at multiple ends instead of applying TDR.

1.3 On-line partial-discharge detection and location

1.3.1 Motivation

Partial-discharge detection and location techniques have become a valuable tool for condition assessment of high-voltage systems. Up to now, practical application of PD measuring methods on medium-voltage cable systems is almost exclusively limited to off-line diagnostics, requiring the cable to be taken out of service for the measurement period and allowing only to take snapshots of its condition (as for all other diagnostic methods mentioned in Section 1.2.1). This points towards the use of a system capable of measuring PDs while the cable is in-service, i.e. on-line and over a long period of time. Obvious advantages emerge:

- The power supply is not discontinued during the measurement. The power can often be rerouted via other connections in the power grid, but especially in countries with a single-feeder power grid topology, or industrial grids, redundancy is not always present. Even rerouting of power means an increased risk in loss of power, since the cable under test is not available as a back-up.
- The cable system is tested under exact operating conditions, including over-voltages and load variations, which can be informative for its actual condition. Influences of switching or the off-line energizing method are no topic of concern.
- After installation, an on-line system hardly requires any personnel effort, which makes it relatively cheap to operate for utilities.
- The data is continuously registered, so time-related information, such as variation of PD activity in time, the effects of sudden over-voltages, and cable-temperature variations are detected. Also PDs occurring shortly before failure can be captured, in contrast with occasionally applied off-line tests.

This last point may be the most important argument from a technical perspective. Fig. 1.7 illustrates the effect in a hypothetical situation. Suppose off-line measurements are conducted at the time instants (1), (2), and (3). At measuring moment (1), some locations show low PD activity, which is no reason for concern. Between measuring moments (1) and (2), however, a PD site has emerged on location (b), which was not identified by measurement (1), and causes breakdown before the next measurement. At measurement moment (2), location (a) shows a small increase in PD activity, but it is PD site (c) that fails between the moments (2) and (3). Location (a) may be repaired before breakdown, since measurement (3) may show sufficient PD activity for taking action. Location (d) is fully missed and fails just after measurement moment (3). (Semi-)continuous monitoring can in principle detect all four defects before breakdown and can therefore potentially deliver a much higher level of information towards maintenance decisions.

On-line monitoring is already applied for other types of medium- and high-voltage equipment, e.g. generators [Pem00], transformers [Ahm98], switchgear [Pem99], etc., where sensors can be installed relatively close to the PD source. For cable systems, this method is also applied for especially extra-high voltage (EHV) cable joints and terminations, for which sensors are either mounted afterwards [Pul95] or implemented by the manufacturer [Hen96]. Also here the sensor is close to the origin of detectable PD activity, i.e. in the accessory itself and sometimes also at a short distance in the adjacent cable [Ahm01]. For underground MV cables, this method is in general not

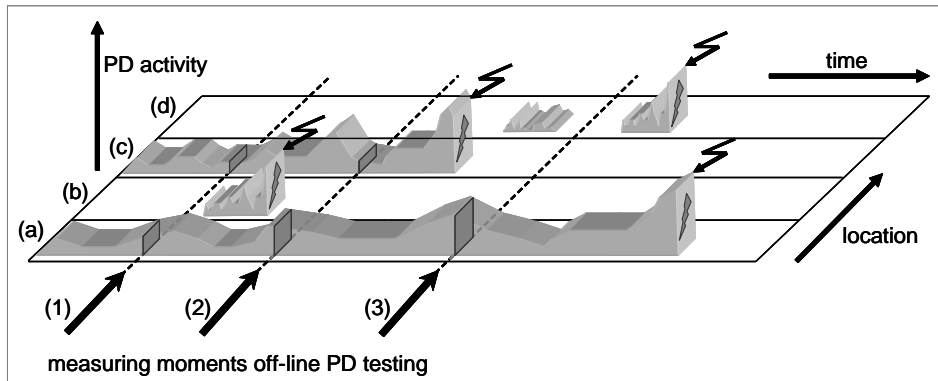


Figure 1.7 Illustration of the impact of (semi-)continuous monitoring versus off-line ‘snap shots’. Different weak spots along the cable are indicated with (a), (b), (c), and (d), off-line measurement moments with (1), (2), and (3). The flash-signs point towards the moment of breakdown.

feasible, since cable accessories are usually not easily accessible and installing the sensors in all accessories would be far too expensive.

A few publications also indicate on-line PD detection on MV cables at the cable terminations, without locating the PDs [Bow00, Ham01]. Some ideas about implementing location of PDs are mentioned, but the main aim for these tests is pre-selection of weak cable connections, which can be examined in more detail by off-line measurements afterwards. Although on-line detection without location already produces valuable information, location of the PD site is, however, a major advantage and results in much better knowledge of the cable-system’s condition:

- The level of PD activity from a few weak spots along the cable length is much more interesting than average PD numbers over the total cable length, since it is often cable joints or local weak spots that cause the fault instead of aging of the overall cable, while both situations can result in a similar total amount of detected PDs.
- The type of cable or accessory can be taken into account, each with its own PD behavior and aging characteristic.
- The history of that specific part of the cable system is known (replacements, failures, etc.).
- Local environmental conditions of the cable also influence the PD behavior (roads, tunnels, water, local temperature, etc.).
- Besides the total amount of PDs (per time unit) also the concentration per length unit can be determined.

When PDs from a cable system are measured on-line, location is even more crucial, because the cable terminations are connected to adjacent cables from which other PDs and disturbances originate too. Without location, it is hard to decide from which connected object (other cable, transformer, switchgear, termination, etc.) the signals originate (see Chapter 5).

1.3.2 Implications

On-line partial-discharge detection implies the measurement of small high-frequency signals on powered conductors. Sensors have to inhibit large frequency discrimination in order to filter the power frequency while being sufficiently sensitive to high frequencies. Safety issues limit applicable sensing principles. To enable on-line installation and to prevent the sensors from becoming a risk to the power system themselves, galvanic contact is not an attractive option.

Besides the type of sensor, also its location is not trivial. The cable under test is terminated in a substation or ring main unit. Depending on the sensor location in this substation or RMU, different signals are measured, some including PD signals, some impeded with extra unnecessary noise. Modelling the different circuits inside a substation and RMU is inevitable for knowledge of what is measured. Furthermore, the total substation/RMU impedance determines the total load impedance for the cable under test and is therefore needed in order to extract correct charge magnitudes of the detected PDs.

Since the cables are connected to the power grid, noise and interference levels are usually much higher as compared to the off-line measurement conditions. Switching transients, PDs from adjacent equipment (and other cables), radio broadcasts, etc. all reduce the signal-to-noise ratio (SNR) of the measured data. Therefore, besides measurement precautions like sensor shielding, optimal measurement locations, and electromagnetic compatibility (EMC) issues, advanced signal processing of the measured data is required, on a much higher level as compared to off-line measurements.

In order to extract the PD signals from data under high-noise conditions, a valid model of the signal characteristics is required. This implies the need for a good model of the cable system, the cable load impedance (substation), and the measurement equipment. As parameters for the models are not always available, on-line identification of the system is preferred to avoid switching.

Location techniques as being employed with off-line measurements may not be applicable for on-line situations. As the cable is not disconnected from the grid implications arise, since the far cable end is not open and does therefore not provide full signal reflection. If multiple measurement set-ups are used (e.g. at both cable ends), accurate synchronization and communication are required.

On-line PD detection opens also the opportunity of (semi-)continuous measurement. As the huge amounts of data from these measurements will be practically impossible to process manually, software has to be designed for automatic processing of measured data. Furthermore, the large bandwidth of PD signals, together with possible high PD rate, results in large demands on processing power. This requires the design of an efficient system.

After PDs are detected and located, interpretation of the results should indicate the cable system's condition. Off-line measurements are usually applied with only one phase-voltage. This results in a different field distribution inside the three-phase structure of a belted cable type (widely used in the Netherlands) as compared to normal, on-line conditions. Different field distributions can imply different induced charge levels and other phase-angle patterns. Knowledge rules, obtained from off-line experience to interpret the detected PD characteristics, may have to be adjusted. Furthermore, as on-line monitoring provides for new results, like variation with time, new knowledge rules will emerge.

1.3.3 Project description

The variety of challenges associated with on-line partial-discharge detection and location requires an approach based on multiple engineering disciplines. To that end, the research is subdivided into different topics, partly addressed in this thesis and partly in [Vee05]. The work presented in [Vee05] focuses on the theories and techniques involved with the signal analysis of partial discharges. This involves signal modelling, signal extraction, and accuracy analysis of discharge location, all in relation with investigation and filtering of noise and interference signals. Part of the work in [Vee05] also discusses the implementation of the signal analysis techniques in a measurement system. The work presented in the thesis at hand is focused on the measurement principle and system, including discharge excitation; propagation; sensor selection, design and location; substation impedance; and PD location methods. Furthermore, this thesis discusses the design of the complete measurement system, with topics such as synchronization and communication. Evidently, both studies are closely related and in many cases the research areas overlap; therefore part of the work was done in close cooperation.

1.4 Thesis outline

The aim for this thesis is to study the several processes and implications of on-line partial-discharge detection and location. The basic structure of this thesis is following the partial-discharge signal from excitation to the final goal in this thesis: extraction of PDs from live circuits into relevant results, e.g. mapping diagrams.

The implications of on-line PD diagnostics to the discharge excitation are studied in Chapter 2. A model is presented for the electrical field inside the three-phase structure of belted cables and accessories, together with corresponding induced charges. Furthermore, implications on the phase-resolved PD patterns are examined. After excitation, the PD signal propagates over the power cable system towards the cable terminations. Chapter 3 discusses the relevant propagation models, together with the involved parameters in order to estimate e.g. pulse shapes and propagation times. Measurement methods are presented to obtain the relevant parameters and validate the models. In Chapter 4, issues related to PD detection at the cable termination(s) are studied. This involves sensors and their location(s), substation impedance, and signal extraction. After detection, the PD sites have to be located. Methods for location, together with the implications, like measurement set-up synchronization with its techniques and possibilities, are examined in Chapter 5. Due to the stochastic behavior of PDs, together with the huge amount of resulting data, the results of on-line PD measurements can practically only be evaluated by an automated system that incorporates all the methods and techniques from the previous chapters. To that end the system design is discussed in Chapter 6. Subjects like data acquisition, communication, and the software model are also incorporated here. In Chapter 7 the system is validated with experiments in on-line situations, and compared with conventional off-line measurements. Obtained on-line PD detection and location results are presented. Chapter 8 summarizes the main conclusions of this thesis, together with recommendations for future work.

Partial-discharge signal excitation

This chapter is focused on aspects related to excitation of a PD pulse. On-line partial-discharge detection of three-phase belted MV cable connections results in a number of interpretation differences as compared to off-line measurements where only one phase is energized. The induced currents and charges in the phase conductors and earth screen resulting from the excitation of a PD not only depend on the discharge site, but also become phase-angle dependent. Furthermore, simulations show that the PD distribution itself varies with the amount of eccentricity of the rotating electric field and may differ from the off-line distributions obtained with a linear field. In this chapter, induced charges and PD distributions are studied by means of theoretical models and computer simulations.

2.1 Introduction

Partial discharges originate from defects in the insulation material of the power cables themselves or in their accessories. As explained in Chapter 1, they occur when the voltage across the defect, a void or whatever is causing the PD, exceeds some inception threshold. Obviously, the magnitude of the PD itself depends on this voltage and the size of the defect. Therefore, this magnitude is an important parameter for the diagnostics on power cables. When a partial discharge occurs, the field is usually largely neutralized by redistribution of charges. This redistribution induces charges in the surrounding conductors, resulting in a small, short duration (< 1 ns) pulse between the conductors. This pulse propagates to both cable ends, enabling us to measure the PD phenomena there. There is much literature describing this process in detail, among which [Kre89].

The relation between the magnitude of the partial discharge itself and the induced charge in the conductors depends on the position of the PD in the dielectric [Abd99, Rob91]. This implies that we are only able to measure what is called the apparent charge and not the real charge of the PD, leaving us with an unknown factor to get the real PD charge. This implies that the focus should not be too much on determining the measured (apparent) charge as accurately as possible, since this unknown factor will usually make this not worthwhile. Besides the magnitude, the phase-angle dependence (the PD pattern or distribution) is often used for PD diagnostics. Knowledge from experience and studies on phase-angle distributions can

help interpretation of measurement results [Kre89, Kre93b, Gro98, Tan95]. Although many nuances are present, most partial discharges from cavities have patterns with maxima between the zero crossings and the maxima of the power frequency field.

The above properties of PDs are valid when dealing with a linear field: every position within the dielectric has a particular and unique electrical field direction. A MV cable consists of three insulated phase-conductors, each with its own or with a common earth screen. Common practice for off-line PD tests is to energize only one phase, while the other phases are connected to ground together with the earth screen (e.g. [Ste01, Gul98, Lem96]). This means that in every location within the dielectric, the electric field only has one direction and its magnitude varies with power frequency between some maximum positive and negative value. So the above mentioned well-known properties of PDs apply.

However, during normal operation of a power grid with belted cables, the system must be regarded as a four-conductor transmission line. In this case, the electrical field in the insulating material is not linear, but rotates with power frequency. This means, the magnitude of the induced PD currents in the conductors will depend on the position of the defect within a cable cross section with respect to the phases and on the phase angle of the energizing voltage. Furthermore, one cannot speak of one power phase-angle anymore, since there are six angles: three phase-ground angles and three phase-phase angles. This, together with the fact that the electrical field in the insulation material is rotating, modifies the observed PD patterns.

In Section 2.2 a model is presented for the rotating electrical field and the excitation of partial discharges in this field. The induced charge on the surrounding conductors due to the PDs is examined in Section 2.3 by means of simulations. In Section 2.4 the change of the PD phase-angle distribution is discussed. Simulations are done to show various possible PD patterns in rotating fields. The conclusions of this chapter are given in Section 2.5.

2.2 Model of electric field and partial discharges in three-phase belted cables

2.2.1 Rotating-field parameters

In conventional off-line measurements on three-phase cable systems, only one phase is energized at a time. This means that the electric field inside this geometry is always linear (i.e. linearly polarized in every point). On-line, however, the three phases are energized simultaneously with a symmetric three-phase voltage:

$$\begin{pmatrix} U_1 \\ U_2 \\ U_3 \end{pmatrix} = U_0 \cos \begin{pmatrix} \varphi + \frac{2}{3}\pi \\ \varphi \\ \varphi - \frac{2}{3}\pi \end{pmatrix} \quad (2.1)$$

where U_0 is the nominal voltage of the phase conductors and φ the phase angle (in radians). In a belted cable system the electric field becomes elliptical: at a certain position (x, y) the field is rotating with varying magnitude, i.e. sinusoidal in two perpendicular directions without necessarily coinciding zero crossings. The geometrical shape of the conductors in a three-phase belted cable is optimized for field control to conserve space. As shown in Fig. 2.1a there is only a small distance between two conductors and also between conductor and earth screen: almost everywhere the electric

field is determined by two conductors. Apparently, here the field is linear except for some small (but maybe critical) regions where three conductors determine the field. A cable joint, in contrast, is a much more open structure (Fig. 2.1b). There, one can expect that over a large region the field is indeed elliptical. This situation is of particular interest, since cable joints are regarded as the most vulnerable components in a cable connection.

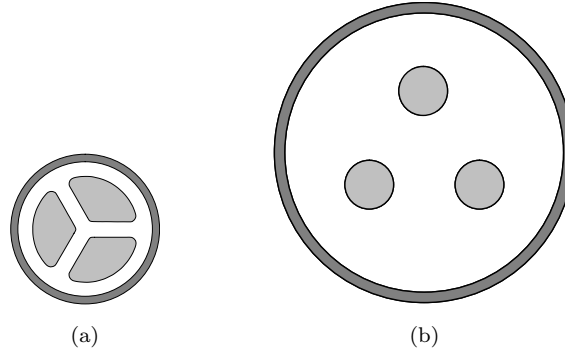


Figure 2.1 Simplified cross-section of a three-phase belted cable (a) and cable joint (b). The lighter gray areas represent the three phase conductors, the white areas the insulation material and the darker gray areas the covering shield.

The elliptic electrical field at a certain position (x, y) can be described by four parameters: the maximum $E_{\max}(x, y)$ and minimum $E_{\min}(x, y)$ field strength, the phase angle of the applied voltage $\varphi_{\max}(x, y)$ at maximum field $E_{\max}(x, y)$, and field direction $\xi_{\max}(x, y)$ at this maximum field.

$$E_a(\varphi; x, y) = E_{\max}(x, y) \cdot \cos[\varphi - \varphi_{\max}(x, y)] \quad (2.2a)$$

$$E_b(\varphi; x, y) = \pm E_{\min}(x, y) \cdot \sin[\varphi - \varphi_{\max}(x, y)] \quad (2.2b)$$

The symbols E_a and E_b describe the field strength along the main axes of the elliptic field, which are rotated over ξ_{\max} with respect to the original (x, y) coordinates, see Fig. 2.2. The \pm sign in Eq. (2.2b) indicates the direction of the rotating field. For the

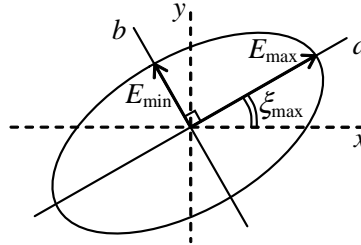


Figure 2.2 Definition main axes a and b of elliptic field at position (x, y)

instantaneous total field strength $E_0(\varphi; x, y)$ and direction $\xi(\varphi; x, y)$ we can write:

$$E_0(\varphi; x, y) = E_{\max} \sqrt{1 + \left[\left(\frac{E_{\min}}{E_{\max}} \right)^2 - 1 \right] \sin^2(\varphi - \varphi_{\max})} \quad (2.3a)$$

$$\xi(\varphi; x, y) = \xi_{\max} \pm \arctan \left(\frac{E_{\min}}{E_{\max}} \tan(\varphi - \varphi_{\max}) \right) \quad (2.3b)$$

All parameters depend on the position inside the dielectrics. For notational convenience this position dependence will be left out for now. The discharge direction is given by the angle $\xi(\varphi; x, y)$, i.e. we assume that a PD follows the external field direction for now. However, if, e.g. in case of a void there is already a (space) charge distribution from previous PDs, the discharge direction must be constructed from both the internal field, due to the charge already present, and the applied external field. The external electric field distribution for a specific geometrical arrangement of the three-phase system can be obtained at any location (x, y) within the dielectrics as a function of the phase angle by means of commercially available numerical techniques, e.g. based on the Boundary Element Method (BEM).

2.2.2 Discharge model

Various mechanisms result in partial-discharge activity in cables and cable accessories: PDs in various kinds of voids, due to water ingress etc. These mechanisms have in common that the PD duration itself is very short, in the nanosecond range (a Dirac pulse for the present purpose). The pulse shape measured at a cable termination is therefore fully determined by the pulse propagation characteristics, not by the original pulse shape. For studying the PD excitation and propagation, it is therefore sufficient to concentrate on one type of defect: a void. As the physical discharge details are of minor importance for the present modelling, we adapt a simplified model to relate the magnitude of a void discharge to the external electric field from the three phase voltages. During a PD it is assumed that this external electric field in the void is neutralized. This means that a charge distribution is formed which counteracts the external field present at the time of discharge. For computational convenience, it is assumed that the void has a cylindrical shape in the direction of the cable. If the radius of the void is small, the external field is locally homogeneous and the charge distribution required for compensating this field can readily be calculated by solving the Laplace equation in cylindrical coordinates:

$$\frac{1}{r} \frac{\partial}{\partial r} r \frac{\partial}{\partial r} U(r, \vartheta) + \frac{1}{r^2} \frac{\partial^2}{\partial \vartheta^2} U(r, \vartheta) = 0 \quad (2.4a)$$

$$\Rightarrow U(r, \vartheta) = -r E_0 \left[1 - \left(\frac{r_v}{r} \right)^2 \right] \cos(\vartheta - \vartheta_0) \quad (2.4b)$$

The angle ϑ_0 corresponds to the direction of the external electric field E_0 during the discharge. The parameter r_v is the radius of the void. The charge distribution follows from the boundary condition for the normal D -field component at $r = r_v$:

$$(D_{n,\text{in}} - D_{n,\text{out}})_{r=r_v} = \sigma_q \quad \Rightarrow \quad \sigma_q(\vartheta) = 2\varepsilon_0\varepsilon_r E_0 \cos(\vartheta - \vartheta_0) \quad (2.5)$$

A spherical void could, of course, also have served as a model. However, the cylinder is preferred because it prevents the need for three-dimensional field calculation software (decreasing accuracy for the same calculation time) to calculate the

induced charge in the conductors later on. Three-dimensional modelling in [Wou03b] has confirmed the findings in this chapter.

2.3 Induced charge in three-phase belted cables

2.3.1 Induced-charge model

Consider a two-electrode system. The induced currents in the conductors upon a moving charge in the dielectrics can be found from energy considerations. The amount of work done by the electrical field to move the charge $\int Q \underline{E}_0 dx$ must be equal to the amount of energy supplied by the source $\int iV dt$. This yields for the current i and the apparent charge Q_{app} :

$$Q_{\text{app}} = \int i dt = Q \frac{\Delta V}{V} \quad (2.6)$$

The apparent charge is determined by the ratio of the voltage over the crossed gap (ΔV) and the total voltage over the electrodes (V). This ratio is independent of the phase angle.

In a multi-electrode system like a three-phase belted cable the situation is more complex. The ‘Ramo-Shockley’ description [Wet89, Ram38, Sho38] can be adopted which relates induced currents in the electrode to a moving charge in between. In the simulations the sudden charge separation in the void caused by a PD is modelled by the introduction of a dipole \underline{p} in the direction of the electric field. The corresponding induced charges are determined from BEM calculations. The magnitude of \underline{p} is taken such that the corresponding field equals the 2-dimensional dipole field from the charge distribution given by Eq. (2.5).

$$\underline{p} = \iiint \underline{r} \sigma_q(\vartheta) \delta(r - r_v) r d\vartheta dr dz = 2\pi \varepsilon_0 \varepsilon_r r_v^2 \underline{E}_0 \ell \quad (2.7)$$

The length of the void is given by ℓ . Further, the value of Q is chosen in accordance with the amount of positive charge on one half of the cylindrical void, which we can refer to as the real charge Q_{real} :

$$\underline{p} = Q_{\text{real}} \underline{d} \quad (2.8)$$

with

$$Q_{\text{real}}/\ell = 4\varepsilon_0 \varepsilon_r r_v E_0 \quad \text{and} \quad d = \frac{1}{2} \pi r_v \quad (2.9)$$

The vector \underline{d} can be regarded as the distance between the ‘center of positive charge’ on one half of the cylinder and the ‘center of negative charge’ on the other half. In a two-electrode configuration the discharge is directed along the field lines between the electrodes. The charge displacement therefore induces an apparent charge of opposite sign in both electrodes. In a three-phase (four-electrode) system a charge displacement will not occur in all conductors to the same extent. This means that if detection is performed at only the earth screen, a PD may remain undetected, depending on the position of the discharge site within the dielectrics and its direction. In principle, one can always find a PD direction for which no charge is induced in the earth screen. The likelihood of such a PD may be negligible in case the field strength in that specific direction is relatively low. For instance, this is the case in a region between a conductor and the cable screen where the field is virtually linear (Fig. 2.3). In regions with nearly circular fields the discharge direction is not prescribed. The

induced charge, however, depends on the actual phase angle. As a consequence, even in case of total absence of a preferred phase angle for the PD, the apparent charge magnitude detected in e.g. the cable screen can still show a phase-angle dependence.

2.3.2 Induced-charge simulations

The eccentricity of the electric field as a function of position within the dielectrics has a strong effect on the induced charge. In Fig. 2.3, for some simplified cable joint configuration, the amount of eccentricity of the elliptical electric field is indicated. As an illustration the fields are numerically determined from BEM simulation along two curves: a circle between the phases and earth screen (I), and a vertical line from the screen to the opposite phase (II). In the insert again the definition of the a - and b -axis, the main axes with respect to E_{\max} and E_{\min} , is indicated. The angle between the a -axis and the normal of the curve (I or II) is denoted by ξ_{\max} , the field direction at phase angle φ_{\max} .

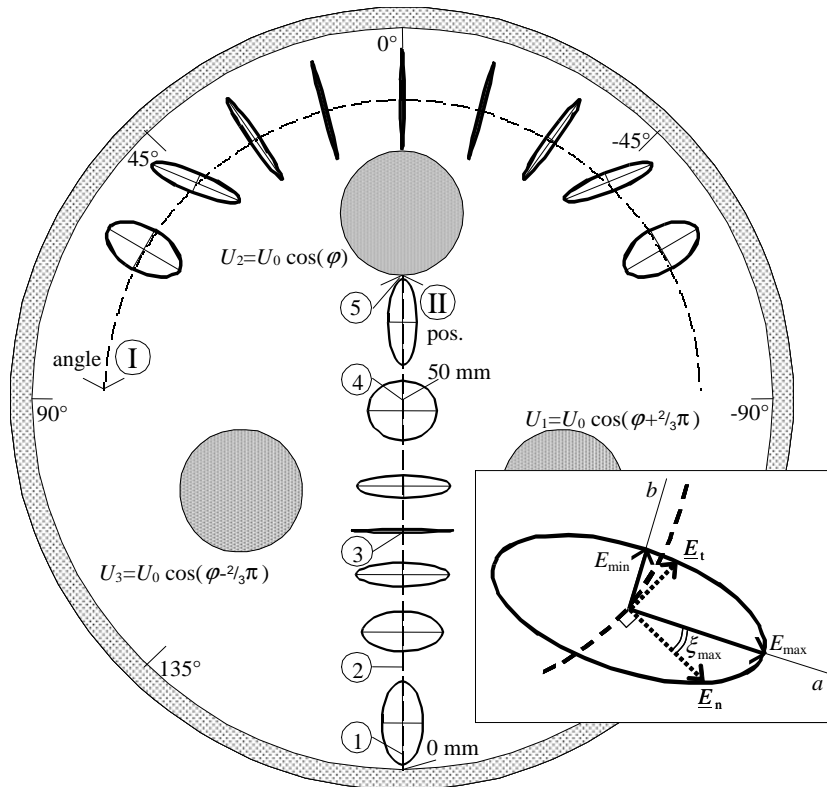
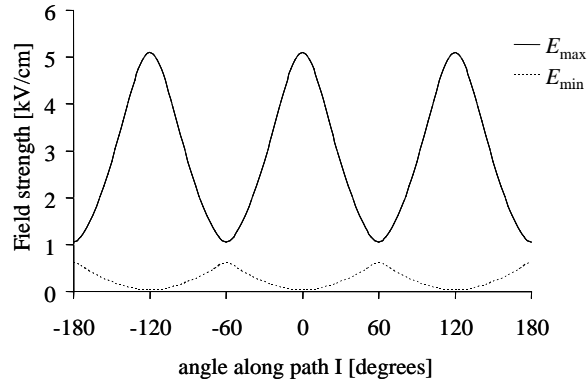
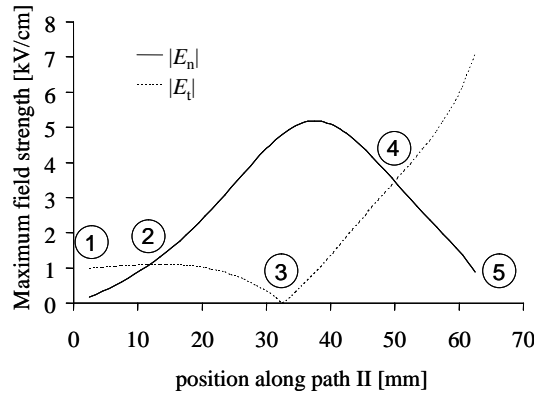


Figure 2.3 A hypothetical three-phase cable joint with normalized (on circumference) elliptical fields. The screen radius is 50 mm, the conductor radii are 10 mm. The conductors are situated symmetrically halfway between center and earth screen. The relative permittivity ϵ_r of the dielectric is 4. The roman numbers I and II indicate the paths (circular or linear) along which electric fields and induced charges are determined. The positions 1..5 serve as reference for later discussion. The insert denotes the several involved symbols, defined in relation to the dashed curve, which is either path I or II.

The calculated field strengths are given in Fig. 2.4a along curve I and in Fig. 2.4b along curve II. The elliptical field distribution in the hypothetical joint configuration of Fig. 2.3 has 120° rotation symmetry. Along the circular path I the field periodically varies from linear ($E_{\min} = 0$, near phase conductors) to elliptical (between two phase conductors). Along line II the field is close to linear at positions 1, 5 (vertical), and 3 (horizontal). In between, the field becomes circular at positions 2 and 4. Apparently, the cable joint contains large regions with strongly eccentric fields.



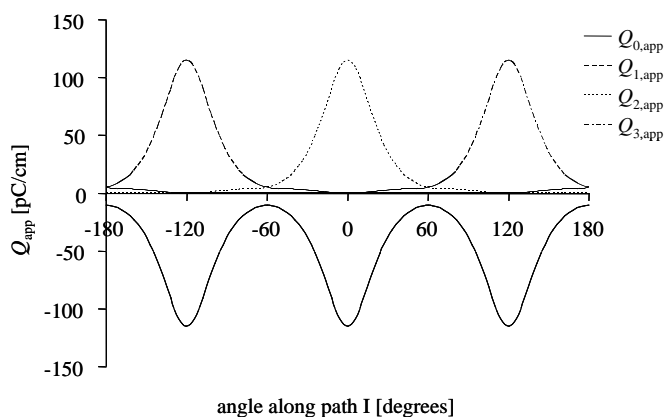
(a)



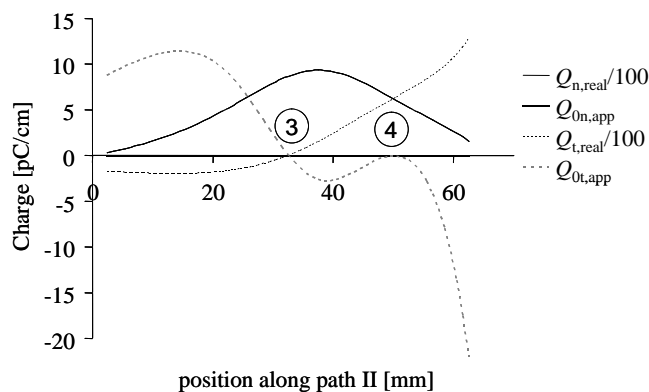
(b)

Figure 2.4 Field strengths along the main axes along path I (a) and II (b) for an applied coupled voltage on the phase conductors of 10 kV. Note that the direction of the main axes in (b) changes such that E_{\max} is either perpendicular (n) or tangential (t) to line (II); therefore the corresponding fields are denoted E_n and E_t respectively. The numbers 1..5 correspond to the positions indicated in Fig. 2.3.

The apparent charges induced in the four conductors are simulated by introducing a dipole according to Eq. (2.7). The dipole is directed parallel to the external field such that the field is cancelled (thereby assuming the void to be initially uncharged). The results for the induced charges along both the curves are plotted in Fig. 2.5.



(a)



(b)

Figure 2.5 (a) Induced charge (in pC per unit length of the void) in earth screen ($Q_{0,app}$) and in phases 1 to 3 ($Q_{1/2/3,app}$) from a dipole ($d = 2$ mm corresponding to a void of radius $r_v = 1.3$ mm, Eq. (2.9)), representing a PD in the direction of maximum field as a function of the position along circular path I (Fig. 2.3); (b) Real and induced charges in earth screen from a PD in horizontal direction (n : perpendicular to path II), and vertical direction (t : tangential to path II) as a function of position along II

Maximum charge is induced in the earth screen when the PD occurs between one phase and the screen (e.g. at angle = 0 in Fig. 2.5a). Obviously, the field is large there and directed favorably (for detection). Opposite charges are induced in the conductors, mainly in the conductor closest to the PD site. The results for real and apparent charge in the earth screen along curve II are given in Fig. 2.5b, both for a PD directed normal and tangential to II. Although the normal field may be larger than the tangential field, PDs in normal direction will remain undetected when signals are measured at the earth screen only, because no charge is induced there ($Q_{0n,app} = 0$). The tangential field is larger close to the screen and close to the conductor at the

opposite side, which is a favorable condition for PD detection at the earth screen. However, at position 3 this field component vanishes and both real and apparent charge for a (hypothetical) PD in that direction would be zero. The induced charge for a PD in the cable center (4) is zero as well, due to the cable (or joint) symmetry.

In Fig. 2.6 the ‘calibration factor’ (defined here as ratio between apparent charge and real charge magnitude) is plotted for the positions in the dielectrics indicated in Fig. 2.3 as a function of the phase angle. In case of a linear field (almost the case in pos. 1 and 5) this factor switches between plus and minus an extreme value according to the applied field. In contrast, for elliptical or circular fields the calibration factor gradually changes with phase angle (pos. 2).

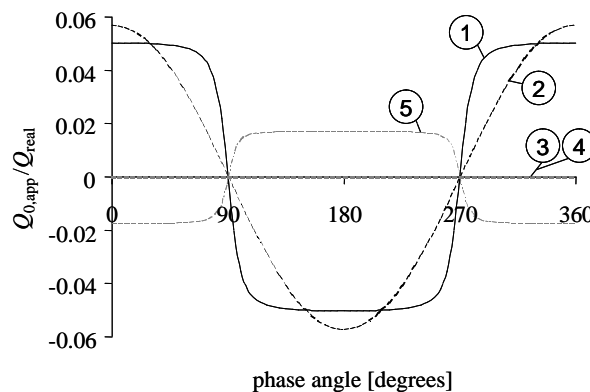


Figure 2.6 Calibration factors between apparent and real charge at various locations on path II (indicated in Fig. 2.3 with 1..5) as a function of phase angle

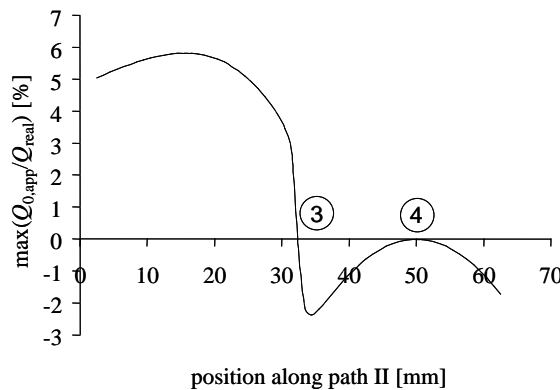


Figure 2.7 Maximum calibration factor (with respect to the phase angle) for induced charge in earth screen along path II

In Fig. 2.7 the maximum calibration factor (occurring at a particular phase angle) is plotted as a function of the position along curve II. ‘Blind spots’, i.e. regions from which no charge is induced in the earth screen, arise at a narrow region around position 3 (horizontally aligned linear field) and around the cable center at position 4 (due to

cable symmetry).

From the simulations it is concluded that the calibration factor between apparent and real charge is dependent on the direction of the discharge and thereby dependent on the direction of the applied field because of their correlation. Therefore, even in case of a circular field, thus without any preference for either a certain discharge direction or phase angle (as discussed in the next section), induced charges may still reveal a phase-angle distribution due to difference in induced charges for different discharging directions. As mentioned earlier, the above simulations assume the PDs to be fully determined by the external field. If some memory effect prevails, then the discharge direction is determined by the superposition of the internal field from charge being already present from previous PDs and the externally applied field.

2.4 Partial-discharge phase-patterns in three-phase belted cables

2.4.1 Phase patterns in a rotating field

In the simple system of the void mentioned in Section 2.2 we assumed that the partial discharge follows the external field, i.e. that the void was initially uncharged. To investigate phase patterns, the *total* electric field must be considered. The total electric field is the external field from the energized phase conductors plus the internal field, remaining from the previous PD in the void. It is assumed that a PD occurs whenever the total electric field inside a void reaches the inception value E_{inc} , upon which the total field inside the void is neutralized. After that, the electric field inside the void rises again until the next discharge takes place. It is further assumed that the time delay between reaching E_{inc} and the occurrence of a PD is negligible. For a linear field this results in the well-known PD concentrations between the positive zero crossing and the maximum, and between the negative zero crossing and the minimum of the applied field [Kre89, Kre93b, Gro98, Tan95].

It can be expected that the distribution will evolve when the eccentricity, defined as $\eta = E_{min}/E_{max}$, increases from 0 (linear field) to 1 (circular field). The principle is illustrated in Fig. 2.8. The elliptic shapes in this figure represent the external electric fields for three locations with different eccentricities. The distance between two points on an ellipsis is the total instant electric field inside a void (external+internal), which will be neutralized upon a PD. The transition of the phase-patterns between linear and circular field can be understood by just considering an initial PD distribution between minimum and maximum field (i.e. the top-right quarters in Fig. 2.8a, b, and c, i.e. between $270^\circ - 0^\circ$). A previous PD between maximum and minimum field (top-left quarter, i.e. between $180^\circ - 270^\circ$) would only result in a successive PD in the quarter being considered.

Assume for now that the PD inception field E_{inc} is close to E_{max} and consider an almost linear field. The position of the following PDs can be constructed by determining the phase angle at which the total field has changed with an amount of E_{inc} since the previous PD (indicated with arrows). From Fig. 2.8a it is seen that in the case of an almost linear field the resulting distribution is projected one half cycle further on the ellipse.

If the ratio η is increased (Fig. 2.8b) the phase angle of successive PDs converges to some point on the opposite half cycle. This corresponds to the occurrence of a

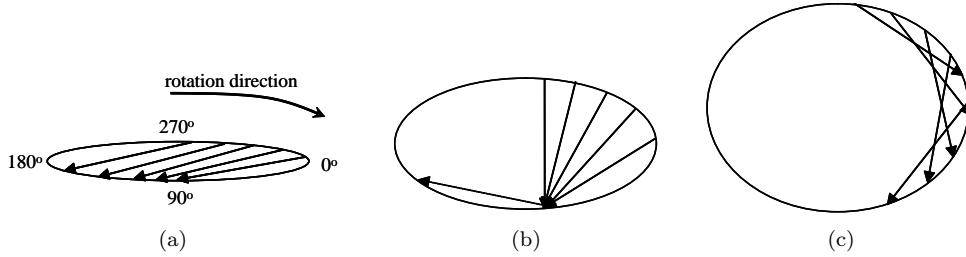


Figure 2.8 PD distributions in transition from almost linear (a), via elliptic (b), to circular field (c). The elliptic shapes represent the external electric fields for three locations with different eccentricities. The rotation direction of these fields is indicated. The distance between two points on an ellipsis is the total electric field inside a void (external+internal field). This total instant field is neutralized upon reaching the inception voltage E_{inc} , indicated by arrows. The indicated phase angles correspond to Eq. (2.2) in case $\varphi_{max} = 0$.

narrow peak in the PD distribution. Since the circumference of the ellipse increases with larger E_{min} (and $E_{inc} \cong E_{max}$), the next PD may occur in the same half cycle, resulting in a double peak structure at each half cycle.

If η is increased even further (Fig. 2.8c) this effect suddenly vanishes and the expected distribution becomes random. This result is obvious in case of a circular field for which the field amplitude is phase-angle independent.

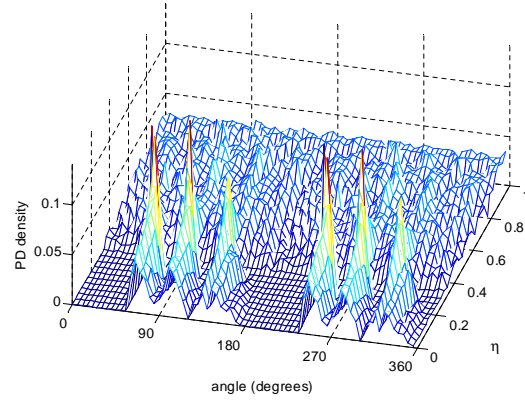
2.4.2 Simulation of partial discharges in a rotating field

To verify the expected transitions of the PD distributions with increasing eccentricity η , simulations have been carried out for three values of the inception field:

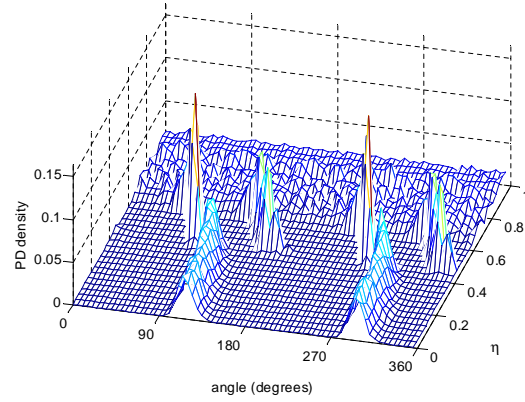
$$E_{inc} = \frac{1}{2}E_{max}, \quad E_{inc} = E_{max}, \quad \text{and} \quad E_{inc} = 1\frac{1}{2}E_{max}.$$

The situation discussed in Section 2.4.1 ($E_{inc} \approx E_{max}$) is shown in Fig. 2.9b. We can clearly distinguish the three stages: at values of E_{min} below $\frac{1}{2}E_{inc}$ the distribution resembles the linear case. The PD convergence is most pronounced at about $E_{min} \approx \frac{1}{2}E_{inc}$, where four narrow peaks arise. For even higher η the distribution becomes random. When the inception field is smaller (Fig. 2.9a), the initial distribution contains various peaks, since PDs can occur already several times in a half cycle. The second stage also starts at about $\frac{1}{2}E_{inc}$ and beyond that point the distribution becomes random too. At large inception field (e.g. $1\frac{1}{2}E_{max}$, Fig. 2.9c) similar stages can be distinguished, except that no extra peaks arise. The inception field is too large for PDs to occur twice in one half cycle.

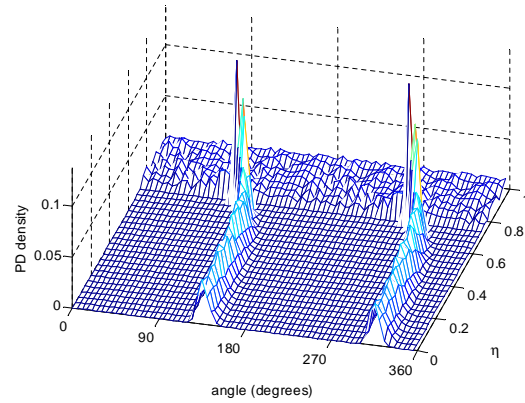
We conclude that the eccentricity of the rotating field, and thus the location of the defect, has a pronounced effect on the PD distribution. The phase-angle dependence measured off-line at a linear field may even be absent for a three-phase field. This may seem to be a disadvantage of on-line measurements in the case of three-phase cables or joints. On the other hand this eccentricity-dependent PD pattern also supplies additional information of the PD location in relation to the cross-section of e.g. a joint, which in turn may give valuable information on the possible type of defect.



(a)



(b)



(c)

Figure 2.9 Simulation of PD distributions from a linear to a circular field for $E_{\text{inc}} = \frac{1}{2}E_{\text{max}}$ (a), $E_{\text{inc}} = E_{\text{max}}$ (b) and $E_{\text{inc}} = 1\frac{1}{2}E_{\text{max}}$ (c). Horizontally the phase angle and eccentricity η are plotted. The PD density along the vertical axis is normalized on the number of simulated cycles and is given per degree of phase angle. Zero phase angle corresponds to maximum field strength.

2.5 Conclusions

The analysis of the induced charges in a rotating field is basically two-dimensional. A three-dimensional approach –along the same lines, e.g. for a spherical void– is in principle not more complicated and gives similar results [Wou03b]. Real voids, however, may vary widely in shape, and may be oriented in any direction. For instance a cylindrical void, partly bridging the dielectrics between conductor and screen, can give rise to higher PD levels as compared to a void perpendicular to the main direction of the field. Placed in a region with a strong elliptical field the measured PD distribution will be a combined effect of the preferential discharge direction, due to the shape of the void, and the effects analyzed in this chapter. Clearly, the orientation of a defect also plays a role in off-line measurements. Depending on the energized phase in relation to the orientation, these defects are sometimes not detected. In regions with a nearly circular field in case of on-line test, the rotating field will be periodically in line with the void direction resulting in relatively large PDs.

Concerning three-phase cables or joints, measurement of signals only at the earth screen will result in position-dependent sensitivity for PDs. Certain regions within the dielectrics form actual blind spots for this measuring principle. To illustrate this, Fig. 2.10 shows the calibration factor, or ‘sensitivity’, for the hypothetical cable joint of Fig. 2.3, assuming PDs to occur in the direction of the maximum field. This figure

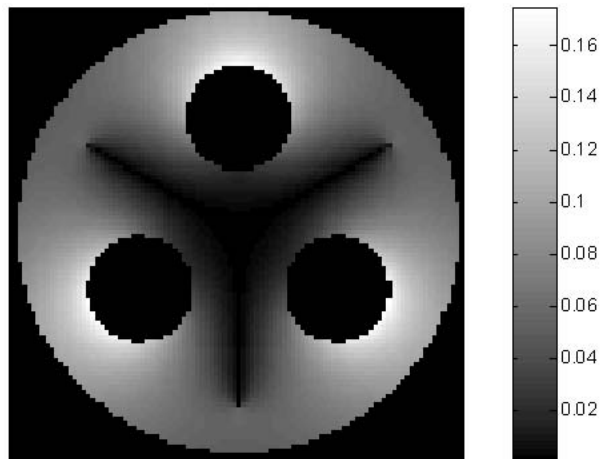


Figure 2.10 Calibration factor between apparent and real charge in the direction of the maximum field in the dielectric of a hypothetical joint

clearly shows that maximum sensitivity is reached in the regions between the phase conductors and the screen. Blind spots appear in the central region stretching out between the phase conductors. As mentioned, in this simulation it is presumed that PDs occur in the direction of the maximum field. Section 2.4, however, showed that this does not necessarily have to be the case. If we would make a similar picture of the sensitivity for PDs (also) occurring at the phase angle where maximum charge is induced in the earth screen, only the center of the dielectric together with three spots in the middle between two phases remain as blind spots.

Real cable joints often have a more complicated structure resulting in displaced

positions of the blind spot(s). However, real defects often extend over a larger region, so it can be expected that some charge will still be induced in the earth screen. Also, larger defects result in larger PD signals, roughly scaling with the void volume.

The amplitude of PDs from the inner region will be relatively small. On the other hand the voltage of interest there is the coupled voltage which is $\sqrt{3}$ higher than the voltage applied during off-line tests with one phase energized (unless above-nominal voltages are applied). Defects may only reveal PD activity at these voltages, and would remain undetected during off-line tests at nominal voltage.

Simulations show that on-line detected PD distributions in a three-phase belted cable system are expected to differ from off-line results due to two reasons:

1. In regions with near circular electric fields the real PD distributions deviate strongly from the distribution obtained for linear fields during off-line tests.
2. Due to the multi-electrode configuration of three-phase cables and joints, the induced charges upon a PD in the conductors and earth screen become a function of the phase angle in case of non-linear electric fields.

Furthermore, the propagation characteristics of a multi-conductor transmission line may rearrange the PD signals to be measured at the various phase conductors and the earth screen at the cable termination, due to the different propagation characteristics of the two distinctive modes. This will be further examined in the next chapter.

It can be expected that in case of three-phase cables or joints the PD distributions obtained during on-line diagnostics do not necessarily have a simple correlation to off-line results. On the other hand, on-line tests will still provide PD distributions, which can contain information about possible locations of the PDs within a cross section of the cable or joint and therefore point towards specific defect types.

Partial-discharge signal propagation

Partial discharges originate from defects in the insulation material of power cables or joints. The discharges induce small pulses on the surrounding conductors, which propagate to both cable ends. Since we are only able to measure at the cable ends in substations or ring main units, the measured PD pulses can be altered or re-arranged by the propagation characteristics of the propagation channel(s) in the power cable. In this chapter, propagation models are discussed for both single-phase and three-phase cables. Simulations and measurements are done to verify the models. Furthermore, the models are extended to be able to describe propagation through a complete cable connection, consisting of a set of cable sections, connected by joints. The resulting model allows us to simulate a PD signal from any location within a cable system.

3.1 Introduction

A PD induces a high-frequency pulse in the cable, starting at the location of the discharge. Since we aim for a measuring system that will detect pulses only at the cable termination(s), the pulse will first have to propagate through the cable. Due to the channels' propagation characteristics, the pulse shape and amplitude will be altered. The PD pulse duration at the defect location where the PD is ignited is small (< 1 ns), so the pulse shape detected at the cable ends (normally many meters away from the defect) will be fully determined by the propagation channel characteristics. In order to be able to extract PD signals from measured data, good knowledge about the propagation channel and its characteristics is vital. Obviously, also decisions with respect to detection bandwidth (sensors, digitizing equipment, etc.) depend upon good understanding of the signal propagation characteristics. Furthermore, good knowledge of the propagation path is needed to determine the optimal sensor locations (as will be further investigated in Chapter 4).

As mentioned in Section 1.1.2, with respect to their high-frequency propagation properties, we can divide all relevant power cable types into two main categories:

- single-phase cables together with multi-phase cables that have separate metal earth screens around each cable core, both denoted further on as 'single-phase' cables, and

- cables with three cable cores, sometimes with a combined insulation in addition (belted cables), and one common metal earth screen, denoted as ‘three-phase’, ‘common screened’, or ‘belted’ cables.

Since the latter group has our main interest, it will be examined in more detail.

In Section 3.2 a propagation model for single-phase cables is described. This model is extended to a multi-conductor description in Section 3.3. The parameters will be deduced in Section 3.4 and complemented with simulations and measurements. In Section 3.5 the model is extended to a complete cable system, i.e. a cascade coupling of cable sections and accessories. Section 3.6 relates the detected amount of charge at a cable end to the original induced charge. In the last section (3.7) the main conclusions from this chapter will be summarized.

3.2 Signal propagation in single-phase cables

This section discusses the basics of single-phase (coaxial) transmission lines, focussing on aspects relevant for power cables. As the cross-section can be regarded as being uniform along its length and the distances between conductors are much smaller than the considered wavelengths, the main propagation mode is TEM (transversal electromagnetic). Since the theory of transmission lines is well known, only the main aspects will be given in this section, serving as a basis for the next sections. Firstly, the propagation model will be given, after which the main cable parameters of this model will be discussed.

3.2.1 Propagation model

The coaxial structure of a single-phase power cable can be described by a normal two-conductor transmission line model. Fig. 3.1 shows the model of an element dz of a transmission line. In this model the transmission line is characterized by the

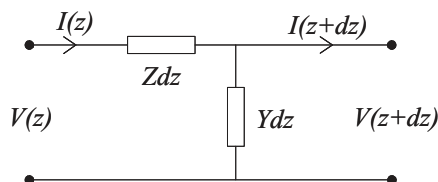


Figure 3.1 Model of element dz of a two-conductor transmission line

per-unit-length impedance (Z) and admittance (Y). The output and input voltages and currents in frequency domain of this element dz are related via:

$$\frac{\partial}{\partial z} \begin{pmatrix} V(z, \omega) \\ I(z, \omega) \end{pmatrix} = - \begin{pmatrix} 0 & Z(\omega) \\ Y(\omega) & 0 \end{pmatrix} \begin{pmatrix} V(z, \omega) \\ I(z, \omega) \end{pmatrix} \quad (3.1)$$

By decoupling the differential equations, the plane wave solutions in terms of forward and backward travelling waves are obtained:

$$V(z, \omega) = V^+ e^{-\gamma(\omega)z} + V^- e^{+\gamma(\omega)z} \quad (3.2a)$$

$$I(z, \omega) = I^+ e^{-\gamma(\omega)z} - I^- e^{+\gamma(\omega)z} \quad (3.2b)$$

where the $^+$ denotes the forward (in positive z -direction) and $^-$ the backward travelling wave. The cable-specific propagation constant $\gamma(\omega)$ is given by:

$$\gamma(\omega) = \sqrt{Z(\omega)Y(\omega)} \quad (3.3)$$

This propagation constant consists of a real and an imaginary part:

$$\gamma(\omega) = \alpha(\omega) + j\beta(\omega) \quad (3.4)$$

The real part $\alpha(\omega)$ describes the attenuation, the imaginary part $\beta(\omega)$ the delay and dispersion of the signals. The ratio of the voltage and current of (forward or backward) travelling waves is defined as the characteristic or wave impedance of the cable, and is given by:

$$Z_c(\omega) = \sqrt{\frac{Z(\omega)}{Y(\omega)}} \quad (3.5)$$

Instead of describing the transmission line by its per-unit-length impedance $Z(\omega)$ and admittance $Y(\omega)$, the system is also fully determined by the propagation constant $\gamma(\omega)$ and the characteristic impedance $Z_c(\omega)$.

3.2.2 Cable parameters

Impedance

Single-phase power cables have a coaxial structure: the phase conductor, surrounded by a concentric neutral (shield), with a dielectric in between. The resistance, caused by imperfect conductance of both the phase conductor and the shield, will slightly increase with temperature, due to the decreasing material's specific conductance. An important effect at high frequencies is the influence of skin-depth, caused by the internal inductance of the conductors. The skin-depth decreases with increasing frequency according to:

$$\delta(\omega) = \sqrt{\frac{2}{\omega\mu\sigma}} \quad (3.6)$$

where σ is the specific conductance and μ the permeability of the material (which, for the materials discussed in this thesis, is the same as the permeability of vacuum, μ_0). Due to the magnetic flux between the conductors, the leaving and returning currents are also drawn towards each other, known as the proximity effect. The current through the conductors is concentrated within a region determined by the skin-depth, so the effective per-unit-length resistance of both phase conductor and metal screen will increase with increasing frequency due to decreasing skin-depth and can be approximated by:

$$R_{1\text{ph}}(\omega) \approx \frac{1}{2\pi r_c \delta_c \sigma_c} + \frac{1}{2\pi r_s \delta_s \sigma_s} \quad (3.7)$$

where r_c and r_s are the phase conductor radius and metal screen inner radius, σ_c and σ_s the specific conductivities, and δ_c and δ_s the skin-depths in the conductor and metal screen.

The inductance of a single-phase cable consists of both the inductance caused by the internal flux of the conductors and inductance of the circuit enclosed between the

two conductors. The internal inductance per-unit-length is approximated by [Kad59]:

$$L_{1\text{ph},i}(\omega) \approx \frac{\mu_0 \delta_c}{4\pi r_c} + \frac{\mu_0 \delta_s}{4\pi r_s} \quad (3.8)$$

The external inductance, can be directly derived by considering the enclosed magnetic flux Φ in surface s , between the central conductor and shield, caused by the current through the central conductor I (using Ampere's law for the transverse magnetic field):

$$\Phi = \oint_s \underline{B}_t \cdot \underline{ds} = \Delta z \frac{\mu_0 I}{2\pi} \ln \frac{r_s}{r_c} \quad (3.9)$$

where \underline{B}_t is the transverse magnetic flux density. In synthetic insulated cables, semi-conducting layers are usually present between the insulation material and the two conductors (phase conductor and metal screen). But since these layers have hardly any effect on the magnetic field, the influence on the inductance can be neglected. This yields for the external per-unit-length inductance:

$$L_{1\text{ph},e} = \frac{\Phi}{I} = \frac{\mu_0}{2\pi} \ln \frac{r_s}{r_c} \quad (3.10)$$

The total impedance for single-phase cables equals:

$$Z_{1\text{ph}}(\omega) = R_{1\text{ph}}(\omega) + j\omega(L_{1\text{ph},i}(\omega) + L_{1\text{ph},e}) \quad (3.11)$$

Admittance

The characteristic capacitance of a coaxial structure can be determined by applying Gauss' law to a closed surface s surrounding the central conductor. This relates the transverse electric field \underline{E}_t to the charge Q causing it:

$$\varepsilon \oint_s \underline{E}_t \cdot \underline{ds} = Q \quad \Rightarrow \quad E_t = \frac{Q/\Delta z}{2\pi r \varepsilon} \quad , \quad r_c \leq r \leq r_s \quad (3.12)$$

where ε is the total dielectric permittivity of the insulation material between the conductors and r is the distance from the center of the conductors in radial direction. The ratio of the charge and the voltage V across the dielectric is the capacitance per-length-unit:

$$C_{1\text{ph}} = \frac{Q/\Delta z}{V} = \frac{Q/\Delta z}{\int_{r_c}^{r_s} \underline{E}_t \cdot \underline{dr}} = \frac{2\pi\varepsilon}{\ln \frac{r_s}{r_c}} \quad (3.13)$$

For power cables without semi-conducting layers, the real part of the admittance through the dielectric –in this thesis entirely denoted as conductance– consists of two contributions: the specific conductance of the insulation and the dielectric losses. The insulation material's specific conductance σ_i , ideally zero, is in reality very small, but non-zero. This part of the conductance is (similar to the capacitance) found by:

$$G_{1\text{ph},c} = \frac{\sigma_i \oint_s \underline{E}_t \cdot \underline{ds}}{\int_{r_c}^{r_s} \underline{E}_t \cdot \underline{dr}} = \frac{2\pi\sigma_i}{\ln \frac{r_s}{r_c}} \quad (3.14)$$

Usually this part of the conductance is small compared to the dielectric losses due to the polarization mechanisms. Alternating electric fields within the cable insulation result in polarization of dipoles in the dielectrics (see [Zae03]). As the dipoles align with the electric field, energy is dissipated as heat. This effect can be implemented in the model by introducing an imaginary part in the dielectric constant (hereby introducing the frequency dependence of the permittivity):

$$\varepsilon(\omega) = \varepsilon_0[\varepsilon_r'(\omega) - j\varepsilon_r''(\omega)] \quad (3.15)$$

where ε_0 is the permittivity of vacuum, $\varepsilon_r'(\omega)$ the relative permittivity of the material, and $\varepsilon_r''(\omega)$ the imaginary part of the relative dielectric constant. With the complex ε_r , Eq. (3.13) becomes:

$$C_{1\text{ph}}(\omega) = \text{Re}(C_{1\text{ph}}) = \frac{2\pi\varepsilon_0\varepsilon_r'(\omega)}{\ln(r_s/r_c)} \quad (3.16)$$

and the part of the conductance caused by the dielectric polarization loss is:

$$G_{1\text{ph,d}}(\omega) = \text{Re}(j\omega C_{1\text{ph}}) = \omega \frac{2\pi\varepsilon_0\varepsilon_r''(\omega)}{\ln(r_s/r_c)} \quad (3.17)$$

For calculation of the influence of semi-conducting layers (present in synthetic insulation cables), the total admittance can be modelled by assigning for each layer its own capacitance and conductance, and placing them in series. This results in equations which can be found in e.g. [Wie00]. Material properties of semi-conducting layers and their influences on high-frequency propagation are further discussed in e.g. [Sto82, Wee84, Mug04]. In this thesis, the main interest is focussed on paper-insulated cables without semi-conducting layers. Therefore, the influence of semi-conductor layers on the capacitance is approximated by adding and subtracting their thicknesses to r_c and from r_s in Eq. (3.16) respectively, since they are assumed to act as metallic surfaces for the considered frequencies. For the conductance, the presence of semi-conducting layers results in a third contribution, which is approximated by [Wou91]:

$$G_{1\text{ph,sc}}(\omega) \approx \omega^2 \frac{4\pi\varepsilon_0^2\varepsilon_r'(\omega)^2}{\sigma_{\text{sc}} \ln^2(r_s/r_c)} \frac{d_{\text{sc}}}{r_s} \quad (3.18)$$

where σ_{sc} is the specific conductance of the semi-conducting layers, which is made large compared to the dielectric's specific conductance, and d_{sc} is the thickness of the semi-conducting layers.

The total admittance of a single-phase cable becomes:

$$Y_{1\text{ph}}(\omega) = G_{1\text{ph,c}} + G_{1\text{ph,d}}(\omega) + G_{1\text{ph,sc}}(\omega) + j\omega C_{1\text{ph}}(\omega) \quad (3.19)$$

The ratio of the real and the imaginary part of the admittance defines the dielectric loss factor $\tan \delta$. In the absence of semi-conducting layers it follows:

$$\tan \delta \triangleq \frac{\text{Re}(Y)}{\text{Im}(Y)} = \frac{\varepsilon_r''(\omega)}{\varepsilon_r'(\omega)} + \frac{\sigma_i}{\omega\varepsilon_0\varepsilon_r'(\omega)} \quad (3.20)$$

The dielectric loss factor is often used to express the dielectric losses in a power cable. The second term in Eq. (3.20) can usually be neglected at high frequencies.

With the expressions for $Z_{1\text{ph}}$ and $Y_{1\text{ph}}$, the propagation channel of single-phase cables is determined according to Eqs. (3.3) and (3.5). Single-phase distribution-class cables usually have synthetic insulation material (XLPE or EPR). This means that dimensions and material properties are relatively accurately known and constant, due to the fabrication process. For cables with paper insulation, this is usually not the case. This will be further examined in Section 3.4, where parameters for three-phase cables (with paper insulation) are discussed.

3.3 Propagation model of three-phase belted cables

For a three-phase cable with a common earth screen, the propagating currents will be distributed over the four conductors. The simple transmission-line model of the former section must be extended to a multi-conductor description. Although the description of a multi-conductor transmission line (MCTL) is well known, e.g. [Pau94, Mer98, Mul99], in this section the main aspects of the theory are summarized, and are specifically applied to power cables. Power cables have a number of symmetry properties that enables us to develop a concise description.

3.3.1 Multi-conductor model

The propagation of signals in a three-phase cable can be described by a four-conductor transmission-line model. The line voltages and the currents in frequency domain are given by the vectors:

$$\underline{V}(z, \omega) = \begin{pmatrix} V_1 \\ V_2 \\ V_3 \end{pmatrix} (z, \omega) \quad (3.21a)$$

$$\underline{I}(z, \omega) = \begin{pmatrix} I_1 \\ I_2 \\ I_3 \end{pmatrix} (z, \omega) \quad (3.21b)$$

where $V_{1/2/3}$ and $I_{1/2/3}$ are the line voltages and line currents. The voltages are related to the ground conductor (shield) and the shield current equals the sum of the phase currents. The per-unit-length impedance and admittance of the four-conductor transmission line are 3×3 matrices $\mathbf{Z}(\omega)$ and $\mathbf{Y}(\omega)$ which relate all three voltages to all three currents, and are given by:

$$\mathbf{Z}(\omega) = \mathbf{R}(\omega) + j\omega\mathbf{L}(\omega) \quad (3.22a)$$

$$\mathbf{Y}(\omega) = \mathbf{G}(\omega) + j\omega\mathbf{C}(\omega) \quad (3.22b)$$

where $\mathbf{R}(\omega)$, $\mathbf{L}(\omega)$, $\mathbf{G}(\omega)$, and $\mathbf{C}(\omega)$ are 3×3 matrices, describing respectively the per-unit-length resistance, inductance, conductance, and capacitance. The set of telegrapher's equations for this system is:

$$\frac{\partial}{\partial z} \begin{pmatrix} \underline{V}(z, \omega) \\ \underline{I}(z, \omega) \end{pmatrix} = - \begin{pmatrix} \mathbf{0} & \mathbf{Z}(\omega) \\ \mathbf{Y}(\omega) & \mathbf{0} \end{pmatrix} \begin{pmatrix} \underline{V}(z, \omega) \\ \underline{I}(z, \omega) \end{pmatrix} \quad (3.23)$$

where $\mathbf{0}$ is a 3×3 null-matrix. Eq. (3.23) is a set of 2 times 3, coupled, first-order, partial differential equations, in principle describing the complete system. The system can be simplified by uncoupling the equations, using symmetry properties existing in the cross-section of power cables.

3.3.2 Propagation channels in power cables

In general the system of Eq. (3.23) can be decoupled by introducing 3×3 transformation matrices that diagonalize both $\mathbf{Z}(\omega)$ and $\mathbf{Y}(\omega)$ simultaneously, see e.g. [Pau94]. Three different propagation channels remain, each of which can be dealt with as a separate two-conductor transmission line. In the case of three-phase belted power cables we can make use of the symmetries of the cross section of this structure. Power cables have both rotation symmetry, meaning that the geometry is invariant under the cyclic permutation of the phases, and reflection symmetry, implying that the structure does not change if we exchange two phases. This results in impedance and admittance matrices that are both circulant and symmetric:

$$\mathbf{Z}(\omega) = \begin{pmatrix} Z_1 & Z_2 & Z_2 \\ Z_2 & Z_1 & Z_2 \\ Z_2 & Z_2 & Z_1 \end{pmatrix} (\omega) \quad (3.24a)$$

$$\mathbf{Y}(\omega) = \begin{pmatrix} Y_1 & Y_2 & Y_2 \\ Y_2 & Y_1 & Y_2 \\ Y_2 & Y_2 & Y_1 \end{pmatrix} (\omega) \quad (3.24b)$$

Circulant matrices can be diagonalized by the Fourier matrix \mathbf{F} , [Bar90, Dav79], in this case:

$$\mathbf{F} = \frac{1}{\sqrt{3}} \begin{pmatrix} 1 & 1 & 1 \\ 1 & e^{-j2\pi/3} & e^{-j4\pi/3} \\ 1 & e^{-j4\pi/3} & e^{-j2\pi/3} \end{pmatrix} \quad (3.25)$$

and the matrices after diagonalization become:

$$\tilde{\mathbf{Z}}(\omega) = \mathbf{F}\mathbf{Z}(\omega)\mathbf{F}^* = \begin{pmatrix} Z_1 + 2Z_2 & 0 & 0 \\ 0 & Z_1 - Z_2 & 0 \\ 0 & 0 & Z_1 - Z_2 \end{pmatrix} \quad (3.26a)$$

$$\tilde{\mathbf{Y}}(\omega) = \mathbf{F}\mathbf{Y}(\omega)\mathbf{F}^* = \begin{pmatrix} Y_1 + 2Y_2 & 0 & 0 \\ 0 & Y_1 - Y_2 & 0 \\ 0 & 0 & Y_1 - Y_2 \end{pmatrix} \quad (3.26b)$$

where $\tilde{\mathbf{Z}}(\omega)$ and $\tilde{\mathbf{Y}}(\omega)$ are the diagonalized matrices, containing the eigenvalues of respectively $\mathbf{Z}(\omega)$ and $\mathbf{Y}(\omega)$. \mathbf{F}^* is the conjugate of \mathbf{F} and for a unitary matrix as the Fourier matrix this is equal to the inverse \mathbf{F}^{-1} . The columns of \mathbf{F}^* contain the eigenvectors of $\mathbf{Z}(\omega)$ and $\mathbf{Y}(\omega)$. With the present symmetry only two distinct eigenvalues remain and therefore only two distinct propagation channels exist.

With this diagonalization a change of variables is introduced:

$$\tilde{\mathbf{V}}(z, \omega) = \mathbf{F}\mathbf{V}(z, \omega) \quad (3.27a)$$

$$\tilde{\mathbf{I}}(z, j\omega) = \mathbf{F}\mathbf{I}(z, \omega) \quad (3.27b)$$

Substitution in Eq. (3.23) results in partial decoupling of the system:

$$\frac{\partial}{\partial z} \begin{pmatrix} \tilde{\mathbf{V}}(z, \omega) \\ \tilde{\mathbf{I}}(z, \omega) \end{pmatrix} = - \begin{pmatrix} \mathbf{0} & \tilde{\mathbf{Z}}(\omega) \\ \tilde{\mathbf{Y}}(\omega) & \mathbf{0} \end{pmatrix} \begin{pmatrix} \tilde{\mathbf{V}}(z, \omega) \\ \tilde{\mathbf{I}}(z, \omega) \end{pmatrix} \quad (3.28)$$

This system can be solved analogously to 3 uncoupled two-conductor transmission lines; the uncoupled second-order equations become:

$$\frac{\partial^2}{\partial z^2} \tilde{\mathbf{V}}(z, \omega) = \tilde{\boldsymbol{\gamma}}^2(\omega) \tilde{\mathbf{V}}(z, \omega) \quad (3.29a)$$

$$\frac{\partial^2}{\partial z^2} \tilde{\mathbf{I}}(z, \omega) = \tilde{\boldsymbol{\gamma}}^2(\omega) \tilde{\mathbf{I}}(z, \omega) \quad (3.29b)$$

where $\tilde{\boldsymbol{\gamma}}(\omega)$ is a diagonal matrix, defined by:

$$\tilde{\boldsymbol{\gamma}}^2(\omega) = \tilde{\mathbf{Z}}(\omega) \tilde{\mathbf{Y}}(\omega) = \mathbf{F} \mathbf{Z}(\omega) \mathbf{Y}(\omega) \mathbf{F}^* \quad (3.30)$$

containing the propagation constants of the different propagation channels in this four-conductor system. The (diagonal) characteristic impedance matrix $\tilde{\mathbf{Z}}_c(\omega)$ of the system is defined as:

$$\tilde{\mathbf{Z}}_c^2(\omega) = \tilde{\mathbf{Z}}(\omega) \cdot \tilde{\mathbf{Y}}(\omega)^{-1} \quad (3.31)$$

Since only two distinct propagation channels exist in this structure, we can describe the multi-conductor propagation in three-phase power cables with a set of two distinct propagation characteristics, found by the eigenvalues of $\mathbf{Z}(\omega)$ and $\mathbf{Y}(\omega)$ according to Eq. (3.26). The first value gives the Shield-to-Phases (SP) channel, the sum of the voltages or currents on the three phase-conductors with the shield as return path and is characterized by:

$$\gamma_{\text{SP}}(\omega) = \sqrt{(Y_1(\omega) + 2Y_2(\omega))(Z_1(\omega) + 2Z_2(\omega))} \quad (3.32a)$$

$$Z_{c,\text{SP}}(\omega) = \sqrt{\frac{Z_1(\omega) + 2Z_2(\omega)}{Y_1(\omega) + 2Y_2(\omega)}} \quad (3.32b)$$

The other, repeated, eigenvalues define the Phase-to-Phase (PP) characteristics:

$$\gamma_{\text{PP}}(\omega) = \sqrt{(Y_1(\omega) - Y_2(\omega))(Z_1(\omega) - Z_2(\omega))} \quad (3.33a)$$

$$Z_{c,\text{PP}}(\omega) = \sqrt{\frac{Z_1(\omega) - Z_2(\omega)}{Y_1(\omega) - Y_2(\omega)}} \quad (3.33b)$$

The forward travelling phase currents at location z are described (analogously to Eq. (3.2b)) by:

$$\underline{\mathbf{I}}^+(z, \omega) = \mathbf{F}^* \begin{pmatrix} e^{-\gamma_{\text{SP}}(\omega)z} & 0 & 0 \\ 0 & e^{-\gamma_{\text{PP}}(\omega)z} & 0 \\ 0 & 0 & e^{-\gamma_{\text{PP}}(\omega)z} \end{pmatrix} \mathbf{F} \underline{\mathbf{I}}^+(0, \omega) \quad (3.34)$$

with

$$\underline{\mathbf{I}}^+(z, \omega) = \begin{pmatrix} I_1^+ \\ I_2^+ \\ I_3^+ \end{pmatrix} (z, \omega) \quad (3.35)$$

Calculating Eq. (3.34) results in:

$$\underline{\mathbf{I}}^+(z, \omega) = \frac{1}{3} \left[e^{-\gamma_{\text{SP}}(\omega)z} \begin{pmatrix} 1 & 1 & 1 \\ 1 & 1 & 1 \\ 1 & 1 & 1 \end{pmatrix} + e^{-\gamma_{\text{PP}}(\omega)z} \begin{pmatrix} 2 & -1 & -1 \\ -1 & 2 & -1 \\ -1 & -1 & 2 \end{pmatrix} \right] \underline{\mathbf{I}}^+(0, \omega) \quad (3.36)$$

If, for instance, the current in the shield of a three-phase power cable at location z is measured, the considered propagation channel is pure SP, and the forward travelling wave current, initiated at location $z = 0$, is described with:

$$\sum_{i=1}^3 I_i^+(z, \omega) = e^{-\gamma_{\text{SP}}(\omega)z} \sum_{i=1}^3 I_i^+(0, \omega) \quad (3.37)$$

Similarly, the difference in current between two phases is purely described by the PP channels (which explains the term PP). The forward travelling currents at position z are:

$$\begin{pmatrix} I_1^+ - I_2^+ \\ I_2^+ - I_3^+ \\ I_3^+ - I_1^+ \end{pmatrix} (z, \omega) = e^{-\gamma_{\text{PP}}(\omega)z} \begin{pmatrix} I_1^+ - I_2^+ \\ I_2^+ - I_3^+ \\ I_3^+ - I_1^+ \end{pmatrix} (0, \omega) \quad (3.38)$$

Observe that the third channel is determined if the other two channels are known. Eqs. (3.34) - (3.38) are also valid for the forward travelling voltages by replacing I_i^+ and \underline{I}^+ with V_i^+ and \underline{V}^+ .

A real cable may deviate to some extent from the perfect symmetries assumed in this section. The asymmetry will result in cross-talk between the SP and PP propagation channels. This cross-talk is studied by injecting a current pulse in the SP channel at one end of a 200 m paper-insulated lead-covered (PILC) cable. Both the SP and PP currents at the other side of the cable were measured. As shown in Fig. 3.2 the SP signal dominates and the PP signals are indeed very small. The observed weak cross-talk may not only be caused by the cable asymmetries, but also by coupling at the injection point. Measurements with injection in the PP channel showed similar results.

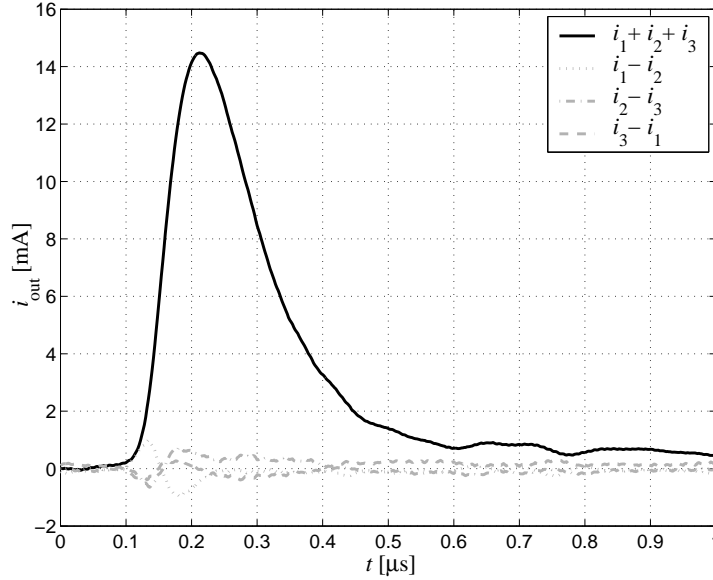


Figure 3.2 Channel responses of a 200 m long (12.5/12.5 kV, $3 \times 95 \text{ mm}^2$ Cu) PILC cable on a pulse injected in the SP channel

3.4 Multi-conductor cable parameters

3.4.1 Model-based approximations

From the two propagation channels, derived in the former section, only the SP channel is of interest if measurements are taken from the earth screen of the cable (see Chapter 4). This channel can be modelled by approximating the three segment-shaped phase-conductors as one solid conductor, which results in a coaxial-shaped cross-section, like single-phase cables. With this assumption, the single-phase description of Section 3.2.2 also applies to the SP channel of three-phase cables with a common earth screen.

For cables with synthetic insulation the dimensions and material properties are usually well known and rather constant. Three-phase belted cables, however, are often constructed with paper insulation. This has important implications on the variability of the parameters. Since belted PILC cables are the most important type of cables in the research project, the parameters of this cable type will be examined in more depth.

Dielectric constant

For XLPE, the permittivity is more or less constant up to 100 MHz [Sri86]; a typical value for ε'_r is 2.26 and $\tan \delta$ around 0.0004 (e.g. [Hap78]). The permittivity of paper insulation, which is applied in belted cables, can vary significantly with frequency. Moreover, it can also vary with paper type, impregnating mass, mechanical pressure, electrical field, aging, temperature, moisture ingress, and other properties that may vary from cable to cable [Cla62]. As a consequence, modelling a paper-insulated cable requires knowledge or, better, measurement of both $\varepsilon'_r(\omega)$ and $\varepsilon''_r(\omega)$. These parameters can be determined, by using the coaxial approximation for the cable model and leaving $\varepsilon'_r(\omega)$ and $\varepsilon''_r(\omega)$ as the single (real and imaginary part of the) unknown parameter. In Fig. 3.3 experimental results (from network analyzer measurements) are shown for two different PILC cables. Both the real and imaginary parts are indeed frequency dependent and differ significantly for both cables. From now on, the models in this thesis will contain dielectric permittivities obtained in this way.

Attenuation

Analogous to Eqs. (3.3) and (3.4), the propagation constant of the SP channel of a three-phase cable is given by:

$$\gamma_{\text{SP}}(\omega) = \sqrt{Z_{\text{SP}}(\omega)Y_{\text{SP}}(\omega)} = \alpha_{\text{SP}}(\omega) + j\beta_{\text{SP}}(\omega) \quad (3.39)$$

with $Z_{\text{SP}}(\omega) = R_{\text{SP}}(\omega) + j\omega L_{\text{SP}}(\omega)$ and $Y_{\text{SP}}(\omega) = G_{\text{SP}}(\omega) + j\omega C_{\text{SP}}(\omega)$, the per-unit-length circuit parameters of the SP channel. These parameters are determined by cable dimensions and material properties and can differ from cable to cable. In general, $\alpha(\omega)$ can be approximated for high frequencies, using $R \ll \omega L$ and $G \ll \omega C$, according to:

$$\alpha(\omega) \approx \frac{1}{2} \left[R(\omega) \sqrt{\frac{C(\omega)}{L(\omega)}} + G(\omega) \sqrt{\frac{L(\omega)}{C(\omega)}} \right] \quad (3.40)$$

The first term in this equation is the attenuation caused by the conductor losses and is mainly determined by the skin effect. When this effect is dominant, using

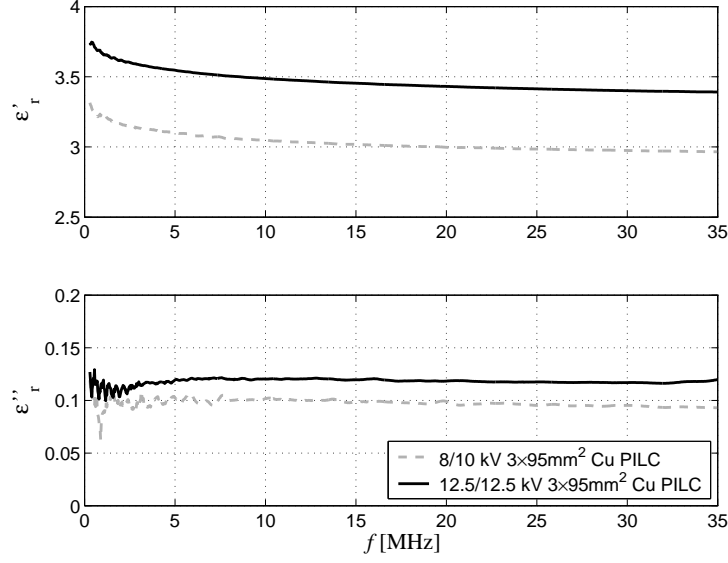


Figure 3.3 Measured dielectric constants for two different PILC cables

the equations in Section 3.2.2, it follows that $\alpha_{sk}(\omega) \propto \sqrt{\omega}$. The second term in Eq. (3.40) is due to the conductance, consisting mainly of dielectric losses (resulting in $\alpha_d(\omega) \propto \omega$) and the influence of semi-conductor layers (resulting in $\alpha_{sc}(\omega) \propto \omega^2$). When considering frequencies in the MHz range, PILC cables without semi-conductor layers usually have their attenuation mainly dominated by dielectric losses. Even though this is a crude approximation, we will examine it in some more detail.

For any geometry, the attenuation caused by dielectric losses is given by:

$$\alpha_d(\omega) \approx \frac{G(\omega)}{2} \sqrt{\frac{L(\omega)}{C(\omega)}} \quad (3.41)$$

The parameters $G(\omega)$, $L(\omega)$, and $C(\omega)$ are normally dependent on this geometry, see e.g. the equations in Section 3.2.2 for the coaxial shape. However, in [Pau94] it is proven that

$$L(\omega)C(\omega) \approx \mu\epsilon_0\epsilon'_r(\omega) \quad (3.42)$$

for *any* geometry. If the dielectric polarization loss is the main contributor to the conductance, the following approximation is derived in a similar way:

$$L(\omega)G(\omega) \approx \omega\mu\epsilon_0\epsilon''_r(\omega) \quad (3.43)$$

Combining Eqs. (3.41) - (3.43) gives:

$$\alpha_d(\omega) \approx \frac{\omega\epsilon''_r(\omega)}{2} \sqrt{\frac{\epsilon_0\mu}{\epsilon'_r(\omega)}} \quad (3.44)$$

This contribution to the attenuation is independent of the geometry of the propagation channel and depends only on material parameters. Since this is a rather crude approximation, Eq. (3.44) should not be used for accurate modelling. However, the

approximation shows us that, for three-phase power cables where the dielectric losses are dominant, both SP and PP channels are expected to have attenuation constants in the same order of magnitude. Fig. 3.4 shows measurements of the attenuation in the two different propagation channels of a typical distribution-class cable. The attenuation of both channels is indeed similar and the dependence on frequency is close to linear, which indicates the dominant effect of dielectric loss on the attenuation and a small amount of skin-effect influence in this particular cable.

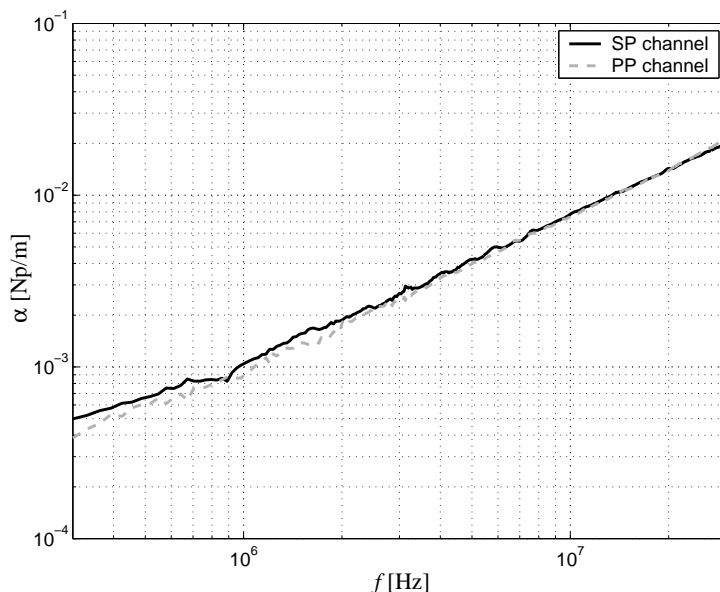


Figure 3.4 Measured attenuation of SP and PP channel of a distribution-class cable (8/10 kV, $3 \times 95 \text{ mm}^2$ Cu, PILC)

To compare the model (not including the approximations above) with measurements, Fig. 3.5 shows both simulation and experimental results of the attenuation for the SP channel of two different MV cables. Despite the difficulties in performing these measurements accurately and also the inaccuracy of the parameters in the model, the result is quite satisfactory.

Dispersion and phase velocity

Dispersion is the effect that different frequency components of a propagation signal have different velocities. The phase velocity for each frequency component is given by:

$$v_p(\omega) = \frac{\omega}{\beta(\omega)} \quad (3.45)$$

Usually lower-frequency components travel with a slower speed than components of higher frequency. The velocity of a pulse obviously depends on the phase velocities of the frequency components it contains. Since attenuation for higher frequencies is stronger, and therefore propagating pulses lose high-frequency components first, the velocity of travelling pulses decreases while the travelled path gets longer.

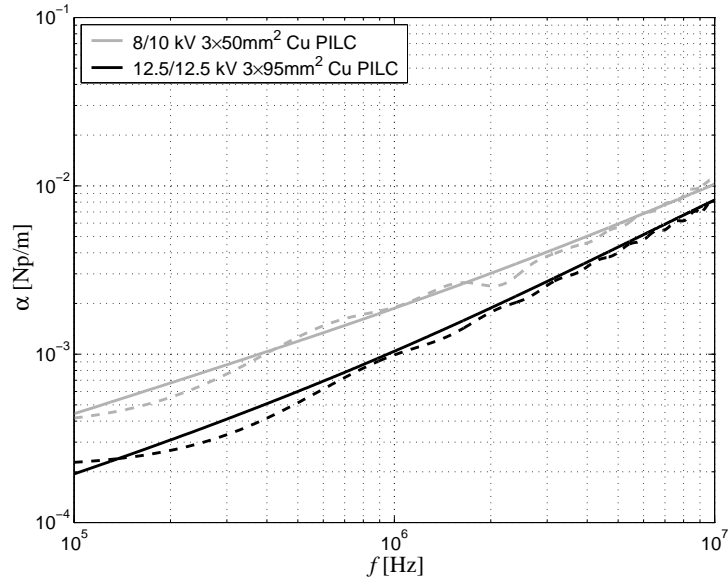


Figure 3.5 SP channel attenuation of two different PILC cables. Solid lines represent model simulations, dashed lines pulse response measurements

The dispersion is found from the imaginary part of the propagation constant. For high frequencies, $R \ll \omega L$ and $G \ll \omega C$ holds and the phase-shift in Eq. (3.4) can be approximated by:

$$\beta(\omega) \approx \omega \sqrt{L(\omega)C(\omega)} \quad (3.46)$$

which, together with Eq. (3.42) results again in an expression, independent of the channel's geometry:

$$\beta(\omega) \approx \omega \sqrt{\mu \varepsilon_0 \varepsilon'_r(\omega)} \quad (3.47)$$

This equation represents a straight line, i.e. no dispersion, if $\varepsilon'_r(\omega)$ would be independent of frequency. This is not the case for PILC cables (Fig. 3.3), so dispersion can not be neglected. Substituting Eq. (3.47) in (3.45) gives:

$$v_p(\omega) \approx \frac{c}{\sqrt{\varepsilon'_r(\omega)}} \quad (3.48)$$

where $c = 1/\sqrt{\mu_0 \varepsilon_0}$ is the velocity of light in vacuum. Again this quantity is only dependent on material constants (only $\varepsilon'_r(\omega)$ in this case) and independent of dimensions or propagation channel. Fig. 3.6 shows the measured velocities of both SP and PP channel of a PILC cable. Both channels have approximately the same phase velocities, since the dielectric properties for both channels are the same. However, for three-phase XLPE cables, there can be a slightly different situation. The dielectric in both channels is still the same, but most XPLE cable types have a screen, consisting of a set of helical wires around the insulation material. The wires are connected to one another by a metal strip around them, but due to the small skin depth and the proximity effect the currents will still follow the path of the individual wires. This causes a longer path-length for high-frequency currents in the SP channel of the cable. Therefore, even if the real phase velocity remains the same, the time for a pulse

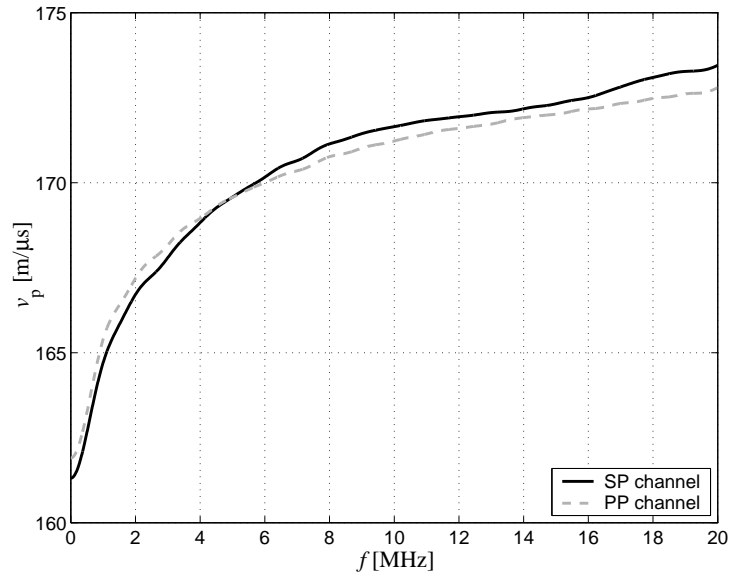


Figure 3.6 Measured velocities of both SP and PP channel of one MV (8/10 kV, $3 \times 95 \text{ mm}^2$ Cu) PILC cable

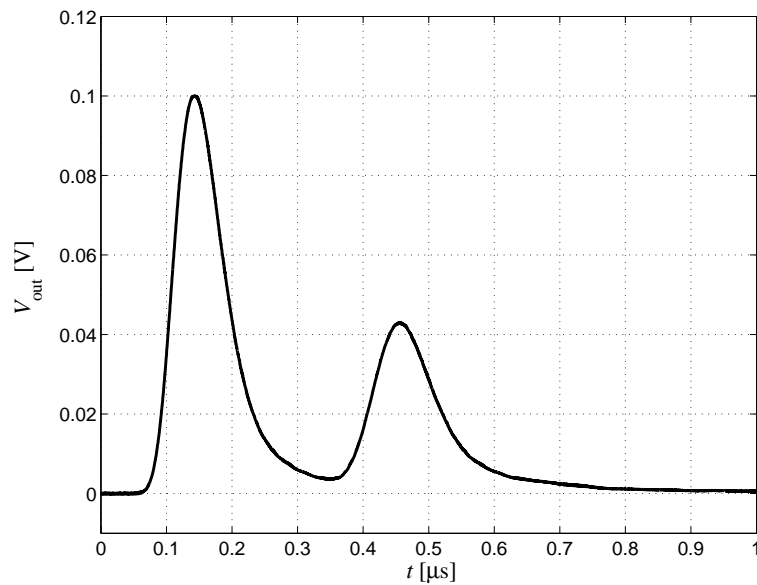


Figure 3.7 Far-end response of a 192 m long (8/10 kV, $3 \times 95 \text{ mm}^2$ AL) XLPE cable to a pulse injected in both propagation channels (between one phase conductor and earth screen)

to propagate a certain distance along the cable increases because of the lengthened channel path. Fig. 3.7 shows the result of a measurement, where one pulse is injected between one phase conductor and the screen (so exciting in both propagation paths) at one cable end and measured at the other end of the same conductor. Two pulses appear, since both channels are measured and have a different path length. Furthermore, the semiconducting layers and their frequency dependent material parameters may influence this effect further, see [Wee84, Mug04].

As different cables can have different dielectric constants, they can have significantly different phase velocities. Fig. 3.8 shows measured and calculated phase velocities for two MV PILC cables having phase velocities differing over 5%.

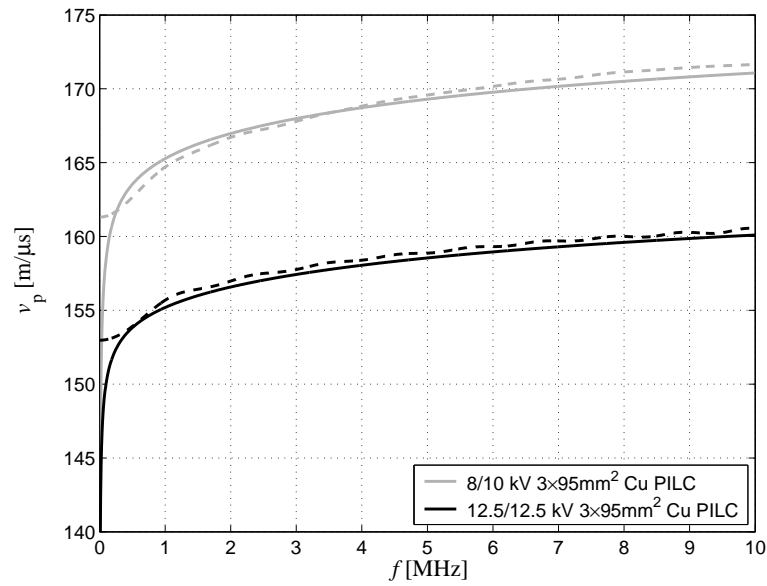


Figure 3.8 SP channel phase velocities of two different PILC cables. Solid lines represent model simulations, dashed lines pulse response measurements.

Characteristic impedance

The characteristic impedance (Eq. (3.5)) cannot be simplified into an expression without geometric dependence. This means that for the two propagation channels in a symmetric three-phase belted cable, two different characteristic impedances can be defined.

For the SP channel the coaxial approximation can be used, which, if again $R \ll \omega L$ and $G \ll \omega C$, can be approximated by:

$$Z_{c,SP}(\omega) \approx \frac{1}{2\pi} \sqrt{\frac{\mu_0 \mu_r}{\varepsilon_0 \varepsilon_r'(\omega)}} \ln \frac{r_s}{r_c} \quad (3.49)$$

Fig. 3.9 shows the experimental results of pulse response measurements on a distribution-class PILC cable. Although some variance exists, one can regard the characteristic impedances of power cables within the frequency range (30 kHz – 30 MHz) as constant.

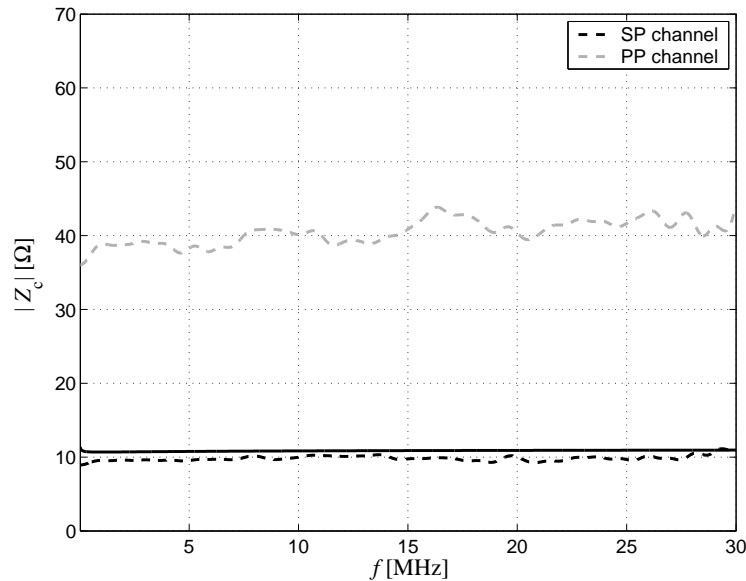


Figure 3.9 Characteristic impedances of SP and PP channel of (8/10 kV, $3 \times 95 \text{ mm}^2$ CU) PILC cable. The solid line represents model simulation of the SP channel, dashed lines represent pulse response measurements.

3.4.2 Propagation-measurement methods

To measure the characteristics of propagation channels across a wide frequency spectrum, a ‘network analyzer’ can be applied, [Pap03a]. The available network-analyzer (HP 8753C, with S-parameter test set HP 85047A) can be used to do a full analysis of an unknown two-port in a frequency range of 300 kHz – 6 GHz. However, for measuring power cables there is a major disadvantage (apart from being expensive and therefore often unavailable): it is vulnerable to static discharges (e.g. from the large cable capacitances, charged due to e.g. recovery voltages). Another method to determine propagation characteristics is measurement of the response to an injected wide-band pulse. In this way only fairly common equipment is necessary, while still a wide frequency spectrum can be analyzed with only one measurement. In this section both the network analyzer and pulse response method will be described and the results are compared.

For measurement of the propagation characteristics of a power cable’s PP channel, an extra complication is introduced, due to grounding of the equipment and balanced injection/measurement. In Appendix A a solution to this problem is given by deriving the PP channel properties from combination of measurements on the SP channel and signal injection between shield and one single phase conductor with the other phases floating.

Network analyzer propagation measurements

A network analyzer is used in combination with an S-parameter set to describe the propagation channels of a power cable as a general two-port. This combination uses scattering (S-)parameters to describe the device under test (DUT). A description

with S-parameters is an alternative representation of input and output impedances and transfer functions (in both directions) of the DUT and is regularly used in e.g. microwave network design. The S-parameter response from a lossy unmatched transmission line with length l , propagation constant γ , and characteristic impedance Z_c in a Z_0 measuring system are [Gup81]:

$$\mathbf{S} = \frac{1}{D_s} \begin{bmatrix} (Z_c^2 - Z_0^2) \sinh \gamma l & 2Z_c Z_0 \\ 2Z_c Z_0 & (Z_c^2 - Z_0^2) \sinh \gamma l \end{bmatrix} \quad (3.50)$$

with $D_s = 2Z_c Z_0 \cosh \gamma l + (Z_c^2 + Z_0^2) \sinh \gamma l$. The S , Z , and γ parameters are all frequency dependent. Extracting γ and Z_c from Eq. (3.50) [Eis92, Car00] gives:

$$\gamma = \frac{1}{l} \cosh^{-1} \left(\frac{1 - S_{11}^2 + S_{12}^2}{2S_{12}} \right) \quad (3.51a)$$

$$Z_c = Z_0 \sqrt{\frac{(1 + S_{11})^2 - S_{12}^2}{(1 - S_{11})^2 - S_{12}^2}} \quad (3.51b)$$

These two parameters describe the complete system in the case of translation symmetric DUTs, such as cables.

Pulse response measurements

The second method to measure a cable's characteristic impedance and propagation constant is by means of a wide-band pulse, injected in one cable end and comparing the different reflections. For this purpose a digitizer and a pulse generator are connected closely together at one side of a long measurement cable. The measurement cable length is chosen sufficiently long to separate direct and reflected pulses in time domain. At the other side, the measurement cable is connected to the propagation channel of the power cable (which is the DUT). When a pulse is injected, three pulses will be recorded: 1) the injected (reference) signal, 2) the reflection on the near end of the power cable, and 3) the reflection on the (open) far end of the power cable. The first reflection, i.e. the second pulse, characterizes the wave impedance of the cable. The third pulse is used to derive the propagation constant.

In order to eliminate the influence of the injection set-up, a calibration measurement must be done first. For this calibration, the measurement cable end is short-circuited at the point where the DUT is connected. In this way a voltage reflection coefficient of -1 at the connection cable end is artificially obtained, meanwhile leaving the rest of the total set-up unaffected. The ratio of the amplitude spectra of the reflection on the short-circuited end and the injected pulse gives the first transfer function $H_{\text{cal}}(\omega)$, comprising losses in the injection circuit and the reflection coefficient of -1 .

After this calibration, the short-circuit is removed and the DUT is measured under normal connection. The transfer function between injected signal and first reflection obtained in this way, $H_1(\omega)$, represents the same losses in the injection circuit, together with the reflection coefficient at the end of the measurement cable - power cable transition:

$$H_1(\omega) = -\rho(\omega)H_{\text{cal}}(\omega) \quad (3.52)$$

where the reflection coefficient $\rho(\omega)$ is defined as the ratio of the voltage of the reflected wave and the incident wave, depending on the characteristic impedance transition by:

$$\rho(\omega) = \frac{Z_c(\omega) - Z_0}{Z_c(\omega) + Z_0} \quad (3.53)$$

where $Z_c(\omega)$ is the characteristic impedance of the power cable and Z_0 the characteristic impedance of the injection cable (50 Ω , independent of frequency). Combining Eqs. (3.52) and (3.53), leaves the characteristic impedance of the power cable as the single unknown:

$$Z_c(\omega) = Z_0 \frac{H_{\text{cal}} - H_1}{H_{\text{cal}} + H_1} \quad (3.54)$$

By using transfer functions instead of frequency spectra of measured reflected signals in this equation, possible variations in injected pulse shape are cancelled out.

The transfer function from the injected pulse to the second reflection $H_2(\omega)$, is the combination of transfer in the injection circuit ($-H_{\text{cal}}(\omega)$), the transmission coefficient at the measurement - power cable junction ($1 + \rho(\omega)$), the propagation through twice the cable length with reflection on an open far end ($e^{-\gamma(\omega)2l}$), and the transmission coefficient from the power cable back to the measurement cable ($1 - \rho(\omega)$):

$$H_2(\omega) = -H_{\text{cal}}(\omega) \cdot (1 + \rho(\omega)) \cdot e^{-\gamma(\omega)2l} \cdot (1 - \rho(\omega)) \quad (3.55)$$

If the cable length l is known, the propagation constant $\gamma(\omega)$ is found by rewriting Eqs. (3.52) - (3.55):

$$\gamma(\omega) = \frac{1}{2l} \ln \left(\frac{H_1^2 - H_{\text{cal}}^2}{H_{\text{cal}} H_2} \right) \quad (3.56)$$

Obviously, it is important to use pulses with sufficient energy in the relevant frequency range in order to minimize the influence of noise. To improve the accuracy even further, multiple signals are recorded (approximately 1000 in our tests) and results are averaged.

Comparing measurements results

In order to compare the two measuring methods, Figs. 3.10 and 3.11 show measurements of the attenuation and the velocity of a 200 m PILC cable. In the frequency range 500 kHz - 10 MHz the two measuring methods show good agreement. Like in Figs. 3.4 and 3.5, the attenuation increases approximately proportional to frequency in this frequency range. This indicates again the dominance of the dielectric losses in the attenuation. For lower frequency the slope of the curve decreases, which is expected since the skin effect will dominate there ($\alpha_{\text{sk}}(\omega) \propto \sqrt{\omega}$). The measured velocity in Fig. 3.11 also shows similar results for the two measuring methods. At frequencies below 500 kHz the method with the network analyzer reaches its limitation due to lack of injected power. For frequencies above 10 MHz the pulse response method begins to show inaccuracies, due to the low signal-to-noise ratio (SNR) that was achieved there. The accuracy of the pulse response method can be improved by using pulses with more energy in the high frequencies.

It can be concluded that the pulse response measurement can be used for estimating the propagation characteristics in the frequency range of interest. This method has an additional advantage which makes it very attractive: the same principle can be used on-line, so without disconnecting the cable. This aspect will be further pursued in Chapter 4.

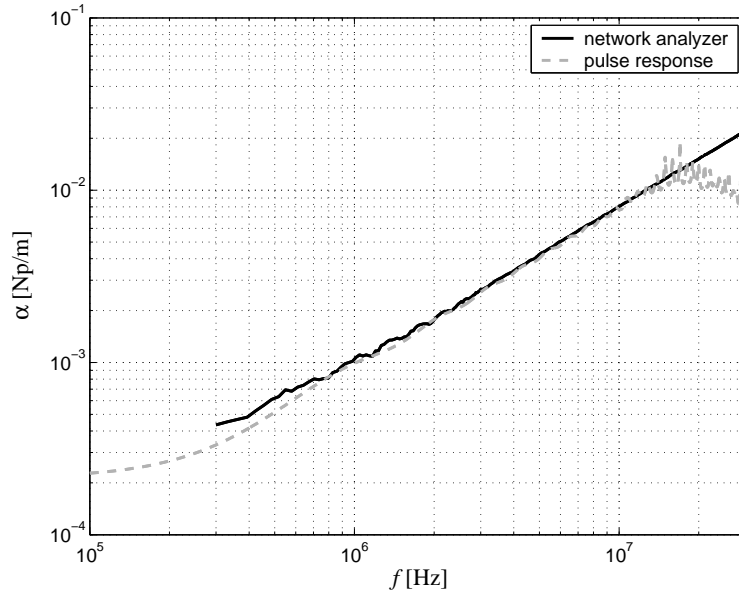


Figure 3.10 Measured attenuation of SP channel of a 200 m (12.5/12.5kV, $3 \times 95 \text{mm}^2$ CU) PILC cable with both pulse response and network analyzer methods

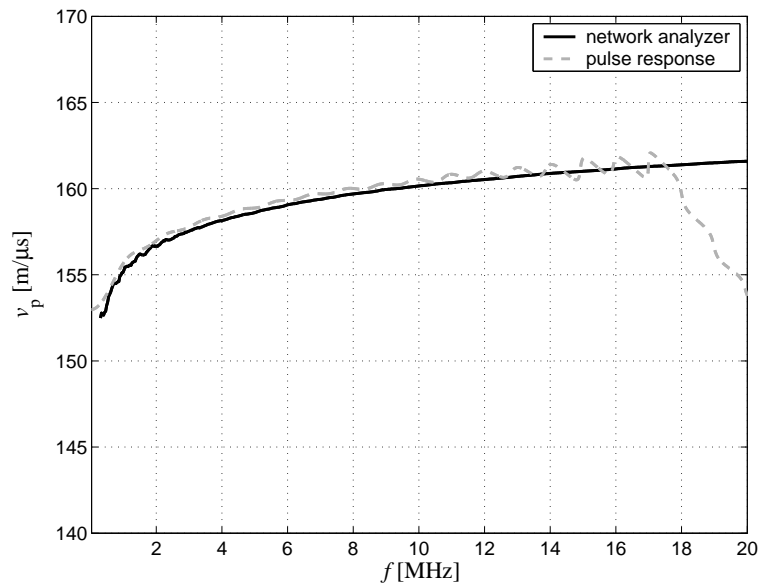


Figure 3.11 Measured phase velocity of a 200 m (12.5/12.5kV, $3 \times 95 \text{mm}^2$ CU) PILC cable with both pulse response and network analyzer methods

3.5 Cascade-coupled cables and accessories: cable systems

3.5.1 Model of cable systems

The models and measurements in the former paragraphs are applicable to connections consisting of one type of cable. In a distribution grid, however, connections usually consist of a sequence of cable sections, interconnected by joints. Each cable section can be modelled by the models presented in the former paragraph and each section can have different propagation characteristics. To obtain a model of the total cable system, a cascade coupling of the single-section models can be used. One propagation channel of one cable section can be characterized as a general two-port. One way of characterizing a general two-port is with a chain parameter Θ or [ABCD] matrix (e.g. [Gup81]):

$$\begin{pmatrix} V_{\text{in}}(\omega) \\ I_{\text{in}}(\omega) \end{pmatrix} = \Theta(\omega) \begin{pmatrix} V_{\text{out}}(\omega) \\ I_{\text{out}}(\omega) \end{pmatrix} \quad (3.57)$$

where the chain parameter matrix $\Theta(\omega)$ characterizes the parameters of the two-port. For transmission lines, the chain parameter matrix is [Wer91]:

$$\Theta(\omega) = \begin{pmatrix} \cosh(\gamma(\omega)l) & Z_c(\omega) \sinh(\gamma(\omega)l) \\ Z_c^{-1}(\omega) \sinh(\gamma(\omega)l) & \cosh(\gamma(\omega)l) \end{pmatrix} \quad (3.58)$$

The voltage and current transfer can be calculated from Eq. (3.57). The impedance of one side of the two-port depends on the load impedance $Z_1(\omega)$ at the other side. From Eqs. (3.57) and (3.58) the input impedance can be derived:

$$Z_{\text{in}}(\omega) = \frac{V_{\text{in}}}{I_{\text{in}}} = \frac{Z_1(\omega) \cosh(\gamma(\omega)l) + Z_c(\omega) \sinh(\gamma(\omega)l)}{Z_1(\omega) Z_c^{-1}(\omega) \sinh(\gamma(\omega)l) + \cosh(\gamma(\omega)l)} \quad (3.59)$$

Obviously, this equation also applies for the output impedance, since a cable is a symmetrical two-port.

Each cable section is characterized by one chain parameter matrix. A convenient property of describing two-ports in this way is that a set of N cascade-coupled two-ports is described by the total chain parameter matrix:

$$\Theta_{\text{T}}(\omega) = \Theta_1(\omega) \Theta_2(\omega) \dots \Theta_N(\omega) \quad (3.60)$$

where $\Theta_j(\omega)$ is the chain parameter matrix of the j^{th} cable section. Using $\Theta_{\text{T}}(\omega)$ in Eq. (3.57) gives the relation between the input and output voltages and currents of the total set of cascade-coupled segments. Similarly to Eq. (3.59), the total input impedance of this total system with load $Z_1(\omega)$ at the output is:

$$Z_{\text{in}}(\omega) = \frac{V_{\text{in}}}{I_{\text{in}}} = \frac{Z_1(\omega) \Theta_{\text{T}(1,1)}(\omega) + \Theta_{\text{T}(1,2)}(\omega)}{Z_1(\omega) \Theta_{\text{T}(2,1)}(\omega) + \Theta_{\text{T}(2,2)}(\omega)} \quad (3.61)$$

where $\Theta_{\text{T}(i,j)}(\omega)$ represents the i^{th} row and j^{th} column of matrix $\Theta_{\text{T}}(\omega)$. Using these equations, the complete cable system is described and the (multiple) reflections of pulses in the system are incorporated. If only the first arriving pulse is of interest, a much simpler expression can be used. For a travelling pulse each section j involves a certain attenuation, time delay, and dispersion, which are incorporated in the specific

$\gamma_j(\omega)l_j$ of that section. Each section change $j \rightarrow j + 1$ introduces a transmission coefficient, caused by the impedance change:

$$\tau_{v(j \rightarrow j+1)}(\omega) = \frac{2Z_{c,j+1}(\omega)}{Z_{c,j+1}(\omega) + Z_{c,j}(\omega)} \quad (3.62a)$$

$$\tau_{i(j \rightarrow j+1)}(\omega) = \frac{2Z_{c,j}(\omega)}{Z_{c,j+1}(\omega) + Z_{c,j}(\omega)} \quad (3.62b)$$

where τ_v is the voltage transmission coefficient and τ_i the current transmission coefficient. This results in the total transfer function of the system for the first arriving pulse in:

$$H_T(z, \omega) = \prod_{j=1}^N e^{-\gamma_j(\omega)l_j} \tau_{(j \rightarrow j+1)}(\omega) \quad (3.63)$$

where H_T is either $(V_{\text{out}}/V_{\text{in}})$ or $(I_{\text{out}}/I_{\text{in}})$ using respectively τ_v or τ_i for τ . The length of the propagation path z is obviously determining the value of N and l_1 . Note that the last transfer coefficient $\tau_{(N \rightarrow N+1)}(\omega)$ represents the transition from the last cable section to the load impedance Z_1 .

Besides different cable sections, the system also incorporates joints to interconnect the cable sections. Usually joints have metal shields that are connected to the cable shields. The cable's phase-conductors are interconnected inside the joint to the other cable and the area between the conductors and shield is filled with some insulation material (liquid or solid). One effect that may upset the propagation characteristics of a cable system is the asymmetry that may be present inside these joints, i.e. the symmetry that allows three-phase cables to be modelled by the two distinctive channels may not always be fully continued inside joints. Many joints, for example, exhibit an extra wire inside the metal shielding to ensure good connection between both cable's earth screens. Furthermore, the set of three phase conductors may be a little out of the center. Both effects introduce small asymmetries for signals propagating through a joint. As a consequence the transition matrices can be mixed and channels start to exhibit cross-talk. In that case one propagation channel in the system cannot be modelled separately anymore and the total propagation characteristics depend on both SP and PP characteristics. However, some symmetry measurements to joints give results similar to the symmetry measurements on cables, depicted in Fig. 3.2. Furthermore, joints usually have a length of about 1 m. For the considered frequency range (up to about 30 MHz) the corresponding wavelengths are much larger. Because of the limited size of joints and the minimal amount of asymmetry, the effect of the joint itself on signal characteristics is marginal.

3.5.2 Measurements on cable systems

In order to compare model simulations with practical measurements, pulse response measurements are discussed for a cable system, consisting of a 200 m (12.5/12.5 kV, 3×95 mm² CU) PILC cable connected via an oil-filled joint to a 100 m (8/10 kV, 3×95 mm² CU) PILC cable. Both cable far ends are short-circuited in order to get full reflection. A pulse is injected at cable end 1 (200 m 12.5 kV cable) and signals are recorded simultaneously on both cable ends. The dielectric constants of both cables are determined in advance and the cable dimensions are known. The joint is not implemented in the model, as its influence is assumed to be negligible. In the top

graph of Fig. 3.12 the measured signal at the injection site is shown. The first pulse is the injected pulse. After twice the cable length ($\approx 4 \mu\text{s}$) the far-end reflections are visible. The bottom graph shows the measured signal at the other cable system end on an aligned time base with respect to the top graph. Fig. 3.12 shows both measurement and model simulation results. As input signal for the model the injected time-domain pulse is recorded and the model from the former sections is applied to calculate the expected time-domain responses.

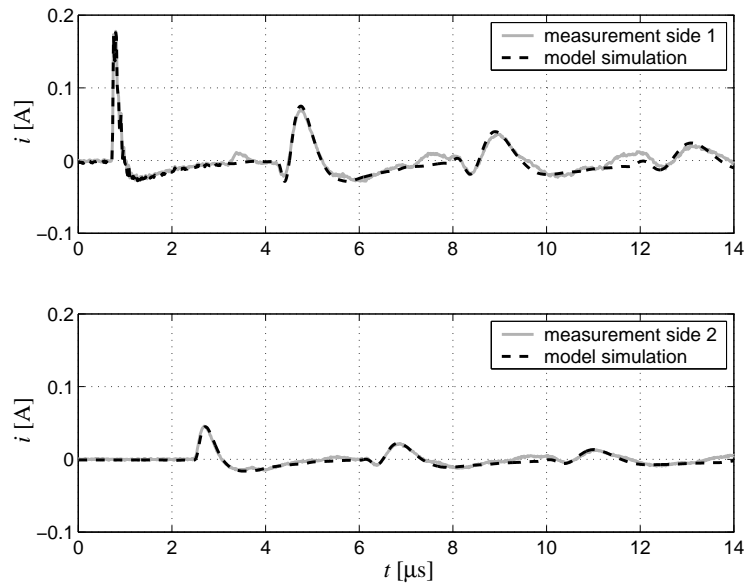


Figure 3.12 Measured and simulated pulse responses on both ends of a cable system, consisting of 200 m (12.5/12.5 kV, $3 \times 95 \text{ mm}^2$ CU) PILC (side 1) and 100 m (8/10 kV, $3 \times 95 \text{ mm}^2$ CU) PILC (side 2) cables, interconnected by a joint

The model simulations show good agreement with the measured signals. In the top graph of Fig. 3.12 small extra reflections are visible between the main reflections. These small pulses are reflections from the joint. These reflections are very small and a model for the joint itself can apparently be omitted. For longer cables, high frequencies will be attenuated more strongly, thereby decreasing the influence of joints even further.

3.6 Charge transport

The charge transport is discussed here for one cable section only, since this illustrates the effect of propagation itself on charge transport more clearly compared to using a complete cable system. This discussion can easily be extended for cascade coupled sections; the only difference is the transfer function from PD site to cable end. For a cable system, the functions of Section 3.5 should be applied instead of the transfer function for one cable section, resulting mainly in an extra multiplying factor for the changes in characteristic impedance along the propagation path.

3.6.1 Charge-transport estimation

The total charge arriving at the cable termination can be found from the time integral of the propagated current pulse. Taking the full frequency content into account, conservation of charge implies that the measured charge is only reduced by the DC component of the attenuation $\alpha(\omega)$ [Wie03a]:

$$Q(z) = Q(0) \cdot e^{-\alpha(0)z} \quad (3.64)$$

Here $Q(z)$ is the measured charge at position z and $Q(0)$ the initial induced charge at the PD site propagating to the detection end of the cable. Since a PD results in both a forward and a backward travelling pulse, $Q(0)$ only corresponds to a fraction (factor $\frac{1}{2}$ if the impedance to the left and right are equal) of the induced charge, since we consider only the forward travelling pulse. As the attenuation at DC is negligible, the total charge at the cable end directly corresponds to the induced charges at the PD site, irrespective of the measured propagation channel. However, measurement of the small charges at DC is clearly impossible for on-line situations due to the present power frequency. Obviously one has to aim for a frequency range with low interference level, and at the same time allowing for accurate PD location. A detection method with a limited bandwidth extending over the low MHz range is usually chosen. The charge obtained from integration over this detected PD current is only indirectly related to the induced charge at $z = 0$. Furthermore, it strongly depends on the detection method and bandwidth of the sensor. Consider a sensor with transfer function $f_{\text{det}}(\omega)$, having a bandwidth of $\pm\Delta\omega$ around the center detection frequency ω_c . Time integration is performed over a narrow range around the center of the detected pulse (say from $t_c - \Delta t$ to $t_c + \Delta t$):

$$\begin{aligned} Q(z) &= \int_{t_c - \Delta t}^{t_c + \Delta t} \mathcal{F}^{-1} \{ f_{\text{det}}(\omega) I(\omega, 0) e^{-\gamma(\omega)z} \} dt \\ &= \frac{2}{\pi} Q(0) \int_{\omega_c - \Delta\omega}^{\omega_c + \Delta\omega} e^{-\alpha(\omega)z} \cos(\beta(\omega)z - \omega t_c) \frac{\sin \omega \Delta t}{\omega} d\omega \end{aligned} \quad (3.65)$$

where $\mathcal{F}^{-1}\{\cdot\}$ denotes the inverse Fourier transform. The initial PD current $I(\omega, 0)$ at $z = 0$ in the frequency domain can be taken constant, because of the very short PD duration (Dirac pulse with content $Q(0)$). If dispersion is neglected, i.e. $\beta(\omega)$ only describes the propagation delay t_c ($\beta(\omega)z = \omega t_c$), and attenuation in the considered frequency range is approximated by a constant mean value $\alpha(\omega_c)$ then Eq. (3.65) can roughly be approximated by:

$$Q(z) \approx K \cdot Q(0) \cdot e^{-\alpha(\omega_c)z} \quad (3.66)$$

The value of K depends basically on the time integration interval in relation to the sensor frequency response and is close to 1 if the detection bandwidth is sufficiently large. From Eq. (3.66) it follows that the measured charge strongly depends on the cable's propagation characteristics via $\alpha(\omega_c)$. Equation Eq. (3.66) can be applied to the existing propagation channels. For the SP channel we find

$$\sum_{i=1}^3 Q_i(z) \approx K e^{-\alpha_{\text{SP}}(\omega_c)z} \sum_{i=1}^3 Q_i(0) \quad (3.67)$$

and the PP channels are described by

$$(Q_i(z) - Q_j(z)) \approx K e^{-\alpha_{PP}(\omega_c)z} (Q_i(0) - Q_j(0)) \quad (3.68)$$

3.6.2 Charge-transport measurements

The involved charges in propagation measurements are examined with pulse response measurements on a 200 m PILC cable. Integration of the current injected into the cable gives the injected charge $Q(0)$. As we analyzed the complete frequency spectrum and time interval, integration of the measured current results in the full charge. To determine the effect of using a bandwidth-limited sensor, the measured data is filtered with a (digital) 1-4 MHz band-pass filter. Integration of the positive part of this signal results in the charge that is approximated by Eq. (3.66). The calculated charges are given in Table 3.1. We conclude that the simplified Eq. (3.66) gives indeed a rough indication of the detected charge magnitudes.

Table 3.1 Measured $Q(z)$ (which is equal to the injected $Q(0)$ when integrated over both full frequency and time domain), the bandwidth limited charge Q_{bwl} by means of a 1-4 MHz band-pass filter, together with the approximated charge Q_{appr} , calculated with Eq. (3.66) with factor K taken as 1, for both the SP and the PP channels.

| | $Q(z)$ [nC] | Q_{bwl} [nC] [% of Q_{in}] | | Q_{appr} [nC] [% of Q_{in}] | |
|----|----------------|------------------------------------|-----|-------------------------------------|-----|
| SP | 3.0 | 0.98 | 33% | 0.77 | 26% |
| PP | 2.0 | 0.86 | 43% | 0.97 | 49% |

For a complete cable system the factor $e^{-\alpha(\omega)z}$ in Eqs. (3.65) – (3.68) should be replaced with $H_T(\omega)$, the transfer function of the complete cable system. With this substitution the impedance changes of the different cable sections are incorporated.

3.7 Conclusions

For cables longer than a few hundred meter, the attenuation of high frequencies in power cables results in an upper limit of frequencies useful to consider of tens of MHz (up to about 30 MHz, depending on the cable length and cable type). Since the cross-section of power cables are much smaller than the corresponding wavelengths, TEM waves dominate and transmission line theory can be applied to model the signal propagation through the cable length.

For single-phase power cables or cables with a shield around each phase-conductor, a simple coaxial model is applied. For three-phase cables with a common earth screen around the cable cores, multiple propagation paths exist, thereby introducing a four-conductor transmission line model, involving many hard to determine parameters. However, because of the symmetries in three-phase power cables, the propagation description can be reduced to a description of two distinctive propagation channel characteristics: Shield to Phases (SP), the travelling wave between the three-phase conductors and the shield, and Phase to Phase (PP), the wave between two phase-conductors. This reduces the system to two-conductor transmission line models.

In on-line situations, the earth screen of the cable is often the only location to measure without safety hazards. Therefore, the SP channel is of major interest to

this thesis. The parameters of the SP channel of a three-phase power cable are easily modelled assuming the SP channel to be approximately coaxial.

In the case of power cables with paper insulation, it is important to use the correct frequency dependent and complex dielectric permittivity for the model. This quantity can only be obtained from measurement.

A complete cable system, consisting of various sections of different power cables, can be modelled by using chain matrices. The total model is a valuable tool to predict the expected signals originating from PDs at all possible locations within the cable system. It also enables us to calculate the original (apparent) charge at the PD site from a measured (band limited) signal at the cable end.

Partial-discharge signal detection

After excitation of partial discharges and propagation along the cable system, the PD signals have to be detected at the cable termination(s). Detection involves both measurement of relevant data and extraction of the important signals from the measured data. This chapter discusses systems and models involved in the detection process. This involves sensors and their locations, the load impedances at the sensor position(s), system identification, and signal analysis.

4.1 Introduction

As distribution-class power cables are normally buried underground, the only place to detect signals propagating through these cables is at the cable termination. In some countries, joints and splices are installed in ‘man holes’ and can in principle be accessed after laying. If sensors are implemented in joints or splices (e.g. [Cra99, Khe98, Pom99, Zho01]), detection can be established at these locations. However, in MV cable systems these sensors are usually not installed and as most joints are completely shielded, installation afterwards without violating the cable system is generally not possible. Furthermore, in many countries the joints are buried underground, usually even without pinpointing their exact locations. MV cables are usually terminated inside substations (supplying multiple MV cables with power, transformed from voltages at transmission level) or ring main units (RMUs, interconnecting multiple MV cable connections and/or transforming the power to a lower voltage). In this thesis, the models are designed for and tested on RMUs, since they are present in much larger numbers. However, the models can serve as a basis or crude approximation for large substations too.

The first step in PD detection is the measurement of relevant signals. For conventional off-line PD detection, measurements are performed with sensors capable of separating high frequencies from the power frequency. As energizing of the cable under test (CUT) is performed with an external source (e.g. a 0.1 Hz or oscillating-wave generator), temporal galvanic connection of the sensor with the high-voltage conductor(s) can be made while the CUT is de-energized. Due to safety reasons, this is not possible for on-line measurements. Many sensor types used for partial-discharge applications require switching of power and/or modification of the installation [Pom99, Pul95, Lee00]. For our application a sensor that can be installed without

switching is preferred. Section 4.2 discusses different types of sensors, each with their specific (dis)advantages. As substations are highly disturbing EM environments (e.g. [Wig94]), shielding of sensors is an important issue too. Measurements of both the sensor transfer function and their shielding show the applicability for the present application.

At least as important as the sensor type itself is its position in the substation. Several positions for safe installation of sensors can be found in a substation. The position of a sensor determines how a PD signal is measured and is therefore crucial for correct signal detection. Furthermore, combination of sensor positions can provide extra information, such as the propagation direction of the detected signal and its originating propagation channel. Section 4.3 discusses various aspects of different sensor locations.

The propagation model in Chapter 3 describes the partial-discharge signal up to the load impedance(s) formed by the substation(s) or RMU(s). Measured data at the cable termination(s) will be dependent on these impedances. In Section 4.4 a model is presented to estimate the substation or RMU impedance. Several high-frequency circuits are defined and components are described by lumped circuit elements. As substations or RMUs can normally not be switched off-line without interruption of power delivery, a method is presented to measure the substation and RMU impedance on-line.

Besides measurement of the substation impedance, the proposed method in Section 4.4 can be extended to identify the complete system, i.e. both the substation(s) impedance(s) and the cable propagation parameters. Section 4.5 presents this method.

The final step in detection is signal analysis, involving both signal extraction and disturbance rejection. An in-depth research of these subjects can be found in [Vee05]. The main principles relevant for the rest of this thesis are given in Section 4.6.

Section 4.7 summarizes the conclusions from this chapter.

4.2 Sensors

4.2.1 Sensor types

Although many types of sensors exist, they can basically be subdivided into three main categories: capacitive, inductive, and directional sensors. The latter category is usually a combination of both capacitive and inductive sensing, implemented in one device. This combination of both measuring principles is not attractive for on-line PD measurements on MV cables, as will be described below. However, there are alternatives for directional sensing in this specific application, as will be discussed in Section 4.3.2.

Capacitive sensors

Capacitive sensors are sensors that provide capacitive coupling to one of the phase conductors, thereby filtering out the high-voltage power frequency and only detecting high-frequency signals on these conductors. Capacitive sensing can be established in several ways.

Separate high-voltage capacitors can be connected to a phase conductor of the cable. The measurement of PDs can be performed over a measurement impedance in

series with this capacitor, resulting in high-pass filtering. This method is successfully applied in conventional off-line PD measurements (e.g. [Ste91]). However, for on-line application there are important implications:

- The high-voltage capacitor can only be mounted when the cable is de-energized, thereby not allowing PD measurements without interrupting the power delivery.
- High-voltage capacitors can be unreliable on long term and may therefore become a cause of fault themselves when being applied for longer measuring times, as is one of the goals of on-line monitoring. This would result in the opposite effect of what is one of the general purposes of diagnostics like on-line PD detection: increasing power-delivery reliability.
- A decent place to connect this high-voltage capacitor can be hard to find. Most modern switchgear completely shields or insulates the high-voltage rail. Mounting would only be possible in substations or RMUs with an open type of switchgear or at the transformer (MV/LV), if present. This latter solution involves inclusion of extra impedances, thereby lowering the sensitivity, see Section 4.4.

Instead of installing a lumped component, capacitive coupling can also be realized through installing an electrode in the vicinity of a phase conductor, resulting in capacitive coupling to this conductor. The obtained capacitance, however, is highly dependent on the layout of the substation, type of switchgear, cable termination, and positioning of this electrode. Furthermore, the capacitance is relatively low.

In some high-voltage cable systems, capacitive coupling is performed in the accessories themselves [Cra99, Khe98, Pom99, Zho01]. As these types of sensors are usually not installed in MV cable accessories, and it would be far too expensive to install them afterwards, this type of sensing is not of interest for our application.

In modern switchgear a capacitor is sometimes integrated to detect the power frequency voltage on each phase conductor. The use of this capacitor for measuring small signals like PDs is in practice hard, due to its small value (usually < 100 pF). Moreover, this method would not be very universal, since it depends on the presence of this particular type of switchgear.

It is concluded that capacitive sensors have crucial disadvantages if applied for on-line PD detection on MV cable systems. In special circumstances, a capacitive solution may be applied if inductive sensing is impossible, but capacitive sensors cannot provide a general, practical solution. A directional sensor also involves capacitive sensing. This type of sensors shares the same disadvantages as pure capacitive sensors.

Inductive sensors

Inductive sensors are sensors where a voltage is induced in a secondary (detection) circuit as a response on the change in enclosed magnetic flux, caused by the current in the primary circuit (with the PD current). The magnetic field, caused by the primary current, can be enhanced by inserting a current transformer in the primary circuit. However, the magnetic field surrounding any conductor of the primary circuit can also be measured by placing a coil in the secondary circuit in the proximity of the primary circuit, thereby enclosing magnetic flux from this primary current. Now, the primary circuit is not altered and no interruption of the primary current is necessary. An example of a widely applied inductive sensor is the Rogowski coil, a toroidal coil with

N_w equally spaced turns, and a constant loop area [Rog12, War93, Hud65, Bos00, Coo63, Nas79]. Although this type of coil is wide spread and model descriptions are widely available (e.g. [Sty82, Coo63, Wag04]), a short derivation of its transfer function is given in Appendix B to demonstrate several specific properties. The mutual inductance M_c is defined as the ratio of induced voltage $V_{\text{ind}}(\omega)$ and change of enclosed current $I_{\text{pr}}(\omega)$:

$$V_{\text{ind}}(\omega) = j\omega M_c I_{\text{pr}}(\omega) \quad (4.1)$$

The mutual inductance for an air coil with rectangular cross section for signal wavelengths much larger than the coil size is given by:

$$M_c = \frac{\mu_0 h N_w}{2\pi} \ln\left(\frac{r_o}{r_i}\right) \quad (4.2)$$

where μ_0 is the permeability of vacuum, h the height, r_i the inner radius and r_o the outer radius of the coil. The mutual induction for other shapes can be found in Appendix B. The rectangular shape is preferable, since the maximum amount of magnetic flux will be enclosed with the minimal outer dimensions. Including transmission-line effects is not required for this application, since the probe dimensions are restricted to the order of 5 cm, the minimal space generally available at the cable terminations in RMUs, while the considered minimum wavelengths are only down to tens of meters. A nice property of Rogowski coils is that the output is independent of the location and angle of the primary conductor within the coil. Furthermore, external magnetic fields, present in substations and RMUs, are inherently cancelled by the symmetric structure of the coil, i.e. the equally spaced turns, together with the routing of the return wire along the path of the windings (Appendix B).

The mutual inductance of the coil can be increased by using core material with high permeability μ_r (up to 10^5). If such core materials are used, additional requirements arise. The material should not saturate, in particular not by the power frequency current. For a coil with air slit d_{air} the mutual inductance becomes (Appendix B):

$$M_c = \frac{\mu_0 A N_w}{d_{\text{air}}} \quad (4.3)$$

where A is the cross sectional area of the turns in the coil. Saturation of the core material can also provide inherent safety. As is explained in Appendix B, it can be used to prevent over-voltages due to e.g. power switching transients or lightning surges.

The transfer impedance of a current probe is defined as:

$$Z_t(\omega) \triangleq \frac{V_m(\omega)}{I_{\text{pr}}(\omega)} \quad (4.4)$$

where V_m is the output voltage of the probe over a measurement impedance Z_m . In Appendix B several equivalent circuits are discussed, valid within different levels of approximation and frequency range. The simplest, most commonly used, circuit is depicted in Fig. 4.1 and gives insight in the behavior of current probes in general. The current probe is modelled as a current-controlled voltage source V_{ind} , representing the induced voltage, and a self-inductance of the coil L_c . The introduced self-inductance in the primary circuit can usually be neglected. Parasitic capacitances have been omitted in this figure. For higher frequencies the inner-winding capacitance should

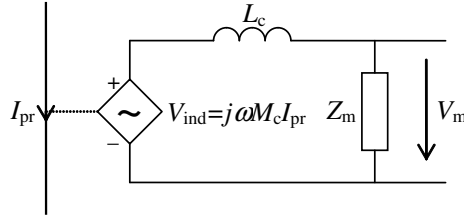


Figure 4.1 Simple equivalent circuit of current probe

be taken into account, which can be represented as a parallel capacitor over L_c . Furthermore, the parasitic capacitance to the shield or environment can be significant. In Appendix B a transmission-line model shows those effects. The transfer impedance of the simple circuit shown in Fig. 4.1 is given by:

$$Z_t(\omega) = \frac{j\omega M_c Z_m}{Z_m + j\omega L_c} \quad (4.5)$$

In general one can distinguish two operation conditions:

- If $\omega L_c \ll Z_m$, usually the case for an air coil in combination with a large Z_m , the measured voltage becomes: $V_m(\omega) = j\omega M_c I_{pr}$; i.e. the measuring system differentiates the current $i_{pr}(\omega)$ with calibration factor M_c .
- If $\omega L_c \gg Z_m$, usually the situation with a ferro-magnetic core and a small Z_m , then: $V_m(\omega) = M_c Z_m I_{pr}(\omega)/L_c$, a flat frequency spectrum as from the cut-off frequency $\omega_{co} = Z_m/L_c$.

Although commercially available current probes with a ferro-magnetic core, a complete shielding, and a transfer impedance of 1Ω in the frequency range of 100 kHz – 100 MHz, are suitable sensors for on-line PD application, some inexpensive Rogowski-type air coils were made to investigate possible alternatives for commercial probes. Calibration of unshielded probes have to be performed in an EMC-well-conditioned situation. To this extent a brass-plate enclosed calibration set-up is used, to minimize environmental influences and provide shielding and/or rerouting of common-mode currents (e.g. over the shield of the measurement cables). A calibration measurement of the transfer impedance of a custom made Rogowski coil, optimized for detection between 100 kHz and 30 MHz, is shown in Fig. 4.2, together with a theoretical calculation. The figure shows good agreement of the measurement and model calculation even though the simple equivalent circuit of Fig. 4.1 is used. For low frequencies (< 500 kHz) the transfer impedance of the Rogowski coil decreases below 0.2Ω . Small signals with low frequencies will be hard to detect. For frequencies above 3 MHz, the transfer impedance increases above the value of the available commercial probe (1Ω), resulting in higher sensitivity. From the average sensitivity (over the frequency domain of interest), it is concluded that, regarding the sensitivity, the custom made air coil is a good alternative to commercial probes.

In Fig. 4.3 a measurement on the same coil is shown, but without EMC precautions. Now resonances due to the environment, e.g. standing waves on the measurement cables, are clearly modifying the transfer impedance. A slight change of the

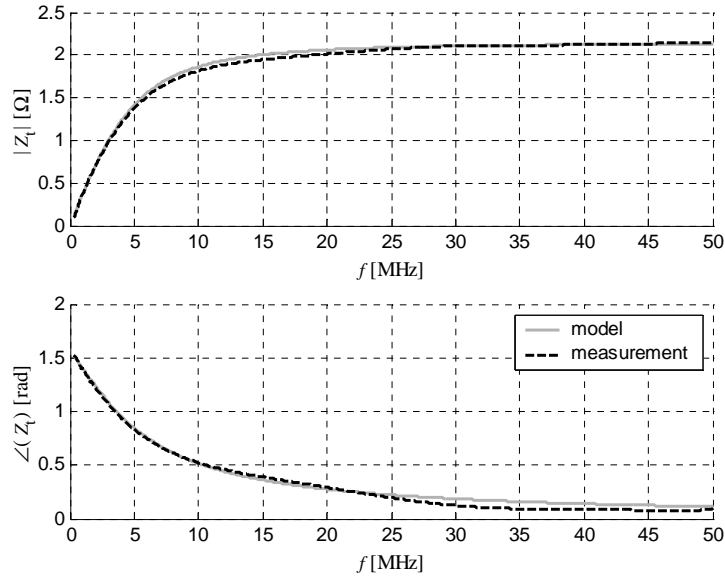


Figure 4.2 Measured and calculated transfer impedance of Rogowski coil

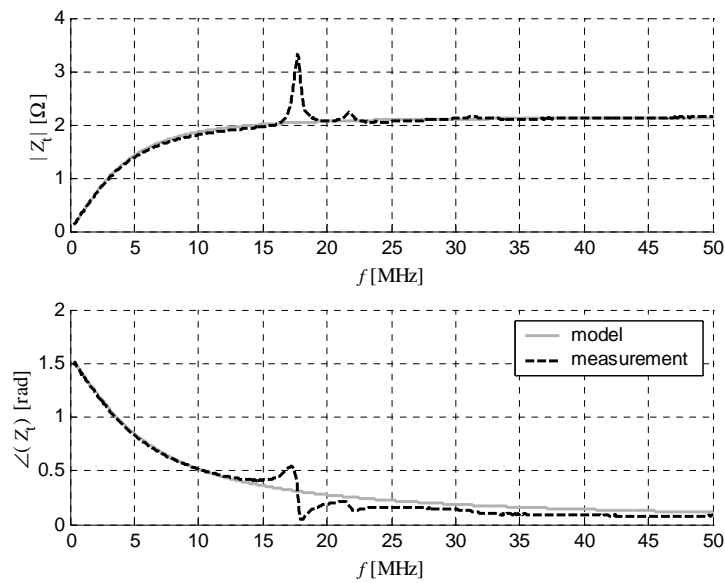


Figure 4.3 Measured and calculated transfer impedance of Rogowski coil without good EMC precautions

layout of the set-up did shift this resonance frequency, indeed indicating the effect of the environment. In the next section, shielding will be discussed more thoroughly.

To summarize, toroidal sensors have important advantages for on-line PD detection:

1. Since toroidal coils measure only the total enclosed current, this sensor is less dependent on the geometry of equipment in a substation or RMU.
2. No galvanic contact with a conductor is required; therefore the sensor can be mounted safely without interrupting the power delivery and can never become a cause of power failure itself.

Since these advantages are essential for on-line PD measurements, we will focus on the application of inductive sensors.

4.2.2 Sensor shielding

The environment can influence the transfer impedance of current probes as was shown by Fig. 4.3. The detection coils are applied in substations or RMUs, environments with severe disturbing electro-magnetic fields [Wig94]. Good design of a Rogowski coil implies that magnetic fields from external currents are automatically cancelled (Appendix B). The remaining coupling to the environment is capacitive. The capacitive coupling can occur to any conductor in the environment, and especially to the enclosed conductor. The transfer function of the detection probe, should be shielded against electric fields to maintain a well defined transfer function.

Usually Rogowski probes have unshielded wires, making them highly sensitive to external electric fields. A common option for shielding such coils is applying a conducting screen around the complete coil [Bos00, Won90]. An air slit must be included so the magnetic field of the enclosed primary current is not cancelled by currents through the screen. This solution is applied in many commercially available coils and is very effective. However, such commercially available coils are usually expensive and we are restricted to available specifications and sizes. The problem (or expense) of constructing self made coils is usually not the windings themselves, but the core material and the shielding. However, if no core is used it is possible to design simple Rogowski coils with an alternative shielding method: the use of coaxial cable for the windings [Nev03]. The shield of the coaxial cable shields the inner conductor, over which the induced voltage is measured. This shield must be interrupted on at least one location, for the same reason as the complete screen required an air slit. If only one interruption is applied, the inter-turn capacitance and self inductance of the screen causes unwanted resonances. To prevent this, the screen of the coaxial cable can be interrupted at every turn. The separated screen segments are then interconnected by a common wire around the coil [Ger02]. This wire also serves as the return conductor of the coil formed by the central conductor of the coaxial cable. In Fig. 4.4 the principle is illustrated. The formulas from Section 4.2.1 are still valid.

A measure for the shielding efficiency is the common-mode transfer impedance, defined as:

$$Z_{t,CM}(\omega) \triangleq \frac{V_m(\omega)}{I_{CM}(\omega)} \quad (4.6)$$

where $I_{CM}(\omega)$ is the common-mode current, flowing over the shield of the probe and the connecting cables, and $V_m(\omega)$ is the voltage in the measuring circuit over the

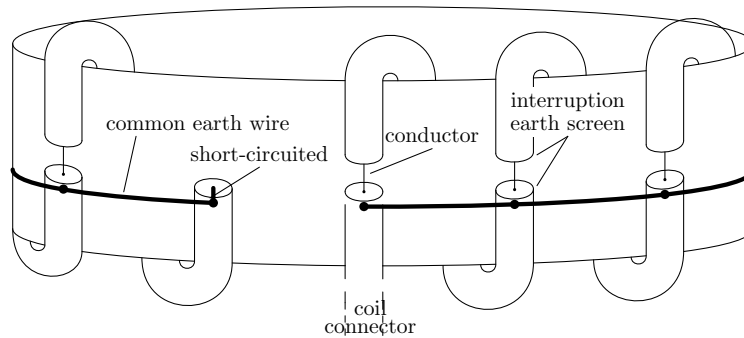


Figure 4.4 Rogowski coil with windings from coaxial cable. The shield from the coaxial cable is interrupted in each turn and interconnected by a common earth wire.

measurement impedance Z_m . In Fig. 4.5 the set-up to determine the common-mode transfer impedance is depicted. A current $I_i(\omega)$ is injected in a primary circuit (left), which has a capacitive coupling C_{ec} to the Rogowski coil. If the coupling would pinpoint to a small region of the coil, the exact place of coupling would have large influence on the test, since the length of the coil over which the current flows is dominant. Therefore, the capacitive coupling is realized by placing an electrode with the typical size of a power cable in the center of the coil, imitating realistic conditions. Hereby, the capacitive coupling will approximately be evenly distributed along the coil length, eliminating the effect of the exact place of current injection. Small variations in positioning confirmed this assumption. Obviously, C_{ec} is dependent on the dimensions of the coil and the electrode and their relative orientation. Since $Z_{t,CM}(\omega)$ is dependent on $I_{CM}(\omega)$ and not on the voltage, the magnitude of the coupling has no influence on the common-mode transfer impedance.

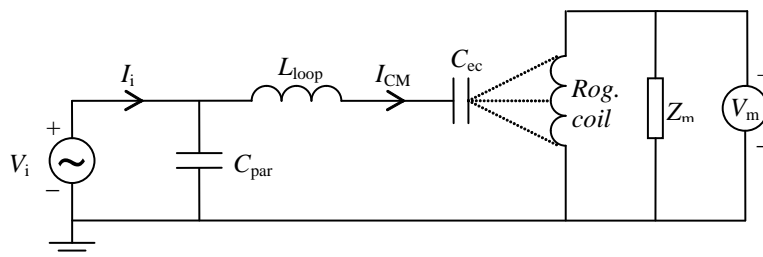


Figure 4.5 Measurement circuit for common-mode transfer impedance of current probes

The injected current in the primary circuit, $I_i(\omega)$ is not equal to the common-mode current to the coil $I_{CM}(\omega)$. The injected current partly flows through a parasitic capacitance C_{par} parallel to the coil (Fig. 4.5) and partly over L_{loop} to the coil. If the test set-up is kept constant, the values of these parameters can be determined by calibration measurements: one with C_{ec} short-circuited and one in absence of capacitive coupling by removing the coil. Although $Z_{t,CM}(\omega)$ is independent of C_{ec} , it is necessary to determine this coupling capacitance before $Z_{t,CM}(\omega)$ is calculated. As both voltage and current are measured at the input circuit, the input impedance

$Z_i(\omega) \triangleq V_i(\omega)/I_i(\omega)$ can be used to determine the coupling capacitance for the specific set-up:

$$C_{ec} = \frac{Z_i(\omega)^{-1} - j\omega C_{par}}{j\omega + \omega^2 L_{loop} Z_i(\omega)^{-1} - j\omega^3 L_{loop} C_{par}} \quad (4.7)$$

Now the common-mode transfer impedance can be corrected for the parasitic capacitance:

$$Z_{t,CM}(\omega) = \frac{V_m(\omega)}{I_i(\omega)} \left(1 + \frac{C_{par}}{C_{ec}} - \omega^2 L_{loop} C_{par} \right) \quad (4.8)$$

The common-mode current, caused by the capacitive coupling described above, also causes an induced voltage over the coil since part of it is enclosed by the coil. As the capacitive coupling is approximately distributed evenly over the coil, about half of this current will contribute to the inductive coupling. The common-mode transfer impedance caused purely by the capacitive coupling is therefore $Z_{t,CM}(\omega)$ from Eq. (4.8) minus $\frac{1}{2}Z_t(\omega)$, half the transfer impedance of the coil.

The electric shielding efficiency is measured for Rogowski coils with (coaxial, see Fig. 4.4) and without shielding. The size and number of turns are about equal for both coils. The resulting absolute value of the common-mode transfer impedances are shown in Fig. 4.6. A reduction of over a factor 6 of the common-mode transfer impedance is found for the shielded coil. It is therefore concluded that coaxial cable windings for a Rogowski coil can improve the shielding efficiency significantly, while production costs and sensitivity remain attractive.

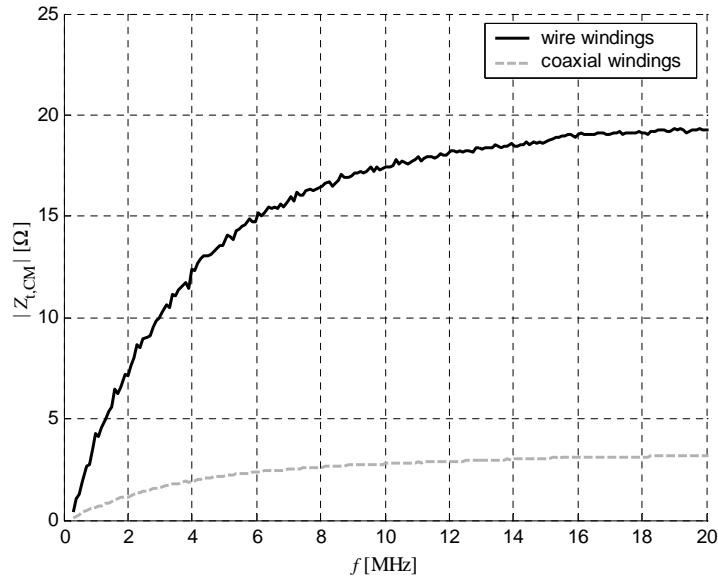


Figure 4.6 Measured common-mode transfer impedance caused by capacitively coupled current of Rogowski coils with windings constructed from wires and from coaxial cable

4.3 Sensor locations

4.3.1 Measurement locations

The location of the sensors at the cable termination in the substation determines to a large extent the signal-to-noise ratio (SNR) of the detected signal and which propagation channel (Shield to Phases, SP, or Phase to Phase, PP, see Chapter 3) is measured and is therefore crucial for the detection sensitivity of the measuring system. In Fig. 4.7 a simple representation of a cable termination as a lumped component is shown. The load in the substation is indicated as impedance Z_1 . Two main current circuits can be defined. The differential-mode (DM) current, flowing through the cable's phase conductor(s), the load impedance at the termination and returning through either the shield of the cable (SP) or an other phase conductor (PP). This current includes PD signals from the cable. The DM circuit along the cable is well shielded, so noise and interference only originate from the connected power grid. The common-mode (CM) current flows through the shield of the cable and back via some other earth path, which is in practice always present. This circuit is actually a large antenna for noise and disturbance and does not contain PD signals from the cable under test.

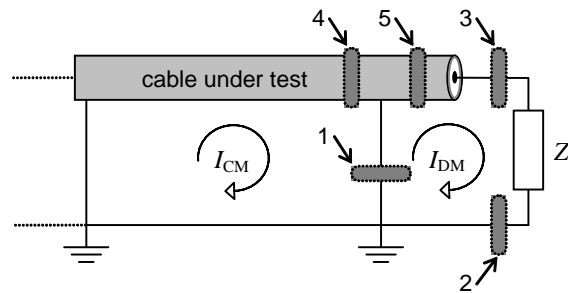


Figure 4.7 Simplified representation of a cable termination in a substation or RMU. The two main current circuits DM and CM are indicated, the numbers indicate locations discussed in the text.

Various locations for the current sensor are indicated with numbers in Fig. 4.7.

- Location 1 is the earth connection of the cable on which a current sensor can be installed without safety hazards. Both the DM and CM currents will be measured; therefore, the DM current is unnecessarily disturbed. Moreover, if the earth connection is branched only a part of the PD signal is detected.
- Location 2 can be considered as the earth connection of all the impedances in the substation, denoted as Z_1 . In reality, this is a complex network of branched earth connections. One main connection can usually not be identified.
- At location 3, the DM current can in theory be measured separately. However, the sensor should be clamped around energized phase conductors, which is obviously not safe and usually difficult due to the dimensions of the cable termination. In modern switchgear the phase conductors inside the termination even cannot be reached. This method can only be applied if the sensor is integrated in the cable termination (as is sometimes applied in EHV cable accessories).

- Location 4: Here a current probe can be installed easily and safely. The enclosed current, however, includes both the DM and CM currents flowing forth through the shield and the DM current flowing back through the phase conductors, resulting in only the CM current, without PD signals from the cable. In the case of an XLPE cable with a helically-wired screen, this location can still be used to detect pulses inside the cable. The helical wires cause a magnetic field with a component in the direction of the cable (z -direction), which can be measured with a simple strap around the cable, functioning as a single-turn coil. However, only high frequencies (> 100 MHz) can be measured, which makes it hardly applicable for PDs from complete cable connections. See further [Wou94].
- Location 5, around the cable shield just before the actual cable termination, but past the last earth connection of the cable (PLEC). A current probe can be installed safely here, and only the DM current is measured. Apparently, this is the optimal location for direct current measurement. If the cable termination lacks space to install the sensor there, one can take location 4 and can re-route the last earth connection, back through the current probe. One direction of the DM current and the CM current is then subtracted from the total signal and only the DM current remains.

A measurement session has been performed in several 10 kV RMUs in order to determine the noise and interference level. Sixteen 10 kV circuits were measured on both sides, so in thirty-two RMUs spread throughout the Netherlands. Fig. 4.8 shows a typical PSDF (Power Spectral Density Function) obtained at the two sensor positions 1 and 5 in Fig. 4.7 of the same cable. Clearly the CM circuit introduces additional noise. Note that the noise level for frequencies below 1 MHz is considerably larger than for higher frequencies. The decrease in noise level for even lower frequency is due to the drop in sensor sensitivity. The noise spectra indicate that the lower bound for the frequency range of interest for PD detection is a few hundred kHz.

In the discussion above, the substation or RMU is considered as one overall impedance Z_1 . As will be shown in Section 4.4, however, several current paths and impedances can be identified in the substation impedance. Fig. 4.9 shows a schematic representation of the relevant MV elements in a substation or RMU. The potentially interesting sensor locations 1 and 5 from Fig. 4.7 are again indicated, complemented with several additional locations.

- Location 6 provides the option to position sensors around one or more of the (in the Netherlands usually three single-phase) transformer-connecting cables (TCC). The transformer, if present, forms an impedance between the high-voltage rail and earth, i.e. PD signals originating from the CUT will produce a current through this impedance. Their shields are earthed, which allows for installation of sensors around these cables while they are energized. If multiple sensors are installed around each single transformer-connecting cable, each sensor measures the current through an individual phase, and SP and PP signals can be distinguished.
- Location 7 is the earth strap of the TCC. Such cables are relatively short (about 5 m) and have a capacitance in the order of 2 nF. The current flowing through the earth connection of this cable is coupled to the voltage of this cable by this capacitance. This current allows a capacitive measurement of the PD voltage.
- Location 8 is also part of the current loop through the transformer. However, the

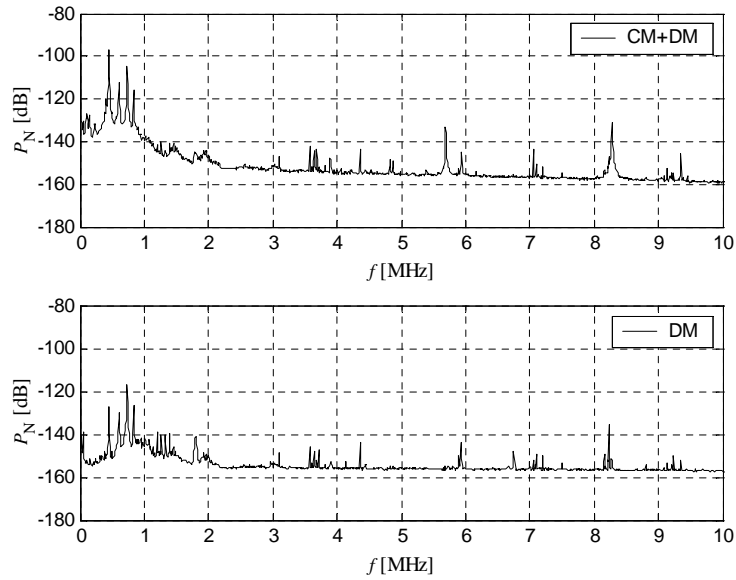


Figure 4.8 PSDF of noise signals measured at position 1 (DM+CM current) and 5 (DM current only) in Fig. 4.7

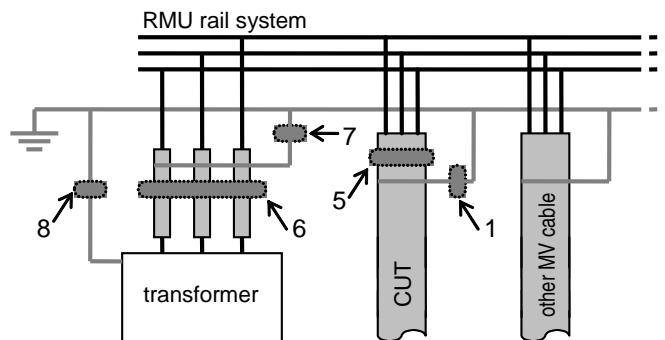


Figure 4.9 Schematic representation of relevant MV elements in a RMU connected to the cable under test. The numbers indicate sensor positions, discussed in the text.

transformer has a metal enclosure, so parasitic capacitances to the environment and conductance to the floor enable high-frequency signals to find other paths to earth than the wired connection. Therefore location 8 will only contain a part of the current at e.g. location 6.

In principle measurement of PD signals in the PP channels has advantages. By detection in the PP channel, a differential measuring method is implicitly applied. Noise and interference that arises through radiation is partly cancelled, since the coupling strength is almost equal to all phases. Moreover, since the earth connections in the substations act as antennas, due to their geometric arrangement the noise and interference contribution of ground conductors is larger than the contribution of the phase-conductor connections and rail systems. A survey of the noise and interference levels in substations has confirmed this assumption. In a typical Dutch cable environment with belted cables, the only location to measure the PP channel currents is on the TCC at position 6 in Fig. 4.9. Therefore, the signal level is determined by the transformer impedance. The SP channel's impedance is usually much smaller, especially when several MV cables are connected to the substation or RMU (see Section 4.4). So although the interference level in the PP channel is in principle lower, the SNR does not necessarily have to be better. Furthermore, the exact position and direction of the PD at the discharge location have pronounced effects on the induced currents in the different channels (Chapter 2).

It is concluded that position 5 (PLEC) provides for the optimal location for measuring SP currents, since the total PD current is enclosed and CM currents are cancelled. Measuring the SP channel is the most general method, as it is least dependent on the actual substation arrangement. For PP channel detection, TCC (position 6) is the only possible location in the case of belted cables.

4.3.2 Directional sensing

Apart from PDs coming from the cable under test, measured high-frequency signals can also originate from other sources, e.g. PDs from adjacent high-voltage equipment (other cables, transformer, etc.) or transients from switching, thyristor pulses, etc. If pulses coming from the cable can be discriminated from other pulses, much interference can be rejected at an early stage of the detection process. Directional sensing of measured signals can be performed by three methods. Signals can be measured by placing sensors at sufficient distance from each other to detect time differences in the outputs. However, the maximum possible distance at feasible sensor locations in a substation or RMU are too short to distinguish between the time of arrivals at the sensor locations. Other options are: detection of the polarity of the energy flow and a cancellation technique of all signals not originating from the desired direction, denoted as differential measurement.

Polarity of pulse energy flow

The direction of a propagating pulse is determined by the direction of the energy flow, given by the Poynting vector \underline{S} according to:

$$\underline{S} = \underline{E} \times \underline{H} \quad (4.9)$$

where \underline{E} and \underline{H} are the electric and magnetic field vectors of the signal, respectively. The principle of directional sensing is based on simultaneous measurement of both

magnetic and electric field, or both current and voltage, [Oli54]. Directional sensing is usually performed by having both coupling methods implemented into one device, e.g. [Sed91, Sch00]. This technique is also used for directional sensing in joints of HV cables, e.g. [Pom99, Cra99]. However, capacitive and inductive coupling can be realized by separate sensors as well.

In the case of on-line PD detection, inductive coupling to the SP channel at the cable termination is established by means of an inductive sensor at e.g. position 5 in Fig. 4.9. A capacitive divider for the capacitive part of the directional coupling, as in [Wen95] has major disadvantages due to the required galvanic contact to the phase conductors. However, the voltage of the SP channel can also be determined from the current through an impedance over this channel. As the impedances in a substation or RMU are not necessarily real (Section 4.4), the pulse shape of the voltage may differ from the current pulse shape. But irrespective of the nature of the impedance, the polarity of an initial current through that impedance is equal to the polarity of the voltage across it, which can be easily seen when considering e.g. the voltage across a resistor, a capacitance, and an inductance: $v_R = R i_R$, $v_C = \frac{1}{C} \int i_C dt$, and $v_L = L \frac{di_L}{dt}$. Combining the initial polarities of the signal current with the current through a positive impedance over the same channel provides for the direction of the pulse. The only restriction to this principle is that the real part of the impedance is positive. This means that the impedance should never act as a source of energy, i.e. should never produce partial discharges itself. As other MV cables and the transformer can produce partial discharges themselves, the best option is the earth connection of the TCC. In the Netherlands these cables are usually XLPE cables and do therefore normally not produce PDs. A sensor at position 7 in Fig. 4.9 measures the current through the capacitance of these cables and is therefore a measure for the voltage across the SP channel of the cable under test. So combination of currents measured at position 5 and 7 provides for direction of energy flow at location 5.

To illustrate this principle an experiment is performed with current sensors around the earth connection of the TCC and around the cable under test PLEC (positions 5 and 7 in Fig. 4.9). Both sensors have equal direction with respect to earth. Pulses are injected at the far ends of two MV cables, connected to the same RMU. The results are shown in Fig. 4.10. Pulses from the cable under test produce different polarities at the start of the signals and pulses originating from a second cable show equal polarity. Note that the currents through the earth of the TCC is indeed the time derivative of the PLEC currents, confirming the presence of a capacitive impedance.

Measurements with pulses coming from the connected transformer show similar results. It is concluded that the principle of comparing the polarity of the start of the signals predicts the signal direction and is therefore a valuable tool for PD measurements. Complications arise when pulses (e.g. from different locations) overlap. Then the start of the pulse signal is hard to determine. Therefore this is only one of the expert rules of the total detection system, see Chapter 6. The presence of these errors, however, will be randomly distributed over the cable length and will therefore not lead to misinterpretation of the results with respect to the cable system's condition.

Differential measurement

It is possible to construct transfer functions which cancel unwanted signals (coming from other directions than the CUT), using the same measured signals and measurement locations as described above. Fig. 4.11 shows a simple representation of the

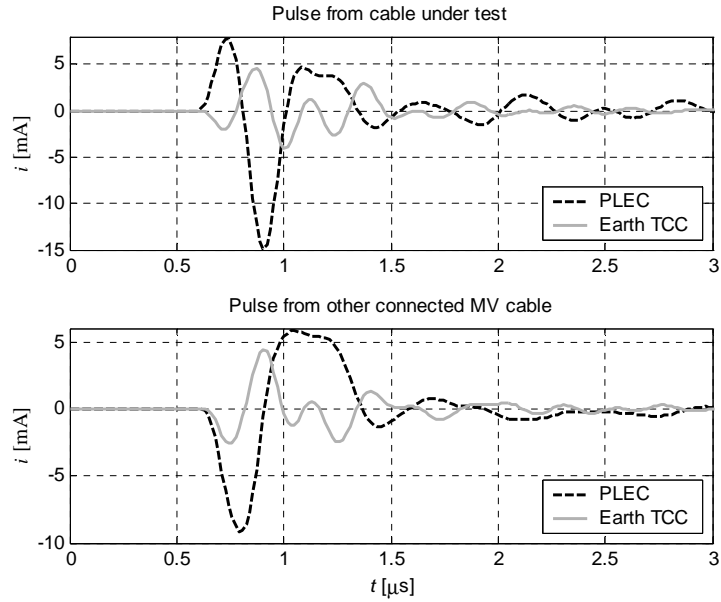


Figure 4.10 Measured currents at the cable under test PLEC and the earth connection of the TCC upon pulse injection in both the CUT (top) and another connected MV cable (bottom)

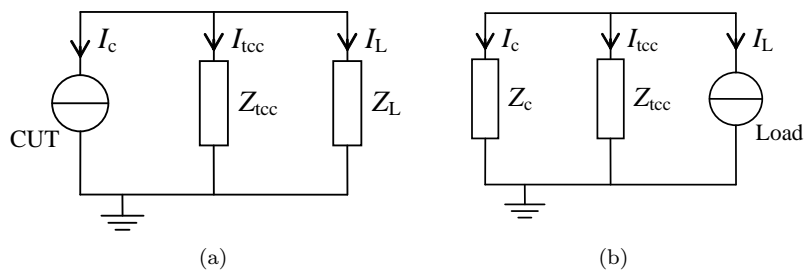


Figure 4.11 Simple representation of the relevant elements inside a substation or RMU upon a pulse coming (a) from the CUT with impedance Z_c and (b) from somewhere else in the load impedance $Z_L(\omega)$. Z_{tcc} denotes the impedance of the TCC to earth.

relevant elements inside a substation or RMU for the situation that a pulse is coming (a) from the CUT and (b) from elsewhere in the load impedance $Z_L(\omega)$. The relations between the indicated currents in Fig. 4.11 depend on the origin of the signal, which is either the CUT, situation (a), or the load, situation (b). The transfer function $H_{tcc,c}(\omega)$ between $I_{tcc}(\omega)$ and $I_c(\omega)$ for both cases is :

$$H_{tcc,c}(\omega) \triangleq \frac{I_c(\omega)}{I_{tcc}(\omega)} = \begin{cases} H_{(tcc,c)c}(\omega) = -\frac{Z_{tcc}(\omega)}{Z_L(\omega)} - 1 & , \text{ for sit. (a)} \\ H_{(tcc,c)L}(\omega) = \frac{Z_{tcc}(\omega)}{Z_c(\omega)} & , \text{ for sit. (b)} \end{cases} \quad (4.10)$$

If $H_{(tcc,c)L}(\omega)$ is used to subtract the transformed $I_{tcc}(\omega)$ from $I_c(\omega)$ for both situations it follows for the filtered differential signal $I'_{dif}(\omega)$:

$$I'_{dif}(\omega) \triangleq I_c(\omega) - H_{(tcc,c)L}(\omega) \cdot I_{tcc}(\omega) \begin{cases} \neq 0 & , \text{ for sit. (a)} \\ = 0 & , \text{ for sit. (b)} \end{cases} \quad (4.11)$$

Signals not originating from the cable under test are cancelled. The original signal $I_c(\omega)$ can be reconstructed from $I'_{dif}(\omega)$ with the transfer function $H'_{dif}(\omega)$:

$$H'_{dif}(\omega) \triangleq \frac{I_c(\omega)}{I'_{dif}(\omega)} = \frac{H_{(tcc,c)c}(\omega)}{H_{(tcc,c)c}(\omega) - H_{(tcc,c)L}(\omega)} \quad (4.12)$$

resulting for the final filtered signal $I_{dif}(\omega)$:

$$I_{dif}(\omega) = H'_{dif}(\omega) [I_c(\omega) - H_{(tcc,c)L}(\omega) \cdot I_{tcc}(\omega)] = \begin{cases} I_c(\omega) & , \text{ for sit. (a)} \\ 0 & , \text{ for sit. (b)} \end{cases} \quad (4.13)$$

Fig. 4.12 shows the results from measurements where pulses are injected in both the CUT and another connected cable in a RMU. The top graph shows that the original signal remains unaffected for a pulse from the cable under test. Signals from the other cable are almost completely cancelled.

For cancellation of signals from the transformer the representation of Fig. 4.11 is too simple, as will be shown in Section 4.4. The same principle can be extended to a more advanced substation model, where different transfer functions for signals originating from the transformer and the other connected MV cables are used. The method depends on accurate knowledge of the needed transfer functions. Section 4.4.3 presents an experimental method to determine these transfer functions while the substation or RMU and all cables remain on-line.

4.4 Substation impedance

This section focuses mainly on RMUs, as a first step of determining the load impedance of the cable under test. The SP channel is considered since sensors at the favorable measurement locations only detect this channel. First, the individual RMU components are discussed, after which the complete RMU is modelled. The measurement method, used throughout this section, is described in Section 4.4.3.

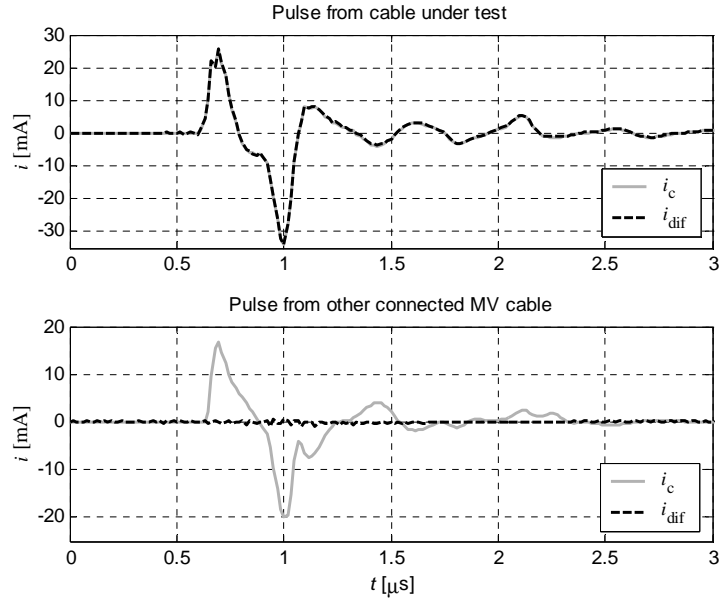


Figure 4.12 Measured and filtered signals using the differential measurement method upon pulse injection in both the CUT (top) and another connected MV cable (bottom)

4.4.1 Components in substations

To model a complete substation or RMU for high frequencies, with several resonating circuits, the individual components should be identified first. Fig. 4.13 shows a schematic drawing of a RMU, having $N + 1$ sections. The sections are referred to by number j , with $0 \leq j \leq N$. The locations for disconnection or switching are indicated by numbers. The components relevant for the discussion are: the MV cable under test and possibly other present MV cables (N), the rail system, the transformer, and the cables to the transformer (TCC).

MV cables

The characteristic impedance of MV cables Z_{c_j} ($1 \leq j \leq N$) can usually be regarded as real and constant (Chapter 3). In this section, the MV cables are assumed to be long, with respect to the considered wavelengths, allowing for elimination of possible reflections by time windowing and model the cables by their characteristic impedances only.

Transformer connection cables

The cables to the MV/LV transformer are usually short (in the Netherlands about 5 m) in comparison with the relevant wavelengths and their impedance to earth can therefore be modelled by a capacitor C_{tcc} . The value can usually be found in data sheets. The cables are also part of the large circuit from the rail system to the transformer and back via earth. The self-inductance of this loop will be included together with the connections and rail system, later on.

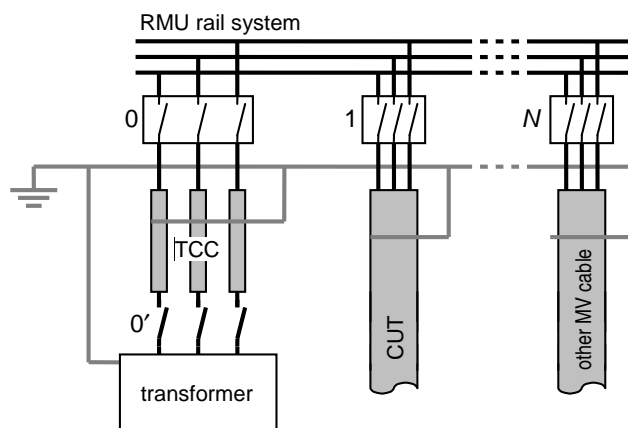


Figure 4.13 Schematic representation of relevant MV elements in a RMU connected to the cable under test. The RMU has N connected MV cables. The numbers are used in the text to indicate switching locations.

(MV/LV) transformer

Models that describe the high-frequency behavior of transformers already exist, e.g. [Dal99, Akb02, Chi95, Mor93]. Most models, however, consider frequencies up to only a few hundred kHz or at maximum 2 MHz. Furthermore, usually the focus is on the transfer function between primary and secondary windings, whereas for our application, the impedance as seen from the MV side is of interest. In [Mor93] it is shown that the three-phase symmetry is maintained inside a transformer. This is in agreement with our findings ([Wou03a, Wie04a]), which also revealed the dominance of capacitive coupling of the transformer's windings to its cabinet for frequencies up to at least 100 kHz. Furthermore, the load at the secondary (LV) side of a transformer was shown to have no influence on the SP impedance at the primary side. For higher frequencies ($\gtrsim 4$ MHz), the self-inductance due to the RMU layout dominates the impedance. If small losses are included (due to e.g. hysteresis losses, skin effect), the simple transformer model results in a series circuit of R_{tr} , L_{tr} , and C_{tr} . As this circuit's impedance has only one zero, at $\omega_r = 1/\sqrt{L_{tr}C_{tr}}$, the values of R_{tr} , L_{tr} , and C_{tr} can be determined independently by splitting the frequency range. Fig. 4.14 shows that for the frequency range between 500 kHz and 20 MHz the model fits the measurements well.

For higher frequencies ($\gtrsim 30$ MHz), a small capacitance (in this case 13 pF) parallel to L_{tr} had to be added to simulate a parasitic capacitance between the conductors forming the loop. This parallel $L_{tr}C_{par}$ -loop forms a pole (in this case at 40 MHz). This extra element is omitted further on, since the relevant frequency range is below 30 MHz.

Connections and rail system

For power frequency, the rail with its connections (e.g. MV cable termination, TCC) are almost ideal conductors. If high frequencies are considered, the inductances L_j ($0 \leq j \leq N$) can not be neglected due to the large loops. Also the parasitic capacitances C_{parj} between several points in the connections of the rail system become

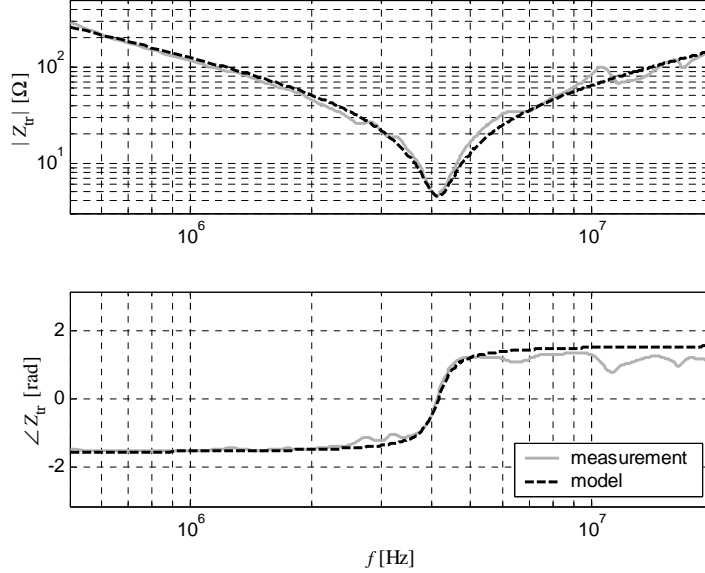


Figure 4.14 Measured and simulated (380V/10kV, 1000kVA) transformer impedance. The values fitted in the model are: $L_{tr} = 1.2 \mu\text{H}$, $C_{tr} = 1.2 \text{ nF}$, $R_{tr} = 4.5 \Omega$.

significant. Although these capacitances are distributed over multiple points, they are modelled as a single lumped-circuit capacitance, parallel to the self inductance of each rail system section j or connection. This reduces the number of parameters without losing much accuracy. Furthermore, losses should be accounted for, mainly in the form of radiation. As indication for the radiation resistance we consider the involved conductors in the substation as a straight antenna with:

$$R_{\text{rad}j}(\omega) = \frac{2\pi}{3} \sqrt{\frac{\mu_0}{\varepsilon_0}} \left(\frac{l_a}{\lambda} \right)^2 \quad (4.14)$$

where l_a is the (effective) length of the antenna, λ the wave-length ($\lambda = c_0/f$) and $\lambda \gg l_a$, e.g. [Kra88, Bal97]. The values of L_j , $C_{\text{par}j}$, and l_a can only be estimated based on crude approximations of typical dimensions.

The MV rail system in a substation or RMU is installed according to several safety and manufacturer regulations and modification should obviously be avoided. Moreover, the geometry itself is dominant for the values of the loop inductances and parasitic capacitances. Therefore, a method is pursued to determine all relevant impedance values by only making use of switching/disconnection that can be applied without altering the layout. In Fig. 4.13 these switch or disconnection locations are already indicated:

- Location 0': The connection of the TCC at the MV/LV transformer, although it is not a switch, can usually be removed relatively easy.
- Location 0: The connection of the TCC to the rail system is often implemented with a switch (and fuses).

- Location 1 . . . N : Each connection of a MV cable to the rail system usually has its own switch.

In Fig. 4.15 a complete equivalent circuit of a typical RMU impedance is depicted, with the individual components modelled as discussed above. Note that the most right section (N), indicated with a box, is repeated for every connected MV cable (index j). To obtain the parameters L_j , $C_{\text{par}j}$, and $R_{\text{rad}j}(\omega)$ for every section, several switching and connection operations must be performed to isolate the various sub-circuits, in order to get unique solutions for the parameter values. For orthogonal parameter fitting, we require a maximum of only one pole and/or one zero in the impedance, and the real part of the impedance to contain only one constant value and one frequency dependent value. If these requirements are not met, allowed parameter ranges must be included for unique solutions. The measurement method, used in this section, is described in Section 4.4.3. For now it is sufficient to know that the method measures the impedance of a closed loop without interrupting the circuit. The impedance measuring method itself can be performed on energized circuits, since no galvanic contact is made.

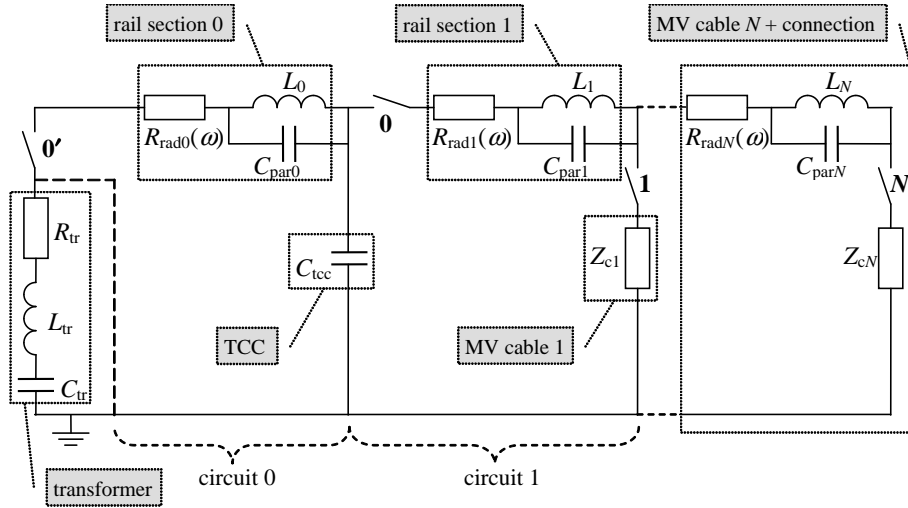


Figure 4.15 High-frequency model of substation or RMU with N connected MV cables

First, consider circuit 0, as indicated in Fig. 4.15. Connection $0'$ is mounted and switch 0 is open. This circuit incorporates the rail and connection parameters of section 0, together with the capacitance of the TCC. The transformer is bypassed to avoid multiple zeros in this loop. Note that the rail and connection parameters L_0 , $C_{\text{par}0}$, and $R_{\text{rad}0}(\omega)$ include the entire connection to the transformer and not only the rail system. Fig. 4.16 presents the measurement results, together with the fitted model. For frequencies below 500 kHz and above 5 MHz, the measurements start to show deviations. This is mainly caused by the lack of injected power due to the high impedance in those frequency ranges. Obviously for higher frequencies the model has to be extended and would become unnecessarily complicated for our purpose. The fitted values are indicated in the figure caption. The value of C_{tcc} is in agreement with the data sheets of the cables. The values for L_0 , $C_{\text{par}0}$, and l_a are values in the

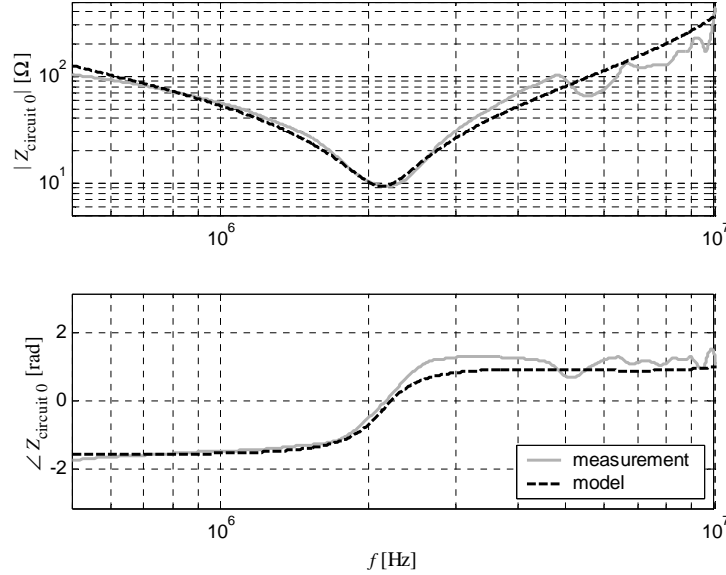


Figure 4.16 Measured and simulated impedance of circuit 0. The parameter values in the model are: $L_0 = 2.1 \mu\text{H}$, $C_{\text{par}0} = 70 \text{ pF}$, l_a in $R_{\text{rad}0}(\omega)$ is 9.7 m, and $C_{\text{tcc}} = 2.4 \text{ nF}$.

order of magnitude for what can be expected, considering approximated dimensions. Measurements of other RMUs show similar results as is e.g. indicated in earlier work [Wie04a].

Circuit 1 is formed by disconnecting point $0'$, closing switches 0 and 1, and opening all other switches. This circuit incorporates the impedance of rail section 1, together with the characteristic impedance of MV cable 1 and, again, C_{tcc} . Fig. 4.17 presents the measurements, together with the fitted model (parameters are indicated in the figure caption). Again good agreement can be established over a large range. For frequencies close to 10 MHz, the measurements start again to show inaccuracies due to low injected energy. The value of the characteristic impedance of MV cable 1 is in agreement with the earlier obtained values by means of propagation measurements (Chapter 3). As the dimensions of the loop, formed by the connections in section 1, are much smaller than those in section 0, the self-inductance of the loop is smaller and the parasitic capacitance is higher with respect to the values in circuit 0. The value of the effective antenna length l_a of 5 m may seem somewhat high, but it should be noted that it is an *effective* value, representing the sum of distributed radiation resistances of all connections. Assuming this effective length can roughly be approximated by the sum of the lengths of the involved conductors, it has the correct order of magnitude.

The procedure can be repeated for N sections for RMUs or substations with N connected MV cables. When measuring circuit j , with $1 < j \leq N$, switch j and $j - 1$ should be closed and all other switches opened. These circuits are similar to circuit 1, with C_{tcc} replaced by $Z_{c(j-1)}$, which is already known from the measurement of section $j - 1$.

For larger substations the same approach can in principle be applied. In a larger

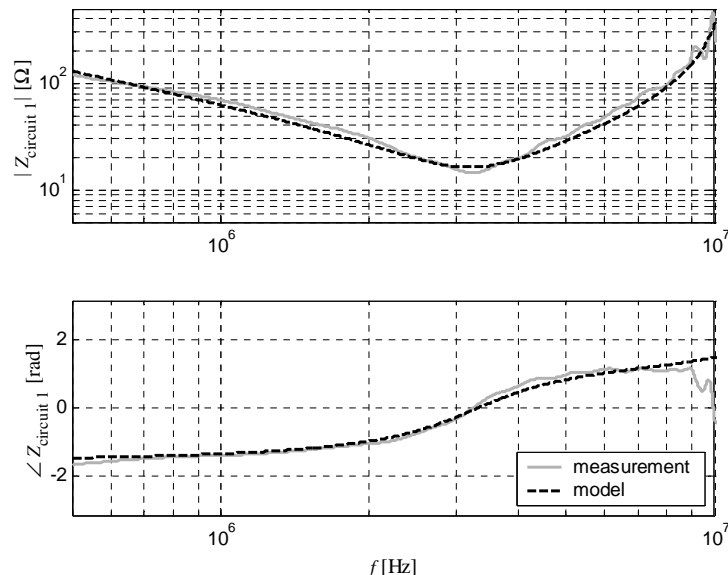


Figure 4.17 Measured and simulated impedance of circuit 1. The parameter values in the model are: $L_1 = 0.86 \mu\text{H}$, $C_{\text{par}1} = 250 \text{ pF}$, l_a in $R_{\text{rad}1}(\omega)$ is 5 m, $C_{\text{tcc}} = 2.4 \text{ nF}$, and $Z_{c1} = 14 \Omega$.

substation, more than one connected transformer may be present, including a HV/MV transformer. Although the same model for all transformers may be used, the connection can differ and dimensions are usually larger. This also refers to dimensions of the rail system. If dimensions approach the wavelengths of a few tens of meters, transmission line effects should be included to represent the introduced time delays. The presented model can serve as a base for more complex situations. The circuit elements in the indicated “rail sections” in Fig. 4.15 should then be replaced by transmission lines.

4.4.2 Total substation impedance

As the values of the single components in a RMU or substation are determined as described in the former paragraph, the total impedance can be modelled. In order to verify the total model, measurements on the same RMU as in Section 4.4.2 are presented in this section. The equivalent total circuit of this particular RMU, containing one MV connection, is depicted in Fig. 4.18.

With the on-line measurement method described in Section 4.4.3, the total RMU impedance is measured at the PLEC location, as is indicated in Fig. 4.18. The resulting impedance is shown in Fig. 4.19, together with the model simulation. The obtained impedances show good agreement up to about 9 MHz, above which deviations become significant. These deviations are again mainly caused by lack of injected power at those frequencies. The fact that high impedances show high measurement inaccuracy is of little concern, since it is the low impedance area that is of most interest for sensitive PD measurements.

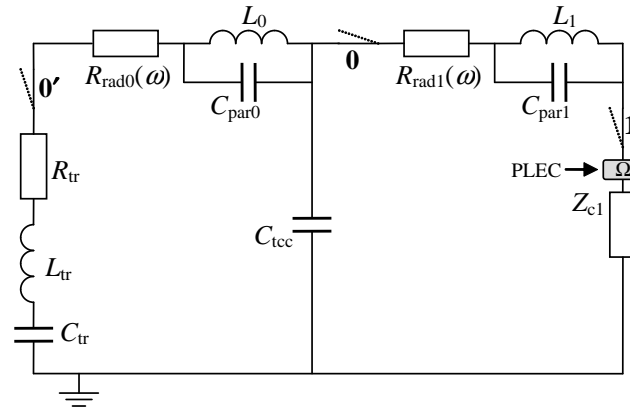


Figure 4.18 Model of RMU with one connected MV cable. The used parameter values are equal to the values given in Figs. 4.14 – 4.17.

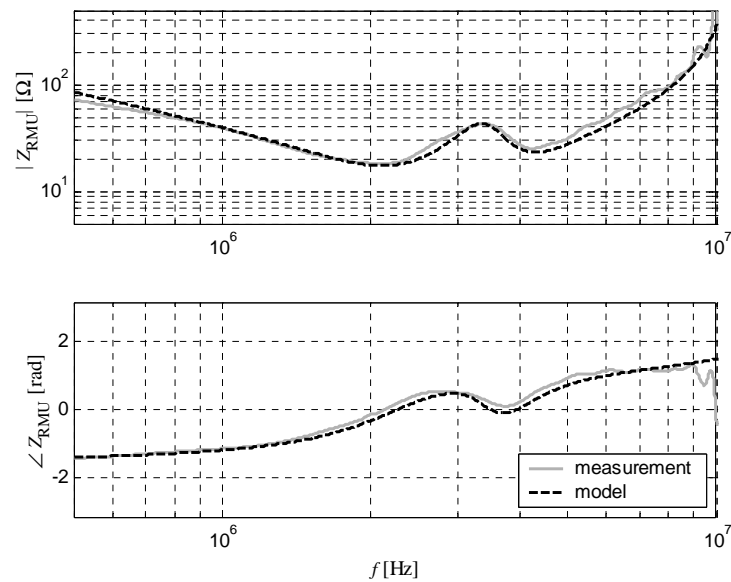


Figure 4.19 Measured and simulated impedance of RMU inclusive of one connected cable. The parameter values in the model are equal to the values given in Figs. 4.14 – 4.17.

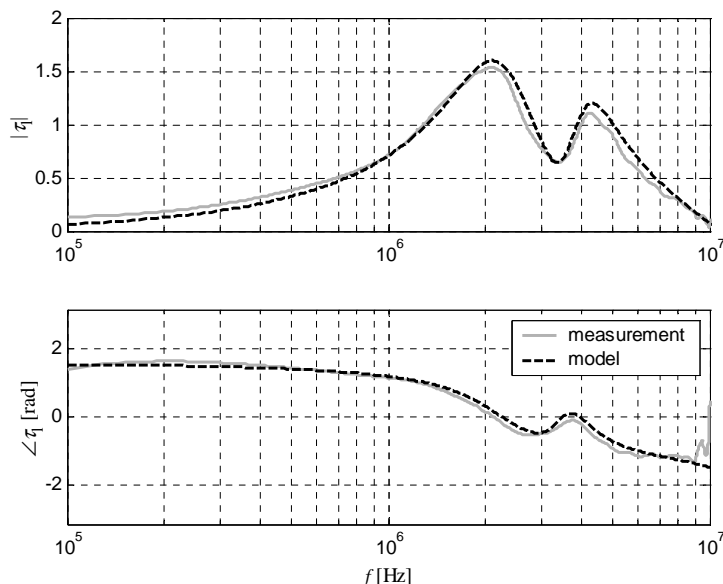


Figure 4.20 Measured and simulated transmission coefficient for current waves from the cable impedance to the load (RMU) impedance

For calculation of the load impedance of the MV cable, Z_1 , the characteristic impedance of the cable Z_{c1} should be subtracted from the total impedance of Fig. 4.19. The current transmission coefficient $\tau_1(\omega)$ for signals from the MV cable to its load impedance is calculated with:

$$\tau_1(\omega) = \frac{2Z_c(\omega)}{Z_c(\omega) + Z_1(\omega)} \quad (4.15)$$

In Fig. 4.20 $\tau_1(\omega)$ is plotted for both measurement and model simulations. It is clearly seen that outside the frequency range of 100 kHz – 10 MHz, only a small fraction of the current (< 5%) remains. This coincides with the earlier results for detection bandwidth based on propagation (Chapter 3) and disturbance level (e.g. Figs. 4.8 and 4.29). If more MV cables are connected to the substation or RMU, the impedance will drop further as can be directly derived from Fig. 4.15, since this results in a relatively small additional parallel impedance. The transmission coefficient in Fig. 4.20 can therefore in principle be regarded as a worst-case scenario for detection sensitivity.

4.4.3 On-line substation-impedance measurement

In Chapter 3 two measurement methods for propagation characteristics of an arbitrary device under test (DUT) are described: network analyzer and pulse response measurements. Both methods are able to determine the impedance of a substation or RMU as well. However, both methods require connection to the conductors of the DUT. A MV cable can usually be switched off relatively easy, since distribution grid structures often allow rerouting of the power delivery. Complete substations or RMUs can, however, not be switched off, since power delivery would be interrupted.

Therefore, it is essential to measure this substation impedance on-line.

To this end, inductive coils as described in Section 4.2 are used. As the magnetic coupling of these probes is reciprocal, they are used for both measurement and injection of current in the enclosed conductor(s). Fig. 4.21 shows a schematic drawing of the principle. The injection circuit (left) contains a probe with a transfer impedance

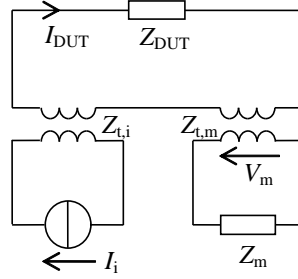


Figure 4.21 On-line impedance measurement method with an injection and measurement probe

$Z_{t,i}(\omega)$. As the coupling of toroidal current probes is small, the influence of the presence of the coils on the impedance of the DUT is neglected. Therefore the circuits can be described independently, using the simple model of Fig. 4.1. The induced current $I_{DUT}(\omega)$ through the impedance of the DUT is dependent on $Z_{DUT}(\omega)$. This current is measured with the circuit on the right-hand side in Fig. 4.21, resulting in a voltage over the measurement impedance Z_m . The total transfer impedance between $I_i(\omega)$ and $V_m(\omega)$ equals:

$$Z_t(\omega) \triangleq \frac{V_m(\omega)}{I_i(\omega)} = \frac{Z_{t,i}(\omega)Z_{t,m}(\omega)}{Z_{DUT}(\omega)} + Z_x(\omega) \quad (4.16)$$

In this equation $Z_x(\omega)$ is implemented to represent a possible direct cross-talk between the two coils if they are in close vicinity. $Z_x(\omega)$ is small for well designed probes as is discussed in Appendix B. As $Z_{t,i}(\omega)$, $Z_{t,m}(\omega)$, and $Z_x(\omega)$ can be calibrated a priori, $Z_{DUT}(\omega)$ is the remaining unknown parameter. In Fig. 4.22 a picture of the designed injection coil, mounted on a commercially available measurement coil is shown.

Fig. 4.23 shows test measurements using known resistor values to validate this method. The figure shows accurate impedance measurements up to at least 100 Ω . If the impedance of the DUT increases, the accuracy of this method decreases, since insufficient current is induced in the DUT. The figure shows a variation of approximately 20% when Z_{DUT} is 820 Ω . However, from Section 4.4.2 it is concluded that even in the ‘worst-case’ situation where no additional MV cables are connected to the substation, the impedance between 500 kHz and 10 MHz is sufficiently low. This validates both this measurement method and the principle of inductive PD measurement.

To verify the applicability of this on-line impedance measurement method for substations or RMUs, the method is applied to a complete RMU impedance and compared with results from the network analyzer and pulse response measurement. The measurements are performed on a full-scale test set-up at KEMA in the Netherlands. This test set-up can, in contrast to normal RMUs in the field, be disconnected from the power to enable methods requiring a galvanic connection. Fig. 4.24 shows the results. All methods are in good agreement between 1 and 10 MHz. Below 1 MHz the



Figure 4.22 Photo of the designed injection coil, mounted to a commercially available measurement coil (Fischer CC F-70)

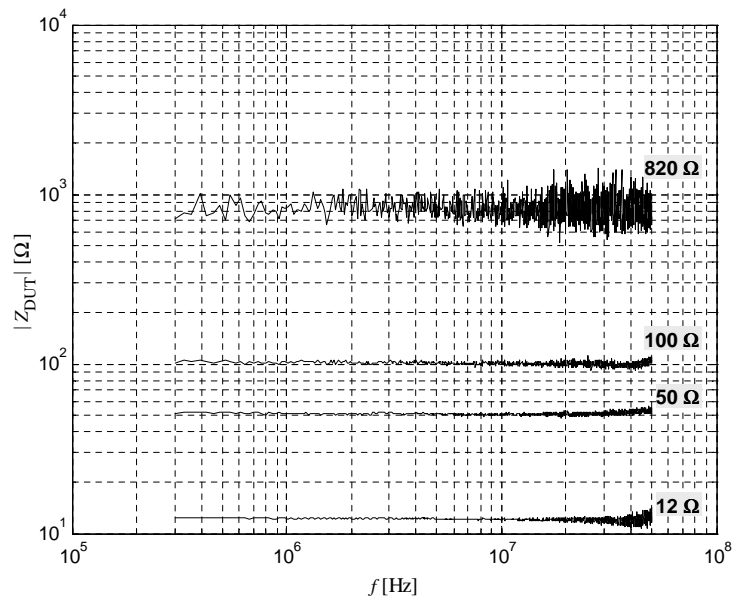


Figure 4.23 Measured impedance with the on-line impedance-measurement method. The lines represent the measured values, the labels on the right the given resistance values.

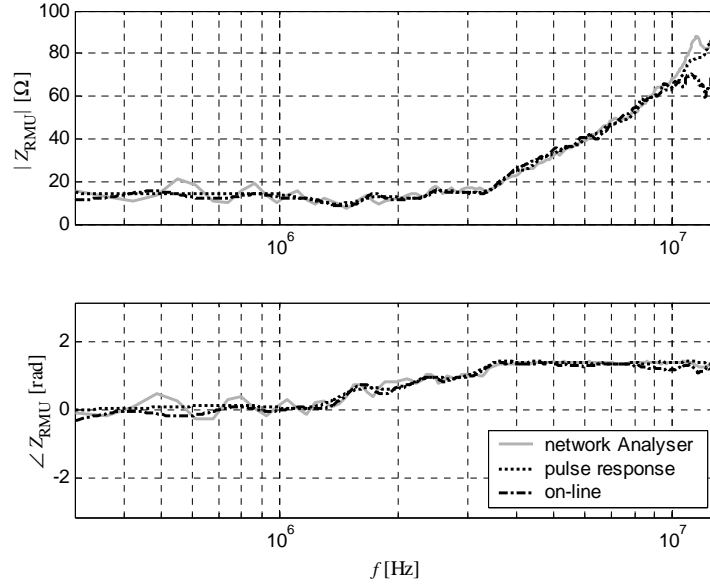


Figure 4.24 Measured impedance of a RMU using three measurement methods. The RMU incorporated a MV/LV transformer and one connected MV cable.

network analyzer measurements show small resonances in the frequency domain due to the presence of reflections from the cable far end. These can be removed as shown in Chapter 3, but this is omitted here, as no extra information would be gained since the two other methods already correspond well for low frequencies. For frequencies above 10 MHz, the on-line measurement method starts to deviate considerably. The available pulse generator, capable of injecting high currents in the injection probe, does not provide enough power above 10 MHz for accurate measurements in that frequency range. Increasing high-frequency power is, however, not advisable, since this can easily interfere or damage other equipment present in a substation.

The described on-line impedance measurement method is able to determine the impedance of a closed circuit. In the case of a complete substation or RMU impedance measurement, the closed circuit also incorporates the characteristic impedance of the CUT itself, see Fig. 4.18. Section 4.5 will provide a method to distinguish the impedance of the CUT from its load impedance if both impedances are unknown.

4.5 On-line system identification

If a measurement is applied, with sensors in the two substations or RMUs connected by the cable under test, the following components should be characterized:

- A MV cable system, consisting of N cable sections of which each section j is characterized by its characteristic impedance $Z_{c,j}(\omega)$, attenuation constant $\alpha_j(\omega)$, phase-shift $\beta_j(\omega)$, and length l_j . All parameters are related to the used propagation channel. Values for N and l_j can in principle be provided by the

utility.

- Two connected substations or RMUs with total impedances $Z_{1,1}$ and $Z_{1,2}$ as relevant parameters for on-line PD detection.

First consider uniform cables, i.e. cables with only one section or more sections with one, equal cable type. In Section 4.4.3 a method was proposed to determine the sum of both the CUT's characteristic impedance Z_c and its load impedances, i.e. the substation impedances $Z_{1,i}$ of the connected substations/RMUs i with $i \in \{1, 2\}$. This sum impedance is denoted as $Z_{T,i}$. If the injected pulse at cable end 1 has sufficient energy in the frequency range of interest to be detected after propagating to cable end 2, reflecting at side 2 and propagating back, the transfer function between injected and reflected pulse is:

$$H_{r,1}(\omega) = \tau_{1,1}(\omega) \cdot (\tau_{1,2}(\omega) - 1) \cdot e^{-\gamma(\omega)2l_c} \quad (4.17)$$

where $\tau_{1,i}(\omega)$ is the transmission coefficient for an incident signal from the cable to the load impedance $Z_{1,i}$:

$$\tau_{1,i}(\omega) = \frac{2Z_c(\omega)}{Z_c(\omega) + Z_{1,i}(\omega)} = \frac{2Z_c(\omega)}{Z_{T,i}(\omega)} \quad (4.18)$$

Now, first assume that the cable's characteristic impedance is known. Then, if $Z_{T,i}$ is determined by the method from Section 4.4.3, both $Z_{1,i}$ and $\tau_{1,i}(\omega)$ are determined and the cable's remaining propagation characteristics result from:

$$\alpha(\omega) = -\frac{1}{2l_c} \ln \left[\frac{|H_{r,1}(\omega)|}{|\tau_{1,1}(\omega)| |\tau_{1,2}(\omega) - 1|} \right] \quad (4.19a)$$

$$\beta(\omega) = -\frac{1}{2l_c} [\angle H_{r,1}(\omega) - \angle \tau_{1,1}(\omega) - \angle (\tau_{1,2}(\omega) - 1)] \quad (4.19b)$$

The remaining unknown parameter is the characteristic impedance of the cable. Since $Z_c(\omega)$ is usually independent of frequency (Chapter 3), the system is now determined up to this factor. This factor is only needed for estimating the PD magnitude. In order to find its value the procedure for pulse injection and determination of the transfer function between injected and reflected pulse (Eq. (4.17)) is repeated on cable end 2, and the ratio between $H_{r,1}(\omega)$ and $H_{r,2}(\omega)$ becomes:

$$\frac{H_{r,1}(\omega)}{H_{r,2}(\omega)} = \frac{\tau_{1,1}(\omega)[\tau_{1,2}(\omega) - 1]}{\tau_{1,2}(\omega)[\tau_{1,1}(\omega) - 1]} \quad (4.20)$$

which, together with Eq. (4.18), provides for the cable characteristic impedance:

$$Z_c(\omega) = \frac{Z_{T,1}(\omega)H_{r,1}(\omega) - Z_{T,2}(\omega)H_{r,2}(\omega)}{2[H_{r,1}(\omega) - H_{r,2}(\omega)]} \quad (4.21)$$

Since $Z_{T,i}(\omega)$ is known, the cable characteristics and thereby the complete system is identified.

For cable systems with more than one cable section, the same approach can be applied. The main difference is that instead of only the reflection on the far end, all reflections from the cable section transitions should be considered. Since reflections

from cable section transitions are in practice very small, presence of noise and interference can impair the accuracy. Furthermore, resonances from the substation(s) or RMU(s) and multiple reflections between joints will make estimating accurate parameters of the single cable sections hard. Due to these practical implications, the method for separation of the cable sections is not further elaborated here. However, a successful preliminary measurement is described in [Vee05].

4.6 Partial-discharge signal analysis

Partial-discharge detection is impeded with noise and other disturbing signals. The subject of signal analysis is described thoroughly in [Vee05]. The basic principles important for this thesis are summarized in this section.

4.6.1 Signal extraction

Signal extraction involves recovery of PD data from measured signals that are impeded by noise. Since the channel characteristics are constant during measurement, the PD signal shapes can be regarded as deterministic. If only the PD pulse waveform is known, a matched filter maximizes the SNR for PD pulse detection [Tre68, Wha71, Wai62]. Therefore a matched filter is theoretically the optimal method for signal detection in the presence of noise, provided that the signal waveform and the noise spectral power distribution are known.

Principle of matched filters

For colored noise, the transfer function of a matched filter is defined as:

$$H_m(\omega) \triangleq A_m \frac{V_{PD}^*(\omega)}{P_N(\omega)} \quad (4.22)$$

where $V_{PD}(\omega)$ is the frequency spectrum of the PD signal to be detected, A_m a scaling factor (explained later), and $P_N(\omega)$ the noise power spectral density function, defined as:

$$P_N(\omega) \triangleq E \{ |V_N(\omega)|^2 \} \quad (4.23)$$

where $E\{\cdot\}$ denotes the expectation and $V_N(\omega)$ the frequency spectrum of the noise. As the expectation of the noise is in principle not known, it is estimated by the average of the noise spectrum of multiple long data records, assuming the signal power can be neglected compared to the noise power. The PD signal spectrum, required for the matched filter, is derived from the cable model of Chapter 3, together with the load impedance of the substation or RMU (incorporated via $\tau_{(N \rightarrow N+1)}(\omega)$) and the sensor transfer impedances $Z_t(\omega)$:

$$V_{PD}(\omega) = Z_t(\omega) \prod_{j=1}^N e^{-\gamma_j(\omega)l_j} \tau_{(j \rightarrow j+1)}(\omega) \quad (4.24)$$

Note that only the first arriving pulse is considered, not its reflections. In addition to its noise suppressing capabilities, a matched filter also provides a means to determine the PD charge. Since the charge of a PD pulse is unknown a priori, the filter is

matched to a scaled (to unity charge at $z = 0$) version of the modelled pulse in Eq. (4.24), with scaling factor A_m . As the maximum filter output upon filtering the expected signal is proportional to the energy of that signal, this value, together with scaling factor A_m , provides for the apparent charge of the PD signal at the place of origin. In Section 5.4 it is shown that also the time of arrival of the measured pulse can be determined accurately by means of matched filters.

A matched filter maximizes the SNR of the filter output signal, [Wha71]. Intuitively this statement becomes clear by recognizing that filtering a waveform is equivalent to calculating the cross correlation of the waveform and the time-reversed filter impulse response. If the time-reversed impulse response equals the waveform itself, which is the case for the matched filter, then the filter output signal equals the autocorrelation function of the waveform. The output signal of any other filter with the same energy as the matched filter has a lower peak value. Fig. 4.25 shows a visualization of the principle of matched filtering by showing both the expected signal frequency spectrum, together with the matched filter transfer function. Each frequency component of the input signal is weighted corresponding to the component's SNR. Frequency components with relatively high SNR contribute strongly to the filter output signal, while signals with low SNR do not, thus optimizing the overall SNR of the output signal.

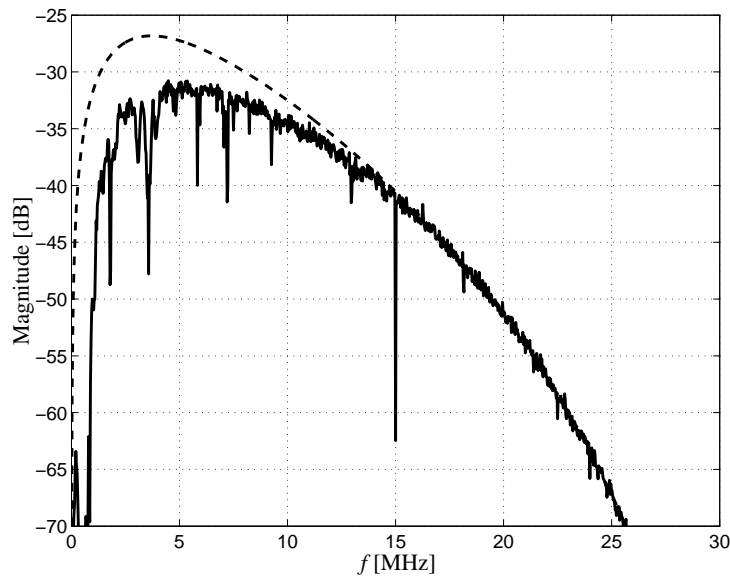


Figure 4.25 Visualization of the principle of a matched filter. The solid line shows an example of the transfer function magnitude of a matched filter for colored noise, preceded by a whitening filter. Frequency components with low SNR are suppressed, for example around $f = 15$ MHz where the SNR is very low. Thus for narrow band noise, the matched filter acts as a notch filter. The dashed line provides the matched filter response for white noise, i.e. the amplitude spectrum of the PD signal.

Matched-filter bank

In practice, partial discharges originate from various locations within the cable under test. As PD pulses propagate through differing paths, a variety of PD waveforms arrives at the detection location, see Fig. 4.26. Thus PD analysis based on matched

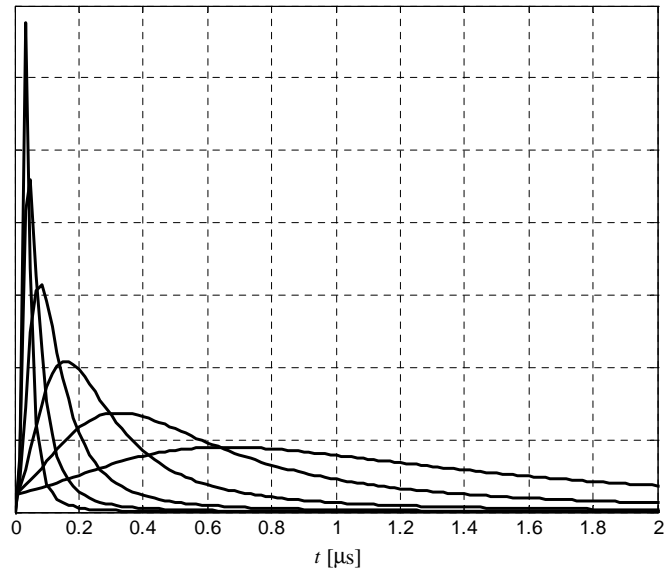


Figure 4.26 Example of MFB templates. The templates are waveforms of a simulated PD that propagated 70, 170, 380, 860, and 1900 m through a 12.5 kV, $3 \times 95 \text{ mm}^2$ PILC cable, [Vee05].

filter technology must employ a range of matched filters, i.e. the system must employ a matched-filter bank (MFB) as depicted in Fig. 4.27. In practice, PD pulses that originate close to each other propagate through nearly the same path, and the waveforms are similar. In the case of power cable testing, a PD pulse that has travelled through 500 m of cable does not differ appreciably from a pulse that has propagated 100 m more (see also Section 5.2.1). Thus a limited number of filters is sufficient to match every PD signal from the test object.

In conventional detection, pre-filters, i.e. analog band-pass filters, which define the detection bandwidth, are generally employed. Since PD pulses may propagate through different paths, their frequency contents may differ considerably, and the detection bandwidth cannot be ideal for every waveform. A matched-filter bank automatically selects the optimal detection bandwidth for each waveform, and therefore brings a practical benefit relative to analog pre-filters.

When a PD signal is filtered by a MFB, multiple output signals are obtained. If the matched filters have equal energy, the filter that matches best to the input signal gives maximum output amplitude, Fig. 4.28. Since the differences between the filters of the MFB are purely based on a PD signal propagation model, the best matching filter also provides an estimate of the PD location.

A MFB can be regarded as a signal analysis bank, comparable to analysis banks

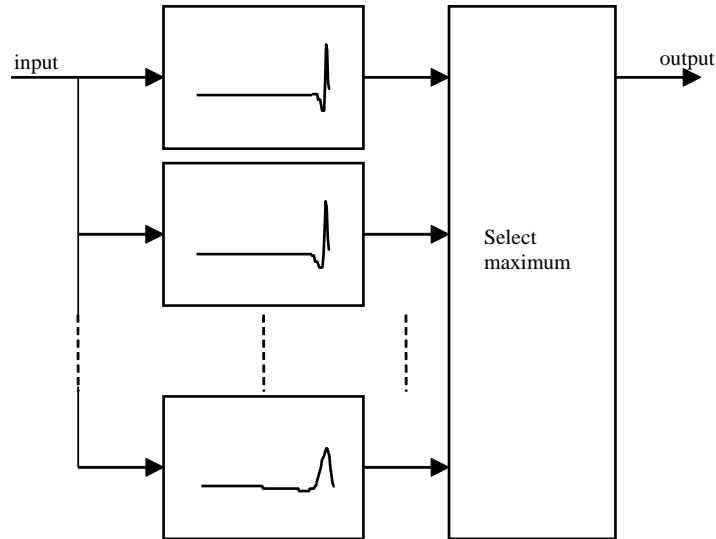


Figure 4.27 Simple representation of a partial-discharge matched-filter bank

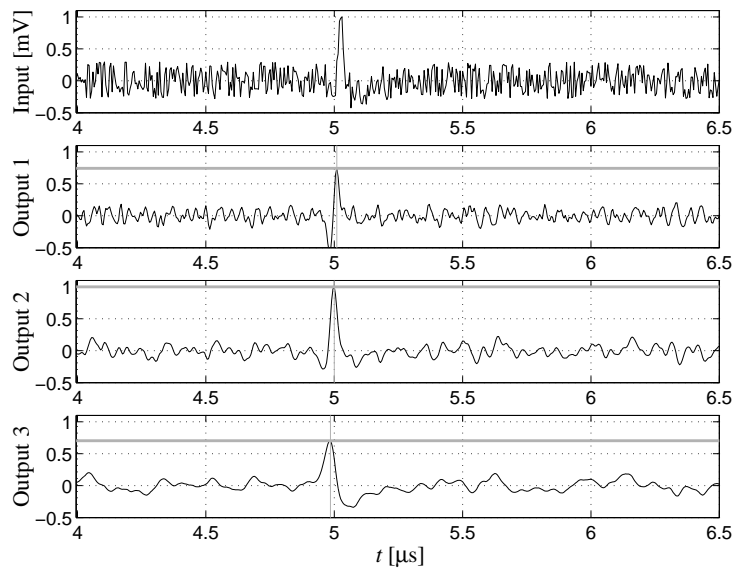


Figure 4.28 A PD signal corrupted by white noise is applied to a matched-filter bank with three filters.

used in decomposition methods such as the wavelet transform (e.g. [Shi01]). Such decomposition methods transform signals to some domain where decisions on the signal properties can be made more easily or where noise can be suppressed. Contrary to a matched filter, a wavelet synthesis bank allows unambiguous reconstruction of the original signal. However, in case of PD detection and location, reconstruction of a signal from the transform coefficients is generally not required, since decisions can be made and parameters can be estimated directly in the transform domain.

4.6.2 Disturbance rejection

Power cables, especially paper-insulated lead-covered cables are well shielded and will not pick up much disturbance along the cable itself. At the cable terminations, in the substations or RMUs, and in the rest of the power grid, however, many open structures will pick up many disturbing signals, from outside but also from the power system itself. The relevant interference that impedes PD detection can be categorized into three main groups: noise, continuous periodic interference, and finite-energy disturbance.

Noise

Stochastic broadband background signals result from a summation of numerous natural and artificial sources. It can therefore be considered to be stationary or slowly-varying. As a consequence, the PSDF can be estimated accurately by former data sets. The possibly small variations can be incorporated if an adaptation process is applied. Fig. 4.29 shows a typical PSDF estimate of an on-line MV cable. The noise level increases considerably below 1 MHz.

Matched filters are the optimal filters for producing a high SNR, provided that good estimation of the PSDF and the expected signal shape can be achieved. Since the only measure against noise (after the signal is acquired) is obtaining maximum SNR by optimal filtering, this type of noise is taken into account.

Continuous periodic interference

Narrow-band broadcast is generally the main type of disturbance when considering measured amplitudes. Preliminary measurements showed continuous wave voltages that were multiples of PD signal amplitudes. Obviously, this depends on the actual PD magnitude at that moment, so general statements about values are hard to make. The PSDF in Fig. 4.29 shows pronounced narrow-band peaks, indicating high levels of carrier waves. As the preliminary measurements showed slow variation of the presence and magnitude of these narrow bands, adaptation of the filtering is necessary. Since the (matched) filtering is performed digitally, high-order notches can be (automatically) implemented in the matched filter so strong suppression is achieved. Furthermore, the continuous periodic interferences are very narrow-banded, while PD signals are in principle very broad-banded. This results in a matched filter with enough remaining frequency content.

However, there is one implication involved with high levels of periodic interference: the data-acquisition system requires a high dynamic range, i.e. many bits in the analog-to-digital conversion (see Chapter 6).

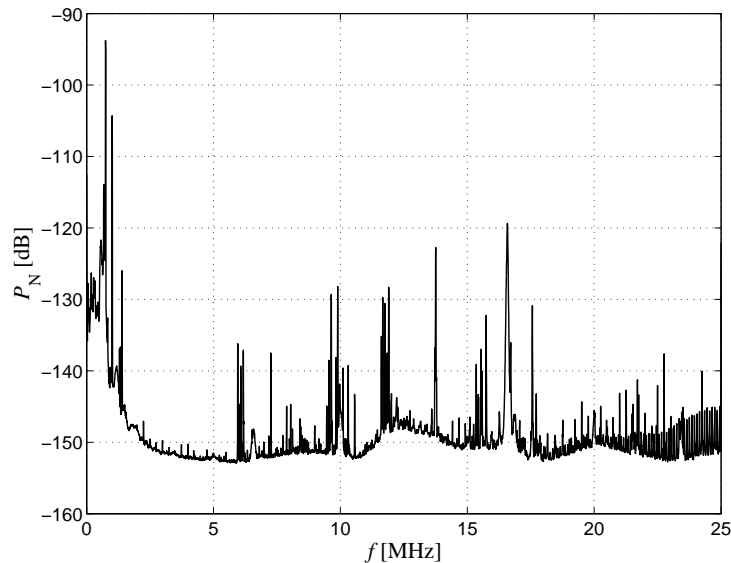


Figure 4.29 Typical power spectral density function of an on-line MV cable, measured with a current probe at the cable termination (PLEC)

Finite-energy disturbance

Finite-energy disturbances are pulses of short duration and can originate from many sources, e.g. thyristor pulses, power switching or PDs from adjacent equipment (transformer, other connected MV cables). As all these types of pulses are regarded as disturbances, the system must incorporate methods to reject them. Matched filters, constructed as discussed earlier, may not contribute to rejection of these signals as they might have frequency content comparable to the PD signals from the CUT. If certain finite-energy pulse-shapes appear often, filters that are matched to these signals can be implemented in the MFB, after which this filter will produce the highest output upon subsequent reception of this signal, and rejection can be established. For further rejection of finite-energy pulses, other expert rules of the system (e.g. directional sensing, charge polarities, see Chapter 6) are applied.

4.6.3 Simulations and measurements

In Fig. 4.30 the matched filter technique is compared with other filtering techniques. A simulated PD signal is corrupted by colored noise and a number of radio stations. Output 1 equals the signal filtered by a simulated analog pre-filter, which consists of a low-pass filter with a cut-off frequency around 8 MHz and notch filters at the appropriate frequencies. Output 2 equals the signal filtered by a matched filter for colored noise, which has been specifically adapted to the specific noise spectrum. Clearly, the matched filter output has the better SNR.

In an experiment, blocks of data were recorded during on-line PD measurements on a 500 m PILC cable system. Based upon knowledge of the cable system which was provided by the utility, a matched-filter bank was designed. The recorded data blocks were used to estimate the noise spectral distribution, and the matched-filter bank was

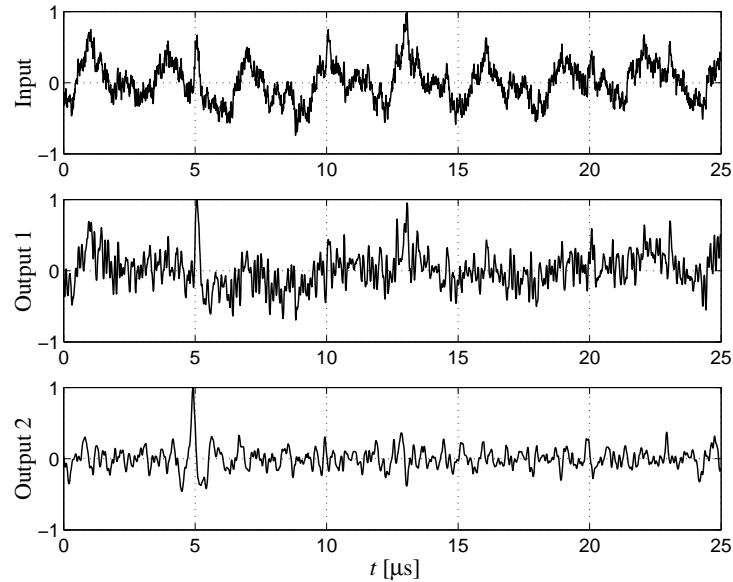


Figure 4.30 Comparison of different filtering techniques upon a simulated PD signal which is corrupted by colored noise and a number of narrow-band carrier waves. Output 1 equals the signal filtered by a simulated analog pre-filters, consisting of a low-pass filter with a cut-off frequency around 8 MHz and some notch filters at the appropriate frequencies. Output 2 equals the signal filtered by a matched filter.

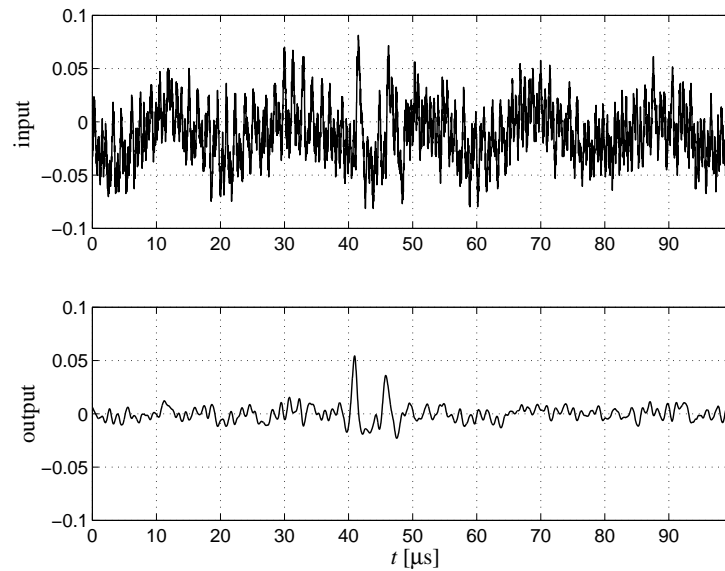


Figure 4.31 PD signals corrupted by colored noise were filtered by a MFB and the output of the best matching filter is selected.

adapted to the noise. Subsequently, the measurements were applied to the matched-filter bank. In Fig. 4.31, a small frame of measurement data and the corresponding output of the best matching filter are plotted. Clearly, the matched filter is able to suppress the noise and enhance the SNR of the PD signal.

4.7 Conclusions

Safety issues for on-line installation of a PD detection system require different sensor types for on-line as compared to off-line PD detection. For on-line partial-discharge measurements, inductive toroidally-shaped sensors are the most suitable sensors. The design of the sensor should prevent high level of EM disturbance by proper shielding. Interference from external magnetic fields can be eliminated by proper design of Rogowski-type coils. Shielding against external electrical fields can be accomplished with a common shield around the complete probe or by using coaxial cable for the windings. The latter method enables relatively simple mechanical construction, thereby providing for a good alternative to commercially available probes. Measurements of the transfer impedance and shielding effectiveness confirmed the applicability for on-line PD diagnostics.

The possible sensor positions in a substation or ring main unit (RMU) depend on the type of switchgear. Generally, for shield-to-phases (SP) channel measurements, the preferred sensor position is around the cable past the last earth connection (PLEC). The cables which connect the transformer, if present, to the HV rail system can provide phase-to-phase (PP) channel measurements, although sensitivity is considerably lower. The earth connection of these cables enables also directional sensing. Combination of the signals from this location, together with the PLEC location, can provide the propagation direction of the detected pulses, thereby rejecting or eliminating disturbing signals from other sources.

A model for the connected substation(s) or RMU(s) is presented to determine the load impedance of the cable under test. An experimental procedure is presented to identify the parameters of the complete cable system, including the substation impedance. Measurements showed that the model is able to describe the cable and the RMU/substation sufficiently accurate in the frequency range optimal for PD detection (1-10 MHz), which coincides with the bandwidth resulting from propagation (Chapter 3) and disturbance considerations.

The extraction of PD signals from field data, which is impeded by noise and interference, is performed with matched filters. For a known system model and noise spectrum, this method optimizes the SNR. Simulations and experiments show the applicability of the matched filtering technique for PD extraction.

Partial-discharge source location

Upon detection of a partial-discharge signal the place of origin, i.e. the place of the PD itself, can be determined to support the interpretation of the results and enhance its reliability. Location involves determination of both the cable system producing PDs and the PD place along its cable length. This chapter will show that these two objectives are connected. As the preferred method for location involves accurate time-base alignment of multiple measurement units, several synchronization methods are discussed. A suitable method, involving pulse injection into the cable under test, is proposed. Furthermore, accurate location requires accurate determination of the time at which signals arrive at the detection location. A general method to perform this time-of-arrival estimation is discussed. Several measurements validate the presented methods.

5.1 Introduction

When detecting PDs in long medium-voltage power cables, several parameters can be defined for interpretation of the results: PD charge, PD density, phase-pattern, etc. (e.g. [Ste91, Kre93a, IECb]). In on-line measurements, these parameters can also be monitored during longer periods of time, so specific trends can be observed [Bow00, Wal01]. To get good estimates of these parameters and to perform optimal detection in a possibly noisy environment, models of the total cable and detection system are essential. In Chapters 3 and 4 these models have been discussed and methods for detection of PDs were presented. These parameters will gain in significance if they can be related to the origin of the corresponding PDs, since:

- Knowledge about the presence of PD activity from a few weak spots along the cable length is usually more interesting than average PD numbers from the overall cable length. A slight increase of PD activity along the total cable length is usually normal behavior for e.g. a paper-insulated lead-covered (PILC) cable and therefore no reason for concern, whereas a severe weak spot in e.g. one joint or localized weak spot can easily produce the same total amount of PD activity; but here, action is needed.
- The type of cable or accessory can be taken into account, each with its own record of PD behavior from earlier experience and aging characteristic (e.g.

[Mas00, Kre93a]).

- The history of that specific part of the cable system can be tracked, including replacements, failures, etc.
- Local environmental conditions of the cable also influence the PD behavior (moisture, temperature, crossings with roads, tunnels, etc.), see e.g. [Ste00].
- For on-line situations, the cable terminations are connected to adjacent cables and equipment from which PDs and disturbances can originate too. Location allows distinguishing between PDs from the cable under test (CUT) and other sources, see Section 5.2.
- Besides the total amount of PDs (per time unit) also the concentration of PDs or charge per length unit can be determined.
- Obviously, the weak spot or section must be located prior to repair.

For off-line PD measurements, location has already been applied for over a decade and is included in several measurement systems, e.g. [Ste91, Mas92, Lem96, Gul98]. Location is often performed by means of time-domain reflectometry (TDR), which is usually the preferred method for off-line cable from lengths up to 4 km. If the length of the cable connection is longer or if it is branched, multiple-sided measurement can be applied [Ste01].

On-line measurement techniques on MV cables already exist, but usually without PD location capability, e.g. [Wal01, Wes02]. In [Ahm01] a system is described to locate PDs for short cables, whereas for longer cables multiple sensors, installed in the accessories, are required. For on-line measurements on HV cables, the method of using multiple sensors, placed in the several accessories along the cable length, is already applied successfully (see e.g. [Pom99, Hen96]). Obviously, this option is too expensive for distribution-class cable connections.

In this chapter research for a general solution for location of on-line measured PDs in distribution-class cables is reported. In Section 5.2 several partial-discharge location methods are evaluated for their applicability to on-line measurements. These methods include pulse-shape detection, TDR, and two- (or multiple-)sided measurement. As systems using the latter method require alignment of the time-bases of the measured records, various methods are evaluated in Section 5.3. Time-base alignment includes both synchronization of the start of measurements and possible time-wander correction. Section 5.4 discusses a general method to obtain accurate time-of-arrival (TOA) estimation of the involved signals. In Section 5.5 the conclusions of this chapter are summarized.

5.2 Methods for partial-discharge source location

5.2.1 Pulse-shape based location

The attenuation of signals that propagate along the cable varies for different frequency components (Chapter 3). This, together with dispersion, results in deformation of the original partial-discharge signal. Both effects increase with increasing distance. Since the PD pulse shape at the source can be approximated to be a delta pulse for the considered frequencies, the measured pulse shape at the cable end is an indication of the travelled distance and therefore of the PD source location.

To discuss this method, we will omit the effects of load impedance and sensor

transfer. These influences are constant and independent of travelling distance and PD location. We are only interested in the effects of the propagation properties, since these are responsible for gradually changing the pulse shape as a function of distance. Results can directly be applied to a complete system incorporating these influences.

Considering the first arriving pulse, the change of (current) pulse shape during propagation through a power cable system can be described by $H_T(z, \omega)$ in Eq. (3.63). The current at the PD origin ($z = 0$) can be modelled by a delta pulse and a scaling factor $Q_{\text{app}}/2$, half the induced charge, since at the point of PD excitation two equal signals start propagating in both directions. Furthermore, the measurement cannot be synchronized with the PD excitation; the time t_0 at which the PD signal starts is unknown. The propagation time of the channel is incorporated in the imaginary part of the propagation constant ($t_c = \beta(\omega)z/\omega$, independent of ω if dispersion is neglected). The measured current at the end of a cable system is given by:

$$I(z, \omega) = \frac{1}{2}Q_{\text{app}}H_T(z, \omega)e^{-j\omega t_0} \quad (5.1)$$

If the propagation channel $H_T(z, \omega)$ is known, the remaining unknowns in this equation are: Q_{app} , t_0 , and z . Q_{app} is just a scaling factor and t_0 a time shift, so the only remaining variable for the pulse shape is z .

The accuracy of this method is determined by the level of pulse shape variation as a function of the propagation distance z . Since we consider the characteristic impedances of the propagation channel to be constant in the frequency range of interest, the transitions between different cable sections in a cable system will only introduce scaling factors $\tau_{(j \rightarrow j+1)}$, independent of frequency. This allows us to examine the efficiency of pulse-shape based location by considering only one cable section with one propagation constant. In Fig. 5.1 pulse shapes are shown for a simulated discharge in a (8/10 kV, $3 \times 95 \text{ mm}^2$ Cu) PILC cable, using the model of Chapter 3 and plotted for propagation distances linearly spaced between 100 and 1000 m. As can directly be seen from this figure, the difference in pulse shape decreases with propagation distance, as can be expected considering the general form of the propagation function (Eq. (3.37)).

If pulses are detected by means of matched filtering (Section 4.6), a good measure to test the resolution mathematically is the maximum cross-correlation of the pulse shape from a specific location with the next location. Since we like to have a location resolution of approximately 20 m, Fig. 5.2 shows the maximum cross-correlation of the signal from each location z with the signal from $z - 20$ m. This normalized maximum cross-correlation approaches 1 very fast as propagation distance increases. As long as this function does differ from 1 with sufficient confidence margin, difference in pulse shape is detectable and location can be performed by means of this method. However, if noise is introduced, the maximum cross-correlation allowed for pulse shape distinction to remain possible decreases, meaning that only very small total propagation distances (tens of meters) can be distinguished. A detailed analysis of the influence of noise can be found in [Vee05].

5.2.2 Time-domain reflectometry

Time-domain reflectometry is used in many off-line PD measuring techniques (e.g. [Ste91, Mas00]). If at the PD location a PD pulse is induced in the cable, the pulse will propagate in both directions. The measuring equipment is installed at one cable

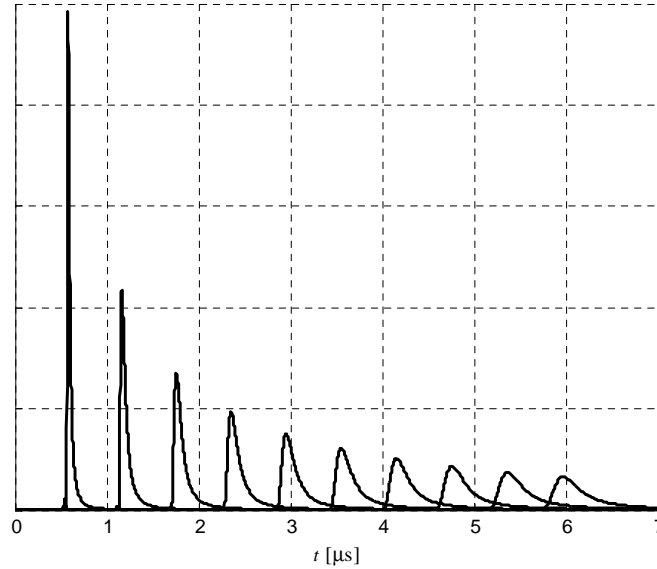


Figure 5.1 Pulse shapes of simulated discharge (modelled as a delta function) in SP channel at propagation distances of (from left to right) 100 up to 1000 m with increments of 100 m. The model from Chapter 3 is used for the SP channel of a (8/10 kV, $3 \times 95 \text{ mm}^2$ Cu) PILC cable.

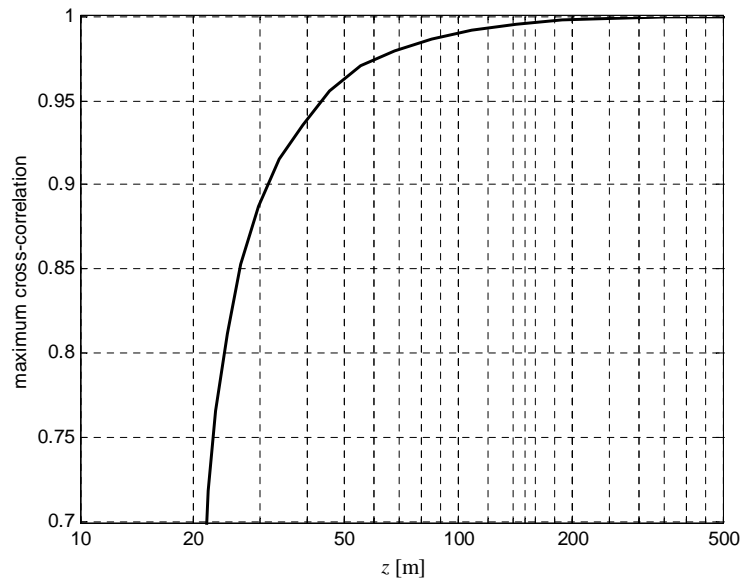


Figure 5.2 Normalized (on power) maximum cross-correlation of the signal at location z with $z - \Delta z$, with $\Delta z = 20$ m. The model from Chapter 3 is used for the SP channel of a (8/10 kV, $3 \times 95 \text{ mm}^2$ Cu) PILC cable with measured dielectric constant.

end. One of the pulses is travelling directly in that direction and arrives at a certain time $t_{\text{oa}1}$. The pulse travelling in the opposite direction will reflect at the far end of the cable after which (part of) it will propagate back through the cable towards the near end and arrive at time $t_{\text{oa}2}$. The difference in time of arrival (DTOA) is defined as:

$$\Delta t_{\text{oa}} \triangleq t_{\text{oa}2} - t_{\text{oa}1} \quad (5.2)$$

and is the time needed for the second pulse to travel from the PD location to the far end of the cable and back. If the total cable length l_c is known and the velocities of the different cable sections are assumed to be equal, the propagation distance of the PD pulse to the near end of the cable is:

$$z_{\text{PD}} = l_c - \frac{\Delta t_{\text{oa}}}{2} v_c \quad (5.3)$$

where v_c is the propagation velocity of the total cable system. In practice, sometimes the length of the measured cable nor its velocity is known. In this case, for installed, buried cables, only the total (single) propagation time t_c can be measured. The factor between brackets in

$$z_{\text{PD}} = \left(1 - \frac{\Delta t_{\text{oa}}}{2t_c}\right) \cdot l_c \quad (5.4)$$

gives the relative distance to the PD origin.

If the velocities of the different cable sections are not equal, v_c in Eq. (5.3) can be replaced with the weighted average velocity \bar{v}_c of the total cable-connection, resulting in an approximation for PD location. This introduces an error which, obviously, is dependent on the variation in the different velocities, see also [Kre93b]. To avoid this error the complete cable model from Section 3.5 can be used to calculate the different propagation velocities of each cable section and the propagation distance becomes:

$$z_{\text{PD}} = l_c - \frac{\Delta t_{\text{oa}}}{2} \bar{v}_2 \quad (5.5)$$

where \bar{v}_2 is the weighted average value of the propagation velocities in the sections of the cable system at the far side (side 2) of the PD location. The average velocities are weighted with respect to propagation time:

$$\bar{v}_x = \frac{\sum_{i \in N_x} l_i}{\sum_{i \in N_x} \frac{l_i}{v_i}}, \quad \text{with } x \in \{1, 2, c\} \quad (5.6)$$

where N_x is the set of numbers indicating the cable sections in part x of the cable, which can be the cable part at the near side (1) of the PD origin, the far side (2) of the PD origin, or the total cable (c).

This method is convenient for PD measurements, since the measurements can be carried out at only one cable end. However, in order to apply TDR, the following conditions have to be met:

1. The total attenuation and dispersion are not too large. As pulses propagate along a cable, both amplitude and shape are altered with propagation distance (Chapter 3). For longer propagation distances the amplitude decreases and the

resulting signal-to-noise ratio (SNR) becomes too low to detect the PD pulses. Furthermore, along with the propagation distance, high-frequency components are lost and TOA estimation becomes less accurate, resulting in inaccurate PD origin estimation ([Kre93b]). Since TDR requires accurate detection of both the first arriving pulse and the far end reflection, propagation lengths vary from 0 up to $2l_c$. For off-line PD measurements this usually results in maximum lengths for cable connections to test of up to about 4 km, depending on the noise level and required sensitivity.

2. The disturbance level is low. In off-line situations the cable under test is disconnected from the grid and disturbances coming from adjacent equipment are eliminated. The cable is powered with a separate generator, where filters can ensure minimal resulting noise levels. With cables on-line, the noise levels can be much higher, since disturbance present on the grid can easily propagate into the CUT.
3. The reflection at the far end is detectable. In case of off-line measurements, the far end is open, providing full reflection. On-line cables are connected to substations or ring main units (RMUs) that have a certain impedance, depending on their configurations (Section 4.4). Since this impedance is neither very low nor very large, compared to the cable's characteristic impedance, the reflection is usually small and PD signal reflections may not be detectable at all.
4. The cable network is not branched. In some countries, a cable system sometimes not only consists of a direct cable connection from one RMU or substation to another, but can also have branches along the connection. The points where the cable system is branched introduce additional reflection points. If only first reflections from each branch are detected, this results in non-unique solutions for PD-site location [Wou96]. As a consequence, multiple reflections should be detected and interpreted. Besides the difficult interpretation itself, this results in even longer propagation distances and is therefore in practical situations not realistic.
5. There are no other power cables, or other possible PD sources, connected to the cable under test. In off-line situations, the CUT is disconnected, so this condition is met. In on-line situations there are usually other adjacent cables connected to the same substation or RMU. In this case, the determined DTOA does not give a unique solution for the PD origin. Two successive pulses can also originate from somewhere else in the adjacent grid, e.g. another connected cable, connected in the same substation. Also the charge polarity of the signal does not give an indication of the originating location of the signal. The method of direction-of-arrival, as described in Chapter 4, can provide the propagation direction, but a signal coming from the CUT can also originate from beyond the far end of that cable. Therefore, measuring at only one location in on-line situations does not even give certainty about the originating cable system and can therefore lead to wrong conclusions, even if PD location is not required.

In conclusion, TDR has proven to be a good method to locate PDs with off-line PD measurements in non-branched cables shorter than about 4 km. For on-line situations, the complications are severe and TDR is not recommended.

5.2.3 Double-sided measurement

To overcome the problems of TDR for on-line PD measurements, a two-sided measurement system can be applied. One measurement set-up is installed at each cable end. To locate detected PD signals, basically the same principle as TDR is used, but only the first arriving pulse is analyzed. In this case, the TOA of the PD signals at cable end 1 and 2 is $t_{\text{oa}1}$ and $t_{\text{oa}2}$ respectively. Again the DTOA (Eq. (5.2)) is used to locate the origin of the PD signal. If the average propagation velocity of all cable sections is applied again, the distance from the PD site to cable end 1 is given by:

$$z_{\text{PD}} = \frac{1}{2} \left(1 - \frac{\Delta t_{\text{oa}}}{t_c} \right) \cdot l_c \quad (5.7)$$

where the factor in front of l_c represents the relative distance again, in case the cable length is unknown. Obviously, this expression assumes that the propagation velocity is equal for all cable sections. The expression for cable systems with different velocities is:

$$z_{\text{PD}} = \frac{1}{2} \frac{\bar{v}_1}{\bar{v}_c} (l_c - \bar{v}_c \Delta t_{\text{oa}}) \quad (5.8)$$

where the average velocities \bar{v}_1 and \bar{v}_c are weighted conform Eq. (5.6).

The problems for TDR given in Section 5.2.2 have mostly disappeared:

1. The total propagation distance is smaller (between 0 and l_c), compared to the propagation distance of reflected pulses with TDR (between l_c and $2l_c$). This results in more sensitive pulse detection and more accurate TOA estimation.
2. The noise level is similar to TDR, but since the propagation distance is smaller, the resulting SNR will be larger. Furthermore, combination of both TOA results in a method to eliminate disturbance originating from outside the CUT (see item 5).
3. There is no need for a reflection at the far cable end, so a large impedance change is not required.
4. If cable systems are branched, the same principle, as described in this section, can be applied if measurement set-ups are installed at all cable ends.
5. Since the TOAs at both cable ends are recorded, combination of the results can eliminate pulses originating from outside the cable under test. PD pulses originating from within the cable under test result in a difference in time of arrival of 0 to the total propagation time t_c . Recorded pulses with a DTOA of t_c are pulses that travelled through the total cable length and are therefore originating from outside the CUT. Furthermore, pulses from outside the CUT should deliver an opposite current polarity at both cable ends, since the direction is opposite, with respect to the CUT. Both properties provide a means to reject disturbing pulses from adjacent connections and are only feasible if two-sided measurement is applied.

Besides the advantages of a two- (or multiple-)sided measurement system, there is one major complication. Since the TOAs of both measurement units are compared, the employed time bases should be extremely well aligned. From Eq. (5.7) it is concluded that the location error is half the error in Δt_{oa} times v_c (which is large). The various options for time-base alignment will be discussed in the next section.

5.3 Time-base alignment

In order to locate PDs within 10 to 20 m, the time bases of the measurement units have to be aligned within a margin in the order of 100 ns. Aligning the complete time-bases of multiple measurement data records incorporates two aspects: (i) performing simultaneous starting of – or correction of the difference between the start of – multiple measurement data records, in this thesis denoted as “synchronization”, and (ii) correction of the time-wander of multiple measurement data records, caused by a small difference in sampling-clock speed used in multiple data acquisition systems, denoted in this thesis as “time-wander correction” (TWC).

5.3.1 Measurement set-up synchronization

In this section several synchronization techniques will be discussed briefly, with their implications for the on-line PD application. The most promising method, pulse injection, will be discussed separately in the next section.

Stable independent clocks

To achieve high time accuracy, very stable clocks like atomic clocks can be used. There are many types of atomic clocks that vary according to the natural element on which they are based (for example, hydrogen, ammonia, rubidium, cesium). All natural elements absorb and release electromagnetic radiation at a certain fixed frequency. Atomic clocks are tuned to the frequency of the electromagnetic waves that are emitted or absorbed when certain atoms or molecules make the transition between two hyperfine energy states. Because the frequency of these waves is in principle only dependent on the element used, the corresponding period of the waves can be used as a standard to define time intervals. The cesium-atom clock is very accurate and remains stable over a long period of time and is therefore used as definition for the unit second in the International System of Units.

Within a limited time span, atomic clocks can provide an accuracy far beyond the requirements for our application. However, even if the clock has a drift of only a fraction of the needed accuracy, it will still have to be calibrated regularly to keep absolute time over long measuring sequences. If we would require a calibration of once every year, the clock would have to maintain its accuracy of 100 ns during this one year. This would result in maximum inaccuracy of $3 \cdot 10^{-15}$. This value is just managed by one of the most accurate atomic clocks of this moment (the “NIST-F1” at the American National Institute of Standards and Technology, $1.7 \cdot 10^{-15}$). Commercially available clocks remain far behind this requirement. Furthermore, external influences in substations and RMUs, like temperature, magnetic fields, and vibration, can jeopardize the stability of these clocks. Anyway, clocks approaching the required accuracy are extremely expensive.

Global positioning system

The Global Positioning System (GPS) is a worldwide radio-navigation system formed by a constellation of 24 satellites and their ground stations. Each satellite transmits very accurate timing information, together with its exact position. From the time these signals take to reach GPS receivers on earth, location can be determined. If

at least four satellite transmissions are received, the three location coordinates and precise time are uniquely determined. The time of arrival of the signals from the satellites can, despite their extremely low power, still be determined very accurately, since a pseudo-random code is included. The GPS receiver is generating the same code and determines the time-shift needed to achieve precise alignment of the two signals.

The accuracy of GPS can be very high, but the following factors can introduce errors:

- Number of visible satellites. The GPS signals are transmitted on a frequency of about 1.5 GHz. This means the satellites have to be in the line-of-sight to receive their signals. Four satellites are necessary to produce results, but more visible satellites enables averaging of results and therefore increased accuracy.
- Signal multi-path effects. Buildings and other large objects reflect the high-frequency GPS signals. If the GPS signals are not received via the direct line-of-sight path, but via some reflected path, the travelled distance changes and the location and timing accuracy is jeopardized.
- Receiver clock errors. In a GPS receiver, a clock is present to determine the difference in TOA of the various signals. Small deviation of this time results in inaccuracy of time and location.
- Satellite location errors. The GPS signal contains information of the exact position of the satellite (monitored from fixed ground control centers). Errors in this satellite position results in time and location inaccuracies for the receiver.
- Relative position of the different visible satellites. The more the visible satellites are separated, the higher the accuracy.
- The US military's "selective availability" (SA). The GPS signals used to be intentionally degraded by the US military to prevent military adversaries to use the high accuracy of GPS. This resulted in the high accuracy only to be available for the US military. This selective availability accounted for the major part in the overall error. Fortunately, this intentional degradation was turned off in May, 2000.
- Variations in atmosphere/ionosphere. The satellite signal propagates through different atmospheric layers (strato/iono/tropo)spheres, having different propagation velocities. As the thickness and composition of these spheres are not completely constant, propagation times can deviate from the assumed travelling delay.

Normal GPS without SA can have an accuracy of about 6-12 m or 20-40 ns. Due to sources of error mentioned above, in practice maximum accuracy of about 10-20 m or 100 ns is reached. Some of the errors mentioned above can be compensated by using a differential GPS (DGPS) receiver. Differential GPS works by placing a GPS receiver (the reference station) at a known location. Since the location of this reference station is known, the (time varying) errors from the GPS signals can be calculated. This correction is then sent to the DGPS receiver, which uses the information to adjust the calculations. DGPS has an inaccuracy that goes down to about 1-5 m or 5-20 ns.

GPS is a widely spread system all across the world. Another advantage of this system is the continuous update of the time base, so the accuracy itself is constant,

and not ‘drifting’ as is the case with independent clocks. GPS is already applied for synchronization of (off-line) PD measurements on long or branched cable systems [Ste01]. Although the results are very satisfactory, especially for on-line applications, the system has some disadvantages too:

- GPS is cheaper than atomic clocks, but a system capable of producing the required time labels is still expensive.
- The reception of GPS signals requires at least four satellites to be ‘in the line of sight’. If large buildings are nearby, visibility is hampered.
- An antenna has to be installed outside the substation or RMU. This is not desirable, since one of the objectives is to minimize personnel effort. Furthermore, special precautions would have to be made when installed for a longer time, due to the vulnerability of such equipment to e.g. vandalism.

Other navigation systems

Besides GPS also other systems exist that have much in common with GPS, but are less known and less widespread. Therefore, only a brief description is given here.

Loran-C (Long range navigation) is the successor to Loran-A, a terrestrial radio-navigation system using ground-based transmitters. Hyperbolic lines-of-position are formed by measuring the difference in reception times of synchronized signals, received from ground systems at frequencies of 100-110 kHz. Reception of signals, transmitted from at least three ground stations determines the location and time (height is omitted). Loran was initially developed in the United States for marine and air navigation. The coverage includes North America (the entire United States), the coastal areas of Europe, and much of east Asia. The maximum time accuracy of Loran-C is about 100 ns. The time drift of the transmitters is compensated, since the transmitters themselves also receive signals from the neighboring transmitters and deviations are sent back. This continuous correction of the complete system is calibrated at one station with the Universal Coordinated Time (UTC) with an accuracy of 100 ns. With the ever increasing popularity of GPS the continuity of Loran is frequently under question. It can serve as an important back-up system for GPS in e.g. military applications, but due to its price, coverage, and uncertain continuity, it is not interesting for our application.

Glonass is the Russian counterpart of GPS and works much alike. Like DGPS there is also a D-Glonass with improved accuracy. Although details differ, the principle and performance are about the same as for GPS. Without going into detail, this system has about the same pros and cons as the GPS system with one additional disadvantage: the small availability of systems in western countries and therefore high price, low support, etc.

Chayka is the Russian counterpart of Loran-C. It is still under operation under Russian sponsorship.

Lorac (Long range accuracy) a comparatively short range system, merely used as portable location system.

Decca, Gee, Consol, Sonne, Elektra, Consolan, Omega (and probably others) are all predecessors of or equivalent systems to the Loran-C system and are therefore not interesting for our application.

The applicability of all these systems for the application at hand is less as compared

to GPS, mainly due to less coverage, less availability, higher prices and/or smaller accuracy.

Long-wave radio clocks

Around the world there are several radio clocks transmitting a time code, synchronized to a time standard like a synchronized atomic clock. The reception of the clock signal and therefore the choice of broadcasting station obviously depends on the location. Two clocks of importance in Western Europe are:

- DCF77: A long-wave time signal radio station, run by the ‘Physikalisch-Technische Bundesanstalt’. The DCF77 signals are broadcasted from Mainflingen and are synchronized with an atomic clock near Frankfurt, Germany. The transmission frequency is 77.5 kHz and the power is about 30 kW, having a range of approximately 2000 km. There are two transmitters, so the signal is rarely off-line.
- MSF: This time signal is a broadcast from Rugby, Warwickshire, UK, based on time standards maintained by the ‘British National Physical Laboratory’, synchronized by an atomic clock near Rugby. The frequency is 60 kHz and the power is 15 kW, reaching much of Northern and Western Europe.

Time-radios like this transmit, e.g. every second, a pulse accompanied with its time-information. The beginning of the pulse gives the accurate moment of time, followed by codes with time-information. Compared to time-signal transmissions in higher bands (short-wave, GPS), signals with low frequencies have a number of advantages and are therefore often used for radio clocks. There is no line-of-sight necessary for good reception, so a single powerful station can cover a large area. Long-wave signals also penetrate walls of most buildings quite well. Furthermore, the propagation is mostly in the form of a ground wave, so less affected by variability of higher atmospheric layers. Long-wave radio clock receivers are quite commonly used and not expensive.

The accuracy of these long-wave radio clocks is usually in the order of 1-10 ms. This is far from the requirements for our application. Phase-locked-loop techniques could probably improve this accuracy but still not reach our requirements. There do exist radio clocks with higher frequency signals, but they also by far do not reach the required accuracy. These short-wave radio clocks also have only a small geographic coverage. However, not the absolute time is of interest for the PD measuring system, but the time difference between the two cable ends. If the time of arrival of the pulses at both cable ends can be determined with sufficient accuracy, the time between the pulses (e.g. one second) can be maintained by a sufficiently stable local clock. The stability for the local clock would have to require maximum deviation of 100 ns in 1 s, or $1 \cdot 10^{-7}$, which is just feasible. The pulse’s time information can be used to identify which pulse is examined, so both sides focus on the same pulse. Remaining problems are:

1. The estimation of the TOA cannot be performed accurately enough with carrier frequencies of long wave radios (77.5 kHz for the DCF77). For these relatively low frequencies the time-accuracy would be in the order of microseconds instead of the required 100 ns. A solution for this problem may be to include also different, higher carrier frequencies already present. The pulse of the time-radio

could be used to pinpoint to a certain cycle in the high-frequency signal. If a certain cycle is chosen, a fixed phase can be chosen (e.g. the zero-crossing, since the slope is at maximum there), and a more accurate time instance can be determined. This step can be cascaded to higher frequencies, until the required accuracy is achieved. Realization, however, is quite complex and would come close to designing a variant of e.g. the Loran system.

2. A time delay can exist between the arrival of the time pulses at the two cable ends, because of difference in propagation distance of the signal from the transmitter(s). The maximum delay is the propagation time along the cable length through air. This difference can be regarded as constant, at least for relatively long time, which means this time can be measured for compensation. Calibration can be performed by e.g. provisional setup of GPS receivers at both cable ends or injection of a pulse in the power cable itself. If the propagation time of the pulse through the cable is known, the timing of the time-radio pulse (and/or phase-shift of the selected carrier frequencies) can be compared and corrected with the TOA of the pulse on the power cable. Such a calibration measurement can be performed repeatedly in order to correct for slow varying propagation time delays, caused by e.g. varying weather conditions, influencing the propagation velocity.

Especially the first complication makes this method of synchronization unfeasible for the PD measurement application. One of the solutions for the second complication, pulse injection, involves installing equipment which can serve as a synchronization method by itself.

5.3.2 Pulse-injection principle

Another (patented [Ste02a, Ste02b]) method is injection of pulses through the cable under test itself. Usually, a power cable is shielded and is a reasonably good transmission medium for high-frequency pulses (Chapter 3). Besides measuring PD signals, from the cable insulation, we can also inject pulses into the cable externally. If pulses are injected at one cable end and measured at the other side, only the propagation time for that cable has to be known to align the time bases. This technique has a number of advantages:

- The power cable itself is used as transmission medium. This channel is well defined, definitely present and insensitive to external influences.
- Even higher accuracy than GPS may be possible.
- The pulse-injection system may be shared for data communication between the set-ups (see Chapter 6).
- Less expensive equipment is needed.

Methods for injecting synchronization pulses in a power cable are equal to the methods described in Chapter 4 for on-line measurement of the substation or RMU impedance. For the same reasons as for detection, injection can also be realized most feasibly with inductive (Rogowski) coils. As the requirements for synchronization-pulse injection are similar to those for pulse response measurements of substation impedances, the same coil can serve for both purposes. See further Chapter 4 for design and calibration issues involved.

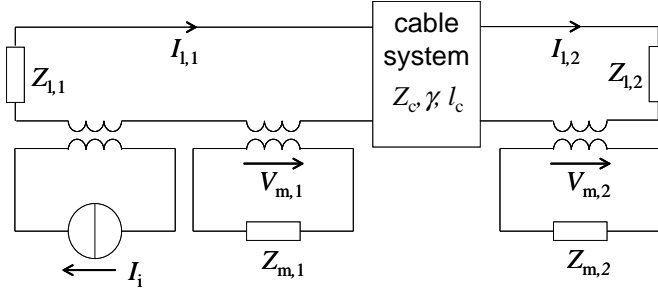


Figure 5.3 Equivalent circuit of pulse injection and measuring set-up. The injection and measuring probes are modelled as transformers, the two substations or RMUs as load impedances $Z_{1,1}$ and $Z_{1,2}$. In between, the cable is depicted as a 2-port, with its relevant parameters: characteristic impedance Z_c , propagation constant γ , and length l_c .

In Fig. 5.3 a situation using an injection coil at one cable end and identical measuring coils at both ends is schematically depicted. At the left hand side (index 1) a pulse is injected into the cable and measured at the same time. At the right hand side (index 2), the pulse arrives after the propagation delay of the cable, and is measured with a similar measuring probe. If the measuring probes at both cable ends have equal characteristics, the relation between the two measured voltages is independent of the coupling characteristics and only dependent on the parameters of the cable system: propagation constant $\gamma(\omega)$, length l_c , characteristic impedance Z_c , and the load (substation) impedance $Z_{1,2}$ at side 2:

$$V_{m,2} = V_{m,1} \cdot e^{-\gamma(\omega)l_c} \cdot \frac{2Z_c}{Z_{1,2} + Z_c} \quad (5.9)$$

If only the first arriving pulse is considered (no reflections) the time delay of the pulse is given by:

$$t_c = \frac{\beta(\omega) \cdot l_c}{\omega} \quad (5.10)$$

where $\beta(\omega)$ is the imaginary part of $\gamma(\omega)$. The time delay is slightly frequency dependent due to dispersion, but if identical pulses are being used, this effect is eliminated. Measured records from both cable ends can be synchronized very precisely by using the pulses as references after compensating for the propagation delay. The travelling time can be calculated from the length of the cable and the wave velocity. Since neither of these two quantities is known accurately (or even not known at all), usually a better method is to measure the time itself by considering the reflection of an injected pulse at the far cable end. By increasing the injection-pulse power, also small reflections at the far cable end can be made visible.

Another ‘synchronization’ method, which also applies pulse injection, is the use of a simpler unit at the far cable end that only acts like a ‘transponder’, i.e. a device that injects a pulse into the cable upon triggering on an incoming PD (briefly mentioned in [Bow00]). At the detection side these injected pulses are interpreted as normal TDR signals, except for an introduced time delay that can be compensated for. This option has the clear advantage that no pulses have to be injected if no PDs are detected. Furthermore, the transponder can be a relatively simple device which replaces a complete measuring set-up. However, for good PD detection under high-noise conditions

an intelligent set-up will be inevitable. If a transponder is used, pulse injection will be required upon every detected PD. Depending on the PD density, this can lead to a tremendous number of injected pulses in the grid, with possibly adverse effects on other equipment or other PD detection sets.

Using the option with repetitive pulse injection, large data records can be taken, containing only a few synchronization pulses per record. These records can contain hundreds or thousands of PDs, all synchronized with only one or two injected pulses. Furthermore, this means that the ‘blind’ periods for PD measurements can be minimal and, more important, are predefined, which is a prerequisite to determine total numbers of PDs or charge per time unit. Furthermore, if two similar measuring set-ups are installed, more intelligent and adaptable PD detection is possible. Especially for on-line measurements, simple triggering on PD signals is usually not possible and intelligent signal processing for PD detection is often indispensable.

5.3.3 Pulse-injection measurements

In order to compare the time synchronization by GPS and by pulse injection, tests have been performed on cables with strongly different lengths. Two experiments are described here: one experiment with an on-line 410 m cable connection and another experiment with an off-line 7.6 km cable. The purpose of the first experiment is to test the feasibility of the principle of pulse injection on a live cable in the field. The second measurement is performed to test the influence of propagation along a long cable on pulse-injection synchronization.

On-line cable connection of 410 m

The cable under test is a three-phase belted PILC cable, which is under normal operating conditions. The injection coil is installed at one cable end and the measuring probes are installed at both ends. The propagation time across the (on-line) cable is measured in advance by means of pulse-injection and considering the far-end reflection. The result is a time of $2.67 \mu\text{s}$. Subsequently, pulses are injected at one side and measured on both sides with 100 MS/s digitizers, coupled to GPS receivers (HP59551A) including a time labelling feature with 100 ns resolution. In Fig. 5.4 two measured records obtained from both sides of the cable are shown for a single injection pulse with the time axis derived from GPS. Correction for the measured propagation time is included in the time axis. The difference in time of arrival is determined by means of matched filters (see Sections 4.6 and 5.4), and is $2.70 \mu\text{s}$, close to the measured cable propagation time, especially with respect to the resolution of the GPS. Over 900 measurements were performed with this configuration, all showing a DTOA with a deviation from the cable’s propagation time less than the GPS resolution.

Also during similar experiments where RMUs are involved that have no additional MV cables connected, which implies large impedances (Section 4.4), pulse-synchronization inaccuracy remains within the GPS resolution. From the above and similar experiments it is concluded that the coupling to and from the cable and the TOA determination provides results having an inaccuracy within the resolution of GPS. One aspect of the pulse synchronization that has to be evaluated is the effect of propagation length on location accuracy. The next experiment deals with this aspect.

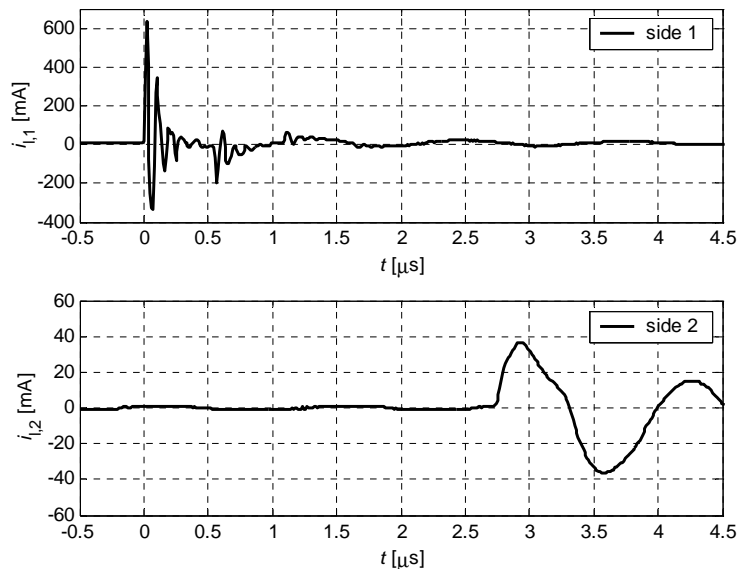


Figure 5.4 Measured injection pulses at both sides of a live 410 m cable system with time axis based on GPS. Side 1 is the injection side. The propagation time over the cable is 2.67 μ s. The oscillations at the back of the pulses are due to the non-characteristic termination of both the injection cable and the MV-cable in the substation.

Off-line cable connection of 7.6 km

In this experiment real PDs in a 7.6 km long cable system are located independently with both GPS and pulse injection. A long cable can be regarded as a ‘worst case’ situation for pulse injection as the attenuation of signals limits the accuracy. For GPS this accuracy is independent of the cable length. So shorter lengths will be advantageous for the pulse-injection method. The cable is measured with an off-line measurement system from KEMA (0.1 Hz), since the on-line system was not fully developed yet. However, off- or on-line tests are similar with respect to propagation influence, and the previous experiment already validated the principles of on-line pulse synchronization for a relatively short cable. So for the purpose of this experiment, off- or on-line test will not produce different outcomes.

PDs are measured with two measurement units at both cable ends. Pulses are injected at one cable end. The two data-acquisition systems (100 MS/s digitizers) are triggered by these pulses and GPS labels are recorded simultaneously. The cable under examination showed a number of spots with large PD concentration that correspond closely with the positions of joints. So the PDs most likely originate from those joints. One joint, at 5154 m, even had to be replaced, and showed clear evidence of large PD activity after inspection. Since we can presume the PDs to originate from these precise locations (each within 1 m), it enables us to use these measurements to evaluate both synchronization methods simultaneously and compare the location results. GPS directly adds the time scales to the data records, so the only parameter to be determined is the TOA of the PD pulses. In the case of synchronization

with the pulse-injection method, the time bases are shifted, using the TOA of the synchronization pulses, estimated by matched filtering.

In Fig. 5.5 the location results of the PDs originating from the joint at 5154 m are shown, using both GPS and pulse-injection alignment. As can be clearly seen both standard deviations are comparable (GPS: 5.2 m, pulse injection: 5.3 m). So for this situation both methods result in comparable location results. Similar analyses are performed for the other PD spots in the cable as well. In Fig. 5.6 the standard deviation of these locations are presented, using the pulse-injection alignment (GPS produced almost exactly the same numbers). The remaining variation, still present in these results, is most probably due to the inaccuracy of TOA determination. Although the matched filtering technique shows much better results than we could achieve with other TOA methods (Section 5.4), this still appears to be the limiting factor. The average deviation is 7.4 m. If the location errors are assumed to be normally distributed, this means that 95% of the PDs are located within a margin of two times the standard deviation, which is 0.2% of the cable length. The mean of the location results in Fig. 5.5 is very close to the location provided by the utility of this power grid. For some measurements this agreement is not this precise, but one should bear in mind that the locations, provided by utilities, are not always accurate.

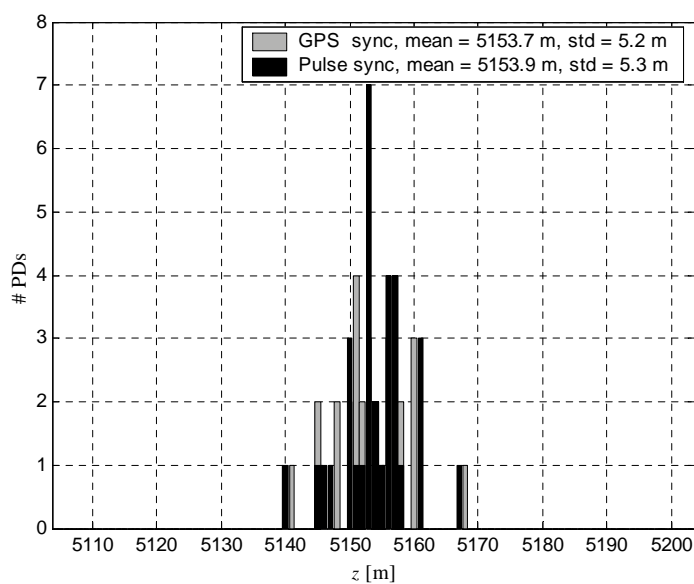


Figure 5.5 Mapping results of PDs, originating from one position, 5154 m, synchronized with GPS and pulse injection

5.3.4 Time-wander correction

When the start times of measured data records are synchronized, data points can still deviate in time due to the (independent) slight difference in sampling-clock speed. Large data records (comprising at least a full power-frequency cycle) should be recorded for phase-resolved PD patterns and reliable PD and charge density values.

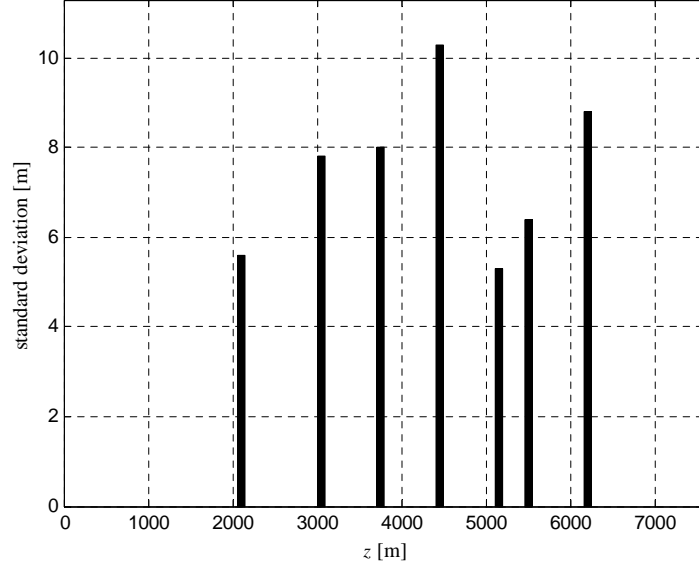


Figure 5.6 Standard deviation of mapping results of PDs, originating from different joint positions along the cable, using pulse-injection alignment

Small variations of sampling-clock speed will result in relatively large deviations in time for sample moments far away from the synchronized start time. This effect is denoted as time wandering.

Pulse injection can be used to compensate for this time-wander. Instead of injecting only one pulse to achieve the synchronization of only one time instant in the recorded frame (usually the starting point), two pulses can be injected. If the exact time delay between the two pulses is known, the time difference in the recorded data should represent this time. The difference between the exact time delay and the interval based on the clock speed in the detection equipment, can be compensated by adjusting the sampling rate. This correction is illustrated in Fig. 5.7. The top graph represents the time axis as if it would be digitized correctly. The difference in TOA (Δt_o) is the known time between the two synchronization pulses, corresponding to a number of samples S_o when using a hypothetical exact sample frequency f_{so} . The middle graph shows the effect if the actual sample rate f_{sm} differs from f_{so} . To correct for this error, the bottom graph shows the result with a reconstructed sample rate f_{sm} , resulting in the correct difference in TOA ($t_{m2} = t_o$). The relation between the corrected and the hypothetical sample rate results from:

$$f_{sm} = \frac{\Delta t_{m1}}{\Delta t_o} f_{so} \quad (5.11)$$

Between the two synchronization pulses a data-block containing one power-frequency cycle is analyzed. If this analysis is done based on sample rate f_{so} , the TOAs $t_{oa,m}$ of the PDs, obtained from this analysis, can be corrected by mapping the signal on

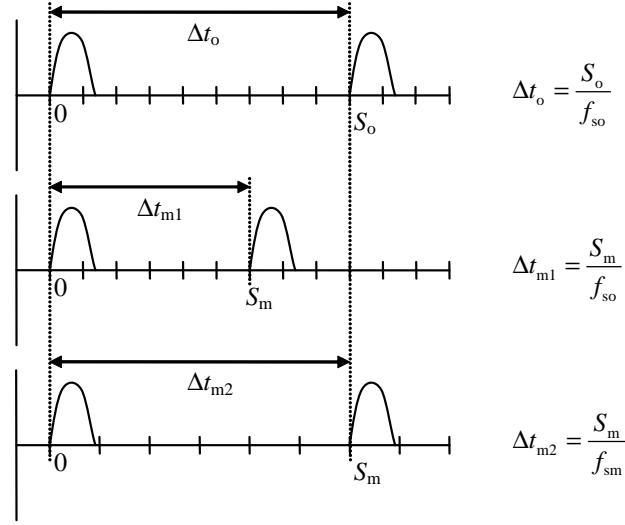


Figure 5.7 Illustration of time-wander correction using two successive injected pulses

the real time axis $t_{oa,r}$ with the function:

$$t_{oa,r} = (t_{oa,m} - t_{oa,p1}) \frac{\Delta t_o}{\Delta t_{m1}} + t_{oa,p1} \quad (5.12)$$

where $t_{oa,p1}$ is the time of arrival of the first synchronization pulse. Synchronization of the beginning of the records includes the cable propagation time. Obviously, the time Δt_o between the two synchronization pulses must be known a priori, since it cannot be determined exactly by the detection equipment with a possibly wandering clock. However, the accuracy of this Δt_o nor its stability have to meet high requirements. Inaccuracy of Δt_o of $x\%$ leads also to an inaccuracy of $t_{oa,r}$ of $x\%$. This can involve large values, since the analyzed data block, and therefore the maximum value of $(t_{oa,m} - t_{oa,p1})$, is one power-frequency cycle. However, the measurement at the other cable end experiences the same deviation of $x\%$. Since we are interested in the differences in TOA from both sides, these DTOAs will also be only $x\%$ deviated. According to Eq. (5.7) a maximum location error of e.g. 0.1% requires a maximum clock inaccuracy of 0.2%, which can be realized easily.

5.4 Time-of-arrival estimation

The location accuracy of a PD relies on the accuracy of its time-of-arrival estimation, according to e.g. Eq. (5.8). For the method of pulse injection, the TOAs of the synchronization pulses have to be determined with at least the same accuracy, since deviation of these TOAs accumulates to the TOAs of all the PD signals in that record, e.g. Eq. (5.12).

One can think of numerous ways to determine the TOA of a pulse-shaped signal, e.g. defining a threshold and use its corresponding time as TOA. However, as the pulse shape depends on the location of the partial discharge, this method introduces

inaccuracies due to attenuation and dispersion (see e.g. [Kre93b]). Furthermore, this method can be severely impeded by the presence of noise. One can also define the average or instantaneous slope of the detected pulse shape and use this slope to cross some amplitude value of which the corresponding time is used. Results can be improved by this method, but still the influence of noise and varying pulse shape remain.

A more general and accurate solution is to use the maximum of the cross-correlation of the detected signal with its template that is constructed a priori, i.e. the required filter is the time-reversed impulse response of the signal's template:

$$h(t) = As(t_0 - t) \quad (5.13)$$

where $s(t)$ is the known signal waveform, A is a filter gain, and t_0 is a time delay to make the filter causal, i.e. $h(t) = 0$ for $t < 0$. Essentially, this is similar to the technique of matched filters, already discussed in Section 4.6, apart from the whitening of noise in case of colored noise. The matched filter, used for the signal detection can be designed by choosing t_0 in Eq. (5.13) such, that the maximum filter output occurs at the time of arrival of the PD pulse, as is shown in Fig. 5.8. In [Ste92, Vee05] a

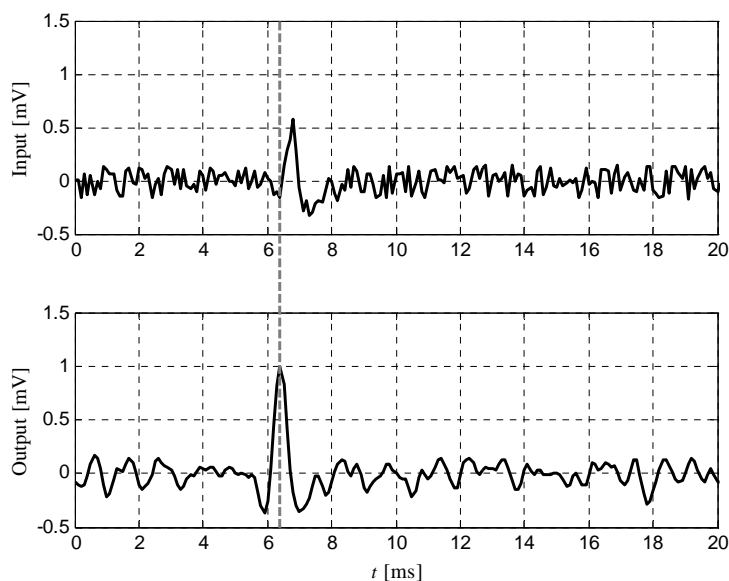


Figure 5.8 Illustration of TOA estimation with a matched filter. The top graph shows the input of the signal, i.e. the measured signal, the bottom plot is the output of the filter with its maximum at the TOA of the PD pulse.

theoretical analysis on the minimum variance of TOA estimation with this filtering method is performed. It is concluded that signals with high-frequency components and high SNR contribute more to the reduction of this variance than low-frequency components. This is in agreement with intuition.

The templates for the realization of this method are deduced from the cable model, together with parameters from system identification measurements, as described in

Chapter 4. For the templates of the synchronization pulses, measured data-records can be used, in which two (identical) injected pulses are recorded.

5.5 Conclusions

PD location based on double-sided measurement enables distinction between signals originating from the cable under test and signals from other locations. This, together with low far-end reflections for on-line cables and lower required propagation distances has resulted in the use of a two-sided measurement topology.

Multiple measuring set-ups require time-base alignment of measured data records. Injection of synchronization pulses appears to be a suitable method for both economical and practical reasons. The presented results show also the technical suitability of pulse injection for both time-base alignment and time-wander correction.

The time-of-arrival (TOA) estimations of the PD signals can be obtained from the matched filters, already used for the PD detection detection. The same technique is used for the TOA estimation of the synchronization pulses.

The principle of pulse injection in combination with matched filtering gives very satisfactory location accuracy of PD signals (approximately 0.2%) even for long cables (up to about 8 km). Besides inaccuracy caused by time-of-arrival estimation of detected pulses, the inaccuracy introduced by the time-base alignment with synchronization pulses is mainly caused by attenuation and deformation of the pulse, due to cable characteristics. This inaccuracy scales with cable length. GPS synchronization inaccuracy is introduced by inaccurate position determination of the measuring set-up, due to e.g. insufficient satellite visibility. The resulting error is independent of the cable length. Furthermore, the maximum resolution of 100 ns will limit the overall PD location accuracy to about 10-20 m. It is therefore concluded that synchronization-pulse injection can be regarded as the most attractive solution for synchronization of multiple measuring set-ups.

CHAPTER 6

System design

In this chapter the methods and techniques from previous chapters are combined into a system prototype, capable of detecting and locating partial discharges on-line in medium-voltage cable systems. The preferential system topology is discussed, together with several hard- and software issues. The resulting system is realized, and validated in Chapter 7.

6.1 Introduction

Excitation of partial discharges can be regarded as a stochastic process, i.e. it is not deterministically known whether, when and where a PD occurs in practical conditions. Since other systems capable of on-line detection and location of PDs in MV cables are not available, simultaneous measurements for validation of individually detected PDs are not possible. Therefore, comparison of the proposed concept with existing off-line techniques can only be performed on the basis of statistical averages of large quantities of measured PDs. On-line PD measurements result in huge amounts of data and therefore necessitates fully automated analysis. Furthermore, since a double-sided measurement topology is chosen (Chapter 5), the data acquisition at both cable ends must be synchronized. To enable these tasks a system prototype is proposed and realized, incorporating the different methods and techniques discussed in previous chapters.

The system design presented here is primarily intended as ‘proof of concept’. This means the system is not optimized for large scale production, which would incorporate aspects like economics, user friendliness, processing speed, etc. Instead, flexibility, modularity, and detection performance are the main arguments for the choices made. This may have led to somewhat over-dimensioned equipment, but due to the modularity, the system components can be scaled (e.g. to optimize price/performance) if necessary.

The system will be installed in a substation or ring main unit (RMU), an environment with high electro-magnetic interference. This implies the need of electro-magnetic compatibility (EMC) precautions, to avoid damage of the equipment and unnecessarily disturbed measurements.

To enable fast prototyping, a standard PC platform with a high-level programming language is chosen for measurement control and analysis software: LabView (from National Instruments), which allows easy and robust interfacing with external

hardware.

In Section 6.2 the system topology is given, explaining the general set-up and system functions. Hardware design considerations are discussed in Section 6.3, including an overview of the required components and their functions. Section 6.4 deals with the general software structure. The most important functions are discussed in detail. The conclusions from this chapter are summarized in Section 6.5.

6.2 System topology

In Chapter 5 it was concluded that a double-sided measurement set-up is preferred, which involves performing synchronized measurements. Two methods for time-base alignment (TBA) are implemented in the system: GPS as a reference system, and the proposed pulse-injection method, which has important advantages for on-line application. The system has two active operation modes: system identification and PD detection. In Fig. 6.1 a simplified block diagram of the main processes after triggering in PD detection mode is shown to illustrate the basic ideas of the concept.

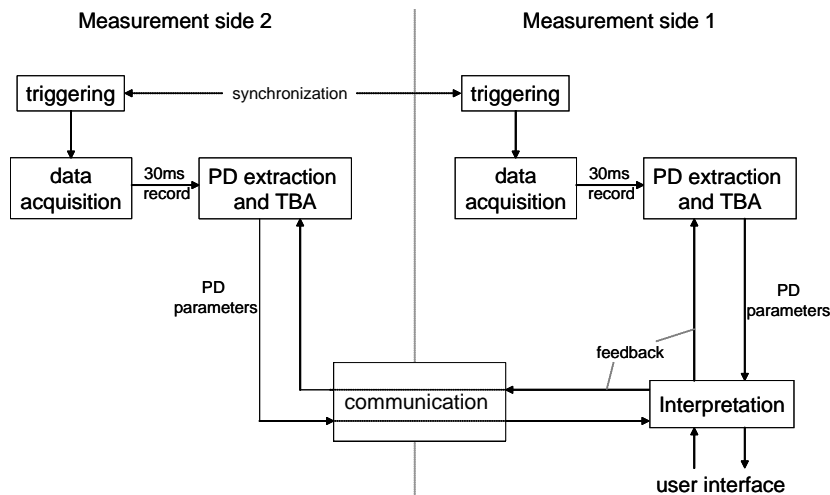


Figure 6.1 Simplified block diagram of the processes involved in PD detection mode upon (synchronized) triggering

In on-line situations, the amplitudes of noise and interference signals are frequently larger than the PD signals. Therefore, simple hardware triggering of the data-acquisition system on PD signals is usually not possible. Real-time processing of measured data requires too much processing power for PC-based systems. However, the aim for the diagnostic system is not to capture *every* occurring PD, but to determine the (insulation) condition of the cable under test (CUT). To this end, detecting only a small percentage of the occurring PDs is sufficient, as long as these PDs are representative for the total PD activity. Therefore, processing delay is allowed and block-based acquisition is applied. The trigger for the data acquisition is indicated in Fig. 6.1 and can be either a pulse from the GPS system (at a predefined

instant) or a synchronization pulse from the cable under test. To enable triggering on synchronization pulses from the cable, the amplitude of these pulses should exceed other present signals. Apart from the triggering and the time-base alignment, the system design is basically independent of the synchronization method.

The size of the acquired data-blocks is adapted to the duration of one power-frequency cycle (20 ms in e.g. the Netherlands). This ensures that possible phase-angle-dependent effects are included. Some extra time is reserved for the synchronization pulses, including possible oscillations. This is clarified in Fig. 6.2, where a measured data-record is plotted with two synchronization pulses (see Chapter 5). The synchronization pulses are allowed to exceed the data-acquisition system's dynamic range, since they only serve as time-reference. The analog front-ends of the system should not be affected by this clipping. Obviously, the matched-filter templates used for the time-of-arrival (TOA) estimation must also include the clipping.

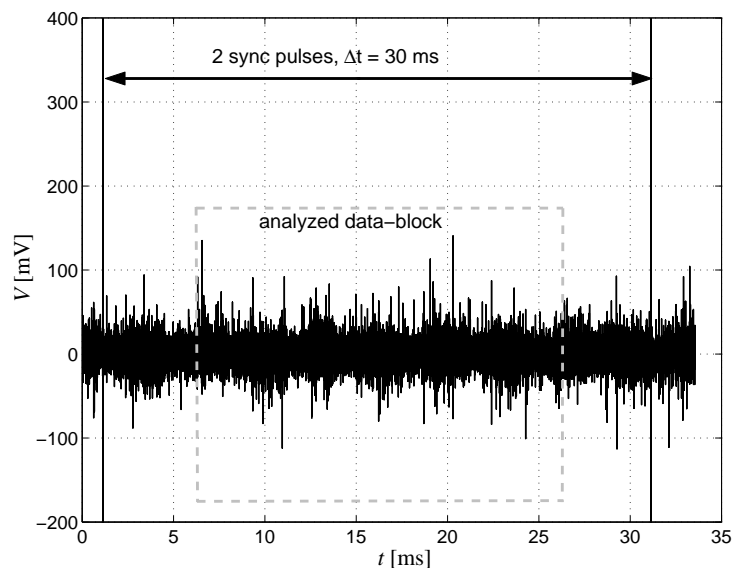


Figure 6.2 Measured data record (33.6 ms) with two large synchronization pulses (clipped) with $\Delta t = 30$ ms and a data-block of 20 ms, indicated by a dashed box

After PD extraction from the data-records and achieving time-base alignment, the results from the two cable ends are combined and interpreted at either measurement side or at a third location, see Fig. 6.1. As the components are separated, a communication link is established. To reduce the amount of communication data, the PD extraction results are parameterized locally (e.g. PD charge, TOA, etc.). After deciding on a higher, centralized, level whether the extraction results are valid PDs, feedback may be necessary to implement this new knowledge in the PD extraction blocks to improve future extraction.

Interpreted results can be stored and presented. This is indicated in Fig. 6.1 as “user interface”, and can be included either locally or at an other location via a communication link (see Section 6.4).

6.3 Hardware-design considerations

6.3.1 General component description

An overview of the components involved at one measuring side is depicted in Fig. 6.3. The measurement coil(s) (CT, only one indicated in Fig. 6.3), are installed at sensor locations discussed in Section 4.3. The signals are amplified by custom-made amplifiers as front-end for the data-acquisition (DAQ) card in the PC. The amplifier and DAQ contain 4 channels, so signals at multiple sensor locations can be measured simultaneously (see further Section 6.3.2). A PC is used for measurement control and data analysis. As only standard interfaces are used, the PC can easily be upgraded or replaced by e.g. microcontroller based systems. The pulse generator, needed for time-base alignment and system identification, is controlled by (the parallel port of) the PC. The output of the pulse generator is amplified and tuned to the injection-coil impedance (see Section 6.3.3). To enable the use of the GPS system as a reference, the signals from a GPS antenna are received by a GPS receiver (HP59551A), which includes a time-labelling feature. Depending on the type of data-communication (Section 6.3.4) a communication device is implemented in the PC. Several components are discussed in more detail in the next sections.

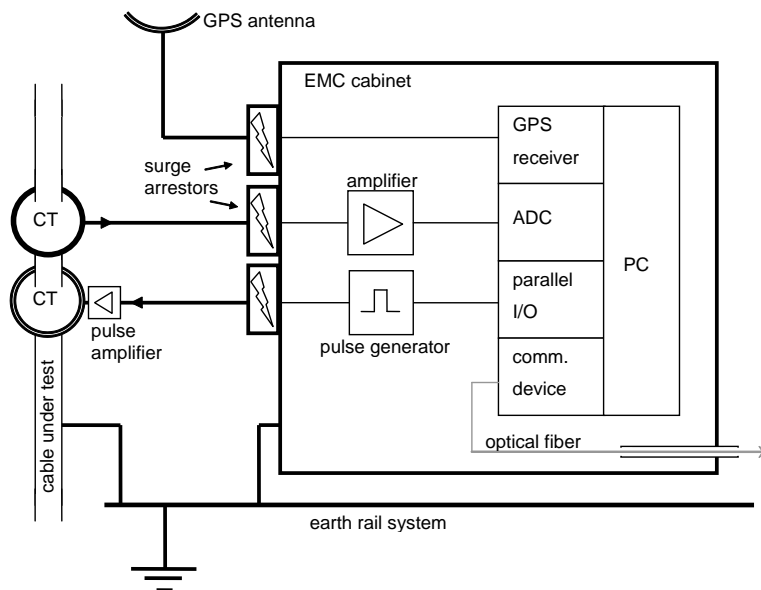


Figure 6.3 Overview of the hardware of one measurement set-up

An important aspect to consider is the EMC of the equipment. The equipment is installed in a substation or RMU, where large electro-magnetic disturbances occur. Magnetic fields at the power frequency are hard to shield, due to the large skin depth at low frequency (see Eq. (3.6)). Thick, highly permeable and conductive material can be used to prevent penetration of these low-frequency magnetic fields (e.g. [Has94]), but this is very unpractical due to the size and costs involved. However, since power frequencies are much lower than the frequency range of interest for PD detection,

disturbances due to these fields remain undetected. Electric fields can be shielded against with a thin earthed metal enclosure (EMC cabinet in Fig. 6.3). The main reason for concern left is the occurrence of high-frequency transients, due to lightning surges and switching operations. These transients can have large amplitudes and can cause both unnecessary disturbance of the measurement data and even cause damage to the equipment. For incident fields due to these transients, shielding is achieved by a relatively thin conductive EMC cabinet. Purely regarding the absorption shielding, the attenuation of EM waves in the shield material is given by the inverse of the skin-depth, $\sqrt{\sigma\mu\omega}/2$, e.g. [Sch88]. For an aluminium shield of 2 mm this results in 100 dB attenuation for frequencies down to approximately 200 kHz.

The large transients, however, also induce currents over the shields of the various connection cables. This coupling can cause disturbance in the measurements or damage to the equipment. To avoid coupling of these common-mode (CM) currents in the measuring circuit, coaxial cables and connectors with adequate shielding (e.g. [Hor98]) are applied and conducted coaxially through the EMC cabinet. The shielding of the sensor is discussed in Section 4.2. Signals for data communication are led through the EMC cabinet by either a coaxial connection as well, in the case of only an external antenna, or by an optical fiber, connected to external communication equipment or directly to an optical network, if available (see further Section 6.3.4). The optical fiber, if applied, is conducted through the EMC cabinet by means of a waveguide, having a diameter $d_{wg} \lesssim \lambda/4$ and a length $l_{wg} \gtrsim 5d_{wg}$, [Hem92, Joh75]. The power supply of the EMC cabinet is filtered, blocking both common- and differential-mode currents above the power frequency.

Besides the coupling of CM currents to the measured signal, the sensor(s) and the attached GPS antenna can also produce high voltages themselves in case of e.g. switching or lightning surges. To protect the equipment against these differential-mode (DM) over-voltages, coaxial surge-arrestors, with a spark-over voltage of 100 V, are applied for every coaxial connection in the EMC cabinet (Fig. 6.3).

6.3.2 Measurement and data acquisition

For the first measurement set-up, commercially available split-core current-probes are used (Fischer CC F-70), having a flat transfer impedance of 1Ω for 100 kHz–100 MHz. These probes are well shielded and their cores do not saturate for power-frequency currents up to 350 A. A good alternative is the use of an air coil with windings constructed from coaxial cable, as was discussed in Section 4.2.

The optimal sensor location for measurement of Shield-to-Phases (SP) current is around the cable under test, past the last earth connection (PLEC). If directional sensing is applied, an additional sensor is installed around the earth strap of the transformer-connecting cables (TCC), see Section 4.3.

The sensor signal is amplified by a custom-made 4-channel amplifier. This amplifier has a voltage gain of 26 dB over a frequency range of 100 kHz–30 MHz and a notch-filter of 50 dB at 50 Hz to eliminate possible power-frequency coupling. Furthermore, the output of this amplifier is limited to 5 V to offer additional protection of the data-acquisition card against over-voltages.

The DAQ system is a 4 channel, 12 bits, 62.5 MHz digitizer card (Spectrum MI.3033). A 12 bits analog-to-digital converter (ADC) is chosen, since the amplitude of measured narrow-band interference from radio broadcast is often large compared to the PD amplitude (Section 4.6.2). A 12 bits ADC corresponds to a theoretical

dynamic range of 72 dB and reduces the quantization noise compared to an 8 bits ADC with 24 dB. As an alternative, an analog front-end with (computer controlled) adjustable notch-filters can serve to filter the narrow-band interferences and reduce the required dynamic range of the ADC. The digitizer card is equipped with 2 MS of internal memory per channel, allowing 33.6 ms data-acquisition time. In order to verify the stability of the internal sampling clocks, an experiment was conducted by comparing the time-wander of two equal digitizers placed in different temperature conditions. The result indicated deviations of several hundreds of ns within 20 ms of data acquisition, with an environment temperature difference of about 5°C. This deviation is clearly too large for accurate PD localization. Compensation by the synchronized GPS clocks or by the time-wander correction method of Section 5.3.4 is needed.

The system consisting of current-probe, cable connections, surge arrestor, and amplifier is calibrated to enhance the accuracy of the measurement results. To this end, the whole system is installed in a shielded measurement set-up, which was also used for the calibration of each current-probe (Section 4.2). The measured data upon wide-band current pulse injection is compared to the output of a calibrated Tektronix current probe (A6302) – amplifier (Tektronix AM503) combination, installed in the same set-up. The detection transfer function is calculated from averaged measurements.

6.3.3 Pulse injection

A pulse generator is needed for both pulse synchronization and system identification. To this end a pulse generator is designed which is optimized for the specific demands [Tal04]. The pulse generator is controlled via a parallel output port of the PC.

The pulse generator is set to produce two pulses with an accurate time difference of 30 ms, controlled by a temperature insensitive oscillator. This time difference serves as reference for time-wander correction of the data-records (Section 5.3.4). The requirement of accurate time-difference between the pulses of 30 ms can be used for discrimination between these pulses and other high-amplitude disturbances or PD signals. Therefore, detection remains possible, even in the case of disturbance levels above the injected pulses.

The amplitude of the generated pulses is controlled by the (8 bits) parallel port of the PC. The output of the pulse generator is connected to an amplifier placed close to the injection coil. Since the final stage of the amplifier also involves impedance matching to the self-inductance of the coil, it is installed directly on the injection coil. For efficient current injection in the coil, the basic principle of the final stage of the amplifier is the discharging of a capacitor over the coil. The value of the capacitor is chosen such that half of the oscillation cycle of the LC-combination corresponds with the desired pulse width. This oscillation is switched with transistors (MOS-FETs), such that the injected pulse shape is blocked after a half oscillation cycle. The maximum peak current through the injection coil is about 10 A.

The injection coil is designed for a frequency range of 500 kHz–10 MHz, optimal for pulse propagation through the cable under test and detection sensitivity. A picture of the coil was shown in Fig. 4.22 and its transfer function is given in Fig. 6.4.

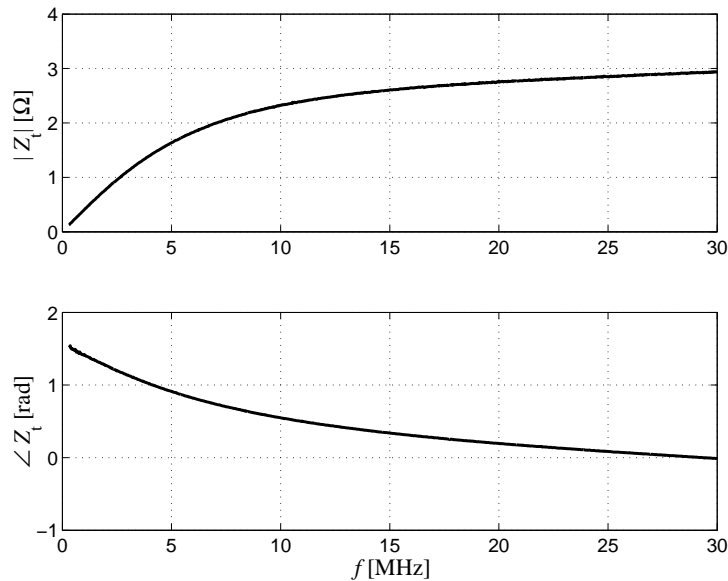


Figure 6.4 Measured transfer function of injection coil

6.3.4 Data communication

Since two-sided measurement is applied, data-communication between the measurement nodes is needed. If communication is possible, a third node is an attractive option for the system to monitor and/or control the system from a remote location. To enable the use of internet in part of the communication link, especially interesting in case of a third node, the TCP-IP protocol is used for all communication in the system. Furthermore, since TCP-IP is today's de-facto standard for transmitting data over networks, its application provides for high interchangeability of specific tasks with other programming languages and platforms. The software architecture is structured such that different software components communicate with TCP-IP messages (Section 6.4.1), independently of the means of communication itself. This topology complies with the modular and flexible approach applied to the complete system design.

The needed data rate is low, in the order of kbps, since measured data-records are analyzed locally and only parameterized results need to be communicated. Speed is not an issue, as processing delay is allowed (Section 6.2). Without going into much detail or specific, country dependent cost aspects, the various options for data-communication between the two measurement set-ups are listed:

Computer network (LAN/WAN, ethernet). If a local- or wide-area computer network is available, data communication is not an issue. Unfortunately, most substations and RMUs do not provide such a connection. In the measurement set-up at KEMA (Section 7.2), data-communication is established via an optical LAN and the optical fiber is conducted through the waveguide in the EMC cabinets, as described in Section 6.3.1.

Telephone lines (analog or digital). In some countries (among which the Netherlands), a large part of the substations and RMUs is equipped with telephone lines, used for voice communication for e.g. switching operations. Generally, these phone-lines are part of an internal telephone system, so in principle no substantial costs are involved when using these lines. If modems are installed in the measurement PCs, data communication is established. Typical data rates are 56 kbps (analog modems) and 128 kbps (ISDN: Integrated Services Digital Network).

Mobile-phone networks. Nowadays, cellular phone networks are commonly used for both voice and data communication. Obviously, if no network is available at the location of the substation or RMU, which may be the case for large, sparsely-populated areas, this type of communication is not an option. However, in many industrialized countries the coverage is almost 100 %. As this type of communication is still increasing in popularity, costs will continue to decrease and coverage increase. The most feasibly types of data communication over cellular networks are:

- GSM CSD (Global System for Mobile communication based upon Circuit Switched Data). A voice call uses a GSM specific codec to transmit the audio over a 9600 bps digital link to the base station. Although the operation of data communication is handled differently inside the GSM network itself, the end user can utilize the 9.6 kbps link for data communication too. One variant is HSCSD (High-speed Circuit Switched Data), which enhances the speed up to (theoretically) 57.6 kbps, by allocating several data channels into one logical link and code enhancement. The costs are usually charged per connection time, like voice connections.
- GPRS (General Packet Radio Service). GPRS is an overlay network on a digital cellular system such as GSM to provide wireless packet switching services, including internet-like packet switching service, to mobile users. Packet-switched data under GPRS is achieved by allocating unused cell bandwidth to transmit data. As dedicated voice (or data) channels are set up by phones, the bandwidth available for packet-switched data in the same cell shrinks. The theoretical limit for packet switched data is 171.2 kbps, but a more realistic bit rate is 30–70 kbps. An enhanced version of GPRS called EDGE (Enhanced Data Rates for Global Evolution) will allow higher bit rates up to a (theoretical) maximum of 384 kbps. This is mostly seen as a step towards a full 3G system (see below).
- 3G (third generation) mobile phone technology. E.g. UMTS (Universal Mobile Telephone System), which is a European version of a 3G system, supports up to 2 Mbps data transfer rates. Just as GPRS the data rates reduce considerably in a heavily loaded real-world system. The packet-switched data is IP-based. In many countries, this technology is just starting to be implemented on a large scale, so the coverage is not large yet, but increasing. Most end-user UMTS equipment, however, automatically switches to GPRS if no UMTS network can be found.

Satellite communication. Although this is a system with global coverage, it has some practical disadvantages of which the relatively high costs are probably the most important for our application. In some rare situations, however, where no other means of communication are available, this technology may provide a solution.

Wireless point-to-point communication. Stand-alone transmitters and transceivers can be used to perform data communication. This solution involves obtaining radio transmission licences, which can be different for every country in which the system is applied. Furthermore, antennas should be installed and radio equipment of enough gain should be applied to bridge the involved distances with possible obstacles in between. A small survey learned that the involved costs were too high for this application to be applied as default communication means. However, if no other communication possibilities exist, this may be a solution.

Power-line communication (PLC). By using the cable itself as a communication medium, the system becomes independent of the availability of other networks or equipment. PLC is to some extent already applied successfully in low-voltage networks. For medium-voltage networks, a few systems are available, but mainly in a test phase. Furthermore, not every system is in agreement with the current standards. Whereas the challenge for PLC over LV networks is the branching of the cables, for MV networks the coupling to the cables is the main problem. Coupling of high-frequency signals from MV cables is extensively discussed in Chapter 4 of this thesis and the same principles are valid for injection and measurement of communication signals. For the same reasons as mentioned in Section 4.2 for PD sensors, inductive coupling is also preferred for communication and the same locations in substations or RMUs as discussed in Section 4.3 are applicable for the location of communication receiver and transmitter coupling. The distinction between the DM and CM circuits is also important for PLC, since injecting in the CM circuit results in much higher (EM) disturbance to the environment, which may also violate EMC standards. Furthermore, the DM circuit is the better propagation channel (Fig. 4.7). In principle, the coil for injecting synchronization pulses and the measurement probe can be shared for communication purposes. The allowed bandwidths in the (European) standards for signalling by utilities in MV networks [IECd] is 3 kHz–500 kHz and for LV networks [CEN] this is 3 kHz–95 kHz. These bandwidths are in principle sufficient for the low data rate that is required for metering and diagnostic purposes. Low frequencies result in low (magnetic: $j\omega M$, or capacitive: $j\omega C$) coupling and usually relatively high impedance of the substation or RMU due to the capacitive behavior at these frequencies of the transformer and the cables connecting the transformer, see Section 4.4. Improvements in coupling can be made via:

- Using a ferro-magnetic core in the injection and detection coils (see Appendix B).
- Using a current-transformer with thick multiple primary windings instead of a Rogowski-type coil. This involves modification of the MV installation in the substation or RMU. However, if these transformers are implemented in the earth connection from e.g. the MV cable itself or the TCC, modifications are minimal. If only a few primary windings with sufficient thickness are used, power frequency currents still experience low impedance.
- Application of alternative modulation schemes which still meet the standards. For instance, the pulse-injection system can be applied to generate successive pulses (repetition rate within the limits of the standards) with modulated time differences or amplitudes. This option has the additional advantage that the communication device is integrated with the pulse synchronization system that is already present in the on-line PD system.

From the above list, power-line communication may be the most attractive method for communication between the two measurement sides of the on-line PD system. Although the principles of coupling to the MV cable, presented in this thesis, may lead to a much more applicable PLC system for MV networks, PLC is not used for the first prototype of the on-line PD system, since the main objective is partial-discharge detection and not the development of a communication system. Furthermore, access to one of the two measurement units from a third, remote location still has to be performed via other means of communication. Therefore, the first prototype communicates via either a computer network, a telephone line (for which a TCP-IP module is developed), or a mobile-phone network. Combinations of these options are obviously also possible.

6.4 Software architecture

6.4.1 Software components

The complete software structure of the on-line PD system is incorporated in several components. The software components run separately from each other on either the same or a different computer and communicate via a distributed messaging system: each message is sent over TCP-IP to activate the routine corresponding to this message on the same or a different software component. This way the total system is highly flexible, the separate messages can be developed merely independently from each other, and the software architecture is independent of the physical implementation of the different functionalities, e.g. whether the user interface should be located on the same PC or on a computer somewhere else on the internet, the data-storage can be chosen on an arbitrary location, etc. Furthermore, in principle every software component can be written in its own specific programming language, as long as communication over TCP-IP is possible. This may be especially useful for a remote user interface. A message-based software architecture is established. The software environment of LabView is dataflow-driven and does not support a message-based architecture. To this end, a messaging system is developed, which monitors the TCP-IP port, queues the received messages, executes the queued messages and sends messages over TCP-IP to other software components. One message engine is started for each software component. The execution of the messages itself (started by the message engine) can be implemented via normal dataflow-driven LabView programming, thereby maintaining its specific advantages on a lower level. Every software component maintains its own status (errors and logs) and appropriate actions can be taken upon reaching certain status levels.

In Fig. 6.5 the component collaboration diagram is depicted. The various software components are connected by arrows, which indicate the direction of the initiating messages. Some messages request answers, e.g. confirmation or data-transfer, which will be in the opposite direction. Without going into detail, the general functions of the several components are as follows. The remote user interface (RUI) is the component where the user can configure the measurement, start procedures, obtain results for presentation, etc. This RUI is usually installed at a different location, where the user can monitor the measurement. Via the preliminary user manager (UM), where user rights can be controlled, the RUI sends commands (messages) to the measurement manager (MM). The measurement manager is the component controlling the

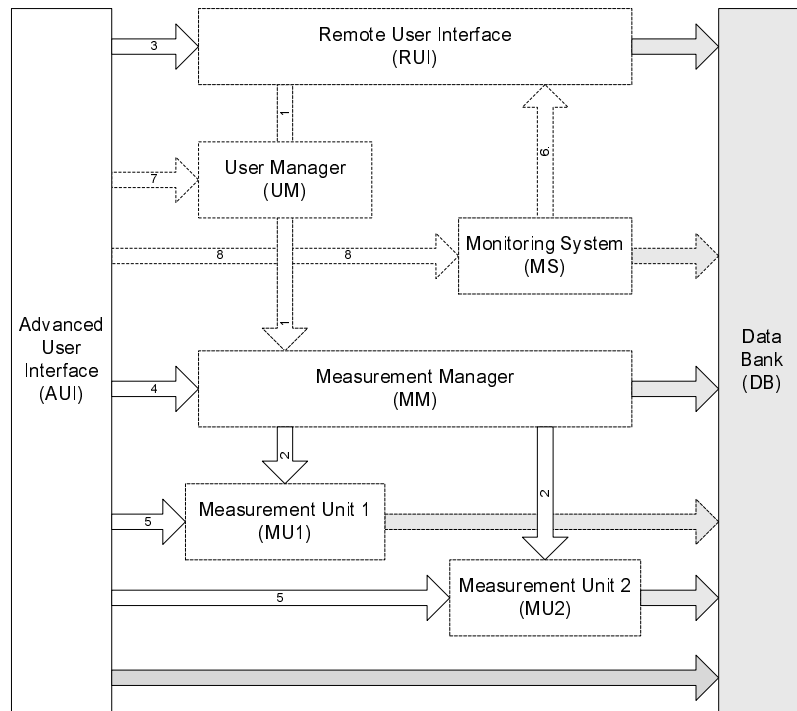


Figure 6.5 Component collaboration diagram. The arrows indicate the direction of the initiating messages (white) or requests for PD data transfer (grey). The components UM and MS and accompanying messages are in a preliminary state.

different procedures for the measurements. Furthermore, the MM combines the results from both measurement sides to determine the PD locations. The MM will usually be running on the same PC as measurement unit 1 (MU1), although this is not necessary. Measurement units 1 and 2 (MU_x , $x \in \{1, 2\}$) are the components controlling the measurement on the lowest level, i.e. the data acquisition, the pulse injector, etc., and perform signal analysis of the raw data in order to extract and parameterize the detected PDs. The PD data is stored in the data bank (DB) in a database. SQL (Structured query language) is used to store and retrieve data from the data bank, since this is the default language to communicate with databases in general. The system is therefore independent of the type of database used. Temporarily data from MU_x is also stored in the database. The advanced user-interface (AUI) is for software development and maintenance and for trouble-shooting. The AUI can therefore interact with all the other software components. The preliminary monitoring system (MS) is intended for pro-active signalling to the RUI in case of exceeding predefined conditions, e.g. excessive PD activity.

Just as the software components can be distributed over several computers, one computer can also run multiple instances of the software components to enable equipment sharing for monitoring multiple cables which are terminated in the same substation or RMU.

Examples of some relevant messages and the structure of the database can be found in Appendix C. Two main tables are defined in the database. The results from the

MUs are stored in the MU1_result and MU2_result tables. These results are combined in the MM and subsequently stored in the MM_result table, which can be viewed by e.g. the RUI. The main tables have links to other tables for preserving information about e.g. used settings, templates, and signals from which the results are obtained. The sub-tables do not necessarily have to be located at the same place. The table of measured raw data, for instance, can be a directory with files on the MU x . The general behavior of a measuring sequence is ‘top-down’, i.e. the RUI sends a message to the MM to start a measuring procedure upon which the MM starts the appropriate actions at the MU1 and MU2. The next sections give a general description of some of the important messages in the system. Since a detailed description would be much too comprehensive, the discussion of the messages is far from complete and only the main aspects are mentioned.

6.4.2 System-identification mode

Fig. 6.6 shows the sequence diagram of the system-identification measuring procedure, following the method of Section 4.5. After initialization, pulses are injected at the near cable end and measured at both sides. Subsequently, the injection is activated at the far cable end. The results are then combined and model parameters are estimated and stored in the data bank as the cable model. The cable model is then available for the MUs for construction of the matched-filter bank, which is stored locally on the MUs. The averaged signals from the system identification measurements are also stored in the data bank and are used as templates for the TOA estimation of synchronization pulses. The power spectral density function (PSDF) of the measurement is calculated and used as the initial PSDF for the signal analysis of the PD measurements (Section 6.4.4).

For optimal signal-to-noise ratio (SNR), the amplitude of the injected pulses is adjusted to a level as high as the digitizer allows without clipping. In contrast to the synchronization pulses, clipping is not allowed for system identification, since transfer functions have to be calculated. If multiple MV cables are connected in the same substation or RMU where the pulses are injected, reflections from the CUT can be discriminated by the direction of arrival technique described in Section 4.3.2. If no reflections from the far side can be detected upon maximum pulse gain due to an insufficiently large reflection coefficient at the far cable end, the cable will have to be disconnected during the system identification. If disconnection is not possible/preferred, cable delay can still be obtained by temporary installation of GPS. However, if the pulse generator can provide sufficient power, it is expected that this should not be necessary at all, since in practical situations there is always some reflection (not enough for PD reflection based measurements, but enough for system identification).

6.4.3 Measurement mode: data acquisition

In Fig. 6.7 the measurement sequence upon activation in the MM is depicted. Before the measurement procedure on the MUs can start, the PC clocks have to be roughly synchronized in order for both MUs to start approximately at the same time to wait for a trigger (from either the GPS or the synchronization pulse). After clock adjustment, the measurement start times (initial time and interval) are uploaded to both MUs and a final measurement decision is made. This extra verification is included, since

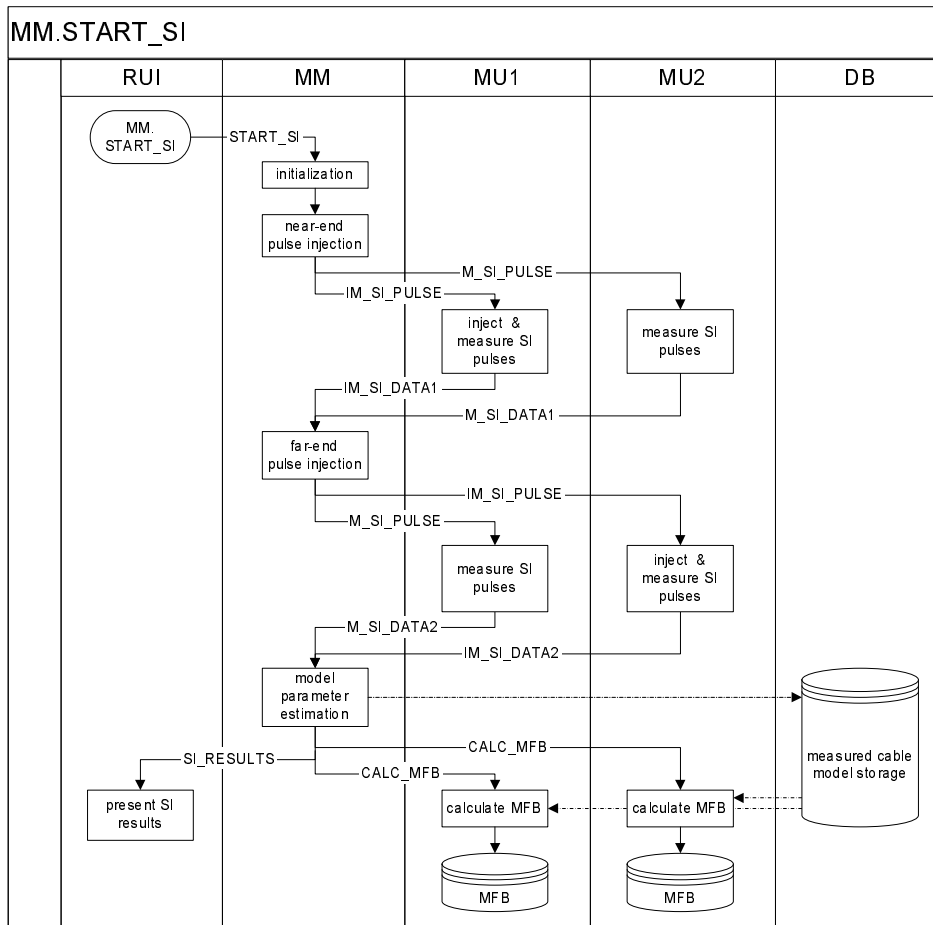


Figure 6.6 Sequence diagram of the system identification (SI) measuring procedure

the MUs will run independently after the start-measurement message has been sent (to reduce load on the communication channel). The analysis sequence on the MM (Section 6.4.5) is then started parallel to the measurement sequence on the MUs.

Fig. 6.8 shows the sequence diagram, which is started at the end of the sequence of Fig. 6.7. At the set time, digitizers are configured to wait for triggering on either a GPS signal or a synchronization pulse from the CUT. The trigger level is determined from results from the system-identification measurements. Upon triggering, the data is digitized and stored locally as raw data for possible future reference. The dynamic range of the digitizer is dynamically adjusted to the signal level. Since the amplitude of PDs can vary to a large extent, this range should be rather loose, which is possible since digitizers with a large dynamic range are used. The data is passed through to the PD extraction routine, where PDs are extracted from the raw data using the MFB (matched-filter bank), see Section 6.4.4. After the extracted PDs are parameterized, the results are stored locally and the process is restarted. The locally stored results are frequently uploaded to the MUX_result database. This results in semi-continuous

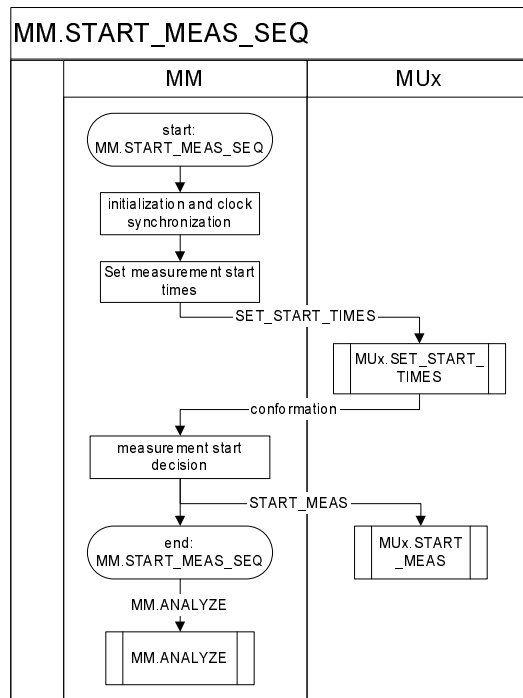


Figure 6.7 Sequence diagram of the measurement sequence on the MM

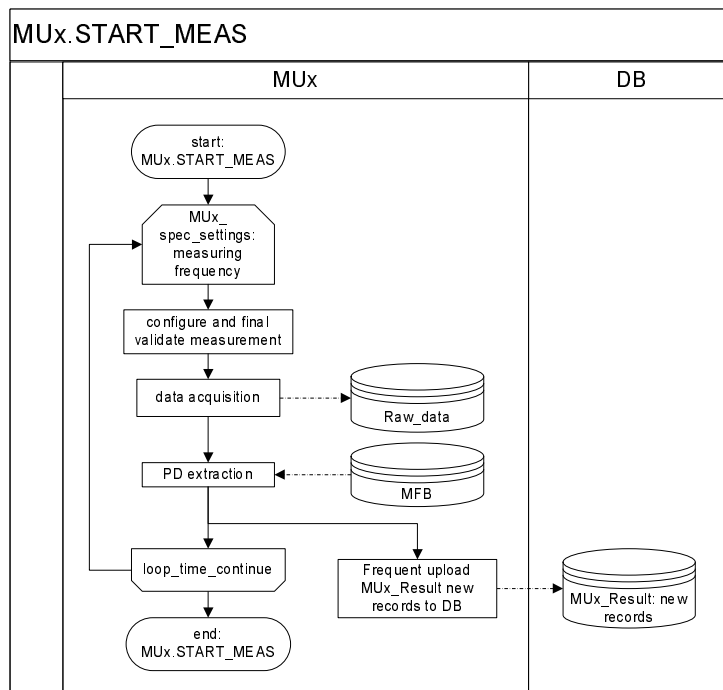


Figure 6.8 Sequence diagram of the measurement message on the MUX

monitoring at pre-defined time intervals and possibly different communication intervals.

6.4.4 Data analysis: partial-discharge extraction

The PD extraction routine is depicted in Fig. 6.9 and incorporates both PD extraction and time-base alignment. If GPS synchronization is used, the routines for TBA are bypassed, since GPS provides both time labels and a reference clock signal to stabilize the digitizer sample clock. For TBA by means of pulse synchronization, an accurate TOA of the synchronization pulses is determined with templates, obtained from the system-identification measurements. The a priori knowledge of the time delay between the two pulses can distinguish them from other possibly-present high-disturbing signals (or PDs). In between the two pulses a data-block of one power-frequency cycle is selected for PD extraction. The matched-filter technique is split into two parts. One part is the whitening filter, which determines its noise spectrum from the present data and previous measurements, and incorporates also some notch filters for pre-filtering narrow-band radio broadcasts, if present. After filtering, the noise is white and a static matched-filter bank, which is determined from the cable model, is applied. If the outputs of the matched filters pass a PSDF dependent threshold, the outputs of the matched filters that are within a small predefined time interval are clustered, since different matched filters will produce slightly different TOAs of the extracted partial discharges. The maximum filter output within one cluster results in the desired PD parameters (TOA, charge, etc.). For a more detailed description of the implementation of the filters and the PD extraction, see [Vee05]. The TOAs from the synchronization pulses are then used to map the TOA results

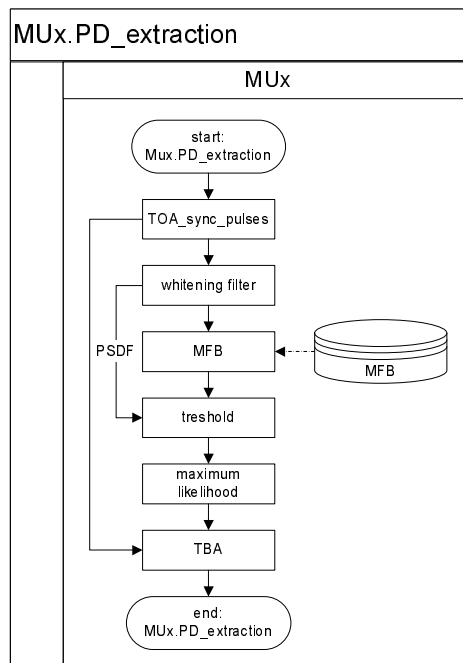


Figure 6.9 Flow diagram of the PD extraction and TBA routine

for correct synchronization and time-wander correction according to the principles of Sections 5.3.2 and 5.3.4.

The processing time of the implemented PD extraction from one power cycle in LabView on a 2.3 GHz Pentium 4 processor is approximately 20 s, which easily allows the chosen data-acquisition time-interval of 1 min.

6.4.5 Result combination: partial-discharge location

To localize the PDs, the results from the two measurement units are combined in the measurement manager. Fig. 6.10 shows the sequence diagram responsible for this task.

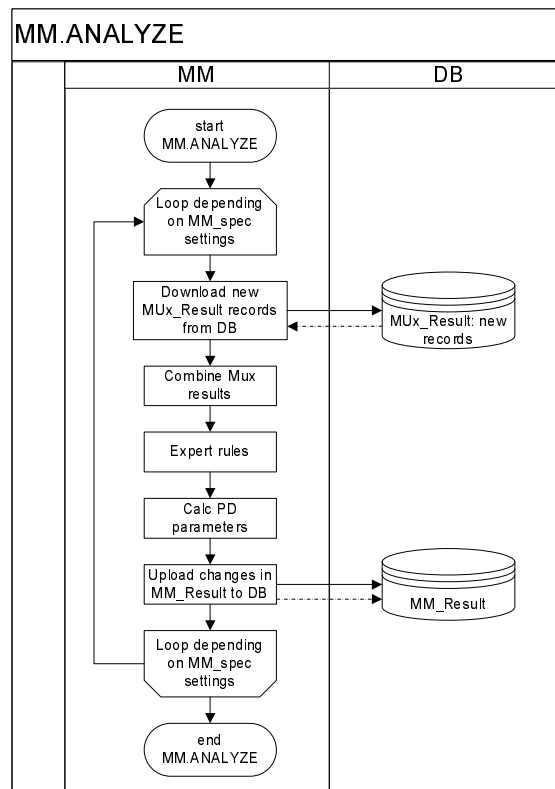


Figure 6.10 Sequence diagram of result analysis routing on MM

After downloading the new MU1_Result and MU2_Result records from the database, results from both cable ends can be combined by finding TOA ‘pairs’ that obey:

$$|t_{oa2} - t_{oa1}| < t_c \quad (6.1)$$

where t_{oa1} and t_{oa2} are the TOAs at cable end 1 and 2 respectively, and t_c is the propagation time of signals over the cable. Obviously, this formula assumes precise TOA estimations. Deviations in TOA determination can result in less robust disturbance rejection. So besides more accurate location results, accurate TOA determination also improves the disturbance rejection effectiveness. However, the combined results

are also passed through to other expert rules which can also reject measured disturbances. This will be further discussed in Section 6.4.6. After the final expert rules, parameters like charge, location, and time of origin are calculated. The location and time of origin are determined by using a velocity look-up table in the cable model to incorporate possibly different velocities in the several cable sections. The resulting parameters are stored in the MM_result database, together with all the information like configuration settings, used cable model, etc. (Appendix C) to be able to trace back the final results to the original signals and check the system's decisions. The time interval for the loop in Fig. 6.10 is independent of other system time intervals and can be chosen as desired.

6.4.6 Expert rules

The system incorporates several techniques to reject disturbances. They are denoted as expert rules. The most important rules are summarized below:

1. Matched filters for disturbance. If interfering signals are extracted and rejected with much certainty by the MM, the signal itself can be used as a template in the matched-filter bank. If this filter produces the highest output, the same disturbance signal is detected and can be rejected in an early stage of the detection process, by the MU_x .
2. Matched-filter output threshold. If the maximum output of the MFB is below a minimal value, the signal deviates too much from an expected PD signal shape and is rejected.
3. Direction of arrival (DOA). If in each substation or RMU a second sensor is used, as described in Section 4.3.2, the direction of arrival can be determined and disturbance can be rejected.
4. Maximum difference in time of arrival (DTOA). Partial discharges originating from the cable under test result in DTOAs between the two measurement setups which are smaller than the cable propagation time. DTOAs longer than this limit result from disturbances outside the cable.
5. Charge polarities. If the charge from the partial discharge at its origin is calculated after extraction of the signal, the polarity of results from both cable ends should obviously be the same. If a signal is entering the CUT from outside the cable, the polarity of the current at one side will be opposite from the other side, since the propagation direction with respect to the CUT is opposite and charge polarity is equal. Comparison of the charge polarities of the extraction results from both cable ends is decisive.
6. Maximum difference in charge. The calculated charge from both locations should also result in approximately equal charge of the partial discharge. Too large a difference indicates that the signals from the two cable ends do not originate from the same source.

Rules 1 to 3 are incorporated in the MUs, rules 4 to 6 in the MM (indicated in Fig. 6.10). The rules which are implemented in the MUs only filter part of the disturbances, but are important since they reduce the amount of communication data. The rules which are implemented in the MM can obviously only be incorporated in the system if a two-sided measurement topology is applied. Rules 3, 4, and 5 are the most powerful ones, as they do not require a priori knowledge of signal characteristics.

Rule 4 in particular is very robust and can in principle only assign a disturbance as a PD, if signals from different locations arrive at approximately the same time. The chance for this to happen is small, and as this is a random process, resulting faults will produce errors which are randomly distributed over the full cable length and will therefore not lead to incorrect assessment of the cable condition.

6.5 Conclusions

A system capable of detection and location of partial discharges from a cable system is designed and realized. The aim for the system is to prove the concept presented in the previous chapters of this thesis. The designed system therefore aims for optimal flexibility, modularity, and detection performance. The applied hardware components can be regarded as starting points for economical optimization. The system's modularity allows easy replacement of all components. EMC measures are taken by applying an EMC cabinet with surge arrestors and appropriately shielded connections. Data acquisition is performed using a 12 bits, 62.5 MHz digitizer having sufficient dynamic range and bandwidth. The internal memory of 2 MS per channel enables data acquisition of a full power-frequency cycle including additional time for synchronization pulses. Pulse injection is performed via a custom-made generator, amplifier, and injection coil to enable system identification and pulse synchronization. Data communication between the nodes is performed via a computer network, telephone line or mobile-phone network, depending on their availability. Power-line communication (PLC) may be a suitable communication method in the future, if methods for coupling to the MV cable discussed in this thesis are applied to communication systems. Efficiency of PLC depends on the available bandwidth in the applicable standards, but this is not an issue since the channel load is low.

The designed software structure allows flexible distribution of the involved components and easy expansion of functionality. A message-handling engine is designed and realized, enabling the distributed message-driven software architecture in the chosen programming language. Messages between the software components are sent via TCP-IP to enable seamless integration with most existing networks and communication methods. Functional procedures in the software components are started by initiating messages and are in principle executed independently. The system incorporates both GPS and pulse synchronization with minimal difference in the software modules. Results are stored in database structures to enable enhanced methods for storage, searching, and back-tracing of signals and system decisions. The communication of PD data via the database enhances the flexibility of location and update-intervals for the various software modules. To avoid disturbances impeding the results, several rejection algorithms are implemented. Some expert rules may seem redundant, but due to the large numbers and types of disturbances at on-line PD measurements, the different rules are often complementary. The expert rule resulting in the strongest disturbance rejection is the maximum of difference in time of arrival of the signal at the two cable ends. If multiple sensors at both cable ends are used, a significant contribution to the rejection can be realized at the lower MU_x level, which reduces the amount of data to be communicated.

On-line partial-discharge measurements

In this chapter the prototype, described in Chapter 6, is tested. The system is validated by comparing the charge and location results with a calibrated conventional off-line system from KEMA. Special validation measurements are performed to test several aspects of the system's accuracy and functionality. Furthermore, the system is employed for real partial-discharge testing, where measurements are done on both a defective joint and old PILC cables. The results are in agreement with the findings from former chapters and promise good performance in practice.

7.1 Introduction

In the former chapters the different aspects of on-line partial-discharge detection have been examined both theoretically and experimentally. The findings have resulted in a prototype for the system design, discussed in Chapter 6. In this chapter the resulting system prototype is tested by investigating its performance for the actual purpose: on-line PD detection and location.

To enable conditioned validation of the system, a test set-up was designed and artificial PDs were produced from a known location. In Section 7.2 the test-grid is described briefly after which in Section 7.3 validation measurements are performed to test the different aspects of the on-line measurement system. The location ability of the system is validated by testing different time-base alignment (TBA) methods. The charge magnitudes are compared with a calibrated off-line system of KEMA. Real partial discharges must be discriminated from external pulses, so tests are performed to validate the most important expert rules of Section 6.4.6.

Next, real PDs are measured and analyzed by the prototype in Section 7.4 and the results are presented such, that comparison with the off-line system is possible. 'Knowledge rules', which incorporate theories and experiences from past behavior of specific types of cables or accessories, are usually applied for the interpretation of PD measurements. Whether the knowledge rules that exist for off-line diagnostics also apply for the on-line system may be indicated by the different presentation methods in Section 7.4. The conclusions of this chapter are summarized in Section 7.5.

7.2 Measurement set-up

A dedicated small MV grid, where we can alter the configuration according to the testing needs, is set up at KEMA in the Netherlands. This set-up consists of two ring main units (RMUs), interconnected by a MV cable connection. The cable consists of two sections, connected with an oil-filled joint. At one RMU an extra MV cable is connected. Fig. 7.1 shows the layout of this experimental set-up. The RMUs are fully equipped to mimic practical operational conditions. The main difference is the energizing method: in this set-up the transformer in RMU1 is used as a step-up transformer from 400 V to 10 kV (coupled voltages). The main reasons for choosing a test set-up to validate the PD-online performance are:

- The configuration can easily be altered for specific tests.
- The voltage can easily be switched off from the complete RMUs in this test set-up, without concern about power delivery.
- Deteriorated cables can be used, which exhibit large partial-discharge activity.
- Joints and cable terminations can be modified, e.g. such that reproducible PDs are guaranteed.
- The cable ends are all close to each other. This allows direct synchronization of time-bases, which can serve as reference for synchronization techniques.

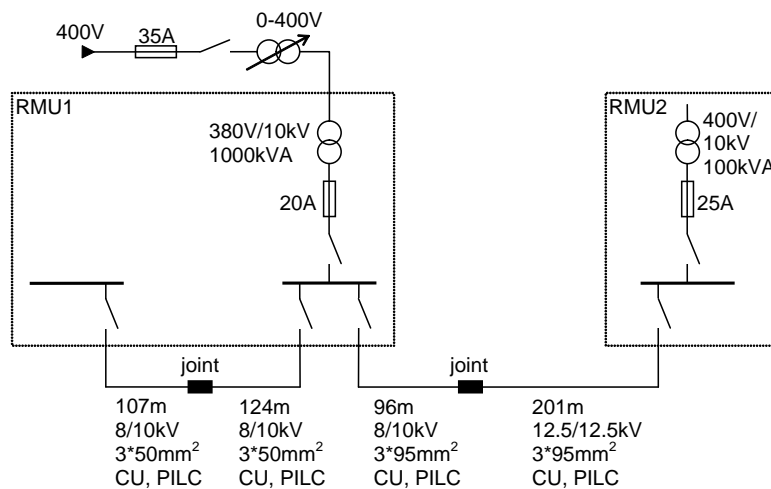


Figure 7.1 Test set-up for experimental on-line PD measurements, consisting of two RMUs, equipped with a 10 kV/380 V, 1000 kVA and a 10 kV/400 V, 100 kVA transformer. The RMUs are interconnected with a 96 m long, 8/10 kV, $3 \times 95 \text{ mm}^2$ CU, paper-insulated lead-covered (PILC) cable and a 201 m, 12.5/12.5 kV, $3 \times 95 \text{ mm}^2$ CU, PILC cable. At one RMU a second MV cable is connected.

This test set-up provides a conditioned environment to produce reliable conclusions. Obviously, in the field longer cables and different noise situations are present. Fig. 7.2 shows the noise power spectral density function (PSDF) for the test set-up. The broad-band noise level is comparable to the noise level for various practical measurement situations in the field, shown in Chapter 4. Often large, narrow-band radio

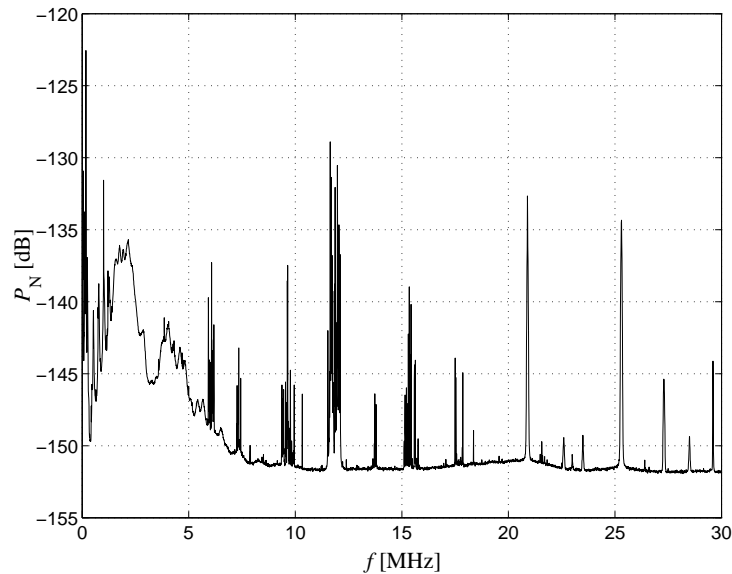


Figure 7.2 Power spectral density function, measured in the test set-up at the cable terminations (PLEC) of the 297 m cable connection

broadcasts are present. But this type of interference can relatively easy be filtered and poses therefore no real limitation for on-line PD detection (see also Section 4.6 and [Vee05]). External interference in the form of short pulses can be injected in the test grid artificially, as will be explained in Section 7.3.4.

7.3 System validation

Partial discharges can in principle originate from any location inside the circuit, can have any charge amplitude, and are therefore not suited to validate the on-line PD system. Instead, pulses are injected artificially in the cable joint. Since the location of the joint is known, the source of the detected pulses is known a priori. The magnitudes of the injected pulses are not known, as the pulses are capacitively coupled to the conductors inside the joint via an unknown capacitance. However, the coupling is constant, so different measuring methods can still be compared.

7.3.1 Off-line reference measurement

For location and charge amplitude validation, measurements are performed on circuit 1, depicted in Fig. 7.3. The cable system under test (CUT) consists of two cable sections: one section of 96 m and a section of 201 m. The CUT is the only connected cable to the two RMUs, so a high and strongly frequency dependent impedance, and therefore higher challenge for on-line PD detection, is ensured. For the off-line measurements, the CUT is disconnected from the RMUs and the three phase-conductors are interconnected to mimic the shield-to-phases (SP) channel in on-line situations. The detection hard- and software from a 0.1 Hz off-line partial-discharge system is used (from KEMA, [Ste91]). This system incorporates a capacitive sensor and a

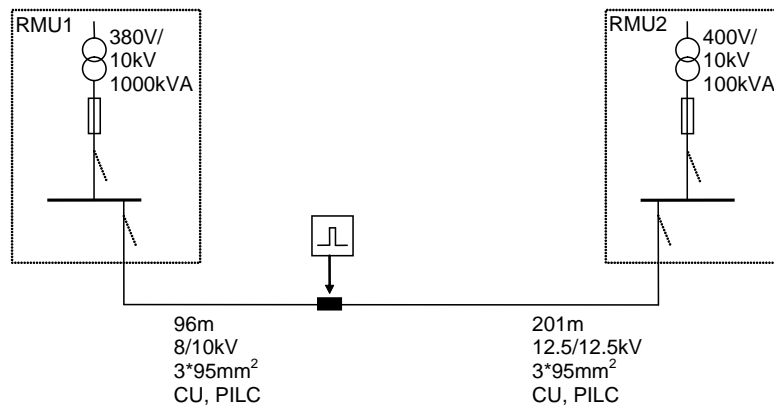


Figure 7.3 Circuit 1. Pulses are injected in the joint between a 96 m and 201 m PILC cable.

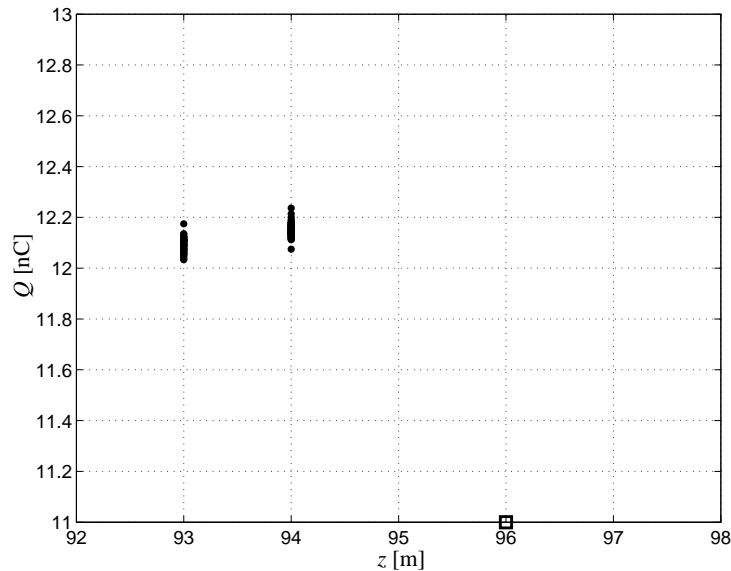


Figure 7.4 Mapping diagram of pulses, injected in joint at 96 m (indicated with \square) and measured with an off-line (0.1 Hz) partial-discharge measurement system. Each dot represents one detected pulse. The software maps to PD locations on a 1 m grid resolution.

100 MS/s oscilloscope which triggers on individual (PD) pulses. The time of arrival (TOA) of the start of each pulse is determined (mainly by eye) and the software uses TDR for location of the PD-sites. The propagation delay of the CUT is determined by pulse injection prior to the PD measurement, as is traditionally done with 0.1 Hz PD testing. The measurement results are given in Fig. 7.4. About 100 detected pulses are plotted, measured during approximately 7 min. The measured charge magnitude has a mean value of 12.1 nC, with a standard deviation of about 0.04 nC. The system's software maps the PD location on a grid with 1 m resolution, so the location results

cannot be interpreted with high resolution. The mean location \bar{z} is about 93.6 m with a standard deviation of about 0.5 m. The mean location is about 2.4 m away from the known joint location. This deviation is mainly caused by the use of a single propagation velocity, while the cable-connection consists of two cable sections with different propagation velocities.

7.3.2 On-line location with different time-base alignment methods

For testing the on-line measurement system, the propagation characteristics were determined in advance by means of pulse response measurements (Chapter 3). Subsequently, both cable ends are connected to the two RMUs, simulating on-line conditions. The RMU impedances are determined by means of the on-line method described in Chapter 4. After these system identification measurements the pulses, injected in the joint, can be measured. The coils were located around both cable ends in the RMUs past the last earth connection. The injected pulses at the joint are recorded with two 12 bit, 62.5 MS/s digitizers, acquiring every minute data records of complete 20 ms frames (one 50 Hz cycle).

Besides the location methods discussed in Chapter 5, GPS and pulse injection, the test set-up provides for a third method. Since the cable ends in the test set-up are close to each other, it is possible to route signals measured at both cable ends to two channels of a single digitizer. This automatically provides for time-base alignment and the calculated location can therefore serve as an objective method for location. Furthermore, the time-of-arrival estimation in the detection software can be tested in this way, since this is the only remaining cause left for location deviation. In this way, 30 records of 20 ms are measured and analyzed resulting in an effective data-acquisition time of 0.6 s. Fig. 7.5 shows a mapping diagram of measurements performed with one digitizer. About 1200 PDs are extracted. The charge magnitudes for the measurements in this section are discussed, in Section 7.3.3. The PD positions can be mapped on a finer grid (≈ 16 cm) compared to the results from the 0.1 Hz analysis. The mean location is very close to the known joint position. The standard deviation is only 4.5 cm, which is very small, considering the 16 ns sample interval of the digitizer, which corresponds to a propagation distance of 2.65 m. It is concluded that the errors introduced by the TOA estimation of the software are very low, and this measurement can serve as a reference measurement.

The next experiment tests the location accuracy when time-base alignment is performed by means of GPS. Again, measurements were done by using circuit 1 (Fig. 7.3). Now both measurement set-ups run separately, but are synchronized by GPS. Again, 30 data blocks of 20 ms were recorded and analyzed. Fig. 7.6 shows the mapping results. The mean of the locations is 99.4 m, 3.4 m biased from the joint's location. Possible sources for this error were discussed in Section 5.3.1. The standard deviation is 6.0 m, which is in agreement with the resolution of the GPS system of 100 ns.

The method of time-base alignment by pulse injection is implemented in the prototype system as well. The pulse-injection coil is mounted together with the measurement coil of RMU1 around the PILC cable past the last earth connection. Synchronization pulses are injected each minute and both systems trigger on these pulses. The resulting diagram is depicted in Fig. 7.7. The mean location of the detected artificial PDs is 95.3 m and the standard deviation from this mean value is 42 cm (0.14% of the cable length, similar to results from Chapter 5). The mean value is closer to the given

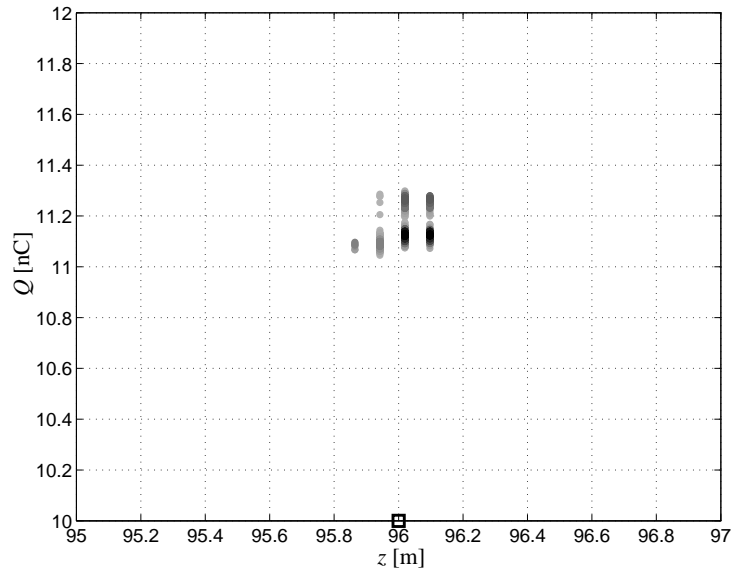


Figure 7.5 Mapping diagram of detected pulses, injected in the joint at 96 m and measured with a single digitizer of the on-line partial-discharge measurement system. Each grey dot represents one detected pulse, the darkness indicates the pulse density. The locations of the PDs are mapped on a grid of about 16 cm, corresponding to 1 ns time resolution.

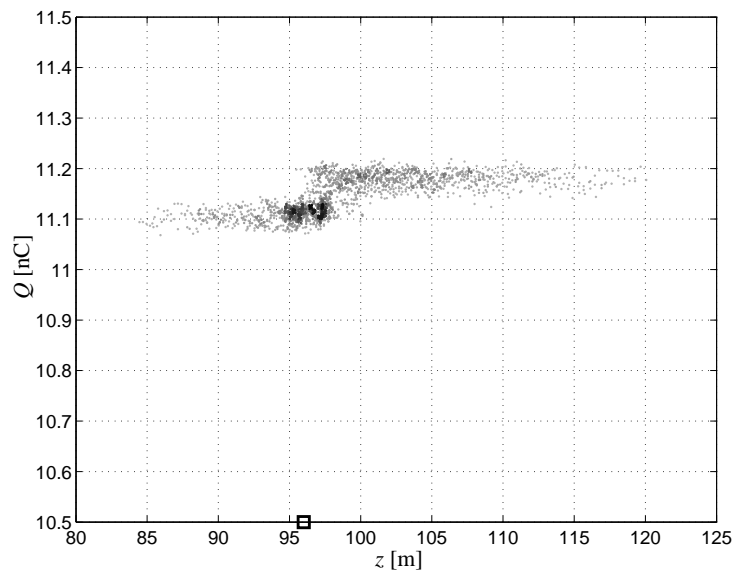


Figure 7.6 Mapping diagram of pulses, injected in the joint at 96 m and measured with the on-line partial-discharge measurement system. Time-base alignment for location is performed with GPS.

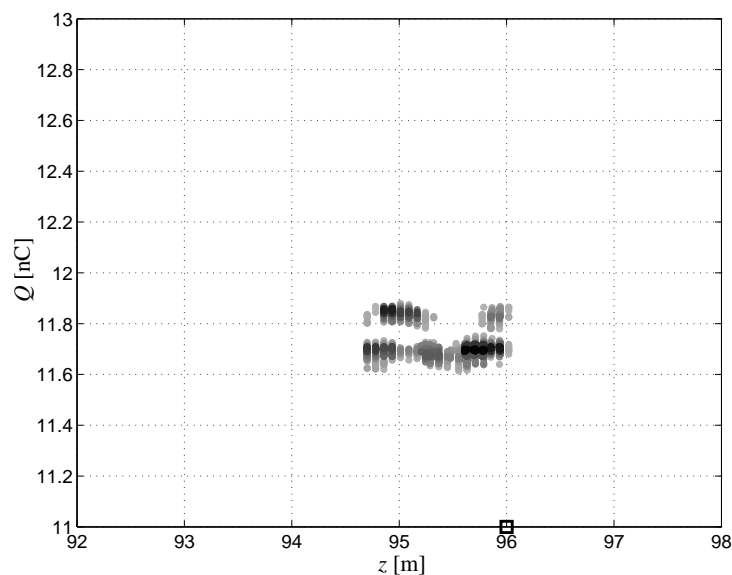


Figure 7.7 Mapping diagram of pulses, injected in the joint at 96 m and measured with the on-line partial-discharge measurement system. Time-base alignment for location is performed with the pulse-injection method.

joint location of 96 m than in the case of the off-line method or GPS synchronization and the deviation is much smaller. Obviously, errors are slightly larger compared to the reference method where only one digitizer was used, but the errors are still much smaller than the sample period of 16 ns. Because of a large number of artificial PDs (about 1200), the estimation of the standard deviation of 0.1–0.2% of the cable length can be considered statistically reliable.

An aspect of time-base alignment still to be tested is the influence of clock jitter on location accuracy. As the two measurement units have two independent digitizing clocks, location calculation can deviate significantly upon small sample-rate variation of these clocks. The solution, presented in Section 5.3.4, employs two pulses with a fixed time-interval. The time interval is detected at both measurement units and time-wander correction is performed. To validate this technique, the sample frequency of one measurement unit was deliberately lowered with 4% (much more than is realistic in practice). The system was fooled by letting it believe that its sample rate was still correct. Firstly, time-wander correction was omitted. The resulting location did deviate to such an extent, that the artificial PDs were located outside the cable length, resulting in zero mapped PDs. Secondly, the time-wander correction was enabled and the mapping results are shown in Fig. 7.8. The figure shows that the resulting locations are corrected and mapped on the same locations as was found without a deliberately altered sample rate. Clearly, the system is insensitive to large variations of the digitizing clocks.

In Table 7.1 the locations and their accuracies are summarized for all tests performed. It is concluded that the method of pulse injection for TBA is most accurate. In fact, it is the most practical method as well.

All previous figures in this section zoom in on the location of the joint, to enlarge

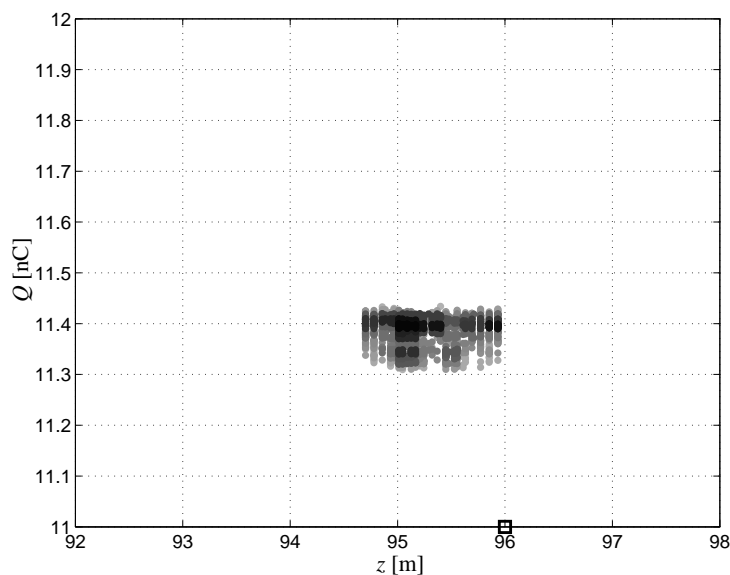


Figure 7.8 Mapping diagram of pulses, injected in the joint at 96 m and measured with the on-line partial-discharge measurement system with deliberately lowered sample frequency of one digitizer. Time-base alignment for location is performed with the pulse-injection method.

Table 7.1 Locations determined from various measurement methods with various synchronization methods when pulses are injected at the joint location z_j (96 m). Δf_s indicates the measurement with deliberately altered sample frequency.

| Measurement method | \bar{z} [m] | $ \bar{z} - z_j $ [% of l_c] | Max deviation | | Standard dev. | |
|------------------------------------|---------------|---------------------------------|---------------|---------------|---------------|---------------|
| | | | [m] | [% of l_c] | [m] | [% of l_c] |
| off-line | 93.6 | 0.81% | 1.0 | 0.34% | 0.50 | 0.17% |
| on-line, single dig. | 96.0 | 0.0% | 0.15 | 0.051% | 0.045 | 0.015% |
| on-line, GPS sync. | 99.4 | 1.1% | 20.6 | 6.9% | 6.0 | 2.0% |
| on-line, pulse sync. | 95.3 | 0.24% | 0.69 | 0.23% | 0.42 | 0.14% |
| on-line, pulse sync., Δf_s | 95.3 | 0.24% | 0.66 | 0.22% | 0.37 | 0.12% |

the deviations. However, normal practice for PD measurements on cables usually shows mapping diagrams of the complete cable connection. In Fig. 7.9 such a graph is plotted for the pulse-synchronization method. Only one pulse was mapped incorrectly at about 102 m and has a lower charge magnitude. This is caused by incorrect positioning of the matched filter in the detection software, resulting in an incorrect estimation of the TOA. Extra checksums in the software could avoid this error, but since this error only occurred once during acquisition of 1200 signals, the error-rate can already be considered to be extremely low.

7.3.3 On-line charge magnitudes

To compare the signal content detected by the off-line and on-line methods, the charge magnitudes mapping diagrams of the previous section are summarized in Table 7.2. In

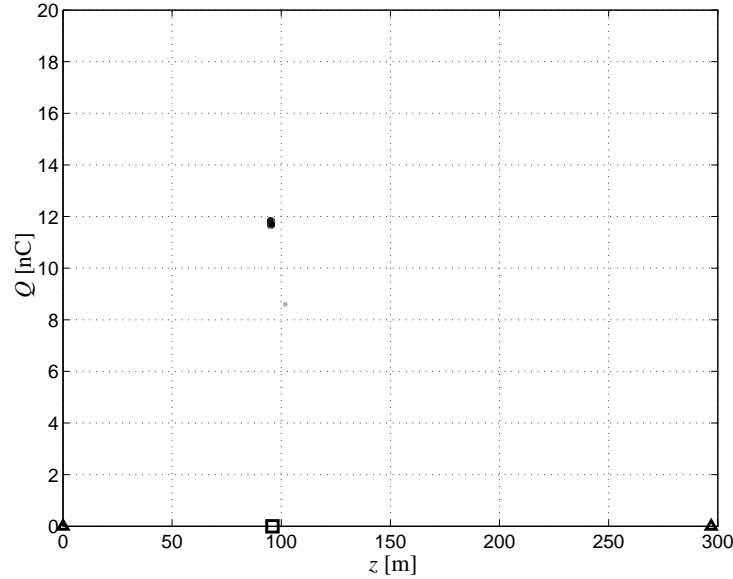


Figure 7.9 Mapping diagram of the full cable connection of pulses, injected in the joint at 96 m and measured with the on-line partial-discharge measurement system. Time-base alignment for location is performed with the pulse-injection method. The joint is indicated with \square , the cable terminations with Δ .

Table 7.2 Determined charge magnitudes from the different measurements, described in Section 7.3.2. The on-line measurements are in the same order as discussed in Section 7.3.2, but just numbered, since the TBA method has no influence on the charge magnitude.

| Measurement method | \bar{Q} [nC] | Max deviation | | Standard deviation | |
|--------------------|----------------|---------------|-------------------|--------------------|-------------------|
| | | [nC] | [% of \bar{Q}] | [nC] | [% of \bar{Q}] |
| off-line | 12.13 | 0.11 | 0.91% | 0.040 | 0.33% |
| on-line 1 | 11.16 | 0.14 | 1.3% | 0.069 | 0.62% |
| on-line 2 | 11.15 | 0.078 | 0.70% | 0.037 | 0.33% |
| on-line 3 | 11.73 | 0.14 | 1.2% | 0.072 | 0.61% |
| on-line 4 | 11.38 | 0.071 | 0.62% | 0.029 | 0.25% |

all cases the deviations within each of the different measurements are extremely small, while larger differences exist between the mean values obtained from the different measurement sets. The overall mean value of all measurement sets is 11.51 nC. The maximum deviation from this value is about 5%, with no substantially larger difference between off- and on-line measurements. The cause of these variations is probably the slight instability of the used pulse generator. The slightly lower value for on-line results is possibly due to the use of a full model from partial-discharge excitation to PD detection to calculate the apparent PD charge at the location of origin of the PD. This is not the case for the off-line system. Nevertheless, it can be concluded that the on-line and the off-line system estimate close to equal charge magnitudes.

7.3.4 Expert-rule validation

The main expert rules for rejection of pulses from outside the cable under test are determination of direction of arrival (DOA), charge polarities, and maximum difference in time of arrival (DTOA), see Section 6.4.6. To test these rules, measurements were performed using circuit 2, depicted in Fig. 7.10. This circuit is basically an extension

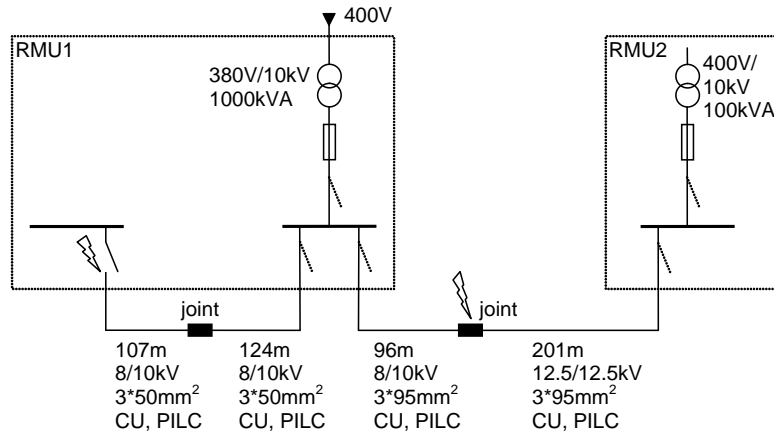


Figure 7.10 Circuit 2. The network is on-line (10 kV). The joint between the 96 m and 201 m PILC cables and the termination of the 107 m PILC cable are damaged.

of circuit 1 with one additional connected MV cable in RMU1. At the end of this cable, PDs can be generated which serve as ‘external’ signals. The 96 + 201 m cable connection is again the cable under test. This time, real PD signals are excited in the joint at 96 m, from an artificial defect generating corona discharge at a sharp point. The PD signals are extracted by sensors around the CUT, past the last earth connection (PLEC) in both RMU1 and RMU2. Furthermore, the signal current through the earth connection of the transformer-connecting cables (TCC) in RMU1 is monitored. All sensors have equal direction with respect to earth. As explained in Section 4.3, the polarity of the first peak in the signals of the PLEC location and the earth of the TCC correlates with the propagation direction of the detected PD pulses: pulses from the CUT should have opposite polarity and signals from anywhere else equal polarity. In RMU1, PD signals can arrive from both directions. Fig. 7.11 shows a signal from a PD originating from the joint at 96 m, measured at the three locations. Indeed, the polarity of the first peak of the two signals measured in RMU1 is opposite. The polarity of the signal at the PLEC location of RMU2, is the same as that of the signal at the same location in RMU1, confirming the origin of the signal. Furthermore, the difference in time of arrival of the signals at both cable ends, indicated in Fig. 7.11, is 667 ns, corresponding with 96 m, the location of the damaged joint that is generating the PDs.

Fig. 7.12 shows a signal where the polarities of the first peak of the signals obtained in RMU1 are the same, so this signal comes from the other direction. This is confirmed by the opposite polarity at RMU2. The indicated DTOA of these signals is 1.79 μ s, corresponding to the propagation time of the CUT, again confirming the signal to come from outside this cable connection.

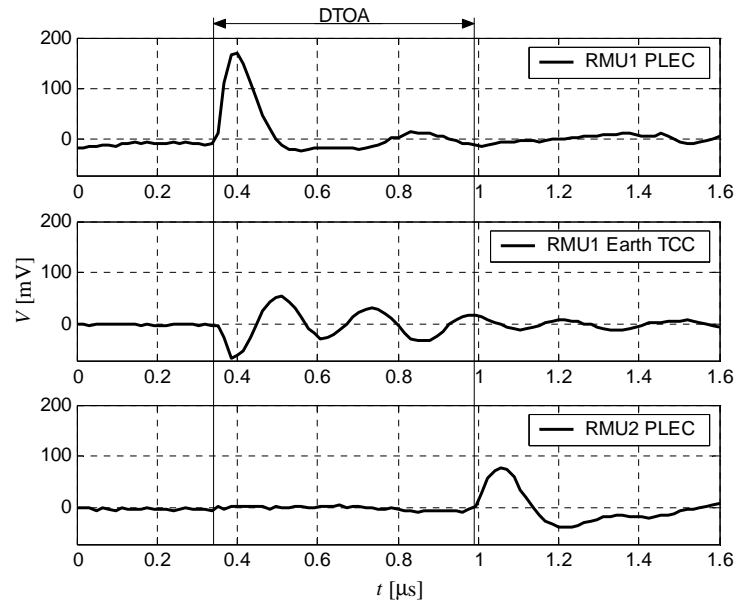


Figure 7.11 PD signal from the damaged joint from the cable under test, measured at three sensor locations

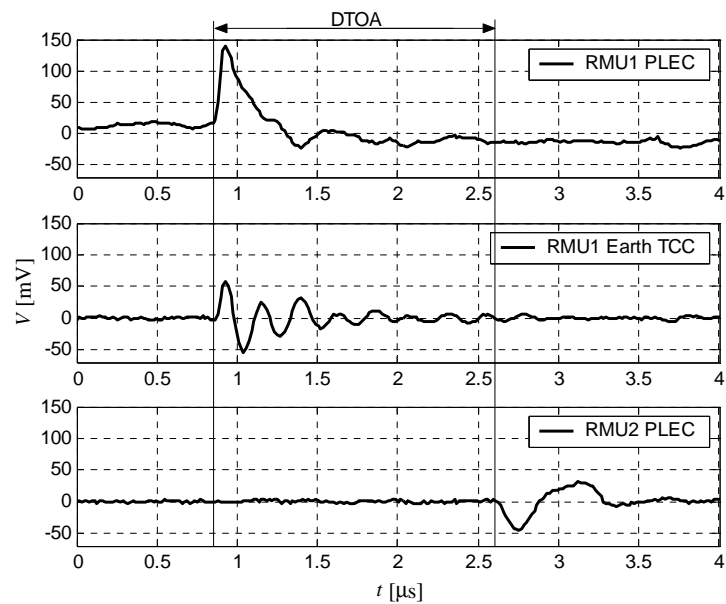


Figure 7.12 PD signal from the damaged termination outside the cable under test, measured at three sensor locations

It is concluded that (i) the method of DOA by means of the polarity of the first peak of the signals, (ii) the method of charge polarities, and (iii) the method of maximum difference in time of arrival are all in agreement, which validates the system's powerful expert rules for interfering pulse rejection.

7.4 Partial-discharge measurements on defective cable and joint

In the previous section, tailored measurements were performed for validation, including one example of a partial discharge in an energized cable. In this section two situations typically occurring in practice are measured at the same time, both with the off-line and the on-line system: a circuit with PDs from cable sections and PDs from a joint.

7.4.1 Partial-discharge mapping

The measurements presented in this section are performed on circuit 3, depicted in Fig. 7.13. The joint between the two cable sections was deliberately damaged to produce PDs.

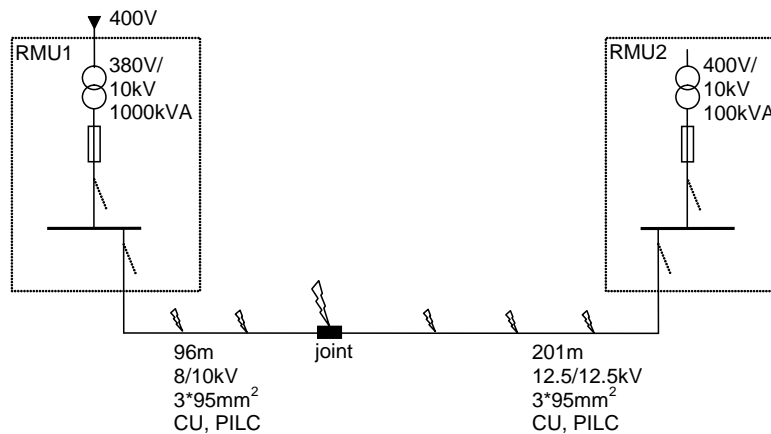


Figure 7.13 Circuit 3. The grid is on-line (10 kV) and the joint between the 96 m and 201 m PILC cables has been damaged to produce PDs. The cables themselves also produce PDs.

First, the cable is disconnected from the RMUs and tested with the 0.1 Hz off-line method. The off-line measurement is performed on the SP channel with the three-phases interconnected, to allow easy comparison with the on-line method. The off-line system is set to a fixed trigger level, just above the noise level. The nominal (phase) voltage of 6 kV is applied. The resulting mapping diagram of the off-line measurement is shown in Fig. 7.14. In 7 minutes approximately 2000 PDs were detected. From this figure it is seen that large PDs arise from the PILC cables, appearing as 'clouds' in the mapping diagram. The left cable section produces PDs up to 6 nC and the right cable even up to 27 nC. The joint of 96 m is also visible in Fig. 7.14, and produces partial discharges up to approximately 2 nC. The visibility of the joint activity is obviously troubled by the high levels of PD from the surrounding cable sections. From the gray-scale, it can be seen that the number of PDs from the joint was high.

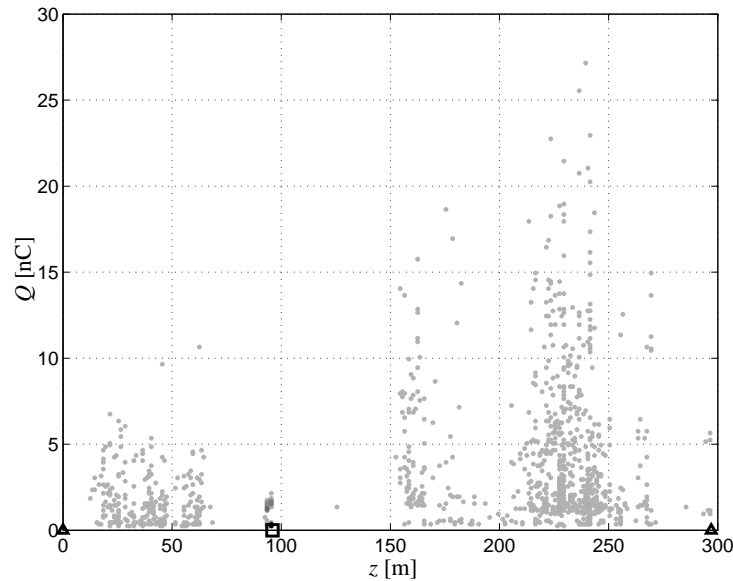


Figure 7.14 Mapping diagram of off-line (0.1 Hz) measurements on circuit 3: partial discharges from a defective joint and PILC cables. The grey scale indicates the PD concentration. The joint is indicated with \square , the cable terminations with \triangle .

Next, the cable-connection and the RMUs are brought on-line up to a coupled voltage of 10 kV. The on-line PD system is synchronized by pulse injection. The mapping diagram is shown in Fig. 7.15 for 60 data-blocks of 20 ms resulting in approximately 13000 PDs. The partial discharges from the joint can clearly be recognized as a narrow line at the joint position. The grey scale at the joint location is dark, indicating a high PD concentration. The magnitude of the majority of the discharges is comparable to the off-line measurement: about 2 nC. PDs from the cable sections are also clearly visible and the locations correspond as well. The magnitude of the PDs from the cables is, however, substantially lower than was the case for the off-line measurements. Apparently, the energizing method (frequency and field distribution) has a pronounced effect on the PDs from the cables (see also Chapter 2). One should also not forget that PD activity in oil-filled cables can change as well upon external condition variation. The location accuracy of the system is high, as shown in Fig. 7.16. In this enlarged mapping diagram the PD concentration occurs within 1.5 m.

7.4.2 Partial-discharge density mappings

In the mapping diagram of the off-line measurement in the previous section, the joint was only visible as a small line, where only the dark color revealed the high PD activity on the joint. Sometimes, instead of their charges, the number of PDs from a certain location is of more interest. The top graph in Fig. 7.17 shows the PD density mapping diagram for the off-line measurement of Section 7.4.1, where the number of PDs (normalized on measurement time and location resolution) is plotted against the location. The location grid is chosen as 3 m, since the validation measurements of Section 7.3 showed higher resolution for off-line measurements to be superfluous. In

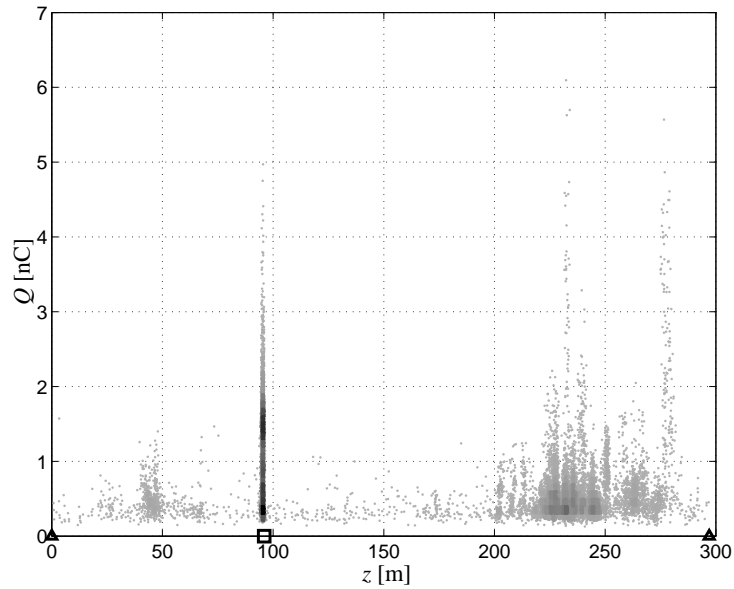


Figure 7.15 Mapping diagram of on-line measurements on circuit 3: partial discharges from a defective joint and PILC cables. The joint is indicated with \square , the cable terminations with \triangle .

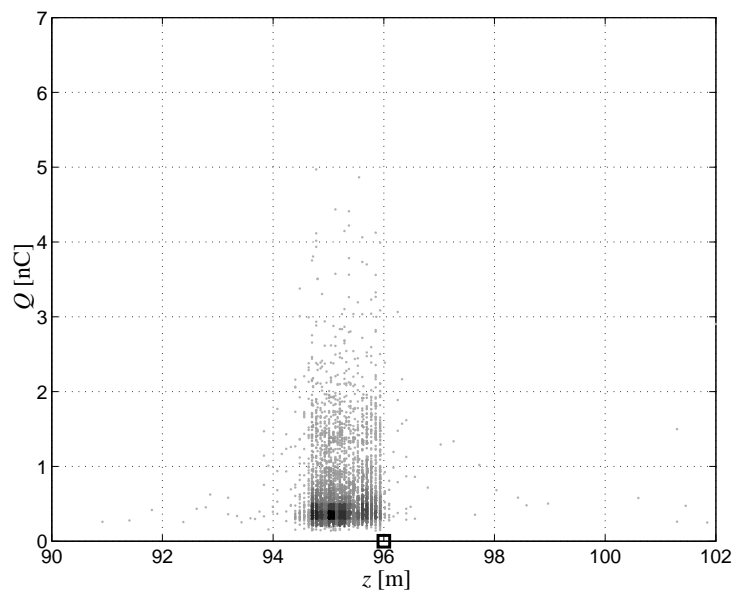


Figure 7.16 Enlarged mapping diagram of on-line measurements on circuit 3: partial discharges from a defective joint

this plot, the PD activity in the joint is pronounced and, since the charge is not taken into account, contributions from the PILC cables are not dominant.

Alternately, the charge density from a certain location can also be a basis for knowledge rules. The total amount of charge (normalized on time and location resolution) is plotted versus the location in the bottom graph of Fig. 7.17. The charge density from PDs in the cable sections is clearer, since their magnitudes were very high compared to the PDs from the joint. It should be noted that the values in these figures may be biased, since the effective measurement time is not precisely known due to dead time after triggering. This is not an issue if data blocks of exactly known duration are recorded at constant time intervals, as is the case for the on-line measurement system.

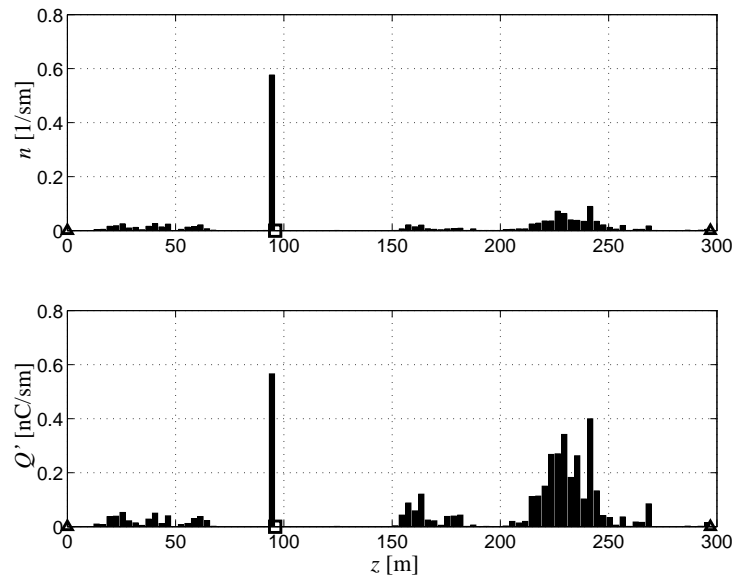


Figure 7.17 PD density mapping diagram (top) and PD charge density mapping diagram (bottom) for off-line (0.1 Hz) measurements on circuit 3: partial discharges from a defective joint

Fig. 7.18 shows the density plots for the on-line measurement. The charge density in the cable sections is relatively low, compared to the off-line measurements, since the charge magnitudes were lower. For on-line measurements, the values in both figures are about a factor 2000 higher than for the off-line test. Apparently, the density of PDs measured on-line is much higher than for off-line. This conclusion is in agreement with the difference between the ratio of the total number of measured PDs for off-line (≈ 2000) versus measurement time (≈ 7 min.), compared to on-line (≈ 13000 PDs in 1.2 s). The ratio between these two totals is also approximately 2000. Part of this effect can be ascribed to the different energizing frequency (factor 500). Furthermore, the dead time after triggering of the off-line system and possible time variance of PD activity can contribute to this effect.

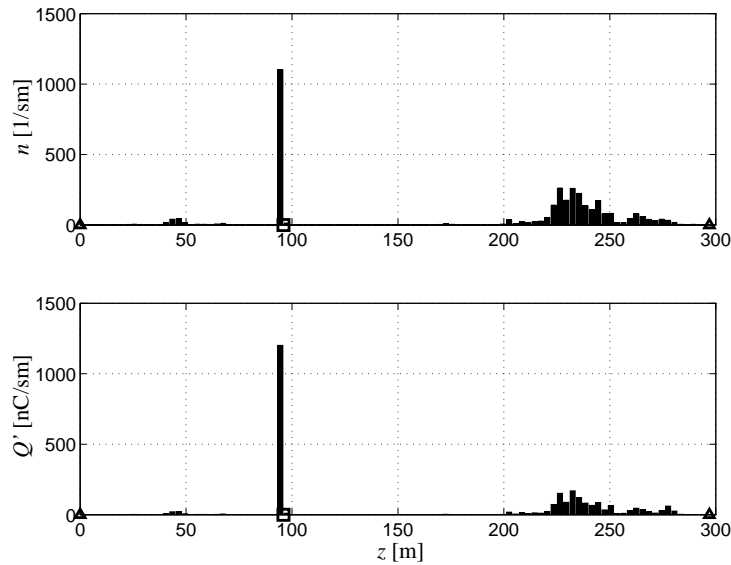


Figure 7.18 PD density mapping diagram (top) and PD charge density mapping diagram (bottom) for on-line measurements on circuit 3: partial discharges from a defective joint

7.4.3 Partial-discharge magnitude histogram

Besides viewing the total length of the cable connections, as described in the previous sections, one specific location may be worth examining in more detail. It can be interesting for result analysis to examine the charge distribution coming from one specific region. Furthermore, the detection sensitivity can be deduced from such a graph. In Fig. 7.19 the PD magnitude histogram is given for the location area of 94 – 96 m of circuit 3, retrieved from off-line measurements. The charge resolution is 20 pC and the distribution function n' is further normalized on the length of the chosen region and measuring time. The maxima in this histogram are visible in the corresponding mapping diagram (Fig. 7.14) at 96 m. The specific shape of this histogram can be dependent on the type of fault and can be useful for knowledge rules. Obviously, n' goes to zero as the charge magnitude increases sufficiently. Below 270 pC the charge distribution function decreases quickly. This is approximately the detection sensitivity of the system in this situation for PDs from that location.

For on-line measured PDs, the charge distribution function is depicted in Fig. 7.20. The same location region and resolution as for the off-line charge distribution is used. Also here, maxima are visible, corresponding to darker areas in the mapping diagram (Fig. 7.15). The values along the vertical axis of this graph are again much larger than the values in Fig. 7.19, due to the reasons mentioned in Section 7.4.2. The shape of this function is also substantially different from the shape of the off-line function. Possible reasons are:

- Different energizing frequency. A different energizing frequency (0.1 Hz versus 50 Hz) may change the behavior of a partial discharge, due to e.g. recovery time of the PD or different field distributions.

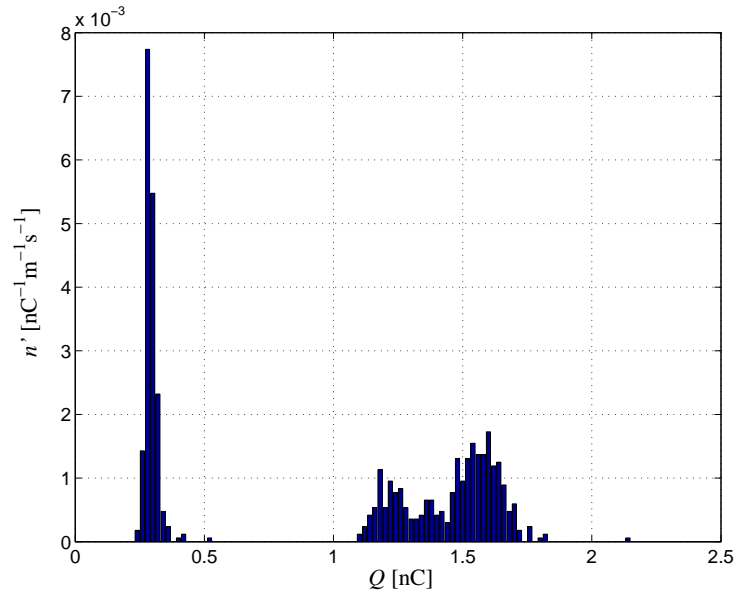


Figure 7.19 PD magnitude histogram of PDs originating from the joint at 96 m, retrieved from off-line measurements on circuit 3

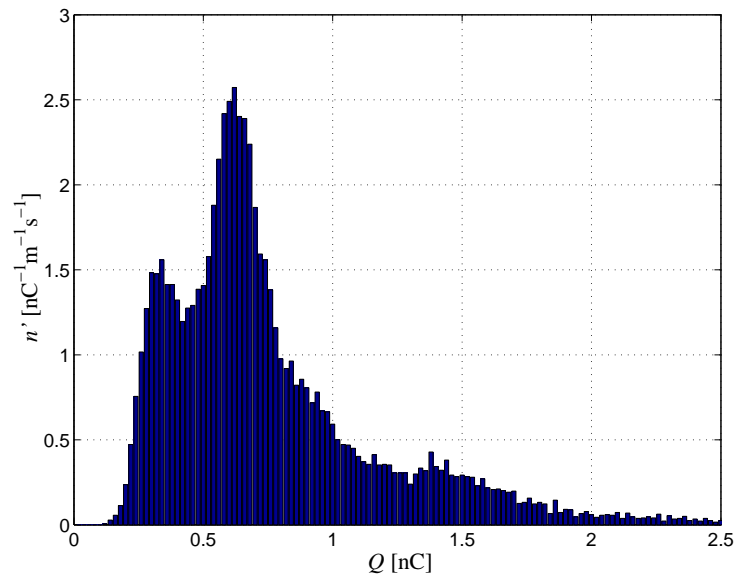


Figure 7.20 PD magnitude histogram of PDs originating from the joint at 96 m, retrieved from on-line measurements on circuit 3

- One-phase energizing voltage versus three-phase, implying different field distributions in the insulation materials (Chapter 2).
- Different triggering method. If the off-line system triggers often on a specific PD, the subsequent PD may be missed each time, which can alter the charge distribution function.
- Time variance of partial-discharge activity. Obviously, the two measurements were not performed at the same time, and time variation of the PD activity causes differences in multiple measurements.

This aspect is beyond the scope of this thesis and is material for future research. Fig. 7.20 also shows clearly that the charge distribution function decreases quickly below 250 pC. The detection sensitivity here is comparable to the sensitivity for the off-line system.

7.4.4 Partial-discharge time-variations

Partial-discharge activity can vary in time. One of the main benefits of the on-line measurement system is the ability to measure over long periods of time or even monitor continuously. To demonstrate this, the set-up of circuit 3 (Fig. 7.15) is monitored for a duration of approximately 7 hours. Data blocks of 20 ms were recorded and analyzed every minute, resulting in almost 100,000 extracted PDs. In Fig. 7.21 the PD charge density Q' is plotted versus location z and time t . The 2-dimensional

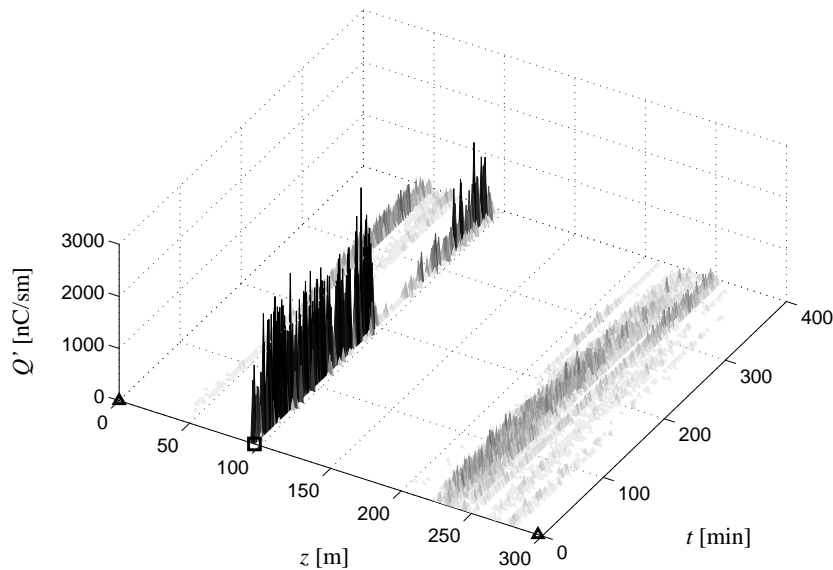


Figure 7.21 PD charge density mapping as a function of time, depicted in 3D

version of this figure is plotted in Fig. 7.22, where the gray-scale indicates the charge density. The density is normalized on length and time grid. Both figures show clearly the variation of PD activity over time. For instance, the PD activity from the joint location (96 m) decreases drastically after 200 minutes, after which it rises again gradually. The PD activity at about 50 m, in the first cable section, increases slowly

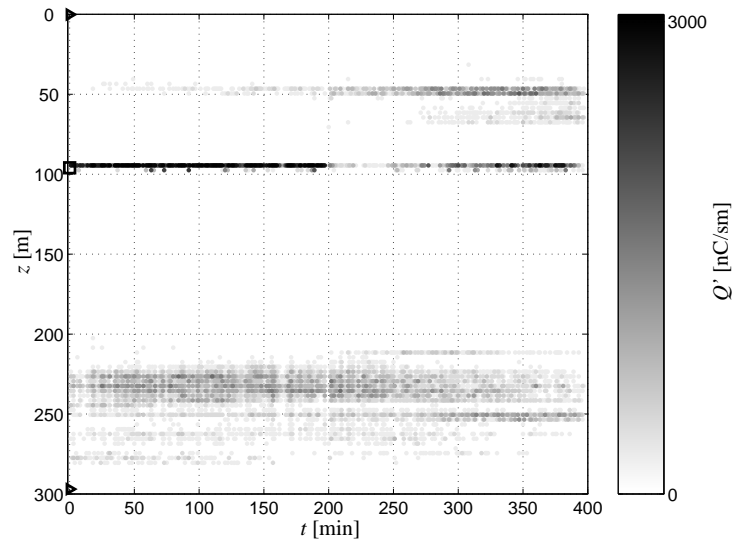


Figure 7.22 PD charge density mapping as a function of time, depicted in 2D

with measurement time. And also the second cable section shows some variation. From literature and practice, possible effects causing variations in time are known. E.g. partial discharges in cavities can stimulate the formation of carbonized paths, after which the field in the cavity is neutralized and the PD stops. It is also known that PILC cables sometimes experience ‘self-healing’ effects and that PD activity changes in time especially directly after energizing. Again, these aspects are beyond the scope of this thesis and their specific behavior for on-line situations requires further investigation.

7.5 Conclusions

The developed on-line partial-discharge measurement prototype has been evaluated in this chapter. A tailored test set-up, consisting of two RMUs and adaptable cable connections, is used to validate the on-line PD system. The test set-up allows more flexible testing than would be possible with live circuits. The level of broad-band noise in the test set-up was comparable to the level determined in the field. Interfering pulses were created deliberately to mimic this class of interference from possible field locations. Large radio broadcast disturbances were not present. But since these are narrow-banded, they are relatively easy to reject anyway and pose therefore no real threat to the PD detection of the on-line system.

For conditioned system validation, pulses were injected in a joint, acting as an artificial PD source. As these pulses are all originating from a single location and have a fixed magnitude, they are used to determine the charge magnitude and location accuracies of the system. Both GPS and pulse injection were tested for the time-base alignment of the on-line system. The method of pulse synchronization resulted by far in the best location accuracy, both concerning the average location (within 0.2% of cable length) and the standard deviation from this value (0.14% of cable length).

The variations in charge, resulting from both off- and on-line measurements are within 5% maximum deviation from the mean value. Probably, real variations of the injected pulses also contributed to these measured variations, since the variations within each (short-duration) measurement set were much smaller (approximately 1%). The number of artificial PDs, captured by the on-line system, is much larger (about a factor 2000) than the number of pulses captured by the off-line system in an equal effective time.

The system includes a number of (partially redundant) methods to eliminate disturbing pulses that are not originating from the cable. The three main rules concern: (1) the direction of arrival of a detected pulse at one cable end, (2) the charge polarities of the pulses from both cable ends, and (3) the maximum difference in time of arrival between pulses detected at the two cable ends. Although also other expert rules are used (see Chapter 6), these three rules are the most powerful, as they do not involve prior knowledge of characteristics of the disturbing signals. All three criteria give decisive answers and are therefore important for robust disturbance rejection. Measurements where disturbing signals were introduced deliberately, showed signal rejection by all three the expert rules, while PDs, originating from the cable under test, were accepted.

Partial discharges were measured on a damaged joint, giving many PDs, situated between two old cable sections. Expected mapping diagrams were obtained: high PD activity from a localized point from the joint position and PD 'clouds' in the old PILC cables. The charge magnitudes from PDs from the joint were comparable for the off- and on-line methods. Although the on-line method resulted in a much larger number of PDs, the same location accuracy is maintained for PDs from a specific location (joint). Several options to present the measurement results were shown and compared to off-line analysis results. Especially the mapping diagram with embedded PD concentration as gray or color scale and the PD charge density diagram (cumulative charge from one location) seem to be a reliable inputs for result interpretation. Measurements made clear that future knowledge rules should be tailored for on-line measurements, since differences with off-line measurements can be substantial. One important advantage of the on-line measuring method is the possibility to measure continuously for long periods of time. Measurements in this chapter already showed the occurrence of large time variations in PD activity, only detectable by long-term measurements. Since location is always determined by this system, all determined variables (charge, density, time-variance) can always be pinpointed to a specific location of interest and different effects from different locations do not influence each other's results.

Conclusions

8.1 Conclusions

On-line partial-discharge diagnostics on medium-voltage cables provides both operational and technical advantages with respect to off-line techniques. Power distribution is not discontinued during testing, since the cable under test remains in service. After installation, an on-line system requires hardly any personnel effort. And, possibly the most important argument from a technical perspective, the cable is continuously monitored, so time variation and intermittent PD activity can be detected, including consequences of operational conditions like over-voltages and load variations. Location of the PD site improves the value and reliability of the result considerably. PD location is even more crucial than in the case of off-line diagnostics, since the detected PD signals can now also originate from adjacent equipment.

Concerning three-phase cables or joints, the electric field in the insulation material differs from off-line measurements where only one phase voltage is applied. In on-line situations, the three phases of the cable system are energized simultaneously, resulting in elliptical field distributions in the insulation. Especially in joints, where the phase conductors are relatively widely spaced, this results in large areas with non-linear electric fields. As a result, for three-phase belted cable systems, a number of differences in interpretation as compared to off-line measurements arise. Dependent on the eccentricity of the electric field, the induced charge magnitude becomes dependent on the direction of the PD, which is related to the phase angle of the power-grid voltage. Furthermore, the phase-angle distributions can deviate strongly from linear-field conditions, depending on the eccentricity of the field at the PD location. Therefore, comparison of results obtained from on-line and off-line PD measurements is not necessarily straightforward. In case of single-core cables, such differences are not present.

After excitation, the PD signal propagates through the cable to the cable terminations. Due to the attenuation of high-frequency signal components in power cables, only frequencies up to a few tens of MHz are useful to consider for cables longer than a few hundred meters. Transmission-line models for TEM waves can be applied. For single-phase power cables with a shield around each phase-conductor, a simple coaxial model applies. For three-phase cables with a common earth screen, multiple propagation paths exist, requiring a multi-conductor transmission-line model. However, the symmetries in a power cable allow reduction to two distinctive channels:

Shield-to-Phases (SP) channel, which concerns the travelling wave between the three phase conductors and the screen, and Phase-to-Phase (PP) channels, which concern the waves between two phase conductors. The preferred measurement location at the cable termination, from a sensor-positioning point of view, involves measurement of the SP channel of the cable. The parameters of this channel can be approximated by using a coaxial model. In the case of paper-insulated power cables, signal attenuation and dispersion are mainly caused by the (frequency dependent) complex dielectric permittivity and must be known or measured for accurate modelling. A complete cable system, incorporating different parameters for every cable section, can be modelled using chain matrices. From the complete cable model, PD waveforms can be predicted and measured signals can be analyzed and interpreted correctly.

Toroidally-shaped coils are the most suitable sensors for detecting partial discharges on-line at the cable terminations in the substations or ring main units (RMUs). Proper design and shielding prevents a high level of EM disturbance. To facilitate practical design for shielding, windings of coaxial cable can provide a good alternative to a common shield around the complete probe. The possible sensor positions in a substation or RMU depend on the type of switchgear present. A highly suitable position, regarding SNR levels and practical issues like safety, is around the part of the cable screen which is extending past its last connection to the earth rail. If this option is not available, a position around the last earth strap is a good alternative. However, extra noise and interference will be measured. Both locations detect signals from the SP channel of the cable under test. If a transformer is present in the substation or RMU, its connecting cables can provide a means to detect the PP channel. The earth connection of these cables provides a possibility to detect the propagation direction of the signals. This way, PD signals from the cable under test can be distinguished from disturbing signals at an early stage of the detection process. Components and circuits in a substation or RMU are identified and modelled in order to determine the load impedance of the cable under test. This load impedance must be known for analysis of PD signals and estimation of the PD charge in on-line measurements. Experiments prove the feasibility of determining the impedances of the substation's elements off-line. The total effective impedance can be obtained while the substation or RMU remains on-line. The impedance can be sufficiently accurately determined in the frequency range that is optimal for PD detection: about 500 kHz–10 MHz, which coincides with the bandwidth of interest found from propagation characteristics and noise levels. The extraction of PD signals from noisy data can be optimally performed by means of a matched-filter bank, which is constructed from the complete signal model.

For on-line PD detection, the cable is connected at both sides to a substation or RMU. This results in low reflection at this point and (possibly PD shaped) disturbances entering the cable at those points. Double-sided measurement enables distinction between signals from the cable under test and signals from elsewhere, and does not rely on far-end reflection for PD location. Multiple measurement set-ups, however, require time-base alignment of the measured data-records. Pulse injection is the most suitable method for both synchronization of the start time, and correction of the time-wander of the local sample clocks at each set-up. Measurements reveal an location accuracy of the pulse-injection method of about 0.2% of the cable length, which is similar to the GPS system for very long cables (around 8 km) and outperforming GPS for shorter lengths.

A system capable of detection and location of partial discharges, based on the concepts in this thesis, is realized, enabling measurement of large quantities of PDs. The system design, chosen hardware and EMC measures were optimized for flexibility and detection performance. This provides a basis for further research and/or commercial production. The data acquisition system incorporates sufficient dynamic range to minimize digitization noise, a large frequency range to accommodate the full bandwidth of interest, and the ability to measure multiple channels for either determination of signal direction or simultaneous diagnostics on several cable connections. The pulse injection is performed via a custom-made pulse generator, amplifier and injection coil, controllable via the measurement computer. GPS synchronization is also implemented as a reference method. The data-communication link between the measurement set-ups depends on the available connections or mobile networks. The flexibility of the system allows easy integration of any communication method. Power-line communication over the MV cables itself may be a suitable method in the future, if methods for coupling to the MV cable discussed in this thesis are applied. The software architecture of the on-line PD system is designed as a set of distributed software components, which communicate via messages over TCP-IP. This allows flexible distribution of the involved components and easy expansion of the functionality. A message handler is realized to enable this distributed messaging set-up. Results are stored in database structures to enable enhanced methods of storage, searching and back-tracing of originating signals and system decisions. For rejection of pulse-shaped disturbances, several expert rules are implemented in the system, providing for robust disturbance-rejecting.

The prototype was validated by controlled experiments, under typical conditions from practice. For location of the PD site, pulse injection outperforms GPS and achieves a location accuracy of approximately 0.2% of the cable length. Charge magnitudes are in agreement with magnitudes found in a calibrated off-line system and maximum deviations are around 5%. On-line partial-discharge measurements on a damaged joint and old PILC-cable sections revealed that the on-line system results in a much larger number of PDs per effective measurement time as compared to the 0.1 Hz method. The same location accuracy is maintained and similar charge magnitudes are found. Several presentation methods can assist the interpretation of the detected PDs for condition assessment purposes, and confirm earlier conclusions that knowledge rules should be tailored to on-line measurements. Furthermore, large variations of PD activity in time are shown, which can only be detected by on-line PD diagnostics.

8.2 Recommendations for future research

This thesis is mainly focused on the detection and location of the PDs. Interpretation of the results is beyond the scope of this study. For off-line measurements, knowledge rules from long experience exist. Several considerations, simulations, and experiments reveal possible interpretation differences between off-line and on-line measurements. Furthermore, the possibility to measure cable systems (semi-)continuously results in extra time-varying parameters. The most important recommendation arising from this thesis is therefore to study the implications of on-line PD detection on knowledge rules, for which the off-line knowledge rules can be used as a starting point

The main application discussed in this thesis is PD diagnostics on medium-voltage

cable systems. Similar theories and methods also apply for high-voltage cable systems. Dimensions and safety aspects will deviate strongly. Furthermore, since the lay-out of the equipment at a high-voltage cable termination differs from medium-voltage systems, practical implementations, like optimal sensor positions, can change. However, many concepts discussed in this thesis are likely to still apply.

The investigation of coupling signals to and from medium-voltage cables leads to a possible spin-off of this project: application of similar techniques for power-line communication (PLC). Especially application of a current transformer in the earth connection of the cables to the transformer (if present) seems to be a promising coupling method for PLC. Another possibility is the integration of PLC techniques with the pulse-injection system, used in this thesis for synchronization and system identification. Alternative modulation schemes, which still meet present standards, may be applied (e.g. pulses with low repetition rate and modulated time differences or amplitudes). Sensors for detection and injection of signals are reciprocal and meet in principle similar requirements, with respect to both frequency range and sensor position. It would be challenging to combine these into a multi-purpose coil, incorporating PD measurement, synchronization-pulse injection and PLC. Obviously, at least two coils are required for on-line impedance measurements as described in this thesis.

The studies performed in this thesis are mainly focused on the situation in the Netherlands. Although the system can be used in many other countries, some complications may arise which may require investigation. Some countries have branched medium-voltage cable systems (e.g. the USA). The proposed system can easily be extended to a multiple-sided system with measurement units at each cable end. Although the general architecture remains the same, details will have to be altered. Furthermore, other types of switchgear may not allow the proposed sensor positions. Some investigation is conducted to switchgear from abroad and the proposed methods are applicable to the majority of the encountered switchgear. A part of the switchgear outside the Netherlands, but strongly depending on the country, needs a different solution for coupling. The data communication between the measurement set-ups in other countries can also involve other available networks and communication standards.

The templates for the matched-filter bank are calculated from the signal model of the total cable system. Another option is to employ a generic cable model and use large detected PD signals to adapt the model in order to increase the extraction sensitivity.

All the theories and methods in this thesis have been tested for their applicability in the PD on-line system. Aspects like speed and costs were not investigated. The implementation of techniques like DSPs (Digital Signal Processors) or FPGAs (Field Programmable Gate Arrays) can improve the efficiency of the system considerably. Furthermore, the use of controllable analog front-ends may eliminate the need for digitizers with a large dynamic range.

APPENDIX A

Measurement of Phase-to-Phase propagation properties

The shield of a power cable is always strongly capacitively coupled to earth. For direct measurements of the PP channels' propagation properties this means that signals should be injected balanced, with e.g. a differential pulse generator. If a normal, unbalanced, pulse generator would be used, the grounding (directly or through capacitive coupling) of one of the poles of the generator would cause an asymmetric injection over the two phase conductors and (an undefined) part of the signal would be injected in the SP channel too. To overcome this complication a different method is presented here. The PP measurements in Chapter 3 are performed using this method.

If a signal is applied between one phase conductor and the shield, with the other phases floating, the signal will be distributed in both the SP and PP channels. This situation is here denoted as Shield to Single Phase (SSP). The resulting propagation characteristics will be determined by both the SP and PP characteristics, i.e. by combination of the results with the SP characteristics, the PP characteristics can be deduced.

The characteristic impedance matrix relates the forward travelling line voltages with the forward travelling line currents:

$$\underline{V}^+(z, \omega) = \mathbf{Z}_c(\omega) \cdot \underline{I}^+(z, \omega) \quad (\text{A.1a})$$

or written out:

$$\begin{pmatrix} V_1^+ \\ V_2^+ \\ V_3^+ \end{pmatrix} (z, \omega) = \begin{pmatrix} Z_{c,1} & Z_{c,2} & Z_{c,2} \\ Z_{c,2} & Z_{c,1} & Z_{c,2} \\ Z_{c,2} & Z_{c,2} & Z_{c,1} \end{pmatrix} (\omega) \cdot \begin{pmatrix} I_1^+ \\ I_2^+ \\ I_3^+ \end{pmatrix} (z, \omega) \quad (\text{A.1b})$$

If a pulse is applied to one phase conductor, with the other two phases floating, the ratio between the (injected) forward travelling wave voltage and current can be determined by e.g. pulse response measurements as in Section 3.4.2. This ratio, denoted as $Z_{c,\text{SSP}}(\omega)$, is equal to the diagonal elements in $Z_{c,1}(\omega)$ in $\mathbf{Z}_c(\omega)$, since initially (at $z = 0$), the currents in the other phases are equal to zero.

$$Z_{c,\text{SSP}}(\omega) = Z_{c,1}(\omega) = \left. \frac{V_i^+(z, \omega)}{I_i^+(z, \omega)} \right|_{I_{j,k}^+(z, \omega)=0, j \neq i, k \neq i}, \quad i, j, k \in \{1, 2, 3\} \quad (\text{A.2})$$

The characteristic impedance matrix, relating the line voltages and currents, is related to the diagonalized characteristic impedance matrix $\tilde{\mathbf{Z}}_c(\omega)$ by reverse transformation:

$$\mathbf{Z}_c(\omega) = \mathbf{F}^* \tilde{\mathbf{Z}}_c(\omega) \mathbf{F} \quad (\text{A.3})$$

with the diagonalized characteristic impedance as:

$$\tilde{\mathbf{Z}}_c(\omega) = \begin{pmatrix} Z_{c,SP} & 0 & 0 \\ 0 & Z_{c,PP} & 0 \\ 0 & 0 & Z_{c,PP} \end{pmatrix} (\omega) \quad (\text{A.4})$$

This results for the characteristic impedance matrix in:

$$\mathbf{Z}_c(\omega) = \frac{1}{3} \begin{pmatrix} Z_{c,SP} + 2Z_{c,PP} & Z_{c,SP} - Z_{c,PP} & Z_{c,SP} - Z_{c,PP} \\ Z_{c,SP} - Z_{c,PP} & Z_{c,SP} + 2Z_{c,PP} & Z_{c,SP} - Z_{c,PP} \\ Z_{c,SP} - Z_{c,PP} & Z_{c,SP} - Z_{c,PP} & Z_{c,SP} + 2Z_{c,PP} \end{pmatrix} (\omega) \quad (\text{A.5})$$

Since the diagonal elements are equal to $Z_{c,SSP}(\omega)$, the characteristic impedance of the PP channels are now determined by:

$$Z_{c,PP}(\omega) = \frac{1}{2} [3Z_{c,SSP}(\omega) - Z_{c,SP}(\omega)] \quad (\text{A.6})$$

The distribution of the applied signal among the SP and PP channels is determined by the impedance matrix in Eq. (A.5). Using Eq. (A.1) this results for the phase voltages at $z = 0$ upon injection on e.g. phase conductor 1:

$$\begin{pmatrix} V_1^+ \\ V_2^+ \\ V_3^+ \end{pmatrix} (0, \omega) = \begin{pmatrix} 1 \\ K_s \\ K_s \end{pmatrix} V_1^+(0, \omega) \quad , \quad K_s = \frac{Z_{c,SP} - Z_{c,PP}}{Z_{c,SP} + 2Z_{c,PP}} \quad (\text{A.7})$$

Now, recall Eq. (3.36) for forward travelling voltages:

$$\underline{V}^+(z, \omega) = \frac{1}{3} \left[e^{-\gamma_{SP}(\omega)z} \begin{pmatrix} 1 & 1 & 1 \\ 1 & 1 & 1 \\ 1 & 1 & 1 \end{pmatrix} + e^{-\gamma_{PP}(\omega)z} \begin{pmatrix} 2 & -1 & -1 \\ -1 & 2 & -1 \\ -1 & -1 & 2 \end{pmatrix} \right] \underline{V}^+(0, \omega) \quad (\text{A.8})$$

The ratio between measured voltage at cable length l_c and injected voltage on phase conductor i upon injection on phase conductor i is:

$$\frac{V_i^+(l_c, \omega)}{V_i^+(0, \omega)} = \frac{1}{3} [e^{-\gamma_{SP}(\omega)l_c}(1 + 2K_s) + e^{-\gamma_{PP}(\omega)l_c}2(1 - K_s)] \quad , \quad i \in \{1, 2, 3\} \quad (\text{A.9})$$

from which $\gamma_{PP}(\omega)$ can be derived. The characteristics of the PP channels are now obtained from combination of results from the SP channel and injection between one phase and the earth screen with the other phases floating.

APPENDIX B

Rogowski-coil principle

B.1 Mutual induction

The theory of a Rogowski coil can be seen as a direct application of Ampere's law, which states that the closed line integral of the magnetic field \underline{H} is equal to the net enclosed current i_{pr} , i.e.

$$\oint \underline{H} \cdot \underline{dl} = i_{\text{pr}} \quad (\text{B.1})$$

where \underline{dl} is a small line element of the integration path. The magnitude of the magnetic field, caused by i_{pr} follows as:

$$H = \frac{i_{\text{pr}}}{2\pi r} \quad (\text{B.2})$$

where r is the distance to the enclosed current.

Consider a helical coil along the loop. If the number of turns per meter n_w is high and constant and we take for simplicity the cross-sectional area A small, i.e. its radius is small compared to the coil diameter, the magnetic flux linking a section \underline{dl} is:

$$d\Phi = An_w \mu \underline{H} \cdot \underline{dl} \quad (\text{B.3})$$

where μ is the magnetic permeability. Integrating the flux over the length \underline{dl} results for the output of the coil:

$$v_{\text{ind}} = \frac{d\Phi}{dt} = \mu n_w A \frac{di_{\text{pr}}}{dt} \quad (\text{B.4})$$

The mutual inductance M_c is defined as the ratio of induced voltage $V_{\text{ind}}(\omega)$ and change of enclosed current $I_{\text{pr}}(\omega)$:

$$V_{\text{ind}}(\omega) = j\omega M_c I_{\text{pr}}(\omega) \quad (\text{B.5})$$

For coils with high winding density and small cross-sectional area, this mutual inductance becomes:

$$M_c = \mu n_w A \quad (\text{B.6})$$

For larger coils, the same approach is valid if the magnetic field is integrated over the relevant cross-section. Analogous to Eqs. (B.3) – (B.6) this results for the mutual inductance of a large coil with N_w rectangularly-shaped windings:

$$M_c = \frac{\mu h N_w}{2\pi} \ln \left(\frac{r_o}{r_i} \right) \quad (\text{B.7})$$

where h is the height, r_i the inner radius, and r_o the outer radius of the coil. For a coil with circularly-shaped windings we find:

$$M_c = \mu N_w \left(r_{\text{coil}} - \sqrt{r_{\text{coil}}^2 - r_w^2} \right) \quad (\text{B.8})$$

where r_w is the radius of the circle of one winding and r_{coil} is the radius of the complete toroidal structure.

B.2 Self inductance

For the self-inductance the relevant enclosed flux is caused by the current i_{sec} through the coil itself, so the total enclosed current becomes $N_w i_{\text{sec}}$. Along the same line as for the mutual induction in Section B.1, this results in the relation between the self induction and mutual induction for the same coil:

$$L_c = \frac{\Phi}{i_{\text{sec}}} = N_w M_c \quad (\text{B.9})$$

B.3 Core material

In principle Rogowski coils are air-filled coils, resulting in $\mu = \mu_0$, the permeability of vacuum. The mutual- (and self-) inductance of the coil is increased by using ferro-magnetic material with high relative permeability μ_r (up to 10^5). If such core materials are applied, extra requirements arise. The material should not saturate, in particular not by the power frequency current. Depending on the location of the probe, this current can reach several hundreds amperes. To avoid saturation, the flux density B in the material should be controlled. This can be done by implementing an air slit of a defined size d_{air} in the core. If l_{coil} is the length of the coil and $\mu_r \gg l_{\text{coil}}/d_{\text{air}}$, the magnetic field inside this air slit is dominant and the mutual inductance becomes independent of μ_r and the shape or size of the windings:

$$M_c = \frac{\mu_0 A N_w}{d_{\text{air}}} \quad (\text{B.10})$$

where A is the cross section area of the turns in the coil. The air slit must be precisely fixed, since the mutual inductance is inversely proportional to d_{air} .

Saturation of the core material also provides for an inherent safety aspect. If the enclosed current becomes too high, the flux density B can reach its saturation value B_s after which the flux density does not increase anymore with increasing magnetic field H . This results in a maximum value of the induced voltage. As the value of B can be controlled by the choice of core material and size of air slit, this characteristic can be used against unwanted over-voltages due to power-switching transients or lightning surges.

B.4 Relevant magnetic fluxes

The following fluxes must be considered for the properties of toroidal coils:

1. The flux relevant for the mutual inductance. This is the flux enclosed by the sum of the windings, i.e. the flux through the cross-sectional loop areas. If a magnetic field from an external current is applied with a component in the direction of the plane of the complete loop, it adds to the enclosed flux on one side of the toroidal coil and is subtracted from the flux at the other side. If the coil windings are equally distributed, the net contribution is zero.
2. The flux that is enclosed by the complete loop. If an external field is applied with a component perpendicular to the area of the complete loop, an external flux will be enclosed by the loop, inducing an extra voltage at the output of the coil. This flux can be caused by not-enclosed currents and is therefore regarded as disturbance. If two coils (e.g. for injection and measurement) are in close proximity, see e.g. Fig. 4.22, this flux can be significant. An effective method to avoid this enclosed flux is to reroute one end of the coil back through the center of the windings to the other end.
3. The flux around single windings. This flux is caused by the secondary current and is ‘leaking’ through the space between two windings. For high winding densities, this flux will be negligible, but if the number of windings becomes small, this flux can become significant. As this flux only contributes to the self-inductance, it should remain small. A method to minimize this contribution is to make use of wide metal strips as windings (as in Fig. 4.22) or use parallel wires for each turn.

If the above conditions are met, the sensitivity for external magnetic fields is minimized.

B.5 Transfer impedance

A commonly used, equivalent circuit of a Rogowski coil, enclosing I_{pr} and loaded by a measurement impedance Z_{m} is depicted in Fig. B.1. The coil is modelled as a

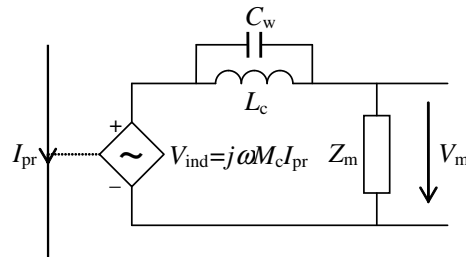


Figure B.1 Equivalent circuit of current probe with inner-winding capacitance

current-controlled voltage source V_{ind} , representing the induced voltage, and a self-inductance of the coil L_c . The distributed inter-winding capacitances are modelled as one lumped capacitance C_w over L_c . The introduced self-inductance in the primary circuit can usually be neglected. The transfer impedance of this circuit is:

$$Z_t(\omega) \triangleq \frac{V_{\text{m}}(\omega)}{I_{\text{pr}}(\omega)} = j\omega M_c \cdot \left(1 + \frac{j\omega L_c / Z_{\text{m}}}{1 - \omega^2 L_c C_w}\right)^{-1} \quad (\text{B.11})$$

At the resonance frequency ($f_r = (2\pi\sqrt{L_c C_w})^{-1}$) the transfer impedance is zero. If the considered frequency range is far below f_r , the inter-winding capacitance can be neglected, resulting in:

$$Z_t(\omega) \triangleq \frac{V_m(\omega)}{I_{pr}(\omega)} = \frac{j\omega M_c Z_m}{Z_m + j\omega L_c} \quad (\text{B.12})$$

In general one can distinguish two conditions:

- If $\omega L_c \ll Z_m$, usually the case for an air coil in combination with a large Z_m , the measured voltage becomes: $V_m(\omega) = j\omega M_c I_{pr}(\omega)$; i.e. the measuring system differentiates the current $i_{pr}(t)$ with calibration factor M_c .
- If $\omega L_c \gg Z_m$, usually the situation with a ferro-magnetic core and a small Z_m , then: $V_m(\omega) = M_c Z_m I_{pr}(\omega)/L_c$, a flat frequency spectrum as from the cut-off frequency $\omega_{co} = Z_m/L_c$.

For high frequencies the parasitic capacitance to the environment can not be neglected. Especially if the coil is shielded, the capacitance to this shield can limit the bandwidth considerably. To model the probe for high frequencies, a transmission-line model can be applied, e.g. [Bos00, Nas79]. In Fig. B.2 the equivalent circuit of a small section dz of the coil is depicted. The circuit elements M' , L , and C are the per-unit-length mutual inductance, self-inductance, and capacitance to the shield or the environment. At $z = 0$ the circuit is short-circuited and at $z = l_{coil}$, the length of the coil, it is terminated with a measurement impedance Z_m .

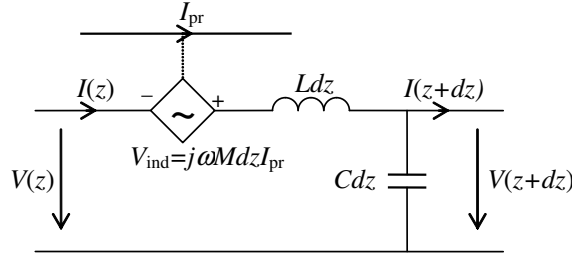


Figure B.2 Equivalent circuit of transmission line section dz of current probe

The input and output voltages are related by the transmission-line equations:

$$\frac{\partial}{\partial z} \begin{pmatrix} V(z, \omega) \\ I(z, \omega) \end{pmatrix} = - \begin{pmatrix} 0 & j\omega L \\ j\omega C & 0 \end{pmatrix} \begin{pmatrix} V(z, \omega) \\ I(z, \omega) \end{pmatrix} + \begin{pmatrix} j\omega M I_{pr}(\omega) \\ 0 \end{pmatrix} \quad (\text{B.13})$$

By decoupling the differential equations, the plane wave solutions in terms of forward and backward travelling waves are obtained:

$$V(z, \omega) = V^+ e^{-\gamma(\omega)z} + V^- e^{+\gamma(\omega)z} \quad (\text{B.14a})$$

$$I(z, \omega) = \frac{V^+}{Z_c} e^{-\gamma(\omega)z} - \frac{V^-}{Z_c} e^{+\gamma(\omega)z} + \frac{M}{L} I_{pr}(\omega) \quad (\text{B.14b})$$

where the “+” denotes the forward and “-” the backward travelling wave. The propagation constant $\gamma(\omega)$ and characteristic impedance Z_c are given by:

$$\gamma(\omega) = j\omega\sqrt{LC} \quad , \quad Z_c = \sqrt{\frac{L}{C}} \quad (\text{B.15})$$

Implementing the boundary conditions:

$$V(0, \omega) = 0 \quad , \quad V_m(\omega) = V(l_{\text{coil}}, \omega) = Z_m I(l_{\text{coil}}, \omega) \quad (\text{B.16})$$

results for the transfer impedance in:

$$Z_t(\omega) = \frac{Z_c Z_m M \sinh(\gamma(\omega) l_{\text{coil}})}{Z_c L \sinh(\gamma(\omega) l_{\text{coil}}) + Z_m L \cosh(\gamma(\omega) l_{\text{coil}})} \quad (\text{B.17})$$

For transmission lines that are short-circuited at one end, the output at the other end becomes zero for frequencies for which the length of the transmission line l_{coil} is an integer multiple of half the wavelength. According to Eq. (B.17) the transfer impedance has discrete resonance frequencies at $\omega_r = k\pi(l_{\text{coil}}\sqrt{LC})^{-1}$ with $k \in \mathbb{N}$. For low frequencies, $|\gamma(\omega)G| \ll 1$, Eq. (B.17) reduces to Eq. (B.12).

APPENDIX C

Software structures

C.1 Software components

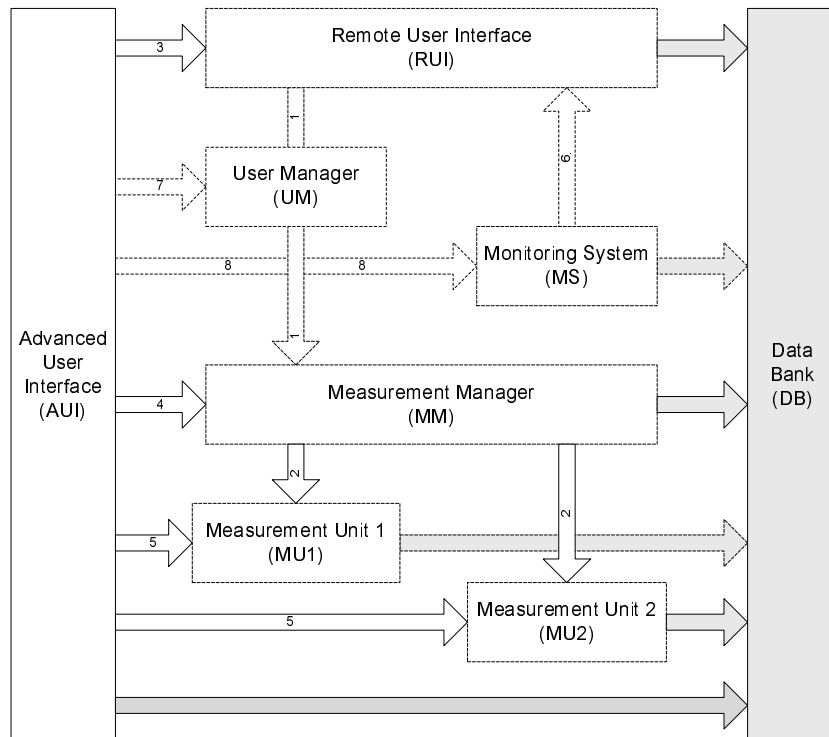


Figure C.1 Component collaboration diagram. The arrows indicate the direction of the initiating messages (white) or requests for PD data transfer (grey). The dashed components UM and MS and accompanying messages are preliminary.

Examples of messages involved:

1. RUI and UM as use cases of MM
 - (a) Set system configuration (SET_SYSCFG)
 - (b) Get system configuration (GET_SYSCFG)
 - (c) Set utility cable configuration (SET_UCABCFG)
 - (d) Get utility cable configuration (GET_UCABCFG)
 - (e) Start system identification (START_SI)
 - (f) Get system identification result (GET_SI)
 - (g) Get cable model (GET_CABMDL)
 - (h) Start measuring sequence (START_MEAS_SEQ)
 - (i) Stop measuring sequence (STOP_MEAS_SEQ)
 - (j) Get measurement results (GET_MM_RESULT)
 - (k) Get Status (GET_STATUS)
2. MM as a use case of MUX
 - (a) Set system configuration (SET_SYSCFG)
 - (b) Set MU configuration (SET_MUCFG)
 - (c) Get MU configuration (GET_MUCFG)
 - (d) Get MUX_Result (GET_MUX_RESULT)
 - (e) Inject and measure system identification pulses (IM_SI_PULSE)
 - (f) Measure system identification pulses (M_SI_PULSE)
 - (g) Calculate MFB (CALC_MFB)
 - (h) Update MFB using current selected templates (UPD_MFB)
 - (i) Initialize measurement (INIT_MEAS)
 - (j) Set measurement starting times (SET_START_TIMES)
 - (k) Start measuring (START_MEAS)
 - (l) Stop measuring (STOP_MEAS)
 - (m) Get Status (GET_STATUS)
3. AUI as a use case of RUI
 - (a) Get Status (GET_STATUS)
4. AUI as use case of MM
 - (a) All messages of 1.
 - (b) Get specific records from tables under MM_Result (GET_SPEC_MM_RESULT)
5. AUI as use case of MUX
 - (a) All messages of 2.
 - (b) Get specific records from tables below MUX_Result (GET_SPEC_MUX_RESULT)
 - (c) Get synchronization details (GET_SYNCDET)
6. MS as a use case of RUI
 - (a) PD alarm (PD_ALARM)
7. AUI as use case of UM
 - (a) Set user definitions (SET_USERS)
 - (b) Get user definitions (GET_USERS)
8. AUI as use case of MS
 - (a) Set alarm conditions (SET_ALARMCFG)

C.2 Database structure

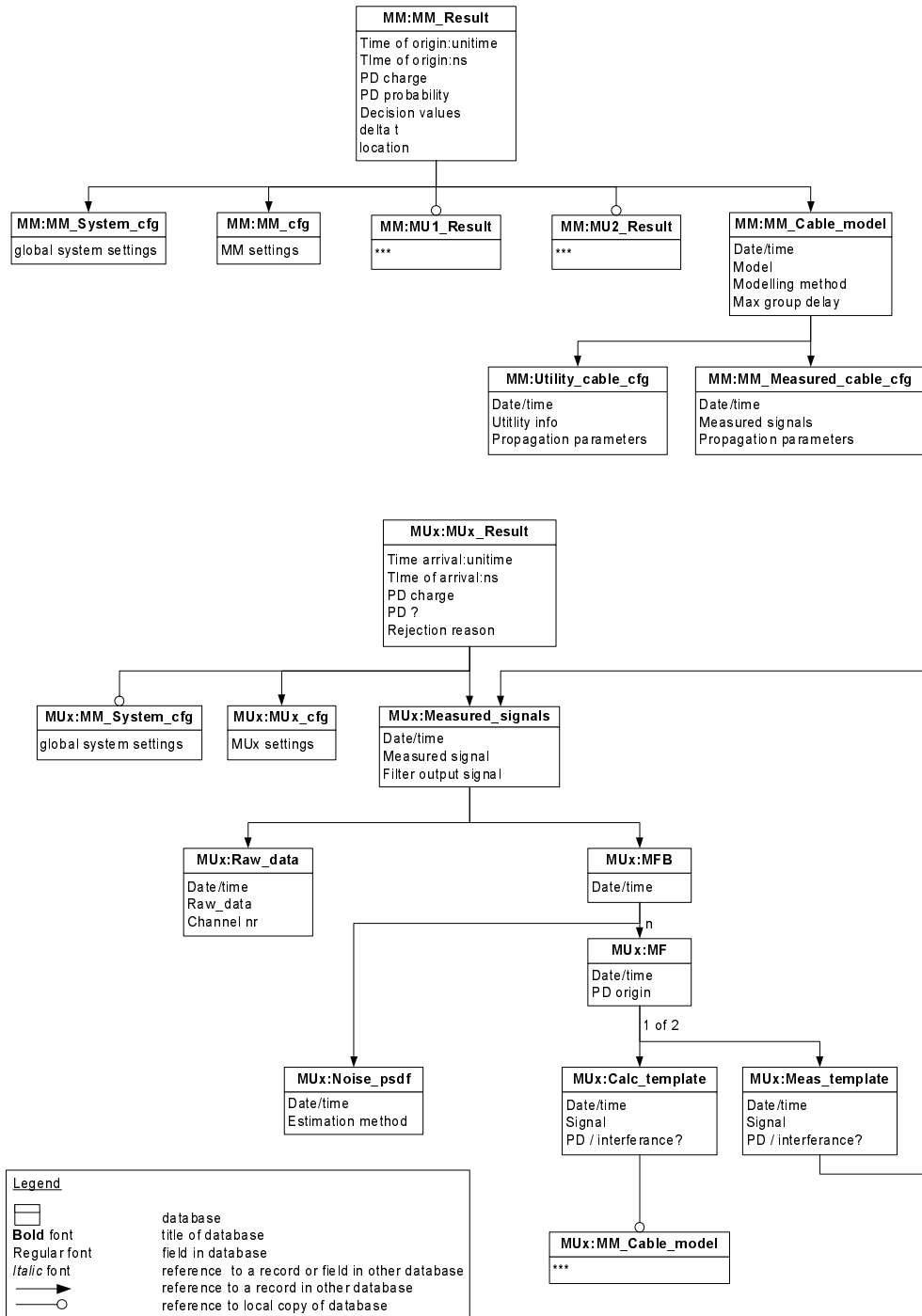


Figure C.2 Database structure

Bibliography

- [Abd99] M. A. Abdallah, “Partial discharge pulses in artificial voids in XLPE-material used in cables insulation”, *Eleventh International Symposium on High Voltage Engineering (Conf. Publ. No. 467)*, vol. 4, pp. 212 – 215, Aug. 1999.
- [Ahm98] N. H. Ahmed and N. N. Srinivas, “On-line partial discharge detection in transformer”, *Conference Record of the 1998 IEEE International Symposium on Electrical Insulation*, vol. 1, pp. 39–42, June 1998.
- [Ahm01] N. H. Ahmed and N. N. Srinivas, “On-line partial discharge diagnostic system in power cable system”, *Proceedings of the IEEE/PES Transmission and Distribution Conference and Exposition*, vol. 2, pp. 853–858, October 2001.
- [Akb02] A. Akbari, P. Werle, H. Borsi, and E. Gockenbach, “A continuous parameter high frequency model based on travelling waves for transformer diagnostic purposes”, *Conference Record of the IEEE International Symposium on Electrical Insulation*, pp. 154–157, Apr. 2002.
- [Auc90] C. Aucourt, W. Boone, W. Kalkner, R. Naybour, and F. Ombello, “Recommendations for a new after laying test method for high voltage extruded cable systems”, *Cigré session 1990*, paper 21-105, Paris, France, Aug/Sep 1990.
- [Bal97] C. A. Balanis, *Antenna theory : analysis and design*, 2nd ed., Wiley, Chichester, UK, 1997.
- [Bar90] S. Barnett, *Matrices: Methods and applications*, Oxford University Press, Oxford, NY, USA, 1990.
- [Bar00] R. Bartnikas and K. Srivastava, *Power and communication cables, theory and applications*, IEEE Press and McGraw-Hill, New York, 2000.
- [Bos00] A. van den Bossche and J. Ghijselen, “EMC combined di/dt current probe”, *IEEE International symposium on Electromagnetic Compatability*, pp. 21–25, Washington, USA, Aug. 2000.
- [Bow00] C. L. Bowmer, “On-line diagnostic trials on london electricity’s 11 kV cable system”, *IEE Seminar on Asset Management of Cable Systems*, vol. 029, pp. 7/1–7/17, 2000.
- [Car00] J. F. Carpentier, S. Gellida, D. Gloria, G. Morin, and H. Jaouen, “Comparison between S-parameter measurements and 2D electromagnetic simulations for microstrip transmission lines on BiCMOS process”, *Proceedings of the 2000 International Conference on Microelectronic Test Structures (ICMTS)*, pp. 235–240, March 2000.
- [CEN] CENELEC EN50065, *Signalling on low-voltage electrical installations in the frequency range 3 kHz to 148.5 kHz*, European Committee for Electrotechnical Standardization (CENELEC).

- [Chi95] S. Chimklai and J. R. Marti, "Simplified three-phase transformer model for electromagnetic transient studies", *IEEE Transactions on Power Delivery*, vol. 10, no. 3, pp. 1316–1325, July 1995.
- [Cig96] Cigré working group 21/22.01, "Comparison of overhead lines and underground cables for electricity transmission", *Cigré Session 1996*, Paper 21/22-01, Paris, 1996.
- [Cla62] F. Clark, *Insulating materials for design and engineering practice*, Wiley, London, UK, 1962.
- [Coo63] J. Cooper, "On the high-frequency response of a Rogowski coil", *Journal of Nuclear Energy Part C, Plasma Physics*, vol. 5, pp. 285–289, 1963.
- [Cra99] P. Craatz, R. Plath, R. Heinrich, and W. Kalkner, "Sensitive on-site PD measurement and location using directional coupler sensors in 110 kV prefabricated joints", *Proceedings of the 11th International Symposium on High Voltage Engineering (Conf. Publ. No. 467)*, vol. 5, pp. 317–321, 1999.
- [Dal99] E. Dallago and G. Venchi, "Analytical and experimental approach to high-frequency transformer simulation", *IEEE Transactions on Power Electronics*, vol. 14, no. 3, pp. 415–421, May 1999.
- [Dav79] P. J. Davis, *Circulant matrices*, Wiley-Interscience, New York, NY, USA, 1979.
- [Eis92] W. R. Eisenstadt and Y. Eo, "S-parameter-based ic interconnect transmission line characterization", *IEEE Transactions on Components, Hybrids, and Manufacturing Technology*, vol. 15, no. 4, pp. 483–490, Aug. 1992.
- [Gäf04] U. Gäfvert, "Dielectric response analysis of real insulation systems", *Proceedings of the 8th IEEE International Conference on Solid Dielectrics (ICSD)*, pp. 5–9, Toulouse, France, July 2004.
- [Ger02] A. Gerasimov, "Wide-range inductive sensors of currents with nanosecond rise times for measuring parameters of high-current pulses (review)", *Instruments and Experimental Techniques*, vol. 45, no. 2, pp. 147–161, 2002.
- [Gro98] D. W. Gross and B. A. Fruth, "Characteristics of phase resolved partial discharge pattern in spherical voids", *IEEE Conference on Electrical Insulation and Dielectric Phenomena (CEIDP), Annual Report*, vol. 2, pp. 412–415, 1998.
- [Gul98] E. Gulski, J. J. Smit, P. Seitz, and J. C. Smit, "PD measurements on-site using oscillating wave test system", *Conference Record of the 1998 IEEE International Symposium on Electrical Insulation*, vol. 2, pp. 420–423, 1998.
- [Gup81] K. C. Gupta, R. Garg, and R. Chadha, *Computer-aided design of microwave circuits*, Artech House, Dedham, MA, USA, 1981.
- [Ham01] B. R. Hamerling, F. J. Wester, E. Gulski, J. J. Smit, and E. R. S. Groot, "Fundamental aspects of on-line PD measurements on distribution power cables", *Proceedings of the 7th IEEE International Conference on Solid Dielectrics (ICSD)*, pp. 408–411, Eindhoven, the Netherlands, June 2001.
- [Hap78] H. Happoldt and D. Oeding, *Elektrische Kraftwerke und Netze*, Springer, Berlin, Germany, 1978.
- [Has94] L. Hasselgren, E. Moller, and Y. Hamnerius, "Calculation of magnetic shielding of a substation at power frequency using FEM", *IEEE Transactions on Power Delivery*, vol. 9, no. 3, pp. 1398–1405, July 1994.
- [Hel98] A. Helgeson and U. Gäfvert, "Dielectric response measurements in time and frequency domain on high voltage insulation with different response", *Proceedings of 1998 International Symposium on Electrical Insulating Materials*, pp. 393–398, Sep. 1998.

- [Hem92] L. H. Hemming, "Applying the waveguide below cut-off principle to shielded enclosure design", *Symposium Record of the IEEE 1992 International Symposium on Electromagnetic Compatibility*, pp. 287–289, Aug. 1992.
- [Hen96] C. G. Henningsen, K. Polster, B. A. Fruth, and D. W. Gross, "Experience with an on-line monitoring system for 400kV XLPE cables", *Proceedings of the IEEE Transmission and Distribution Conference*, pp. 515–520, Los Angeles, USA, 1996.
- [Het95] E. Hetzel and R. Mackinlay, "Diagnostic field testing of paper-insulated lead-covered MV cables", *Jicable 1995*, paper B.8.6.4, 1995.
- [Hor98] F. B. M. van Horck, *Electromagnetic compatibility and printed circuit boards*, Ph.d. thesis, Eindhoven University of Technology, Eindhoven, The Netherlands, 1998.
- [Hud65] R. H. Huddleston and S. L. Leonard, *Plasma diagnostic techniques*, Academic Press, London, 1965.
- [Hvi98] S. Hvidsten, E. Ildstad, B. Holmgren, and P. Werelius, "Correlation between AC breakdown strength and low frequency dielectric loss of water tree aged XLPE cables", *IEEE Transactions on Power Delivery*, vol. 13, no. 1, pp. 40–45, Jan. 1998.
- [Hvi00] S. Hvidsten, H. Faremo, J. Bentjaminsen, and E. Ildstad, "Condition assessment of water treed service aged cables by dielectric response measurements.", *Cigré Session 2000*, paper 21-2001, Paris, 2000.
- [IECa] IEC60055, *Paper-insulated metal-sheathed cables for rated voltages up to 18/30 kV (with copper or aluminium conductors and excluding gas-pressure and oil-filled cables)*, International Electrical Commission (IEC), Geneva, Switzerland.
- [IECb] IEC60270, *High-voltage test techniques - Partial discharge measurements*, 13 ed., International Electrical Commission (IEC), Geneva, Switzerland.
- [IECc] IEC60502, *Power cables with extruded insulation and their accessories for rated voltages from 1 kV ($U_m = 1,2$ kV) up to 30 kV ($U_m = 36$ kV)*, International Electrical Commission (IEC), Geneva, Switzerland.
- [IECd] IEC61334, *Distribution automation using distribution line carrier systems*, International Electrical Commission (IEC), Geneva, Switzerland.
- [Ild82] E. Ildstad, *Water migration and watertreeing in cross-linked polyethylene cables.*, Ph.d. thesis, University of Trondheim, Trondheim, Norway, 1982.
- [Joh75] C. T. A. Johnk, *Engineering electromagnetic fields and waves*, Wiley, Chichester, 1975.
- [Jon89] E. W. P. Jones, "The great dielectric phenomenon", *Power Engineering Journal*, vol. 3, no. 1, pp. 33–37, Jan. 1989.
- [Kab] *Medium Voltage Power Cables Catalogue*, Kabelwerk Eupen AG, Eupen, Belgium.
- [Kad59] H. Kaden, *Wirbelströme und Schirmung in der Nachrichtentechnik*, Springer-Verlag, Berlin/Göttingen/Heidelberg, Germany, 1959.
- [Kam96] K. Kaminaga, M. Ichihara, M. Jinno, O. Fujii, S. Fukunaga, M. Kobayashi, and K. Watanabe, "Development of 500-kV XLPE cables and accessories for long-distance underground transmission lines. V. long-term performance for 500-kV XLPE cables and joints", *IEEE Transactions on Power Delivery*, vol. 11, no. 3, pp. 1185–1194, July 1996.
- [Khe98] A. Kheirmand, M. Leijon, and C. Tornkvist, "Detection and localization of partial discharge in high voltage power cable joints", *Proceedings of the IEEE 6th International Conference on Conduction and Breakdown in Solid Dielectrics, ICSD '98*, pp. 145–148, Västerås, Sweden, June 1998.

- [Kra88] J. D. Kraus, *Antennas*, 2nd ed., McGraw-Hill, Boston, USA, 1988.
- [Kre89] F. H. Kreuger, *Partial discharge detection in high-voltage equipment*, Butterworths, London, UK, 1989.
- [Kre91] F. H. Kreuger, *Industrial high voltage, part 1*, Delft University Press, Delft, The Netherlands, 1991.
- [Kre93a] F. H. Kreuger, E. Gulski, and A. Krivda, "Classification of partial discharges", *IEEE Transactions on Electrical Insulation*, vol. 28, no. 6, pp. 917–931, Dec. 1993.
- [Kre93b] F. H. Kreuger, M. G. Wezelenburg, A. G. Wiemer, and W. A. Sonneveld, "Partial discharge xviii: Errors in the location of partial discharges in high voltage solid dielectric cables", *IEEE Electrical Insulation Magazine*, vol. 9, no. 6, pp. 15–24, November/December 1993.
- [Lee00] C.-Y. Lee, S.-H. Nam, S.-G. Lee, D.-W. Kim, and M.-K. Choi, "High frequency partial discharge measurement by capacitive sensor for underground power cable system", *Proceedings on the International Conference on Power System Technology (Powercon 2000)*, vol. 3, pp. 1517–1520, 2000.
- [Lem96] E. Lemke, P. Schmiegel, P. Elze, and D. Russwurm, "Procedure for evaluation of dielectric properties based on complex discharge analyzing (cda)", *Conference Record of the 1996 IEEE International Symposium on Electrical Insulation*, vol. 1, pp. 385–388, June 1996.
- [Mas92] M. S. Mashikian, F. Palmieri, R. Bansal, and R. Northdrop, "Location of partial discharges in shielded cables in the presence of high noise", *IEEE Transactions on Electrical Insulation*, vol. 27, no. 1, pp. 37–43, February 1992.
- [Mas00] M. Mashikian, "Partial discharge location as a diagnostic tool for power cables", *Proceedings of the IEEE Power Engineering Society Winter Meeting*, vol. 3, pp. 1604–1608, Jan. 2000.
- [Mer98] J. van der Merwe, H. Reader, and J. Cloete, "S-parameter measurements yielding the characteristic matrices of multiconductor transmission lines", *IEEE Transactions on Electromagnetic Compatibility*, vol. 40, no. 3, pp. 249–256, Aug. 1998.
- [Mor93] A. Morched, L. Marti, and J. Ottevangers, "A high frequency transformer model for the emtp", *IEEE Transactions on Power Delivery*, vol. 8, no. 3, pp. 1615–1626, July 1993.
- [Mug04] G. Mugala, R. Eriksson, U. Gäfvert, and P. Petterson, "Measurement technique for high frequency characterization of semiconducting materials in extruded cables", *IEEE Transactions on Dielectrics and Electrical Insulation*, vol. 11, no. 3, pp. 471–480, June 2004.
- [Mul99] G. Muller, J. Wendei, and K. Reiss, "Efficient analysis of coupled multiconductor transmission lines", *International Symposium on Electromagnetic Compatibility*, pp. 646–649, 1999.
- [Nas79] V. Nassisi and A. Luches, "Rogowski coils; theory and experimental results", *Review of Scientific Instruments*, vol. 50, no. 7, pp. 900–902, 1979.
- [Nev03] P. Nevalainen and K. Nousiainen, "Rogowski coil in partial discharge measurements on MV networks", *Nordic Insulation Symposium (NORD-IS03)*, Tampere, Finland, June 2003.
- [Oli54] B. M. Oliver, "Directional electromagnetic couplers", *Proceedings of the Institute of Radio Engineers*, vol. 42, pp. 1686–1692, 1954.
- [Pap03a] R. Papazyan and R. Eriksson, "Calibration for time domain propagation constant measurements on power cables", *IEEE Transactions on Instrumentation and Measurement*, vol. 52, no. 2, pp. 415–418, Apr. 2003.

- [Pap03b] R. Papazyan and R. Eriksson, "High frequency characterisation of water-treed XLPE cables", *Proceedings of the 7th International Conference on Properties and Applications of Dielectric Materials*, vol. 1, pp. 187–190, June 2003.
- [Pau94] C. R. Paul, *Analysis of multiconductor transmission lines*, John Wiley, New York, NY, USA, 1994.
- [Pem99] A. J. M. Pemen, W. R. Rutgers, T. J. M. van Rijn, and Y. H. Fu, "On-line partial discharge monitoring of hv components", *Eleventh International Symposium on High Voltage Engineering (Conf. Publ. No. 467)*, vol. 5, pp. 136–139, Aug. 1999.
- [Pem00] A. J. M. Pemen, *Detection of partial discharges in stator windings of turbine generators*, Ph.d. thesis, Eindhoven University of Technology, Eindhoven, The Netherlands, 2000.
- [Pes99] E. Peschke and R. Olshausen, *Cable Systems for High and Extra-High Voltage*, Pirelli, 1999.
- [Pom99] D. Pommerenke, T. Strehl, R. Heinrich, W. Kalkner, and W. Schmidt, F. and Weiß enberg, "Discrimination between internal PD and other pulses using directional coupling sensors on HV cable systems", *IEEE Transactions on Dielectrics and Electrical Insulation*, vol. 6, no. 6, pp. 814–824, Dec. 1999.
- [Pul95] E. Pultrum and M. J. M. van Riet, "Hf partial discharge detection of hv extruded cable accessories", *Proceedings of the 3rd International Conference on Insulated Power Cables (JICABLE)*, pp. 662–665, Versailles, France, June 1995.
- [Ram38] S. Ramo, "Currents induced by electron motion", *Proceedings of the IRE*, vol. 27, pp. 584–585, 1938.
- [Rob91] G. Robinson, "Discharges in asymmetric cavities under AC stresses", *IEE Proceedings Science, Measurement and Technology*, 2, vol. 138, pp. 119–126, March 1991.
- [Rog12] W. Rogowski and W. Steinhaus, "Die messung der magnetischen spannung", *Archiv für Elektrotechnik*, vol. 1, no. 4, pp. 141–511, 1912.
- [Sch88] R. B. Schulz, V. C. Plantz, and D. R. Brush, "Shielding theory and practice", *IEEE Transactions on Electromagnetic Compatibility*, vol. 30, no. 3, pp. 187–201, Aug. 1988.
- [Sch99] N. van Schaik, W. Boone, E. Hetzel, and B. Grotenhuis, "MV cable maintenance, practices and results", *Proceedings of the International Conference on Insulated Power Cables (JICABLE)*, Versailles, France, June 1999.
- [Sch00] G. Schoffner, "A directional coupler system for the direction sensitive measurement of UHF-PD signals in GIS and GIL", *Annual Report Conference on Electrical Insulation and Dielectric Phenomena*, vol. 2, pp. 634–638, 2000.
- [Sed91] H. G. Sedding, S. R. Campbell, G. C. Stone, and G. S. Klempner, "A new sensor for detecting partial discharges in operating turbine generators", *IEEE Transactions on Energy Conversion*, vol. 6, no. 4, pp. 700–706, Dec. 1991.
- [Shi01] I. Shim, J. Soraghan, and W. Siew, "Detection of PD utilizing digital signal processing methods part 3: Open-loop noise reduction", *IEEE Electrical Insulation Magazine*, vol. 17, no. 1, pp. 6–13, Jan./Feb. 2001.
- [Sho38] W. Shockley, "Currents to conductors induced by a moving point charge", *Journal Applied Physics*, vol. 9, pp. 635–636, 1938.
- [Sri86] N. Srivallipuranandan, *Series impedance and shunt admittance matrices of an underground cable system*, Master's thesis, University of British Columbia, Vancouver, Canada, 1986.

- [Sri95] N. Srinivas and B. Bernstein, "Effect of DC testing on XLPE insulated cables", *Jicable 1995*, paper A.6.1, Versailles, France, June 1995.
- [Ste89] E. F. Steennis, *Water treeing, the behaviour of water trees in extruded cable insulation*, Ph.d. thesis, Delft University of Technology, Delft, The Netherlands, 1989.
- [Ste91] E. F. Steennis, E. Hetzel, and C. W. J. Verhoeven, "Diagnostic medium voltage cable test at 0.1Hz", *Proceedings of the 3rd International Conference on Insulated Power Cables (JICABLE)*, pp. 408–414, Versailles, France, June 1991.
- [Ste92] J. P. Steiner, P. H. Reynold, and W. L. Weeks, "Estimating the location of partial discharges in cables", *IEEE Transactions on Electrical Insulation*, vol. 27, no. 1, pp. 44–59, February 1992.
- [Ste00] E. F. Steennis, F. van den Boogaard, C. G. N. de Jong, M. J. M. van Riet, and G. P. T. van der Wijk, "Learning from high-voltage xlpe cable system testing and monitoring", *Cigr*, 21-203, 2000.
- [Ste01] E. F. Steennis, R. Ross, N. van Schaik, W. Boone, and D. M. van Aartrijk, "Partial discharge diagnostics of long and branched medium-voltage cables", *Proceedings of the IEEE 7th International Conference on Solid Dielectrics ICSD '01*, pp. 27–30, 2001.
- [Ste02a] E. F. Steennis, P. A. A. F. Wouters, P. C. J. M. van der Wielen, and J. Veen, "Method and system for transmitting an information signal over a power cable", Int. Patent No. WO 2004/013642, June 2002.
- [Ste02b] E. F. Steennis, P. A. A. F. Wouters, P. C. J. M. van der Wielen, and J. Veen, "Werkwijze en system voor het overbrengen van een informatiesignaal over een vermogenskabel", Dutch Patent No. NL 1020925, June 2002.
- [Ste03a] E. F. Steennis, *KEMA course on power cables: production, installation, ageing, testing and asset management*, KEMA T&D Testing Services, Arnhem, The Netherlands, Oct. 2003.
- [Ste03b] E. F. Steennis, P. C. J. M. van der Wielen, J. Veen, and P. A. A. F. Wouters, "Aspects and implications of on-line PD detection and localization of MV cable systems", *Conference Record of the International Conference on Insulated Power Cables (JICABLE)*, pp. 666–671, Versailles, France, June 2003.
- [Sto82] G. C. Stone and S. A. Boggs, "Propagation of partial discharge pulses in shielded power cables", *Annual report of the conference on electrical insulation and dielectric phenomena*, pp. 275–280, National Academy of Science, Washington DC, USA, 1982.
- [Sty82] W. Stygar and G. G., "High frequency rogowski coil response characteristics", *IEEE Transactions on Plasma Science*, vol. PS-10, no. 1, pp. 40–44, 1982.
- [Tal04] M. Talbi, *De puls injector*, Master thesis, Avance University, Breda, The Netherlands, 2004.
- [Tan83] T. Tanaka and A. Greenwood, *Advanced power cable technology, present and future.*, vol. II, CRC Press, Boca Raton, Florida, 1983.
- [Tan95] T. Tanaka, "Partial discharge pulse distribution pattern analysis", *IEE Proceedings on Science, Measurement and Technology*, vol. 142, no. 1, pp. 46–50, Jan. 1995.
- [Tre68] H. L. van Trees, *Detection, estimation, and modulation theory, part 1*, Wiley, New York, 1968.

- [Vee02] J. Veen, P. C. J. M. van der Wielen, and E. F. Steennis, "Propagation characteristics of three-phase belted paper cable for on-line PD detection", *Conference Record of the IEEE International Symposium on Electrical Insulation (ISEI)*, pp. 96–99, Boston, MA, USA, June 2002.
- [Vee03a] J. Veen and P. C. J. M. van der Wielen, "Online partial discharge detection in power cables using matched filters", *Proceedings of the 18th Nordic Symposium on Electrical Insulation (NORDIS)*, pp. 71–78, Tampere, Finland, June 2003.
- [Vee03b] J. Veen and P. C. J. M. van der Wielen, "Partial discharge detection and localization using matched filters", *IEEE Electrical Insulation Magazine*, vol. 19, no. 5, pp. 20–26, Sept./Oct. 2003.
- [Vee04a] J. Veen and P. C. J. M. van der Wielen, "PD location in power cables using parametric models", *Proceedings of the 8th IEEE International Conference on Solid Dielectrics (ICSD)*, pp. 711–714, Toulouse, France, July 2004.
- [Vee04b] J. Veen, P. C. J. M. van der Wielen, and E. F. Steennis, "Cancellation of continuous periodic interference for PD detection", *Proceedings of the 8th IEEE International Conference on Solid Dielectrics (ICSD)*, pp. 707–710, Toulouse, France, July 2004.
- [Vee05] J. Veen, *On-line signal analysis of partial discharges in medium voltage power cables*, Ph.D. thesis, Eindhoven University of Technology, Eindhoven, The Netherlands, 2005.
- [Wag04] P. Wagenaars, *Inductive sensors and directional sensing for PD monitoring in RMUs*, Master thesis, Eindhoven University of Technology, Eindhoven, The Netherlands, 2004.
- [Wai62] L. A. Wainstein and V. D. Zubakov, *Extraction of signals from noise*, Prentice-Hall, Englewood Cliffs, 1962.
- [Wal01] C. Walton, "Detecting and locating MV failure before it occurs", *Proceedings of the 16th International Conference on Electricity Distribution (CIRED)*, 482, vol. 1, Amsterdam, The Netherlands, June 2001.
- [War93] D. A. Ward and J. La T. Exon, "Using rogowski coils for transient current measurements", *Engineering Science and Education Journal*, vol. 2, no. 3, pp. 105–113, 1993.
- [Wee84] W. L. Weeks and Y. M. Dao, "Wave propagation characteristics in underground cable", *IEEE Transactions on Power Apparatus and Systems*, vol. PAS-103, no. 10, pp. 2816–2826, Oct. 1984.
- [Wen95] D. Wenzel, U. Schichler, H. Borsi, and E. Gockenbach, "Recognition of partial discharges on power units by directional coupling", *Proceedings of the 9th International Symposium on High Voltage Engineering, paper 5626*, vol. 5, Graz, Austria, Aug–Sep 1995.
- [Wer91] J. J. Werner, "The HDSL environment [high bit rate digital subscriber line]", *IEEE Journal on Selected Areas in Communications*, vol. 9, no. 6, pp. 785–800, Aug. 1991.
- [Wer01] P. Werelius, P. Tharning, R. Eriksson, B. Holmgren, and U. Gäfvert, "Dielectric spectroscopy for diagnosis of water tree deterioration in XLPE cables", *IEEE Transactions on Dielectrics and Electrical Insulation*, vol. 8, no. 1, pp. 27–42, Feb. 2001.
- [Wes02] F. Wester, E. Gulski, J. Smit, and E. Groot, "Aspect of on-line and off-line PD diagnosis of distribution power cables", *Conference Record of the 2002 IEEE International Symposium on Electrical Insulation*, pp. 553 – 556, April 2002.

- [Wet89] J. M. Wetzter and P. C. T. van der Laan, "Prebreakdown currents: basic interpretation and time-resolved measurements", *IEEE Transactions on Electrical Insulation*, vol. 24, no. 2, pp. 297–308, April 1989.
- [Wha71] A. D. Whalen, *Detection of signals in noise*, Academic press, New York, 1971.
- [Wie00] P. C. J. M. van der Wielen, *Corrosiediagnostiek voor loodmantelkabels*, Master's thesis, Eindhoven University of Technology, Eindhoven, The Netherlands, 2000.
- [Wie02] P. C. J. M. van der Wielen, P. A. A. F. Wouters, and E. F. Steennis, "Signal interpretation of partial discharges in three-phase medium voltage cable systems measured on-line", *Conference Record of the IEEE International Symposium on Electrical Insulation (ISEI)*, pp. 542–545, Boston, MA, USA, June 2002.
- [Wie03a] P. C. J. M. van der Wielen, E. F. Steennis, and P. A. A. F. Wouters, "Fundamental aspects of excitation and propagation of on-line partial discharge signals in three-phase medium voltage cable systems", *IEEE Transactions on Dielectrics and Electrical Insulation*, vol. 10, no. 4, pp. 678–688, Aug. 2003.
- [Wie03b] P. C. J. M. van der Wielen, J. Veen, and P. A. A. F. Wouters, "Evaluation of different types of sensors and their positioning for on-line PD detection and localisation in distribution cables", *Proceedings of the 18th Nordic Symposium on Electrical Insulation (NORDIS)*, pp. 367–374, Tampere, Finland, June 2003.
- [Wie03c] P. C. J. M. van der Wielen, J. Veen, P. A. A. F. Wouters, and E. F. Steennis, "Sensors for on-line PD detection in MV power cables and their locations in substations", *Proceedings of the 7th International Conference on Properties and Applications of Dielectric Materials (ICPADM)*, pp. 215–219, Nagayo, Japan, June 2003.
- [Wie03d] P. C. J. M. van der Wielen, P. A. A. F. Wouters, J. Veen, and D. M. van Aartrijk, "Synchronization of on-line PD detection and localization setups using pulse injection", *Proceedings of the 7th International Conference on Properties and Applications of Dielectric Materials (ICPADM)*, pp. 327–330, Nagoya, Japan, June 2003.
- [Wie04a] P. C. J. M. van der Wielen, J. Veen, P. Wagenaars, and P. A. A. F. Wouters, "Determination of substation model for correct interpretation of on-line measured PD signals from MV cable systems", *Proceedings of the 8th IEEE International Conference on Solid Dielectrics (ICSD)*, pp. 747–750, Toulouse, France, July 2004.
- [Wie04b] P. C. J. M. van der Wielen, J. Veen, P. A. A. F. Wouters, and E. F. Steennis, "Time-base alignment of PD signals measured at multiple cable ends", *Proceedings of the 8th IEEE International Conference on Solid Dielectrics (ICSD)*, pp. 648–652, Toulouse, France, July 2004.
- [Wig94] C. Wiggins, D. Thomas, F. Nickel, T. Salas, and S. Wright, "Transient electromagnetic interference in substations", *IEEE Transactions on Power Delivery*, vol. 9, no. 4, pp. 1869–1884, Oct. 1994.
- [Won90] K. Wong and T. Chen, "Studies of a slow-wave rogowski coil", *IEEE Transactions on Plasma Science*, vol. 18, no. 2, pp. 219–222, 1990.
- [Wou91] P. A. A. F. Wouters, W. J. S. Bollen, P. C. T. van der Laan, and E. F. Steennis, "Lokalisatie van partiële ontladingen in XLPE-kabels", Internal rapport EHC/RAP/91/011, Eindhoven University of Technology, The Netherlands, 1991. (in Dutch).
- [Wou94] P. A. A. F. Wouters, P. C. T. van der Laan, and E. F. Steennis, "Inductive ultra-wide band detection and location of partial discharges in high-voltage cables", *European Transactions on Electrical Power Engineering*, vol. 4, pp. 223–229, 1994.

- [Wou96] P. A. A. F. Wouters, “Simulatie pulssequentie van een partiele ontlading in een vertakt kabelsysteem”, Internal rapport EVT/RAP/96073, Eindhoven University of Technology, The Netherlands, Aug. 1996. (in Dutch).
- [Wou03a] P. A. A. F. Wouters and P. C. J. M. van der Wielen, “Effects of cable load impedance on coupling schemes for MV power line communication”, *Proceedings of the IEEE Bologna Power Tech’03 (BPT)*, Bologna, Italy, June 2003.
- [Wou03b] P. A. A. F. Wouters and P. C. J. M. van der Wielen, “Implications of on-line PD measurement on phase distributions for three-phase belted MV cables”, *Proceedings of the 7th International Conference on Properties and Applications of Dielectric Materials (ICPADM)*, pp. 83–87, Nagoya, Japan, June 2003.
- [Wou03c] P. A. A. F. Wouters, P. C. J. M. van der Wielen, and E. F. Steennis, “Challenges related to development of an on-line PD-detection and localization system”, *Proceedings of the 18th Nordic Symposium on Electrical Insulation (NORDIS)*, pp. 3–10, Tampere, Finland, June 2003.
- [Wou03d] P. A. A. F. Wouters, P. C. J. M. van der Wielen, J. Veen, and E. F. Steennis, “On-line PD measuring system for MV cables: some practical aspects and implications”, *XIIIth International Symposium on High Voltage Engineering (ISH)*, Delft, The Netherlands, Aug. 2003.
- [Wou05] P. A. A. F. Wouters, P. C. J. M. van der Wielen, J. Veen, P. Wagenaars, and E. F. Steennis, “Effect of cable load impedance on coupling schemes for MV power line communication”, *accepted for publication in the IEEE transactions on Power Delivery*, 2005.
- [Zae03] W. S. Zaengl, “Dielectric spectroscopy in time and frequency domain for HV power equipment. I. Theoretical considerations”, *IEEE Electrical Insulation Magazine*, vol. 19, no. 5, pp. 5–19, Sep–Oct 2003.
- [Zho01] L. Zhong, Y. Xu, G. Chen, A. Davies, Z. Richardson, and S. Swingler, “Use of capacitive couplers for partial discharge measurements in power cables and joints”, *Proceedings of the 2001 IEEE 7th International Conference on Solid Dielectrics (ICSD ’01)*, pp. 412–415, 2001.

Glossary

| | |
|--------------------------|--|
| Accessory | Generic term for components within a cable system other than cables, viz. joints or splices, and terminations. |
| Cable | Either a cable section or a cable system. In this thesis usually a medium-voltage distribution class is meant. |
| Cable section | Uniform cable with accessories only at the cable ends. |
| Cable system | Cascade of cable sections that are interconnected by joints. |
| Calibration | Determination of the relationship between the physical variable measurement input and the system output of some part of the measurement system. |
| Detection | The combined process of measurement and extraction of partial-discharge signals. |
| Estimation | Determination of signal or model parameter values from indirect or disturbed observations. |
| Excitation | Partial discharge and its consequently induced charges in nearby conductors. |
| Extraction | Recovery of partial-discharge signals from measurements. |
| Interference | (Disturbance) Any signal originating from outside the cable under test. |
| Joint | (Splice) Connection device between two cable sections. |
| Location | Pinpointing the origin of a partial discharge within a cable system. |
| Measurement | Conversion of an electrical or electromagnetic signal into a form that is suitable for analyzing. |
| On-line | Energized by the power grid. |
| Partial discharge | Local breakdown of the electric field that only partially bridges the insulation between the conductors. |
| Partial-discharge signal | Current or voltage that results from a partial discharge within the cable system under test. |
| Ring main unit | Junction of cable terminations and other high-voltage equipment located in small common housing, usually also incorporating a MV/LV transformer. |
| Rotating field | Electric or magnetic field with rotating direction. |
| Signal analysis | The combined process of interference rejection, signal extraction, and parameter estimation from measurements. |
| Substation | Junction of cable terminations and other high-voltage equipment located in a large common housing, also incorporating a HV/MV transformer. |
| Synchronization | Performing simultaneous starting of – or correction of the difference between the start of – multiple measurement data records. |

| | |
|------------------------|--|
| Termination | Electrical and mechanical reliable end device of a cable that allows interconnection of other high-voltage equipment to the cable system. |
| Time-base alignment | Aligning the complete time-bases of multiple measurement data records. This incorporates both synchronization and time-wander correction. |
| Time-wander correction | Correction of the time wander of multiple measurement data records, caused by a small drift of sampling-clock speed used in multiple data-acquisition systems. |

List of Abbreviations

| | |
|--------|---|
| 3G | Third generation |
| AC | Alternating current |
| ADC | Analog-to-digital converter |
| AUI | Advanced user interface |
| BEM | Boundary element method |
| CBM | Condition-based maintenance |
| CM | Common mode |
| CSD | Circuit Switched Data |
| CT | Current transformer |
| CUT | Cable (system) under test |
| DAQ | Data acquisition |
| DC | Direct current |
| DM | Differential mode |
| DOA | Direction of arrival |
| DSP | Digital signal processor |
| DTOA | Difference in time of arrival |
| DUT | Device under test |
| EDGE | Enhanced data rates for global evolution |
| EHV | Extra-high voltage |
| EM | Electro-magnetic |
| EMC | Electro-magnetic compatibility |
| EPR | Ethylene-propylene-rubber |
| FPGA | Field programmable gate array |
| GPRS | General packet radio system |
| GPS | Global positioning system |
| GSM | Global system for mobile communication |
| HF | High frequency |
| HSCSD | High-speed circuit switched data |
| HV | High voltage |
| ISDN | Integrated Services Digital Network |
| LAN | Local-area network |
| LV | Low voltage |
| MCTL | Multi-conductor transmission line |
| MM | Measurement manager |
| MOSFET | Metal-oxide semiconductor field effect transistor |
| MS | Monitoring system |
| MU x | Measurement unit x , $x \in \{1, 2\}$ |
| MV | Medium voltage |
| OWTS | Oscillating-wave test system |
| PD | Partial discharge |
| PE | Polyethylene |

| | |
|--------|--|
| PLC | Power-line communication |
| PILC | Paper-insulated lead-covered |
| PLEC | Past last earth connection (of the cable under test) |
| PP | Phase to phase |
| PSDF | Power spectral density function |
| PVC | Polyvinyl chloride |
| RMU | Ring main unit |
| RUI | Remote user interface |
| SA | Selective availability |
| SI | System identification |
| SNR | Signal-to-noise ratio |
| SP | Shield to phases |
| SQL | Structured query language |
| SSP | Shield to single phase |
| TBA | Time-base alignment |
| TCC | Transformer-connecting cables |
| TCP-IP | Transmission Control Protocol - Internet Protocol |
| TDR | Time-domain reflectometry |
| TEM | Transversal electromagnetic |
| TL | Transmission line |
| TOA | Time of arrival |
| TWC | Time-wander correction |
| UHF | Ultra-high frequency |
| UM | User manager |
| UMTS | Universal mobile telephone system |
| VLF | Very low frequency |
| WAN | Wide-area network |
| XLPE | Cross-linked polyethylene |

Notation and Symbols

General Notations

| | |
|--------------------------------------|--|
| x | scalar in time domain |
| X | phasor in frequency domain, Fourier transform of x |
| $\underline{x}, \underline{X}$ | vector |
| \mathbf{x}, \mathbf{X} | matrix |
| $x^{-1}, X^{-1}, \mathbf{X}^{-1}$ | inverse of x, X, \mathbf{X} |
| $\underline{X}^T, \mathbf{X}^T$ | transpose of $\underline{X}, \mathbf{X}$ |
| $X^*, \underline{X}^*, \mathbf{X}^*$ | complex conjugate of $X, \underline{X}, \mathbf{X}$ |
| $\text{Re}\{X\}$ | real part of X |
| $\text{Im}\{X\}$ | imaginary part of X |
| $ x , X $ | absolute value of x, X |
| $\angle X$ | angle of X |
| $\mathcal{F}\{x\}$ | Fourier transform of x |
| $\mathcal{F}^{-1}\{X\}$ | inverse Fourier transform of X |
| $E\{x\}$ | expected value of x |
| $\text{std}(x)$ | standard deviation of x |
| Δx | difference in x |
| dx | infinitely small difference in x |
| \bar{x} | average of x |
| $=$ | is equal to |
| \triangleq | is defined as |
| \approx | is approximately, is approximated by |
| $<$ | is smaller than |
| $>$ | is larger than |
| \ll | is much smaller than |
| \gg | is much larger than |
| \leq | is smaller than or equal as |
| \geq | is larger than or equal as |
| \lesssim | is smaller than approximately |
| \gtrsim | is larger than approximately |
| \propto | is proportional to |

List of Symbols

| Symbol | Description | Unit |
|---------------------------|---|------------------|
| α | per-unit-length attenuation constant | Np/m |
| α_d | per-unit-length attenuation due to dielectric losses | Np/m |
| α_j | per-unit-length attenuation of j^{th} cable section; $j \in \mathbb{N}$ | Np/m |
| α_{sc} | per-unit-length attenuation due to semi-conducting layers | Np/m |
| α_{sk} | per-unit-length attenuation due to skin effect | Np/m |
| α_{SP} | per-unit-length attenuation of SP channel | Np/m |
| β | per-unit-length phase constant | rad/m |
| β_j | per-unit-length phase constant of j^{th} cable section; $j \in \mathbb{N}$ | rad/m |
| β_{SP} | per-unit-length phase constant of SP channel | rad/m |
| γ | propagation constant; $\gamma = \alpha + j\beta$ | Np/m |
| $\mathbf{\Gamma}$ | propagation constant matrix | Np/m |
| $\tilde{\mathbf{\gamma}}$ | diagonalized propagation constant matrix | Np/m |
| γ_{PP} | propagation constant of PP channels | Np/m |
| γ_{SP} | propagation constant of SP channel | Np/m |
| δ | skin-depth | m |
| δ_c | skin-depth in central conductor | m |
| δ_s | skin-depth in shield conductor | m |
| ε | total dielectric constant; $\varepsilon = \varepsilon_0 \varepsilon_r$ | F/m |
| ε_0 | dielectric permittivity of vacuum; $\varepsilon_0 = 1/\mu_0 c^2 = 8.854187 \cdot 10^{-12}$ | F/m |
| ε_r | relative dielectric constant; $\varepsilon_r = \varepsilon'_r - j\varepsilon''_r$ | – |
| ε'_r | relative dielectric permittivity | – |
| ε''_r | imaginary part of relative dielectric constant | – |
| η | electric field eccentricity; $\eta = E_{\min}/E_{\max}$ | – |
| Θ | chain parameter matrix | – |
| Θ_j | chain parameter matrix of j^{th} cable section; $j \in \mathbb{N}$ | – |
| Θ_T | chain parameter matrix of total cable system | – |
| ϑ | cylindrical coordinate, angle | rad |
| ϑ_0 | direction of electric field \underline{E}_0 | rad |
| λ | wavelength | m |
| μ | total permeability; $\mu = \mu_0 \mu_r$ | H/m |
| μ_0 | permeability of vacuum; $\mu_0 = 4\pi \cdot 10^{-7}$ | H/m |
| μ_r | relative permeability | – |
| ξ | electric field direction | rad |
| ξ_{\max} | direction of maximum electric field | rad |
| ρ | reflection coefficient | – |
| σ | specific conductance | 1/ Ω m |
| σ_c | specific conductance of central conductor | 1/ Ω m |
| σ_i | specific conductance of insulation material | 1/ Ω m |
| σ_q | surface charge density | C/m ² |
| σ_s | specific conductance of shield conductor | 1/ Ω m |
| σ_{sc} | specific conductance of semi-conducting layers | 1/ Ω m |
| τ | transmission coefficient | – |
| τ_i | current transmission coefficient; $\tau_i = 1 - \rho$ | – |
| τ_v | voltage transmission coefficient ; $\tau_v = 1 + \rho$ | – |
| $\tau_{i \rightarrow j}$ | current transmission coefficient from section i to j ; $i, j \in \mathbb{N}$ | – |
| $\tau_{l,i}$ | current transmission coefficient from cable to load impedance $Z_{l,i}$; $i \in \{\emptyset, 1, 2\}$ | – |
| φ | phase angle | rad |

| | | |
|--|---|---------------------|
| φ_{\max} | phase angle at maximum field | rad |
| Φ | magnetic flux | Wb |
| ω | angular frequency; $\omega = 2\pi f$ | rad/s |
| ω_{co} | cut-off angular frequency | rad/s |
| ω_r | resonance angular frequency | rad/s |
| \emptyset | <i>empty</i> | – |
| a, \underline{a} | cartesian coordinate in direction of maximum electric field | m |
| A | cross-section area of turns in a coil | m ² |
| A_m | scaling ‘factor’ for matched filtering | A or V |
| b, \underline{b} | cartesian coordinate in direction of minimum electric field | m |
| B | flux density | T |
| B_s | saturation level of flux density | T |
| \underline{B}_t | transverse magnetic flux density vector | T |
| c | velocity of light in vacuum; $c = 2.997925 \cdot 10^8$ | m/s |
| C | per-unit-length capacitance | F/m |
| \mathbf{C} | per-unit-length capacitance matrix | F/m |
| $C_{1\text{ph}}$ | per-unit-length capacitance of single-phase cables | F/m |
| C_{SP} | per-unit-length capacitance of SP channel | F/m |
| C_{ec} | parasitic capacitance between coil and environment | F |
| C_{par} | parasitic capacitance | F |
| $C_{\text{par}j}$ | parasitic capacitance of section j in substation; $j \in \mathbb{N}_0$ | F |
| C_{tcc} | capacitance of transformer-connecting cables | F |
| C_{tr} | transformer HF capacitance | F |
| C_w | inter-winding capacitance | F |
| d | distance of dipole | m |
| \underline{d} | distance vector of dipole | m |
| d_{air} | thickness air slit in coil | m |
| d_{sc} | thickness of semi-conducting layers | m |
| d_{wg} | diameter waveguide | m |
| $D_n, D_{n,\text{in}}, D_{n,\text{out}}$ | perpendicular electric flux density | C/m |
| D_s | factor to relate S-parameters to conventional parameters; $D_s = 2Z_c Z_0 \cosh \gamma l + (Z_c^2 + Z_0^2) \sinh \gamma l$ | Ω^2 |
| \underline{E} | electric field vector | V/m |
| \underline{E}_0 | total electric field vector | V/m |
| \underline{E}_t | transverse electric field vector | V/m |
| E_0 | total electric field strength | V/m |
| E_a | electric field strength along maximum-field (a -) axis of elliptical field | V/m |
| E_b | electric field strength along minimum-field (b -) axis of elliptical field | V/m |
| E_{inc} | inception (electric) field strength | V/m |
| E_{min} | minimum electric field strength of elliptic field | V/m |
| E_{max} | maximum electric field strength of elliptic field | V/m |
| E_n | perpendicular electric field strength | V/m |
| E_t | tangential electric field strength | V/m |
| f | frequency | Hz |
| f_{so} | assumed exact sample rate | Hz |
| f_{sm} | measurement sample rate | Hz |
| f_{det} | transfer function of detection device (sensor) | – |
| \mathbf{F} | Fourier matrix | – |
| G | per-unit-length conductance | 1/ Ωm |
| \mathbf{G} | per-unit-length conductance matrix | 1/ Ωm |

| | | |
|--|--|--------------------|
| $G_{1\text{ph},c}$ | per-unit-length conductance of single-phase cables due to materials specific conductance | $1/\Omega\text{m}$ |
| $G_{1\text{ph},d}$ | per-unit-length conductance of single-phase cables due to dielectric polarization loss | $1/\Omega\text{m}$ |
| $G_{1\text{ph},sc}$ | per-unit-length conductance of single-phase cables due to semi-conducting layers | $1/\Omega\text{m}$ |
| G_{SP} | per-unit-length conductance of SP channel | $1/\Omega\text{m}$ |
| h | height | m |
| \underline{H} | magnetic field vector | A/m |
| H_1 | transfer function between injected and first reflected pulse | – |
| H_{cal} | transfer function from calibration measurement | – |
| H_{m} | transfer function of matched filter | – |
| $H_{\text{T},i}$ | transfer function between injected and reflected pulse spectrum at cable end i ; $i \in \{1, 2\}$ | – |
| H_{T} | total transfer function of system | – |
| $H_{u,v}$ | transfer function from current through impedance u to current through impedance v | – |
| $H_{(u,v)w}$ | transfer function from current through impedance u to current through impedance v , coming from source w | – |
| H_{T} | total transfer function of system | – |
| i | current in time domain | A |
| i_{C} | current through capacitor | A |
| $i_{\text{enc}}, I_{\text{enc}}$ | enclosed current | A |
| i_{L} | current through inductor | A |
| $i_{\text{pr}}, I_{\text{pr}}$ | primary current | A |
| i_{R} | current through resistor | A |
| I | current | A |
| \underline{I} | line (phase) current vector; $\underline{I} = (I_1, I_2, I_3)^{\text{T}}$ | A |
| \tilde{I} | transformed current vector | A |
| \mathbf{I} | identity matrix | – |
| I^+ | current of travelling wave in positive (z) direction | A |
| I^- | current of travelling wave in negative ($-z$) direction | A |
| $i_{1/2/3}, I_{1/2/3}$ | line (phase) currents | A |
| $I_{1/2/3}^+$ | line (phase 1/2/3) current of travelling wave in positive (z) direction | A |
| I_{c} | cable current | A |
| I_{CM} | common-mode current | A |
| $I_{\text{i}}, I_{\text{in}}$ | injection / input current | A |
| I_{ind} | induced current | A |
| I_{dif} | differential current | A |
| I'_{dif} | transformed differential current | A |
| I_{DUT} | current through device under test | A |
| I_{L} | current through load impedance | A |
| $I_{1,i}$ | current through load impedance $Z_{1,i}$; $i \in \{\emptyset, 1, 2\}$ | A |
| $i_{\text{o}}, i_{\text{out}}, I_{\text{o}}, I_{\text{out}}$ | output current | A |
| I_{tcc} | current through TCC earth connection | A |
| j | imaginary unit | – |
| K | factor for charge approximation | – |
| K_{s} | factor for to relate the line currents upon SSP injection | – |
| l | length | m |
| l_{a} | effective antenna length | m |
| l_{c} | cable length | m |
| l_{coil} | length coil | m |

| | | |
|--------------------------|---|-------------------|
| l_j | length cable section j ; $j \in \mathbb{N}$ | m |
| l_{wg} | length waveguide | m |
| ℓ | length of void in z -direction | m |
| L | per-unit-length inductance | H/m |
| \mathbf{L} | per-unit-length inductance matrix | H/m |
| $L_{1\text{ph},e}$ | external per-unit-length inductance of single-phase cables | H/m |
| $L_{1\text{ph},i}$ | internal per-unit-length inductance of single-phase cables | H/m |
| L_c | self inductance coil | H |
| L_j | inductance of section j in substation; $j \in \mathbb{N}_0$ | H |
| L_{loop} | (parasitic) inductance of loop | H |
| L_{SP} | per-unit-length inductance of SP channel | H/m |
| L_{tr} | transformer HF inductance | H |
| M | per-unit-length mutual inductance | H/m |
| M_c | mutual inductance coil | H |
| n | PD density | 1/sm |
| n' | charge distribution function | C/sm |
| n_w | winding density | 1/m |
| N | number of cable or substation sections | – |
| N_w | number of windings | – |
| N_x | set of cable-section numbers in part x of the cable; $x \in \{1, 2, c\}$ | – |
| \mathbb{N} | Set of natural numbers, i.e. $\{1, 2, 3, \dots\}$ | – |
| \mathbb{N}_0 | Set of natural numbers, including 0, i.e. $\{0, 1, 2, \dots\}$ | – |
| \underline{p} | charge dipole vector | Cm |
| \underline{P}_N | Noise power spectral density function | V ² |
| Q | charge | C |
| $Q_{0n,\text{app}}$ | apparent (induced) charge in earth screen from charge displacement in perpendicular direction | C |
| $Q_{0t,\text{app}}$ | apparent (induced) charge in earth screen from charge displacement in tangential direction | C |
| $Q_{0/1/2/3,\text{app}}$ | apparent (induced) charge in earth/phase1/2/3 conductor | C |
| Q_{app} | apparent (induced) charge | C |
| Q_{appr} | approximated charge | C |
| Q_{bw1} | bandwidth limited charge | C |
| Q_i | apparent charge in phase conductor i ; $i \in \{1, 2, 3\}$ | C |
| $Q_{n,\text{real}}$ | (real) charge displacement in perpendicular direction | C |
| Q_{real} | real charge displacement | C |
| $Q_{t,\text{real}}$ | (real) charge displacement in tangential direction | C |
| Q' | charge density | C/sm |
| r, \underline{r} | cylindrical coordinate, radial direction | m |
| r_{coil} | radius of the middle of the toroidal structure of a coil with circularly-shaped windings | m |
| r_i | inner radius coil | m |
| r_c | radius of central conductor | m |
| r_{coil} | radius of the middle of the toroidal structure of a coil with circularly-shaped windings | m |
| r_o | outer radius coil | m |
| r_s | inner radius of shield | m |
| r_v | radius of void | m |
| R | per-unit-length resistance | Ω/m |
| \mathbf{R} | per-unit-length resistance matrix | Ω/m |
| $R_{1\text{ph}}$ | per-unit-length resistance of single-phase cables | Ω/m |
| $R_{\text{rad}j}$ | radiation resistance of section j in substation; $j \in \mathbb{N}_0$ | Ω |
| R_{SP} | per-unit-length resistance of SP channel | Ω/m |

| | | |
|-------------------------|--|--------------|
| R_{tr} | transformer HF resistance, representing internal losses | Ω |
| s, \underline{s} | surface, surface vector | m^2 |
| S_0 | number of samples between two synchronization pulses at correct sample rate | – |
| S_m | measured number of samples between two synchronization pulses | – |
| S_{ij} | scattering parameters, $i, j \in \{1, 2\}$ | – |
| \mathbf{S} | scattering-parameter matrix | – |
| \underline{S} | Poynting vector | W/m^2 |
| t | time | s |
| t_0 | PD excitation time | s |
| t_c | cable propagation time | s |
| t_{oa} | time of arrival of a PD signal | s |
| $t_{oa,m}$ | measured time of arrival of a PD signal | s |
| $t_{oa,p1}$ | time of arrival of first synchronization pulse | s |
| $t_{oa,r}$ | real time of arrival of a PD signal | s |
| t_{oax} | time of arrival of a PD signal at cable end x ; $x \in \{1, 2\}$ | s |
| Δt_0 | time between two synchronization pulses | s |
| Δt_{m1} | measured time between two synchronization pulses | s |
| Δt_{m2} | corrected time between two synchronization pulses | s |
| U | electric potential | V |
| U_0 | nominal voltage of phase conductors | V |
| $U_{1/2/3}$ | electric potentials of phase 1/2/3 conductor | V |
| v | velocity | m/s |
| v_c | propagation velocity of cable | m/s |
| v_C | voltage over capacitor | V |
| v_L | voltage over inductor | V |
| v_P | phase velocity | m/s |
| v_R | voltage over resistor | V |
| \bar{v}_x | weighted average propagation velocity in part x of the cable system; $x \in \{1, 2, c\}$ | m/s |
| V | voltage | V |
| \underline{V} | line voltage vector; $\underline{V} = (V_1, V_2, V_3)^T$ | V |
| $\tilde{\underline{V}}$ | transformed voltage vector | V |
| V^+ | voltage of travelling wave in positive (z) direction | A |
| V^- | voltage of travelling wave in negative ($-z$) direction | A |
| $V_{1/2/3}$ | line voltages | V |
| $V_{1/2/3}^+$ | line (phase 1/2/3) voltage of travelling wave in positive (z) direction | V |
| V_i, V_{in} | input voltage | V |
| V_{ind} | induced voltage | V |
| $V_{m,i}$ | voltage over measuring coil i ; $i \in \{\emptyset, 1, 2\}$ | V |
| V_N | frequency spectrum of noise voltage | V |
| v_{out}, V_o, V_{out} | output voltage | V |
| V_{PD} | frequency spectrum of PD signal | V |
| x, \underline{x} | cartesian coordinate, perpendicular to direction of propagation | m |
| y, \underline{y} | cartesian coordinate, perpendicular to direction of propagation | m |
| Y | per-unit-length admittance | $1/\Omega m$ |
| \mathbf{Y} | per-unit-length admittance matrix | $1/\Omega m$ |
| $\tilde{\mathbf{Y}}$ | diagonalized per-unit-length admittance matrix | $1/\Omega m$ |
| Y_{1ph} | per-unit-length admittance of single-phase cables | $1/\Omega m$ |
| Y_{SP} | per-unit-length admittance of SP channel | $1/\Omega m$ |

| | | |
|---------------------------|--|--------------------|
| Y_1 | diagonal elements in \mathbf{Y} | $1/\Omega\text{m}$ |
| Y_2 | non-diagonal elements in \mathbf{Y} | $1/\Omega\text{m}$ |
| z, \underline{z} | cartesian coordinate, in direction of propagation | m |
| z_0 | location of PD origin | m |
| z_{PD} | propagation distance from PD site to near cable end / cable end 1 | m |
| Z | per-unit-length impedance | Ω/m |
| \mathbf{Z} | per-unit-length impedance matrix | Ω/m |
| $\tilde{\mathbf{Z}}$ | diagonalized per-unit-length impedance matrix | Ω/m |
| Z_0 | characteristic impedance of measuring system | Ω |
| Z_1 | diagonal elements in \mathbf{Z} | Ω/m |
| Z_2 | non-diagonal elements in \mathbf{Z} | Ω/m |
| Z_c | characteristic (wave) impedance (of cable under test) | Ω |
| \mathbf{Z}_c | characteristic (wave) impedance matrix | Ω |
| $\tilde{\mathbf{Z}}_c$ | diagonalized characteristic impedance matrix | Ω/m |
| $Z_{1\text{ph}}$ | per-unit-length impedance of single-phase cables | Ω/m |
| Z_{SP} | per-unit-length impedance of SP channel | Ω/m |
| $Z_{c,1}$ | diagonal elements in \mathbf{Z}_c | Ω |
| $Z_{c,2}$ | non-diagonal elements in \mathbf{Z}_c | Ω |
| $Z_{c,j}$ | characteristic impedance of j^{th} MV cable in substation | Ω |
| $Z_{c,j}$ | characteristic impedance of j^{th} cable section in cable system | Ω |
| $Z_{c,\text{PP}}$ | characteristic impedance of PP channel | Ω |
| $Z_{c,\text{SP}}$ | characteristic impedance of SP channel | Ω |
| Z_{DUT} | impedance of device under test | Ω |
| Z_i, Z_{in} | input impedance | Ω |
| $Z_{1,i}$ | load impedance at cable end i ; $i \in \{\emptyset, 1, 2\}$ | Ω |
| Z_L | load impedance | Ω |
| $Z_{m,i}$ | measuring impedance over measuring coil i ; $i \in \{\emptyset, 1, 2\}$ | Ω |
| Z_t | transfer impedance | Ω |
| $Z_{t,\text{CM}}$ | common-mode transfer impedance | Ω |
| $Z_{t,i}$ | transfer impedance of injection coil | Ω |
| $Z_{t,m}$ | transfer impedance of measurement coil | Ω |
| $Z_{T,i}, Z_{\text{RMU}}$ | sum impedance of cable impedance and load impedance $Z_{1,i}$; $i \in \{\emptyset, 1, 2\}$ | Ω |
| Z_{tcc} | impedance of TCC to earth | Ω |
| Z_x | transfer impedance due to cross talk | Ω |

Acknowledgement

First of all I would like to thank my professor and first promotor Fred Steennis, whose profound expertise, creative ideas and enthusiasm were highly encouraging and essential for the complete project. Special acknowledgements also go to my coach and copromotor Peter Wouters, whose fundamental and theoretical insight in the encountered problems and critical, but pleasant, feedback were highly constructive. Furthermore, I would like to thank my fellow Ph.D. candidate in this project, Jeroen Veen, for the fruitful and pleasant cooperation and his thorough work.

Most of the practical work was carried out at KEMA in Arnhem. I would like to thank KEMA for the opportunity and support to do the work like this. Several people were involved in some way or another and my appreciation goes to all of them. I would especially like to mention Dick van Aartrijk and Osrick Anita who both did a great job in transforming many of the ‘crazy’ ideas into practice.

The scientific part of the work was mostly done at the university, where I owe gratitude to my second promotor Jan Bergmans and Martin Bastiaans for their fruitful discussions, critical views and constructive comments. Furthermore, the colleagues at the Electrical Power Systems group of the university helped me to broaden my interest and knowledge in different subjects in the power and high-voltage areas. I would like to thank them for all the formal and informal discussions.

During the project I got the opportunity to guide students, who were attracted to the wide subject-area of this project, during their internships or graduation projects. In the mean time, various subjects of my work gained help from these students. In random order I would like to thank Willem Dekker, Remco Melius, Bart Lubberdink, Paul Wagenaars, Mohamed Talbi, Mohamed Abbadi, Guy Vaessen, and Pim Jacobs for their contributing work.

Obviously, a project like this has to be financed. Therefore, I would like to thank the contributors that supported this project: Technology Foundation STW, KEMA Nederland B.V., N.V. Continuon Netbeheer, ENECO Netbeheer B.V. At the two contributing utilities, Maarten van Riet and Marko Kruithof were the representatives and participated in the various discussions and meetings, where they gave constructive feedback from their practical point of view. Furthermore they enabled us to do various measurements in their medium-voltage grids. I would like to thank them for this.

Finally, I would like to thank my family and my friends for their support and understanding. Special and many thanks goes to my parents, who enabled me to study and support me in everything I do. Last, but certainly not least, I owe my girlfriend, Angelique, a large debt of gratitude for all her patience, support, motivation, and especially, all that she is.

Curriculum vitae

Peter van der Wielen was born in Hulst, The Netherlands, on March 6, 1973. After finishing his secondary school at the “Jansenius Scholengemeenschap” (V.W.O., Athenaeum) in Hulst, he started studying Electrical Engineering at the Eindhoven University of Technology in the Netherlands. During this study he was also an active member of the IEEE Student Branch Eindhoven, where he joined the board and various committees for several years. He received his M.Sc. degree in 2000 after a graduation project on corrosion diagnostics for lead-shielded power cables at KEMA, Testing and Diagnostics Power, the Netherlands.

Afterwards, he started pursuing a Ph.D. degree, doing a study on power-cable diagnostics at both the Electrical Power Systems group at the Eindhoven University of Technology and KEMA, Transmission and Distribution Testing Services (TDT). This research was primarily focussing on the different aspects related to on-line partial-discharge monitoring of medium-voltage power-cable systems, as described in this thesis. During this study, he has also been software coordinator/designer for this project at KEMA TDT.

STELLINGEN

behorende bij het proefschrift

On-line Detection and Location of Partial Discharges in Medium-Voltage Power Cables

door

P.C.J.M. van der Wielen

7 april 2005

1. On-line gemeten fasepatronen van partiële ontladingen van gordelkabels kunnen significant afwijken van off-line gemeten fasepatronen.
(Dit proefschrift, hoofdstuk 2)
On-line measured partial-discharge phase patterns from belted cables can differ significantly from off-line obtained phase patterns.
(This thesis, chapter 2)
2. Zowel de diëlektrische constante als de propagatie-constante zijn allesbehalve constant.
(Dit proefschrift, hoofdstuk 3)
Both the dielectric constant and the propagation constant are anything but constant.
(This thesis, chapter 3)
3. De combinatie van propagatiekarakteristieken, ruisspectra en onderstations-impedanties dicteert dat partiële ontladingen van middenspannings-kabelsystemen het best tussen 1–10 MHz kunnen worden gemeten.
(Dit proefschrift, hoofdstuk 3 en 4)
The combination of propagation characteristics, noise spectra, and substation impedances dictates that partial discharges in medium-voltage cables can be measured best between 1–10 MHz.
(This thesis, chapters 3 and 4)
4. Voor on-line partiële ontladingsdetectie aan middenspannings-kabels is PLEC (Past the Last Earth Connection) dé plek.
(Dit proefschrift, hoofdstuk 4)
For on-line partial-discharge measurements on medium-voltage cables, PLEC (Past the Last Earth Connection) is just the PLEC (Preferable Location for the Enclosing Coil).
(This thesis, chapter 4)
5. Zoals een groot deel van de wereld toegang heeft tot het internet, zijn partiële ontladingsmetingen aan middenspannings-kabels nu ook ‘on-line’.
(Dit proefschrift, met name hoofdstuk 7)
Like a large part of the world has access to the internet, partial-discharge measurements on medium-voltage cables are now also ‘on-line’.
(This thesis, especially chapter 7)
6. Capaciteitsproblemen worden geëlimineerd door inductieve koppeling.
(Dit proefschrift, hoofdstuk 4)
Problems with capacity are eliminated by inductive coupling.
(This thesis, chapter 4)
7. De meeste informatie op het internet gaat over het internet zelf (en alles wat daarmee samenhangt), hetgeen internet hoofdzakelijk inherent redundant maakt.
Most information on the internet deals with the internet itself (and everything related to it), which makes the internet mainly inherently redundant.
8. Sportscholen zouden in plaats van alleen energieconsumptie ook moeten zorgen voor energieopwekking uit de arbeid die nodig is voor het verplaatsen van gewichten.
Besides just taking care of energy consumption, sports centers should also supply energy by useful reuse of the labor that is necessary for moving weights.

9. Iemand die zich beroept op zijn of haar autoriteit toont daarmee zijn of haar gebrek daaraan.
Someone who appeals to his or her authority demonstrates his or her lack of it.
10. De bewering van veel mensen dat ze het druk hebben is tamelijk relatief in vergelijking met andere diersoorten die er helemaal geen hobby op na kunnen houden.
The statement of many people to be busy is rather relative compared to other animal species that cannot even have any hobby.
11. Aangezien men tijdens publieke debatten alleen maar goed lijkt te scoren indien men een zo extreem en onwrikbaar mogelijk standpunt inneemt, worden problemen als extremisme en integratie er met eindeloos debatteren niet kleiner van.
Since the appreciation during public debates seems high only if extreme, uncompromising opinions are expressed, problems like extremism and integration will not reduce from endless debating.
12. De oorzaak en bestrijding van terrorisme hebben een grote gemeenschappelijke factor.
The cause of and measures against terrorism have a large common factor.
13. Waarden en normen die kunstmatig worden opgelegd aan een maatschappij zijn geen waarden en normen van die maatschappij.
Values and standards that are imposed on a society are not the values and standards from that society.
14. Met de komst van mobiele telefonie is het vermogen van de mens fatsoenlijke afspraken te maken verloren gegaan.
With the arrival of mobile telephony, the ability of people to make decent appointments has been lost.
15. De meest succesvolle mensen krijgen in de huidige samenleving niet de meeste nakomelingen. Dit ondermijnt de grondbeginselen van de evolutietheorie.
Society's most successful people are not the people that get most children. This undermines the basic principles of the evolution theory.
16. Mensen gedragen zich in de regel anders dan dat ze vinden hoe mensen zich zouden moeten gedragen.
Usually, people behave differently from the way they think people should behave.
17. Men praat vaak over dingen waar men niet over te spreken is.
<no translation possible>
18. Succesvolle stellingen missen nuance.
Successful statements lack in nuance.